REPORT DOCUMENTATION PAGE

AFRL-SR-AR-TR-06-0112

1. AGENCY USE ONLY *(Leave blank)*	2. REPORT DATE	3. REPORT TYPE AND DATES COVERED
		01 Jul 2002 - 31 Dec 2005 FINAL

4. TITLE AND SUBTITLE
COLLISION DYNAMICS OF RYDBERG ATOMS AND MOLECULES AT ULTRALOW ENERGIES

5. FUNDING NUMBERS
61102F
2301/DX

6. AUTHOR(S)
DR FLANNERY

7. PERFORMING ORGANIZATION NAME(S) AND ADDRESS(ES)
GEORGIA TECH RESEARCH COPR
505 TENTH STREET NW
GEORGIA INSTITUTE OF TECHNOLOGY
ATLANTA GA 30332-0420

8. PERFORMING ORGANIZATION REPORT NUMBER

9. SPONSORING/MONITORING AGENCY NAME(S) AND ADDRESS(ES)
AFOSR/NE
4015 WILSON BLVD
SUITE 713
ARLINGTON VA 22203
Dr Anne Matsuura

10. SPONSORING/MONITORING AGENCY REPORT NUMBER
F49620-02-1-0338

11. SUPPLEMENTARY NOTES

12a. DISTRIBUTION AVAILABILITY STATEMENT
DISTRIBUTION STATEMENT A: Unlimited

12b. DISTRIBUTION CODE

13. ABSTRACT *(Maximum 200 words)*

First Major Highlight: Collisional Stark Mixing at ultralow energies in Rydberg Plasmas.

Atoms in high (n,l) states formed in cold Rydberg plasmas decay to the ground state in a succession of radiative transitions populating intermediate excited states. Which states are populated during cascading and with what probability can be obtained from known transition probabilities.

Classical models simplify the calculation. considerably, reveals the "trajectory" in nt space followed during the cascade, scaling rules and other aspects hidden within the quantal approach. Conserved Quantity (quantal analogue obscure).

Quantal-Classicat correspondence in radiative recombination and decay is directly demonstrated.

Classical transition probabilities and radiative.recombination cross-section are in excellent agreement with quantal results.

Cross section for three body collisional capture formulated for arbitrary electron-energy distributions.

20060601087

14. SUBJECT TERMS			15. NUMBER OF PAGES
			16. PRICE CODE
17. SECURITY CLASSIFICATION OF REPORT	18. SECURITY CLASSIFICATION OF THIS PAGE	19. SECURITY CLASSIFICATION OF ABSTRACT	20. LIMITATION OF ABSTRACT
Unclassified	Unclassified	Unclassified	UL

Final Report on AFOSR Grant: 49620-02-1-0338

Contents

Activities and Findings

I. FINAL REPORT ON AFOSR GRANT: 49620-02-1-0338

II. TITLE: COLLISION DYNAMICS OF RYDBERG ATOMS AND MOLECULES AT ULTRALOW ENERGIES

III. PERIOD: 01-JUL-2002 TO 31-DEC-2005

IV. PRINCIPAL INVESTIGATOR: M. R. FLANNERY

V. ADDRESS: SCHOOL OF PHYSICS, GEORGIA INSTITUTE OF TECHNOLOGY, ATLANTA, GA 30332-0430

VI. BACKGROUND: ULTRACOLD RYDBERG PLASMAS

Advances in cooling and trapping of neutral gases have made possible a new branch of atomic physics namely interactions, dynamics and collisions in ultracold ($T \ll 1K$) systems. When atoms, initially prepared in the ground state at sub-millikelvin temperatures, are laser excited to highly excited Rydberg levels a gas of slowly moving Rydberg atoms is produced. The sufficiently dense sample of highly excited atoms then ionizes spontaneously with very high efficiency producing extremely cold plasma containing Rydberg atoms, electrons and ions. The ionization is caused by collision with the small number of Rydberg atoms at cold temperature or by absorbing background radiation. Most of the electrons are trapped by the ions and collide, de-excite and ionize the Rydberg gas creating an electron avalanche. The fact that the plasma can be sustained is evidence of the importance of "super-elastic" (de-excitation) collisions. The plasma state can also revert back to Rydberg atoms via three-body recombination between electrons, ions and neural gas atoms. We wish to study the interaction and collisions between two Rydberg atoms in the Rydberg gas. This interaction may result in Rydberg molecules and in ionization which produces a frozen Rydberg plasma. We are also interested in the dynamics/interplay between the gas and the plasma, a hybrid which we shall refer, for brevity, as an ultracold Rydberg plasma.

VII. FOCUS: ULTRACOLD RYDBERG PLASMAS

The focus of the research reported here is based on providing, in as complete as possible format, theoretical descriptions of the basic interactions and processes involved in ultracold Rydberg plasmas. Not only will the present theory of atomic and molecular collision physics be advanced (in a form for future textbooks), but also the basic physical rates and cross sections will find extensive application in more basic simulations, not only of Rydberg plasmas but also of astrophysical plasmas associated with HII regions of hot stars and of the experiments at CERN on the formation of anti-hydrogen.

A. Physical Processes: Interactions and collisions

The basic processes in Rydberg plasmas we have investigated during the period of the grant included:

1. Stark Mixing (via ion-collision): $Ry^+ + Ry(n,\ell) \rightarrow Ry^+ + Ry(n,\ell')$
2. Radiative Cascade: $Ry(n\ell) \rightarrow Ry(n'\ell') + h\nu \rightarrow Ry(n''\ell'') + h\nu' \rightarrow ....groundstate$

3. Interactions between polar Rydberg atoms: $Ry(n\ell) + Ry(n', \ell') \rightarrow Ry(n'' < n, \ell'') + Ry^+ + e$

4. Possibility for formation of long-range Rydberg-Rydberg molecules: $Ry_2 \rightarrow Ry(n\ell) + Ry(n', \ell')$

where f and s denote faster and slower electron speeds. These four topics have been successfully investigated and developed. The work resulted in seven publications.

VIII. PUBLICATIONS

The following 11 publications was attained under the grant:

A. Research

1. *Equivalent multipole operators for degenerate Rydberg states*, by V. Ostrovsky, D. Vrinceanu and M. R. Flannery, Phys. Rev. A (2006, submitted).

2. *Plasma Screening within Rydberg Atoms in Circular States*, by M. R. Flannery and E. Oks, J. Phys. B: Atom. Molec. and Opt.Phys., (2006, submitted).

3. *Magnetic stabilization of a Rydberg quasimolecule in circular states*, by M. R. Flannery and E. Oks, Phys. Rev. A **73**, 013405 (2006)

4. *The enigma of nonholonomic constraints*, by M. R. Flannery, Am. J. Phys., **73** (2005), pp. 265-272.

5. *Long-range interaction between polar Rydberg atoms*, by M. R. Flannery, D. Vrinceanu and V. N. Ostrovsky, J. Phys. B: Atom. Molec. and Opt.Phys., **38** (2005), pp. S279-S293.

6. *Quantal and Classical Radiative Cascade in Rydberg Plasmas*, by M. R. Flannery and D. Vrinceanu, Physical Review A **68** (2003),030205(R) pp. 1-4 .

7. *Stark Mixing in Rydberg Systems by Ultralow energy Collisions with Ions*, by M. R. Flannery and D. Vrinceanu in **Dissociative Recombination of Molecular Ions with Electrons**, ed. S. L. Guberman (Kluwer Academic/Plenum Publishers, 2003), pp. 151-166.

8. *Stark Mixing in Rydberg Atoms by ultralow energy collisions with ions*, by M. R. Flannery and D. Vrinceanu, Int. Journ. Mass Spectrom. **223-224** (2003), pp. 473-489.

9. *Atomic and Molecular Collision Processes*, by M. R. Flannery, in **Physicists' Desk Reference, Third Edition** (AIP-Springer Press, New York, 2003), Chap. 6, pp 145-241.

10. *David Bates, 1916-1994*, by M. R. Flannery, in **Physicists of Ireland** (Institute of Physics Press, London, 2003), pp 262-272.

11. *Classical and Quantal Atomic form factors for $n\ell m \rightarrow n'\ell' m$ transitions*, by M. R. Flannery and D. Vrinceanu , Phys. Rev. A **65** (2002), 022703 pp. 1-10.

IX. INVITED PAPERS PRESENTED AT SCIENTIFIC CONFERENCES

During the grant period, the following seven invited papers were presented:

1. *Recombination and cascade in Rydberg plasmas*, by M. R. Flannery, **Invited Paper**, presented to **Cold and Ultra Cold Plasma and Rydberg Physics** Workshop at the Institute of Theoretical Atomic and Molecular Physics, Harvard University, Cambridge, MA , September 26-28, 2005.

2. *Interactions and Collisions in Ultracold Rydberg Plasmas*, by M. R. Flannery, **Invited Paper**, presented at **2005 DAMOP, Division of Atomic, Molecular and Optical Physics, American Physical Society** Lincoln, Nebraska, May 17-21, 2005.

3. *Ultracold Rydberg-Rydberg Interactions*, by M. R. Flannery, **Invited Paper**, presented at **Sixth International Conference on Dissociative Recombination: Theory, Experiment and Applications**, Mosbach, Germany, July 12-17, 2004.

4. *Ultracold Rydberg-Rydberg Interactions and Collisions*, by M. R. Flannery, **Invited Paper**, presented at **International Workshop on Rydberg Physics**, Dresden, Germany, May 2-7, 2004.

5. *Non-Adiabatic Transitions in Ultracold Collisions of Rydberg Atoms* , by M. R. Flannery, **Invited Paper**, presented at **Moscow-Chernogolovka Workshop on Nonadibatic Transitions in Quantum Mechanics**, Moscow and Chernogolovka, August 4-7, 2003.

6. *Processes in Ultracold Rydberg Plasmas and in antihydrogen formation*, by M. R. Flannery, **Invited Paper**, presented at **Symposium on Applicatiom of Plasma Processes**, Liptovska Sielnica, Slovensko, Slovakia, January 13-18, 2003.

7. *Stark Mixing in Rydberg Atoms/Molecules by ultralow energy collisions with ions*, by M. R. Flannery, **Invited Paper**, presented at **European Conference on Dynamics of Molecular Collisions**, (*Molec 14*), Koc University, Istanbul, Turkey, September 1-6, 2002.

In addition to those above, various contributed papers were routinely presented at the annual meetings of APS-DAMOP (Division of Atomic, Molecular and Optical Physics) and at the GEC (Gaseous Electronics Conference).

X. PRIZES AWARDED FOR RESEARCH

During the grant period, the PI was the recipient of the following prizes awarded by professional societies for his research:

- Recipient of the 2002 Beams Award of the Southeastern Section of the American Physical Society (SESAPS) for Outstanding Research. *Cited: "For his pioneering, seminal, influential and enduring contribution to Atomic and Molecular Collision Physics."*
- Recipient of the 2002 Bates Prize of the Institute of Physics, London. *Cited: "For his distinguished contributions to the field of theoretical atomic physics and, in particular, for his studies of recombination processes with applications to astrophysics and plasma physics."*

XI. PROGRESS ACHIEVED DURING PERIOD 2001-2005

A. First Major Highlight: Collisional Stark Mixing at ultralow energies in Rydberg Plasmas

$$Ry^+ + Ry(n,\ell) \rightarrow Ry^+ + Ry(n,\ell')$$

The 40 year-old problem of $n\ell - n\ell'$ transitions (Stark Mixing) in a Rydberg atom induced by the time-dependent (dipole) electric field generated by (adiabatic) collision with a slow ion was solved exactly in a very elegant and novel way. The exceptional rich SO(4) dynamical symmetry of the hydrogen atom ennabled the development of a radically new theory of the collision process and the construction of both the exact classical and quantal solutions in a unified way. The classical-quantal correspondence obtained transcends the well-known Ehrenfest's theorem just because of the SO(4) group symmetry of the hydrogen atom. An advantage of the classical treatment is that it was able to expose essential physics, which remains obscured in the quantal treatment. The exact classical and quantal solutions exposed the analytical beauty of the problem and the solutions are applicable to a wide range of problems, ranging from ultracold Rydberg plasmas, antihydrogen formation to ZEKE (zero-energy-electron-kinetic-energy spectroscopy). The research has resulted in three publications (4, 6 and 7 above), where the results are shown in great detail. Three invited talks (7 - 9, above) on the work were presented to Professional Societies.

B. Classical and Quantal Atomic form factors for $n\ell m \rightarrow n'\ell' m$ transitions

An analytical expression for the classical form factor or impulsive probability $P_{if}(\mathbf{q})$ for $nlm \rightarrow n'l'm$ transitions is derived directly from the "phase-space distribution" method previously proposed (Phys. Rev. A **60**, (1999) 1053) and is compared with quantal results. Exact scaling laws are derived for the classical probability for any $i \rightarrow f$ transition. As n is increased, convergence to the classical results is obtained and becomes even more rapid upon averaging in succession over the m and then the ℓ substates. The classical results reveal the basic reason for the underlying structure in the variation of P_{if} with momentum transfer $\mathbf{q}$. They can operate as an effective averaged version of the exact quantal counterpart. The form factor appears as a basic atomic kernel in the quantal impulse cross section which we derived (M. R. Flannery and D. Vrinceanu, Phys. Rev. Lett., **85**, (2000), pp. 1-5) in a novel form suitable for exposing direct classical correspondence. This basic result is useful for atomic collisions involving highly excited Rydberg atoms. This work *Classical and Quantal Atomic form factors for $n\ell m \rightarrow n'\ell' m$ transitions*, by M. R. Flannery and D. Vrinceanu was published in Phys. Rev. A **65** (2002), 022703.

C. Second Major Highlight: Radiative Cascade in ultracold Rydberg Plasmas

Atoms in high (n,ℓ) states formed in cold Rydberg plasmas decay to the ground state in a succession of radiative transitions populating intermediate excited states. We have investigated the energy route preferred in radiative cascade of an excited atom in an initially prepared Rydberg level $n\ell$. In so doing, we advanced a remarkably accurate classical theory of the subsequent trajectory in $n\ell$-space produced by radiative cascade and illustrate a powerful classical-quantal correspondence at work. A classical treatment of the transition probability (Einstein A-coefficient) was also provided. It is worth noting that classical theory of radiative decay, until now, was not vigorously pursued after 1930, presumably due to its prediction that the accelerating spiralling electron will ultimately pass through the Coulomb force center, an untenable feature evident for those lowest n and ℓ states, the only states then accessible to experimental observation. For high n states, however, we have shown that the classical picture developed here works remarkably well, even for states with $\ell/n \geq 0.2$ which includes the majority of Rydberg states created in the ultracold Rydberg plasmas recently observed. The work *QuantalandClassicalRadiativeCascadeinRydbergPlasmas*, by M. R. Flannery and D. Vrinceanu, was published in Physical Review A **68** (2003),030205(R). Two invited talks (1 and 2 above) on the subject were recently presented by the PI at DAMOP 2005 and at an ITAMP workshop on Rydberg Physics.

D. Third Major Highlight: Interactions between polar Rydberg atoms

The most attractive and the most repulsive potential-energy curves for interaction between two Rydberg atoms in a broad superposition of internal angular momentum states were studied. The extreme Stark states have the largest dipole moments and provide the dominant contribution to the interaction which is then expressed as a long-range expansion involving the *permanent* multipole moments Q_j of each *polar* atom. Analytical expressions were obtained for all Q_j associated with principal quantum number n of $H(n)$ and permit the long range expansion for the H(n)-H(n') *first-order interaction* to be explicitly expressed analytically in terms of n, n' and internuclear distance R. Possible quasi-molecular formation was investigated. Direct calculations show that the H($n = 2$)-H($n' = 2$) interaction is capable of supporting 47 bound vibrational levels. As n increases, the long-range interaction becomes increasingly attractive so that molecular formation at large internuclear distances is expected to be scarcely possible for these extreme Stark levels. The work *Long − rangeinteractionbetweenpolarRydbergatoms*, by M. R. Flannery, D. Vrinceanu and V. N. Ostrovsky was published in J. Phys. B: Atom. Molec. and Opt.Phys., **38** (2005), pp. S279-S293. Four invited talks on the subject were presented to Professional Societies (Talks 2-5, above).

E. Broader impact of proposed activity

The theory and computational techniques under development here are important not only for understanding present and future experiments in Rydberg plasmas but also the trapping experiments at CERN on antihydrogen formation and on other issues as dipole blockade. The research is of fundamental significance in helping provide new theories of the basic interaction between two Rydberg atoms and the basic collision mechanisms involving Rydberg atoms and molecules at ultralow energies. The research will also have an impact on and may well establish new classical-quantal correspondences, which have a broad appeal for physical transparency and illumination of the underlying atomic and molecular mechanisms. The framework of these complex atomic processes could possibly be understood in terms of classical mechanics. This approach may help develop nice educational tools for illustrative and various pedagogical aspects of Rydberg dynamics.

F. Educational and Outreach Activities

The invited paper *Recombination and cascade in Rydberg plasmas* by M. R. Flannery was presented to **Cold and Ultra Cold Plasma and Rydberg Physics** Workshop at the Institute of Theoretical Atomic and Molecular Physics, Harvard University, Cambridge, MA , September 26-28, 2005. This 30 min talk was web-cast to all DAMOP scientists and was made available to all who choose to view it. Moreover, the two book chapters

1. *Atomic and Molecular Collision Processes*, by M. R. Flannery, in **Physicists' Desk Reference, Third Edition** (AIP-Springer Press, New York, 2003), Chap. 6, pp. 145-241.
2. *Electron, Atom and Ion Scattering*, by M. R. Flannery, in **Encyclopedia of Chemical Physics and Physical Chemistry** (Institute of Physics Press, London, 2001), vol.2, Chap.B2.2, pp. 1773-1819.

were solicited to be standard desk references in Atomic and Molecular Physics and Chemistry.

G. Some Representative Results

1. Radiative Cascade

The present classical treatment presents radiative cascade in a physically transparent way and revealed the "trajectory" in $n\ell$ space obeyed by the cascade, scaling rules and other aspects hidden within the quantal approach. Quantal-Classical correspondence in radiative decay is directly demonstrated. Classical transition probabilities are also presented and are in excellent agreement with quantal transition probabilities, even for moderate quantum numbers. This work was recently published as a Rapid Communication as M. R. Flannery and D. Vrinceanu, Physical Review A **68** (2003), 030205(R) pp. 1-4. Some results are illustrated in Figs. 1-3. The classical treatment of radiative presented has proven to be accurate, particularly for Rydberg states with $\ell/n \geq 0.1$ (preponderant in recombination) and has provided an accurate yet physically transparent picture of radiative cascade of Rydberg states. The deduced trajectory in $n\ell$ -space obeyed by radiative cascade origination from a constant source is confirmed by quantal calculation. The deduced classical invariant

$$C(n_0, \ell_0) = \frac{1 - \ell_0^2/n_0^2}{\ell_0^3} = \frac{1 - \ell^2/n^2}{\ell^3} \tag{1}$$

has, as yet, no quantal analogue and indicates a hidden symmetry to radiative processes which has not yet been found. The theory has been further developed to provide here a symmetrized new version of the Bohr Power Correspondence Principle and a classical version of Einstein transition rates, to a high degree of accuracy. It is particularly appropriate for the analysis of Rydberg plasmas over (n, ℓ) and for the proposed deactivation of the high $n \geq 50$ states in the ATRAP experiment by laser de-excitation methods, subjects of intense current theoretical and experimental interest.

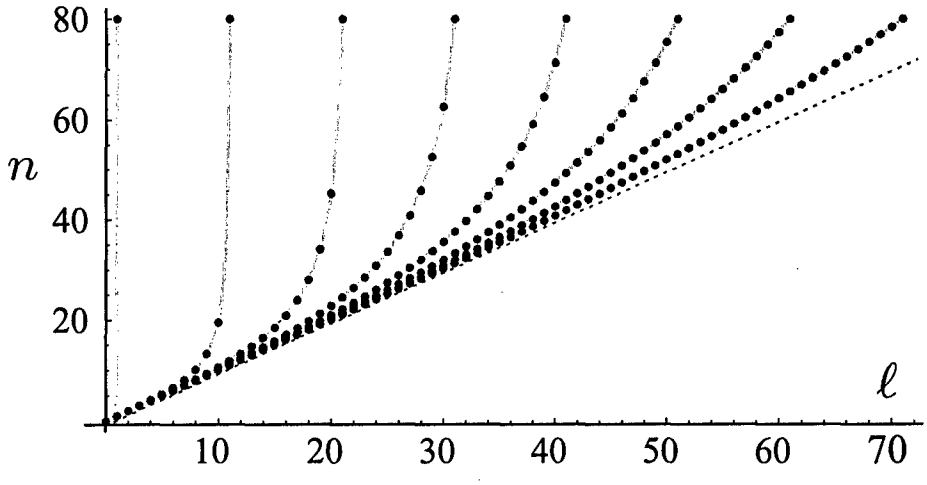

FIG. 1. "Trajectories" in (n, ℓ) space for initial states $l_0 = 1, 11, 21, 31, 41, 51, 61, 71$ within the $n_0 = 80$ shell. Dots correspond to a change of one unit of angular momentum quantum number ($\Delta\ell = -1$). Dashed diagonal line $\ell = n$ represents transitions between circular states. (From M. R. Flannery and D. Vrinceanu, Physical Review A **68** (2003), 030205(R)).

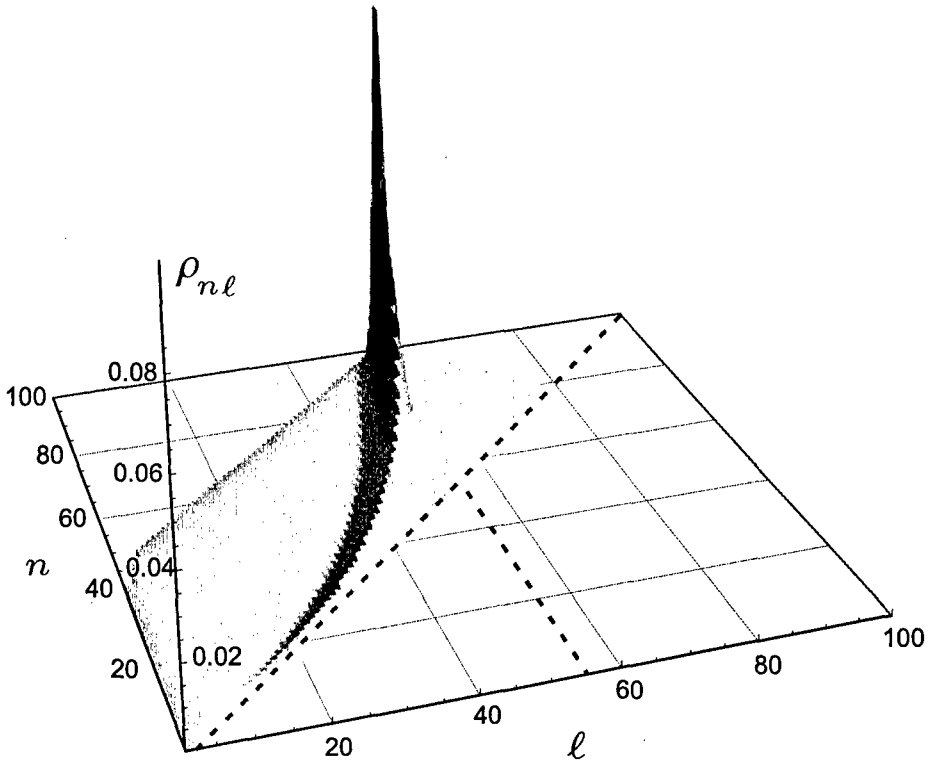

FIG. 2. The steady-state quantal distribution $\rho_{n\ell}$ of $n\ell$ states populated by radiative cascade originating from a source maintained at level $n_0 = 100$, $\ell_0 = 55$. The quantal ridge follows our analytically prescribed classical trajectory Eq.(1). (From M. R. Flannery and D. Vrinceanu, Physical Review A **68** (2003), 030205(R)).

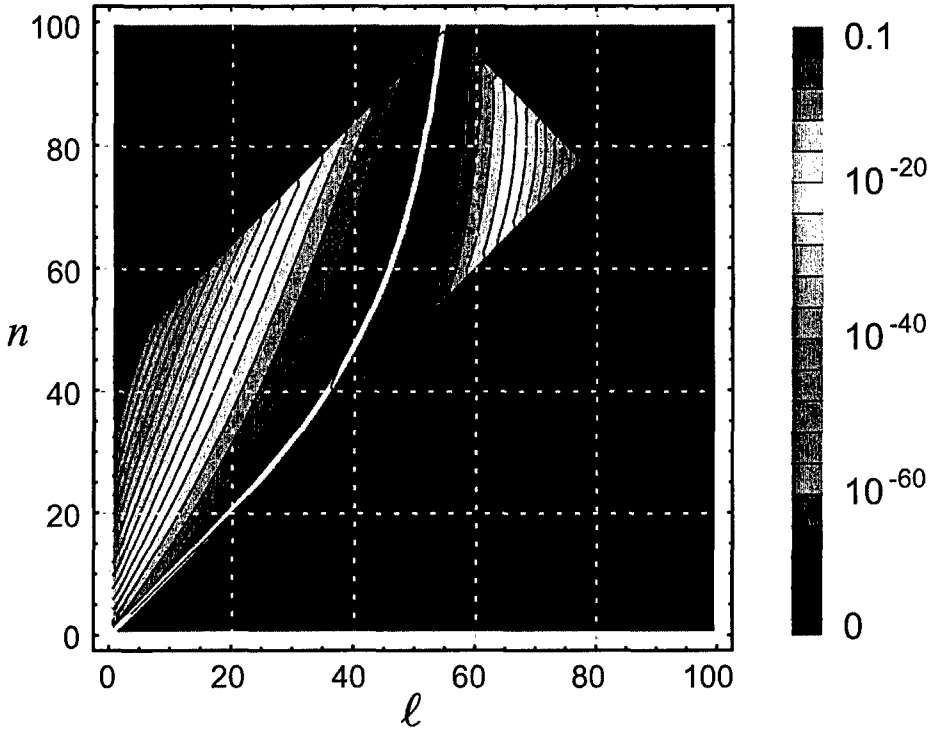

FIG. 3. Two-dimensional representation of Fig. 2 but with quantal iso-distributions represented by lines with magnitudes determined by each color code on RHS . White line is our analytically prescribed classical ridge Eq.(1). (From M. R. Flannery and D. Vrinceanu, Physical Review A **68** (2003), 030205(R)).

2. Stark mixing in ion-Rydberg collisions

Representative probabilities as a function of ℓ' are presented in Fig. 4 for the $n = 28, \ell = 18 \rightarrow 28, \ell'$ transitions in atomic hydrogen. The increasing values of $\chi \sim 1/bv \sim \tau_{coll}/b^2$ corresponds to a series of collisions either at fixed impact parameter b and decreasing v, or vice-versa. Increasing χ therefore corresponds to lengthening the duration τ_{coll} of a collision at fixed b. Since the dipole interaction couples $\ell \rightarrow \ell \pm 1$ states, the sequence of transitions which occur during the time τ_{coll} of collision is then $\ell \rightleftharpoons (\ell - 1) \rightleftharpoons (\ell - 2) \rightleftharpoons .... \rightleftharpoons \ell'_{min}$ and $\ell \rightleftharpoons (\ell + 1) \rightleftharpoons (\ell + 2) \rightleftharpoons .... \rightleftharpoons \ell'_{max}$. For the shorter collision times τ_{coll}, corresponding to small χ, ℓ'_{min} and ℓ'_{max} do remain well within the boundary values 0 and $n - 1$ of the angular momentum. There is insufficient time to sequentially access the highest or lowest values of ℓ' during the collision. Steps then appear in the classical structure. Within the classical inaccessible regions, the quantal results exhibit the characteristic exponentially decreasing and increasing variation. When the extreme limits, $\ell' = 0$ and $\ell' = n - 1$, of angular momentum can be accessed during the collision, then these limits act, in turn, as additional sources which then proceed to populate the $\ell' = 1, 2, ..$ and $\ell = n-2, n-3, ...$ states from below and above, throughout the duration of the collision. The classical probabilities then exhibit two distinct cusps arising from these secondary sources. These cusps merge into one as the collision duration time continues to increase with increasing values of the collision parameter χ. Expressions have been provided for the ℓ'-locations of the classical steps and cusps and the structure explained in physically transparent form. What has been done here is what would be achieved from numerical solution of a n^2 by n^2 array of closely coupled states. This is a very effective demonstration of the tremendous power of analytical theory based on the SO (4) group symmetry of the hydrogen atom. We aim to develop similar theory for Stark mixing in Rydberg-Rydberg collisions which operate via the dipole-dipole orientation dependent R^{-3} interaction.

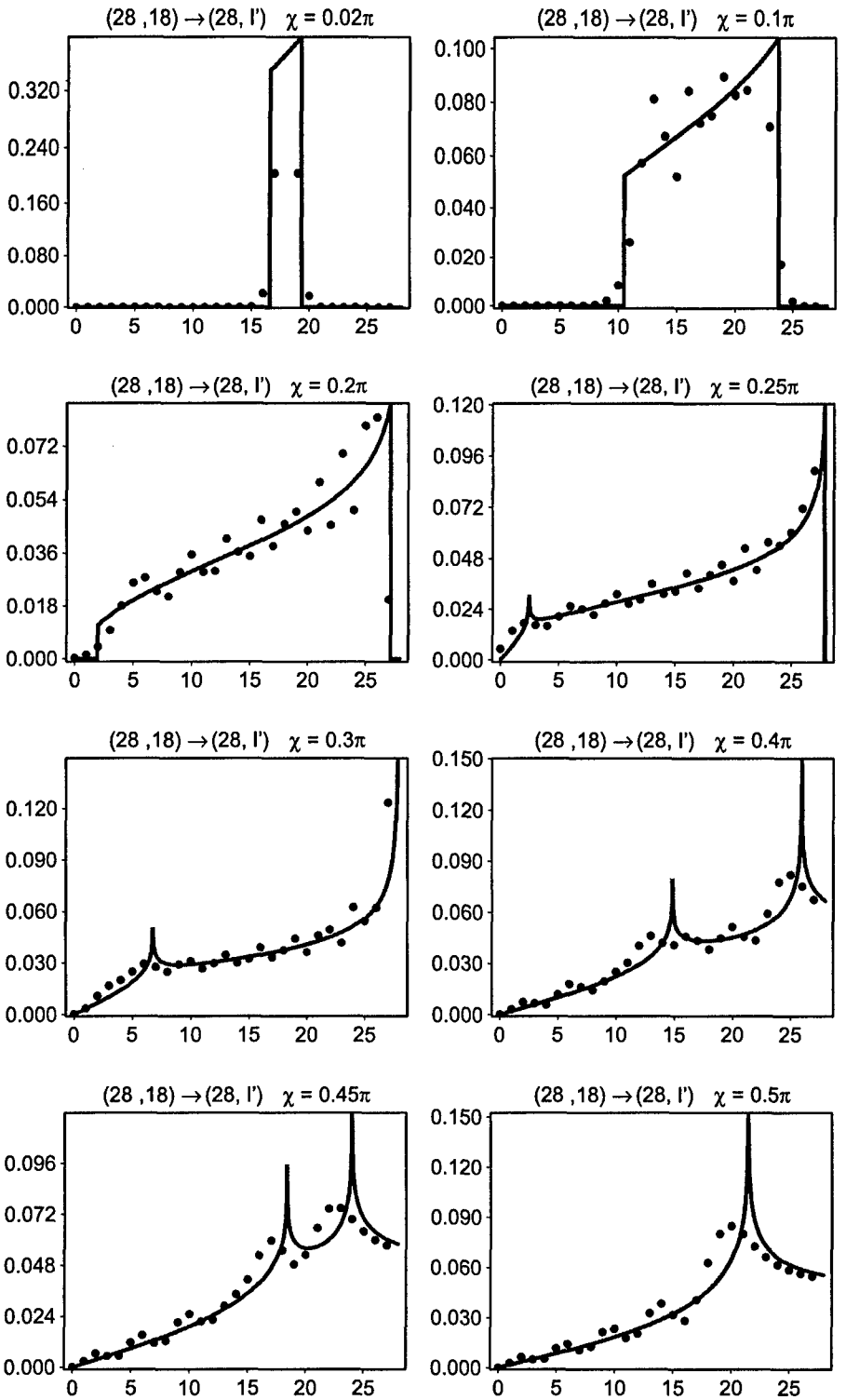

FIG. 4. Quantal and Classical transition probabilities $P^{(n)}_{\ell'\ell}(\chi)$,(ordinates), for Stark Mixing from initial $\ell = 11$ to final ℓ' states, (abscissae), within the $n = 28$ energy shell at specific values of the collision parameter χ which is essentially a measure of and increase with the duration τ_{coll} of the collision. (From M. R. Flannery and D. Vrinceanu, 2003)

3. Long-range interactions between "polar" Rydberg atoms

By 'polar' Rydberg atoms, we mean a Rydberg atom with electronic angular momentum spread over a large number of angular momentum ℓ states associated with a given principal quantum number n. These states are sufficiently flexible that a *permanent dipole* and higher *permanent multipoles* Q_j are created quite easily out of the large number $\sim n^2$ of degenerate angular momentum states ℓ within the energy shell. These Rydberg atoms can be called "polar" because they possess permanent multipole moments. We have investigated the physics of the long-range interaction between these polar Rydberg atoms and investigated the possible formation of long-range molecules from two Rydberg atoms with the same (or different) principal quantum numbers n, but with a broad superposition of many degenerate (non core-penetrating) angular momentum states ℓ.

Our aim was to first The long-range interactions so determined are of basic interest in this rapidly evolving field and will also be useful for various processes involving ultracold Rydberg atoms e.g., for Penning ionization, an important process required to sustain ultracold Rydberg plasmas.

The flexibility of the energy shell of a Rydberg atom in a broad superposition of angular momentum states changes dramatically the nature of the interaction between such atoms. These Rydberg atoms are termed "polar" because they have permanent multipoles Q_j. Higher-order permanent multipoles are introduced as n increases. The highest non-zero multipole associated with level n is Q_N where $N = 4j = 2(n-1)$. In the long-range interaction between two Rydberg atoms, the degeneracy of the energy shells has profound and decisive consequences. Its account represented a challenging quantum mechanical problem which had not received any previous theoretical attention until our present work.

First, we identified the physics and mechanism of the interaction between two degenerate Rydberg atoms. The wavefunction for the case when the two dipoles of the Rydberg atoms are aligned parallel is shown in Fig. 5.

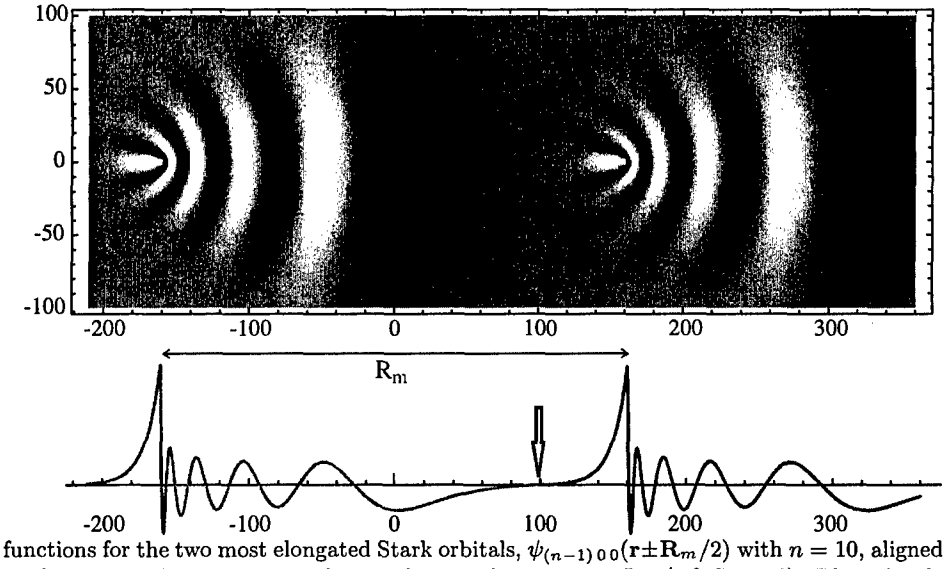

FIG. 5. Wave functions for the two most elongated Stark orbitals, $\psi_{(n-1)\,0\,0}(\mathbf{r}\pm\mathbf{R}_m/2)$ with $n = 10$, aligned along internuclear axis $\mathbf{R}$. Each orbital is centered at its own nucleus with typical separation R_m (c.f. Sect. 6). The orbital overlap is strongly suppressed and is maximum at the arrow.

We then obtained analytical expressions for the various multipoles Q_j as a function of n which allows the coefficients of the long-range expansion to be calculated purely in algebraic terms. Analytical expressions for the electrostatic long-range first-order interaction between polar Rydbergs in extreme (the most stretched) Stark states were provided in terms of Q_i, expressed analytically as functions of principal quantum number n. Each multipole Q_i varies as n^{2i}.

By including only the attractive dipole-dipole $\sim R^{-3}$ and the repulsive quadrupole-quadrupole $\sim R^{-5}$ interactions, we have shown (Fig. ??) that molecules could possibly be formed with relatively large equilibrium separations $R_m \approx 3.7n^2$. Addition of the dipole-octupole attraction, which also $\sim R^{-5}$, however offsets the quadrupole-quadrupole repulsion and destroys this possibility; except for the $n = 2$ case, which has no octupole and higher moments.

We have found, in general, that all permanent multipoles must be included in order to determine the correct coefficients of the first-order long-range expansion. Explicit calculations, including all multipoles $Q_j; j = 1, 2, 3, .., N = 2(n-1)$ appropriate for a given $n = 2, 3, .., 50$, show that the net contribution arising from all the multipoles except that due to the last multipole, Q_{2n-2}, are all attractive. Net repulsion arises only from the final multipole which introduces terms $\sim R^{2N-1} = R^{4n-3}$ into the expansion. Potential wells are indeed exhibited for all H(n)-H(n) and the steepness of the repulsive wall increases with n. Representative results are shown in Fig. 6.

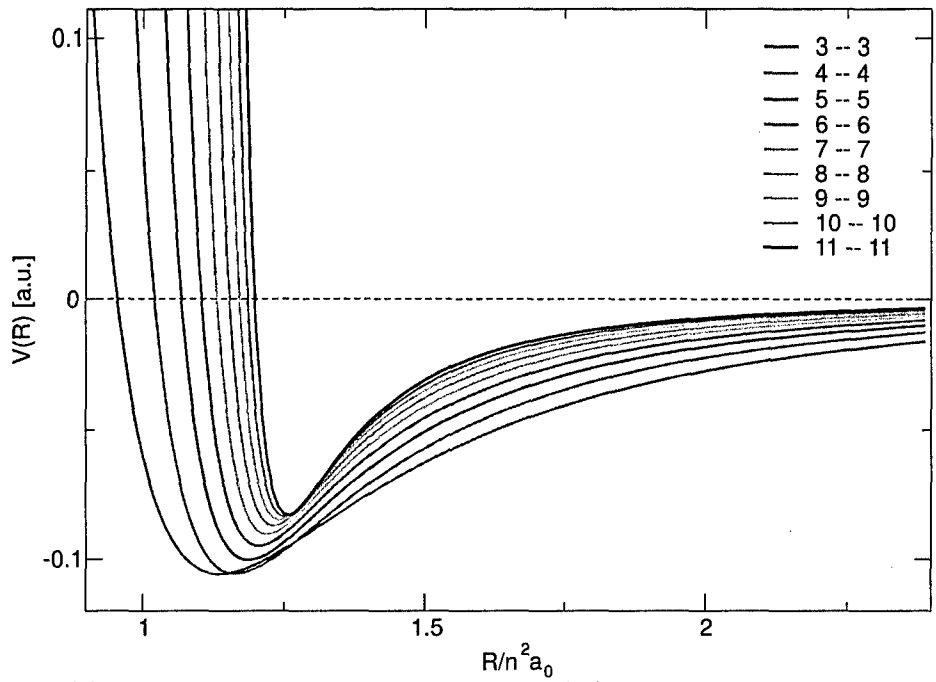

FIG. 6. H(n) - H(n) Rydberg-Rydberg molecular potentials (??) for several adjacent $n - n$ manifolds with $n = 3, 4, 5, 6, 7, 8, 9, 10, 11$.

Fig. 7 illustrates several potential curves for interaction between two 'polar' Rydberg atoms in different levels n and n' but having their dipoles oriented in the same direction. The principal quantum number of one of the atoms is $n = 10$, while the other Rydberg atom has n' ranging from 3 to 11. It is seen that the well becomes much deeper and steeper as n' increases, as expected from the increasingly attractive contributions from the additional multipoles. The minima, however, are still located at about 1.2 min (n^2, n'^2), where distortions, mentioned previously for the $n = n'$ case may also be in evidence. It therefore seems highly unlikely that long-range Rydberg-Rydberg molecules can be formed from the extreme Stark states with the greatest dipole moment. The attraction proves just too overwhelming so that repulsion finally sets in at separations R too small for validity of the long range expansion.

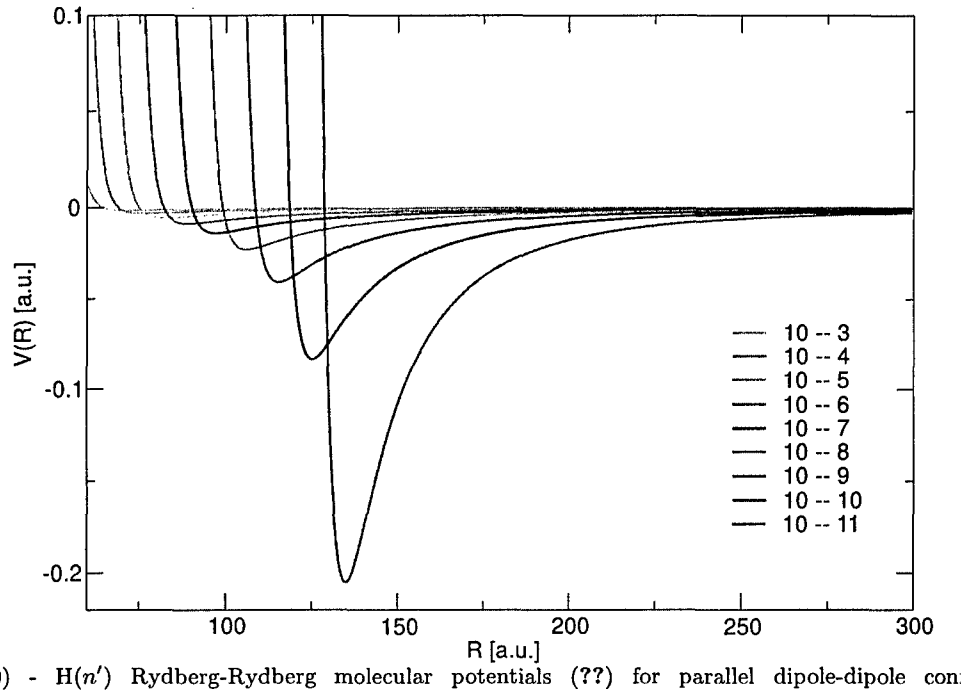

FIG. 7. H(10) - H(n') Rydberg-Rydberg molecular potentials (??) for parallel dipole-dipole configuration with $n' = 3, 4, 5, 6, 7, 8, 9, 10, 11$.

In summary, we have also shown that all the multipoles associated with a given n must be included within the long range expansion in order to determine the correct nature of the first-order interaction. The net contribution from all the multipoles is purely attractive, except for the last multipole $Q_{2(n-1)}$ which provides repulsion, which becomes increasingly steeper with n. Potential minima however occur at relatively modest internuclear distances $R \approx 1.2n^2$, where other effects as second-order van der Waal's attraction and electron overlap become effective, thereby compromising validity of the long-range expansion at such low R. As n increases, the interaction becomes increasingly attractive so that long-range molecular formation is expected to be scarcely possible for these extreme Stark levels.

We have therefore provided the first detailed investigation of the full first-order long-range interactions between 'polar' Rydberg atoms. This work has opened up a very promising and interesting new field with many theoretical and experimental possibilities and challenges ahead.

XII. REPRINTS OF 6 PUBLISHED PAPERS AND PREPRINTS OF 2 PAPERS SUBMITTED FOR PUBLICATION

Attached are reprints of 6 papers published in professional scientic journals and preprints of 2 papers submitted for publication to Physical Review A and to J. Physics B: Atom. Molec. Opt. Phys.

1. *Stark Mixing in Rydberg Atoms by ultralow energy collisions with ions*, by M. R. Flannery and D. Vrinceanu, Int. Journ. Mass Spectrom. **223-224** (2003), pp. 473-489.
2. *Classical and Quantal Atomic form factors for $n\ell m \rightarrow n'\ell' m$ transitions*, by M. R. Flannery and D. Vrinceanu , Phys. Rev. A **65** (2002), 022703 pp. 1-10.
3. *Quantal and Classical Radiative Cascade in Rydberg Plasmas*, by M. R. Flannery and D. Vrinceanu, Physical Review A **68** (2003),030205(R) pp. 1-4 .
4. *The enigma of nonholonomic constraints*, by M. R. Flannery, Am. J. Phys., **73** (2005), pp. 265-272.
5. *Long-range interaction between polar Rydberg atoms*, by M. R. Flannery, D. Vrinceanu and V. N. Ostrovsky, J. Phys. B: Atom. Molec. and Opt.Phys., **38** (2005), pp. S279-S293.
6. *Magnetic stabilization of a Rydberg quasimolecule in circular states*, by M. R. Flannery and E. Oks, Phys. Rev. A **73**, 013405 (2006)
7. *Equivalent multipole operators for degenerate Rydberg states*, by V. Ostrovsky, D. Vrinceanu and M. R. Flannery, Phys. Rev. A (2006, submitted).
8. *Plasma Screening within Rydberg Atoms in Circular States*, by M. R. Flannery and E. Oks, J. Phys. B: Atom. Molec. and Opt.Phys., (2006, submitted).

Three other publications:

1. *Stark Mixing in Rydberg Systems by Ultralow energy Collisions with Ions*, by M. R. Flannery and D. Vrinceanu in **Dissociative Recombination of Molecular Ions with Electrons**, ed. S. L. Guberman (Kluwer Academic/Plenum Publishers, 2003), pp. 151-166.
2. *Atomic and Molecular Collision Processes*, by M. R. Flannery, in **Physicists' Desk Reference, Third Edition** (AIP-Springer Press, New York, 2003), Chap. 6, pp 145-241.
3. *David Bates, 1916-1994*, by M. R. Flannery, in **Physicists of Ireland** (Institute of Physics Press, London, 2003), pp 262-272.

have been published as Chapters in books for which reprints are not available.

ELSEVIER

International Journal of Mass Spectrometry 223–224 (2003) 473–489

International Journal of Mass Spectrometry

www.elsevier.com/locate/ijms

Stark mixing in Rydberg atoms by ultralow energy collisions with ions

M.R. Flannery*, D. Vrinceanu

School of Physics, Georgia Institute of Technology, Atlanta, GA 30332, USA

Received 4 February 2002; accepted 24 May 2002

Abstract

Quantal and classical theories developed recently for the full array of $n\ell \rightarrow n\ell'$ transitions (Stark mixing) in Rydberg atoms by collision with slow ions are summarized. Quantal and classical probabilities $P^{(n)}_{\ell'\ell}$ are provided for transitions in atomic hydrogen, induced by the time-dependent (dipole) electric field generated by adiabatic collision with charged particles. A universal classical scaling law permits examination of the (rapid) convergence of the quantal probabilities onto the classical background as n is increased. The structure exhibited in the variation of $P^{(n)}_{\ell'\ell}$ with ℓ' is explained and a quantal–classical correspondence is manifest. A modification to take account of quantum defects in Rydberg systems (with quantum defects) is presented. Essential agreement is obtained with measurements of Na^+–Na(28d) collisions. (Int J Mass Spectrom 223–224 (2003) 473–489)

PACS: 34.50.Pi; 34.60.+z; 34.10.+x

Keywords: Stark mixing; Rydberg atoms; Collision

1. Introduction

The ion-Rydberg atom/molecule collisional process

$$A^{Z+} + Ry(n, \ell) \rightarrow A^{Z+} + Ry(n, \ell') \quad (1)$$

is called collisional Stark mixing since the ℓ-changing transitions $\ell \rightarrow \ell'$ occur within the same energy shell n of the Rydberg species and are induced by the time-dependent electric field generated by the passing ion A^{Z+}. The process is significant over a broad range of interest and applications. For example, the formation of anti-hydrogen by three-body recombination $e^+ + \bar{p} + e^+ \rightarrow \bar{H} + e^+$ at ultralow energies, where the sequence [1] is collisional capture into high $\ell \rightarrow$ states, followed by Stark mixing collisions $n\ell \rightarrow n\ell'$ and by radiative relaxation. Since the n-changing collisions are relatively unimportant at ultralow energies, the ℓ-mixing collisions are essential in producing the low angular momentum states required to radiatively decay at relatively high rate to low n-levels, thereby stabilizing the recombination. In zero-kinetic-energy-photo-electron spectroscopy (ZEKE-PES), high ℓ states are produced [2] from low ℓ states by electric fields. It is also significant in dissociative recombination [3–5]. Experiments [6] on Na^+–Na(28d) collisions have measured large ℓ-mixing cross-sections, even for dipole-forbidden transitions.

The process is also interesting from a theoretical point of view and has remained largely unsolved for

* Corresponding author.

1387-3806/02/$ – see front matter
PII S1387-3806(02)00931-4

four decades. Notable historical landmarks include a modified first-order impact parameter treatment [7], a classical diffusion theory [8], hydrogen atom in weak E–B fields [9], a truncated closely-coupled channel system of equations [10], Monte-Carlo simulations [11], and quantal and classical treatments of $0 \rightarrow \ell'$ transitions [12–15].

Exact solutions of Stark mixing in atomic hydrogen induced by the time-dependent (dipole) electric field generated by (adiabatic) collision with a slow ion and probabilities for the full array $n\ell \rightarrow n\ell'$ of transitions were only recently presented [16–19] in both classical and quantal formulations. The exceptionally rich dynamical symmetry of the hydrogen atom provides the key foundation which enables both the classical [16,17] and quantal solutions [17–19] to be constructed in a unified way, by using group representation theory. In this paper (dedicated to Werner Lindinger), a full case study of collisional Stark mixing is presented, together with exploration of classical–quantal convergence and correspondence for the full transition array.

2. Group symmetry

Conserved quantities for Coulomb attraction are the unperturbed Hamiltonian

$$H_0 = \frac{p^2}{2m_e} - \frac{e^2}{r},$$

the angular momentum $\boldsymbol{L} = \boldsymbol{r} \times \boldsymbol{p}$ and also the classical Runge–Lenz vector

$$\boldsymbol{A} = p_n^{-1}\left[\boldsymbol{p} \times \boldsymbol{L} - m_e e^2 \frac{\boldsymbol{r}}{r}\right],$$

directed toward the pericenter and normalized to angular momentum units, are all conserved. The operator $\boldsymbol{A}$ has the symmetrized (Pauli–Lenz) quantal form

$$\boldsymbol{A} = \frac{1/2(\boldsymbol{p} \times \boldsymbol{L} - \boldsymbol{L} \times \boldsymbol{p}) - m_e e^2 \hat{\boldsymbol{r}}}{p_n}$$

where $p_n = (-2m_e E_n)^{1/2}$ and the eigenenergy $E_n = -(1/2n^2)(e^2/a_0)$. Components of $\boldsymbol{A}$ satisfy the following relationships:

$$[A_j, H] = 0 \quad : \text{i.e., } \boldsymbol{A} \text{ is a conserved quantity,}$$
$$[L_j, A_k] = i\hbar\epsilon_{jkn}A_n \quad : \text{i.e., } \boldsymbol{A} \text{ is also a system vector,}$$
$$[A_j, A_k] = i\hbar\epsilon_{jkn}L_n \quad : \text{i.e., } \boldsymbol{A}\text{'s components do not commute,}$$
$$\boldsymbol{A} \cdot \boldsymbol{L} = \boldsymbol{L} \cdot \boldsymbol{A} = 0 \quad : \text{i.e., the vector } \boldsymbol{A} \text{ is orthogonal on } \boldsymbol{L},$$
$$A^2 + L^2 = (n^2 - 1)\hbar^2 \quad : \text{i.e., } A \text{ is constant for intrashell transitions,}$$

where ϵ_{kjn} is the Levi–Civita antisymmetric symbol for any $k, j = 1, 2, 3$. Hence $(E_n, \boldsymbol{L}, \boldsymbol{A})$ provide five independent conserved quantities. These commutation relations define the SO(4) dynamic symmetry group for the restricted motion of the orbital electron to the energy shell. The SO(4) operators can be disentangled by introducing $\boldsymbol{J}_\pm = (\boldsymbol{L} \pm \boldsymbol{A})/2$. Each $\boldsymbol{J}_+$ and $\boldsymbol{J}_-$ operator separately generates a SO(3) subalgebra, such that SO(4) $\equiv$ SO(3)$\oplus$SO(3). The $\boldsymbol{J}_\pm$ operators therefore commute i.e., $[\boldsymbol{J}_+, \boldsymbol{J}_-] = 0$, obey usual angular momentum rules $[J_j, J_k] = i\hbar\epsilon_{jkn}J_n$ and have integral or half-integral eigenvalues $J_\pm^2 = j(j+1)\hbar^2$ where $j = (n-1)/2$. In classical treatments, the quantum operators $\boldsymbol{L}$ and $\boldsymbol{A}$ are replaced by their classical vectors and the quantal commutators $(i\hbar)^{-1}[B, C]$ by the corresponding Poisson brackets. The classical analogy is that the set of coupled equations for $\boldsymbol{L}$ and $\boldsymbol{A}$ in a constant electric field $\boldsymbol{\mathcal{E}}$ become decomposed into an uncoupled set for the vectors $\boldsymbol{J}_\pm$ which independently precess [20] with Stark frequency $\omega_S = (3e/2p_n)\mathcal{E}$ about the electric field direction $\boldsymbol{\mathcal{E}}$ according to

$$\frac{d\boldsymbol{J}_\pm}{dt} = \pm\boldsymbol{\omega}_S \times \boldsymbol{J}_\pm. \tag{2}$$

3. Collision interaction

Fig. 1 illustrates the collision dynamics. The frequencies of the Rydberg electron and the collision are $\omega_n = v_n/a_n$ and $\omega_R = |\dot{\Phi}|$, respectively. Here $a_n = n^2 a_0$ and $v_n = p_n/m_e = v_0/n$ are the orbital

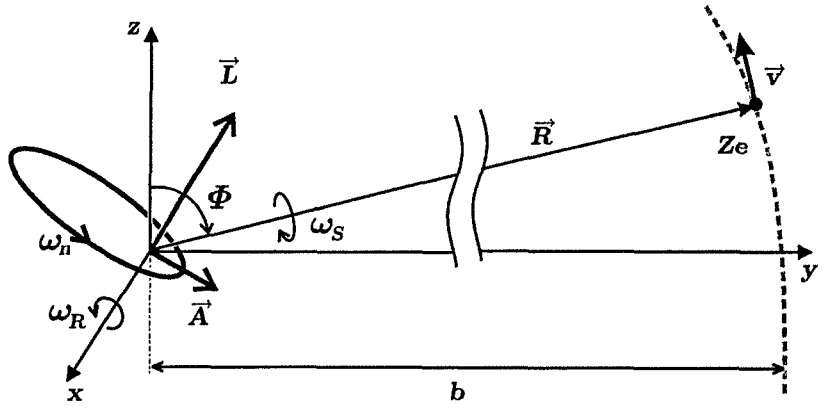

Fig. 1. Ion-Rydberg collision dynamics and the characteristic frequencies ω_n (orbital), ω_R (collisional) and ω_S (Stark).

radius and velocity, averaged so that $e^2/a_n = p_n v_n$. For slow variation of the electric field $\mathcal{E}$, generated by the passing ion, our simulation of the collision in Fig. 2 shows that the frequencies are ordered as $\omega_S < \omega_R < \omega_n$. It also shows that, although $\boldsymbol{L}$ and $\boldsymbol{A}$ change little during one orbit, significant change is accomplished during the collision over the course of many (~50) electron orbits. It also indicates that the ℓ-changing collision at ultralow impact energies satisfies the following three approximations:

3.1. Orbital adiabatic

This means that the collision is much slower than the much more rapid motion of the orbital Rydberg electron. The collision frequency $\omega_R \ll$, the orbital frequency ω_n of the Rydberg electron. In classical treatments, the electron position vector $\boldsymbol{r}$ can then be replaced by its average $\langle \boldsymbol{r} \rangle = -(3/2p_n)\boldsymbol{A}$. For quantal matrix elements within the same energy shell,

$$\langle n\ell'm'|\boldsymbol{r}|n\ell m\rangle = -\left(\frac{3}{2p_n}\right)\langle n\ell'm'|\boldsymbol{A}|n\ell m\rangle \qquad (3)$$

which is Pauli's replacement rule [21]. The collision is orbital adiabatic in the region $b > (v/v_n)a_n$.

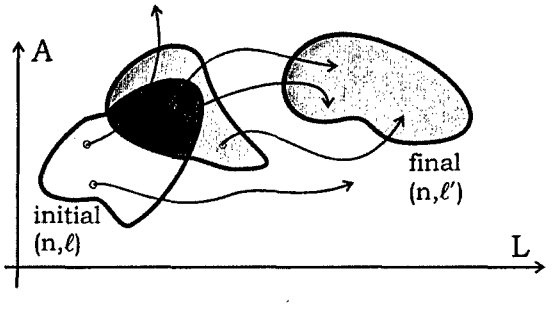

Fig. 2. The classical probability is a ratio of the two phase space volumes: the volume of the region within that part of the initial-state manifold containing coordinates which can evolve into the final state manifold, and the total volume of the initial-state manifold.

3.2. Weak field

Collisions which change only angular momentum occur at large impact parameters b where the ion-Rydberg atom interaction potential is the ion–dipole potential $V = -\boldsymbol{d} \cdot \mathcal{E}$, where $\boldsymbol{d} = -e\boldsymbol{r}$ is the dipole strength and where the electric field $\mathcal{E} = -Ze\hat{\boldsymbol{R}}/R^2$ is constant over the spatial extent of the atom. The Stark frequency is then

$$\omega_S = \frac{3e}{2p_n}\mathcal{E} = -\left(\frac{3Ze^2}{2p_nR^2}\right)\hat{\boldsymbol{R}}$$

Under these adiabatic and dipole assumptions, interaction with the electric field is then characterized by

$$V(\boldsymbol{A}, \boldsymbol{R}) = -\boldsymbol{d} \cdot \mathcal{E} = -\omega_S(\boldsymbol{R}) \cdot \boldsymbol{A}. \qquad (4)$$

The weak field region is where the Stark energy splitting $\hbar\omega_S \ll \hbar\omega_n$, the separation between neighboring

energy levels, i.e., the region $b \approx R \gg (3Z/2)^{1/2}a_n$ where the dipole assumption is valid.

3.3. Classical path

Since the angular momentum $\mu R^2\dot{\Phi}$ of relative motion of the heavy-particle collision system of reduced mass μ is very much greater than the angular momentum $\ell\hbar$ of the Rydberg electron, it is conserved to $-\mu v b$ so that $R^{-2} = -\dot{\Phi}/bv$.

Under the dipole and classical path assumptions, the Stark frequency is

$$\omega_S = \frac{3e}{2p_n}\mathcal{E} = (\alpha\dot{\Phi})\hat{\boldsymbol{R}} \tag{5}$$

where the dimensionless Stark parameter is defined as the ratio

$$\alpha = \frac{\omega_S}{\omega_R} = \frac{3Z}{2}\left(\frac{a_n v_n}{bv}\right) = \frac{3Z}{2}\left(\frac{a_n}{b}\right)^2\left(\frac{\tau_{coll}}{\tau_0}\right) \tag{6}$$

of Stark to collision frequencies. Also $\tau_{coll} = b/v$ is a measure of the collision duration and $\tau_0 = a_0/v_0$ is the au of time. The ion–hydrogen adiabatic interaction is then

$$\begin{aligned} V(A, \Phi; \alpha) &= -\omega_S \cdot A \\ &= -\alpha\frac{d\Phi}{dt}(A_2 \sin\Phi + A_3 \cos\Phi) \end{aligned} \tag{7}$$

which has the advantage that it is expressed only in terms of the generators of the SO(4) group. Moreover, the components $\{L_1, A_2, A_3\}$ generate a subgroup of the original symmetry group. Under the above three approximations, the resulting set of quantal and classical equations governing the problem of collisional Stark mixing at ultralow energies can be solved exactly.

4. Quantal theory

4.1. Quantal intrashell dynamics

The Schrödinger equation for the time evolution operator $U(t, t_0)$ is

$$i\hbar\frac{\partial U}{\partial t} = (H_0 + V)U \tag{8}$$

where H_0 is the free atom Hamiltonian and V is the interaction potential. In the interaction representation, the corresponding equation is

$$i\hbar\frac{\partial U_I}{\partial t} = V_I U_I \tag{9}$$

where $V_I = e^{iH_0t/\hbar}Ve^{-iH_0t/\hbar}$ and $U_I(t, t_0) = \exp(iH_0t/\hbar)U(t, t_0)\exp(-iH_0t_0/\hbar)$ are the corresponding potential and evolution operators in the interaction representation. The transition probability for a general $i \to f$ transition at time t is

$$\begin{aligned} a_{fi}(t) &= \langle\Phi_f(\boldsymbol{r}, t)|\Psi_i(\boldsymbol{r}, t)\rangle \\ &\equiv \langle\Phi_f(\boldsymbol{r}, t)|U(t, t_0)|\Phi_i(\boldsymbol{r}, t_0)\rangle \\ &= \langle\phi_f(\boldsymbol{r})|U_I(t, t_0)|\phi_f(\boldsymbol{r})\rangle \end{aligned} \tag{10}$$

where Ψ_i is the target wavefunction under external interaction V. In the asymptotic limits ($t \to \pm\infty$), it tends to the unperturbed basis set $\Phi_j(\boldsymbol{r}, t) = \phi_j(\boldsymbol{r})\exp(-iE_jt/\hbar)$. The transition amplitude for a Stark mixing process is $a^{(n)}_{\beta\alpha} = \langle n\beta|U_I(\infty, -\infty)|n\alpha\rangle$ where α and β now label the states within the same energy shell. The potential matrix elements $\langle n\beta|V_I(t)|n\alpha\rangle = \langle n\beta|V(t)|n\alpha\rangle$ are then identical. The superscript n will now be omitted, since all dynamics is restricted to the energy shell described by quantum number n. Eq. (9) with $V_I = V$ is then

$$\begin{aligned} i\hbar\frac{\partial U_I}{\partial\Phi} &= -\alpha(A_2 \sin\Phi + A_3 \cos\Phi)U_I \\ &= -\alpha\left(e^{i\Phi L_1/\hbar}A_3\, e^{-i\Phi L_1/\hbar}\right)U_I \end{aligned} \tag{11}$$

in which the basic identity

$$e^{\lambda A}B\, e^{-\lambda A} = B + \frac{\lambda}{1!}[A, B] + \frac{\lambda^2}{2!}[A, [A, B]] + \cdots \tag{12}$$

and the commutation relation $[L_j, A_k] = i\hbar\epsilon_{jkn}A_n$ above are invoked. The exact solution of (11) is

$$\begin{aligned} U_I(t, t_0) = e^{i\Phi L_1/\hbar}\exp\left[-\frac{i}{\hbar}\Delta\Phi(L_1 - \alpha A_3)\right] \\ \times e^{-i\Phi_0 L_1/\hbar} \end{aligned} \tag{13}$$

This can also be directly verified from (11) with use of the appropriate commutator algebra. The

probabilities for full array of Stark mixing transition $\ell \to \ell'$ transitions can be obtained from

$$P^{(n)}_{\ell'\ell} = \frac{1}{2\ell+1} \sum_{m=-\ell}^{\ell} \sum_{m'=-\ell'}^{\ell'} |\langle n\beta|U_I(\infty,-\infty)|n\alpha\rangle|^2 \tag{14}$$

The direct use of (15) permitted analytical probabilities [17,18] to be obtained only for low $n = 2, 3$. Numerical calculations were required for higher n. However, upon the decomposition $\boldsymbol{L} = \boldsymbol{M} + \boldsymbol{N}$ and $\boldsymbol{A} = \boldsymbol{M} - \boldsymbol{N}$, the solution separates as

$$U_I = U_M \otimes U_N$$

where the operators U_M and U_N are defined by

$$U_M = \mathrm{e}^{i\Phi M_1/\hbar}\, \mathrm{e}^{-i\Delta\Phi(M_1-\alpha M_3)/\hbar}\, \mathrm{e}^{-i\Phi_0 M_1/\hbar}$$

and

$$U_N = \mathrm{e}^{i\Phi N_1/\hbar}\, \mathrm{e}^{-i\Delta\Phi(N_1+\alpha N_3)/\hbar}\, \mathrm{e}^{-i\Phi_0 N_1/\hbar}$$

and where $\Delta\Phi(t) = \Phi(t) - \Phi(t_0)$ is the polar angle swept out by $\boldsymbol{R}$ within time interval $(t - t_0)$. Since the angular momentum-like operators $\boldsymbol{M}$ and $\boldsymbol{N}$ commute, the corresponding evolution operators U_M and U_N act independently as rotations in carrier spaces of dimension $2j + 1 = n$. The probability for transition $\ell \to \ell'$ between states with given angular momentum is defined by

$$P^{(n)}_{\ell'\ell} = \frac{1}{2\ell+1} \sum_{m=-\ell}^{\ell} \sum_{m'=-\ell'}^{\ell'} \left| a^{(n)}_{\ell' m' \leftarrow \ell m} \right|^2 \tag{15}$$

where the $(\ell, m) \to (\ell', m')$ transition amplitude between angular momentum states within the energy shell of quantum number n is

$$a^{(n)}_{\ell' m' \leftarrow \ell m} = \langle n\ell' m'|U_M \otimes U_N|n\ell m\rangle = \sum_{\mu\nu\mu'\nu'} C^{\ell m}_{j\mu j\nu} C^{\ell' m'}_{j\mu' j\nu'} \mathcal{D}^{(j)}_{\mu'\mu}(U_M) \mathcal{D}^{(j)}_{\nu'\nu}(U_N) \tag{16}$$

and where $\mathcal{D}^{(j)}(R)$ is Wigner's $2j + 1$ dimensional matrix representation of the finite rotation R.

4.2. Quantal transition probability: exact solution

The 10 folded summation within the quantal probability (15) has been contracted [19] to yield the following compact form,

$$P^{(n)}_{\ell'\ell}(\chi) = \frac{2\ell'+1}{n} \sum_{L=|\ell'-\ell|}^{n-1} (2L+1) \times \begin{Bmatrix} \ell' & \ell & L \\ j & j & j \end{Bmatrix}^2 H^2_{jL}(\chi) \tag{17}$$

for the transition $\ell \to \ell'$ probability between any states with given angular momentum. This involves only one summation. Here $\{\cdots\}$ is the $6 - j$ symbol for coupling of three angular momenta, $j = (n-1)/2$ and H_{jL} is a special matrix element of the irreducible representation of the group O(4). This function (also called the generalized character χ^j_L, associated with the irreducible representation of the rotation group) is well studied (see, for example, the books by Talman (1968) and Varshalovich et al. (1988)). In terms of ultraspherical polynomials $C^{(\alpha)}_n$, defined as the coefficients of the expansion

$$(1 - 2xy + y^2)^{-\lambda} = \sum_{n=0}^{\infty} C^{\lambda}_N(y) x^n,$$

it can be written as

$$H_{jL}(\chi) = (2L)!! \sqrt{\frac{(2j+1)(2j-L)!}{(2j+L+1)!}} \times (\sin\chi)^L C^{(L+1)}_{2j-L}(\cos\chi)$$

The angle χ is determined by

$$\cos\chi = \frac{1 + \alpha^2 \cos\Delta\Phi\sqrt{1+\alpha^2}}{1+\alpha^2} \tag{18}$$

and is called a *collision* parameter defined both by the Stark parameter $\alpha = 3Z/2\tilde{b}\tilde{v}$ and by the polar angle $\Delta\Phi$ swept out by the internuclear vector $\boldsymbol{R}$ during the collision time τ_{coll}. Eq. (17) is capable of providing exact numerical results [19] even for large quantum numbers n, in contrast to previous expressions [17,18] where the number of terms to be summed increases

dramatically with n. Note that the capacity of the projectile to produce angular momentum changes is governed solely by the parameter χ, the argument of H_{jL} in Eq. (17). Since $\Delta\Phi$ varies with time t, expression (17) furnishes $P^{(n)}_{\ell'\ell}$ as a function of t and Stark parameter α, all absorbed within *collision* parameter χ.

It can be shown from (17) that both detailed balance $(2\ell+1)P^{(n)}_{\ell'\ell} = (2\ell'+1)P^{(n)}_{\ell\ell'}$ and probability conservation $\sum_{\ell'} P^{(n)}_{\ell'\ell} = 1$ are satisfied. It is important to note that the above solution (17) for $P^{(n)}_{\ell'\ell}$ is equivalent to the numerical solution that would, in principle, be obtained from the very large $(n^2 \times n^2)$ set of coupled differential equations resulting from closely-coupling all n^2 quantal $n\ell m$ states. Since the dipole interaction alone couples $\ell \to \ell \pm 1$ transitions, the sequence of transitions occurring during the collision time $\tau_{\rm coll} \approx b/v$ is then $\ell \rightleftharpoons (\ell+1) \rightleftharpoons (\ell+2) \rightleftharpoons \cdots \rightleftharpoons \ell'_{\rm max}$ and $\ell \rightleftharpoons (\ell-1) \rightleftharpoons (\ell-2) \rightleftharpoons \cdots \rightleftharpoons \ell'_{\rm min}$. This physical sequence is acknowledged theoretically by the exponential nature of the interaction evolution operator (13).

4.3. Transitions from $\ell = 0$

For the special case of zero initial angular momentum, the $6-j$ symbol is (formula (1) page 299 in [22])

$$\begin{Bmatrix} \ell' & 0 & L \\ j & j & j \end{Bmatrix} = (-1)^{\ell'+n+1} \frac{\delta_{\ell' L}}{\sqrt{n(2\ell'+1)}}$$

to give the transition probability for $0 \to \ell'$ transitions as

$$P^{(n)}_{\ell' 0}(\chi) = \frac{2\ell'+1}{n^2} H^2_{j\ell'}(\chi),$$

which is identical with the previous result of Kazansky and Ostrovsky [14]. Eq. (17) can then be written in the interesting form as

$$P^{(n)}_{\ell'\ell}(\chi) = n(2\ell'+1) \sum_{L=|\ell'-\ell|}^{n-1} \begin{Bmatrix} \ell' & \ell & L \\ j & j & j \end{Bmatrix}^2 P^{(n)}_{L0}(\chi)$$

Since the square of $6-j$ symbol is the probability of coupling three angular momenta, a physical interpretation may be given for the above formula. The Stark mixing transition may therefore be viewed as a multi-step process involving partial waves of angular momentum L.

4.4. Weak coupling approximation

The weak coupling limit of the exact quantal probability is obtained from the limit of (19) as $\alpha \to 0$. Then $\chi \approx 2\alpha + O(\alpha^3)$, $\cos\chi \to 1$ and $\sin\chi = 2\alpha$. The ultraspherical polynomial $C^{\lambda}_N(1) = (2\lambda + N - 1)/n$ so that (17) tends to

$$P^{(n)}_{\ell'\ell}(\alpha \to 0) = \frac{2\ell'+1}{n} \sum_{L=|\ell'-\ell|}^{n-1} (2L+1) \begin{Bmatrix} \ell' & \ell & L \\ j & j & j \end{Bmatrix}^2 \times \left[\frac{2^{2L} L!}{(2L+1)!} \sqrt{\frac{n(n+L)!}{(n-L-1)!}} \alpha^L \right]^2 \tag{19}$$

where $j = 2n+1$. This weak-coupling result allows all $\ell \to \ell'$ transitions. The leading term of the probability (19) varies as α^{2L}, with $L = |\ell - \ell'| = 1$ for optically allowed and $L = 2, 3, 4, \ldots$ for forbidden transitions. Since

$$\begin{Bmatrix} \ell \pm 1 & \ell & 1 \\ j & j & j \end{Bmatrix}^2 = \frac{(n^2 - \ell_>^2)\ell_>}{n(n^2-1)(4\ell_>^2 - 1)},$$

the dipole ($L = 1$) contribution to the weak-coupling probability (19) is

$$P^{D}_{n\ell \to n'\ell\pm 1} = 3Z^2 \frac{\ell_>}{2\ell+1} n^2(n^2 - \ell_>^2) \left(\frac{a_0 v_0}{bv}\right)^2 = \frac{4}{3} \frac{\ell_>}{2\ell+1} n^2(n^2 - \ell_>^2)\alpha^2 \tag{20}$$

which varies as α^2. This result (20) satisfies detailed balance and agrees with the Born limit (Section 6) for $\ell \to \ell \pm 1$ dipole transitions.

4.5. Integral cross-section

The integral cross-section for Stark mixing is

$$\sigma_{n\ell \to n\ell'} = 2\pi \int_0^{\infty} P^{(n)}_{\ell'\ell} b \, {\rm d}b = 4.5 Z^2 \pi a_n^2 \left(\frac{v_n}{v}\right)^2 \times \int_{\alpha_{\rm min}}^{\infty} P^{(n)}_{\ell'\ell}(\alpha, \Delta\Phi) \frac{{\rm d}\alpha}{\alpha^3} \tag{21}$$

A lower limit $\alpha_{\min}$ is imposed [17] in order to account for physical effects as quantum defects, spin-orbit coupling and Debye screening in a plasma, which depend, of course, on the specific problem considered. This prevents the well known logarithmic divergence which originates in (21) from the $\alpha \to 0$ weak coupling limit (20) of (17) for $\ell \to \ell \pm 1$ transitions. The cross-sections for optically forbidden transitions exhibit no such divergence.

5. Classical theory

5.1. Classical intrashell dynamics

In the presence of an electric field of intensity $\boldsymbol{\mathcal{E}}$, the angular momentum $\boldsymbol{L}$ changes at the rate

$$\frac{\mathrm{d}\boldsymbol{L}}{\mathrm{d}t} = -e\boldsymbol{r} \times \boldsymbol{\mathcal{E}}$$

The collision is adiabatic with respect to the electronic orbital motion, ($\omega_{\mathrm{R}} = \dot{\Phi} \ll \omega_n$), so that $\boldsymbol{\mathcal{E}}$ is constant over one period τ_n and the collision lasts over many ($\simeq$50) periods. The secular change of $\boldsymbol{L}$ during the collision is then the classical average

$$\frac{\mathrm{d}\boldsymbol{L}}{\mathrm{d}t} = \frac{\Delta \boldsymbol{L}}{\tau_n} = -\frac{e}{\tau_n}\int_{t-\tau_n/2}^{t+\tau_n/2} (\boldsymbol{r} \times \boldsymbol{\mathcal{E}})\,\mathrm{d}t' = -\left(\frac{3e}{2p_n}\right)\boldsymbol{\mathcal{E}}(t) \times \boldsymbol{A}(t)$$

over one orbital period τ_n. Although the vectors $\boldsymbol{L}$ and $\boldsymbol{A}$ change very little during each τ_n, consistent with the weak field approximation ($\omega_{\mathrm{S}} \ll \omega_n$), they do suffer significant change over many τ_n. The following set of coupled equations can then be deduced [8,20]

$$\frac{\mathrm{d}\boldsymbol{A}}{\mathrm{d}t} = -\boldsymbol{\omega}_{\mathrm{S}} \times \boldsymbol{L}, \qquad \frac{\mathrm{d}\boldsymbol{L}}{\mathrm{d}t} = -\boldsymbol{\omega}_{\mathrm{S}} \times \boldsymbol{A}$$

where $\boldsymbol{\omega}_{\mathrm{S}} = \alpha\dot{\Phi}\hat{\boldsymbol{R}}$ varies with time. Under the substitution

$$\boldsymbol{M} = \frac{\boldsymbol{L}+\boldsymbol{A}}{2}, \qquad \boldsymbol{N} = \frac{\boldsymbol{L}-\boldsymbol{A}}{2} \tag{22}$$

the above set decouples to yield the set

$$\frac{\mathrm{d}\boldsymbol{M}}{\mathrm{d}\Phi} = -\alpha\hat{\boldsymbol{R}} \times \boldsymbol{M}, \qquad \frac{\mathrm{d}\boldsymbol{N}}{\mathrm{d}\Phi} = +\alpha\hat{\boldsymbol{R}} \times \boldsymbol{N} \tag{23}$$

of uncoupled equations. Since the averaged energy-change rate

$$\frac{\mathrm{d}E}{\mathrm{d}t} = \frac{\Delta E}{\tau_n} = -\frac{e}{\tau_n}\int_{t-\tau_n/2}^{t+\tau_n/2} \boldsymbol{\mathcal{E}} \cdot \dot{\boldsymbol{r}}\,\mathrm{d}t = -e\boldsymbol{\mathcal{E}}(t) \cdot \langle \dot{\boldsymbol{r}} \rangle \approx 0$$

there is no secular change to the Rydberg energy E. The magnitudes $M^2 = N^2 = (L^2 + A^2)/4 = n^2\hbar^2/4$ therefore remain constant throughout the collision. This set (23) can be solved exactly and solutions for $\boldsymbol{A}(t)$ and $\boldsymbol{L}(t)$ obtained [16,17] in terms of their initial values, α and $\Delta\Phi$.

5.2. Classical transition probability

The hypersurface in the $\{\boldsymbol{L}\} \otimes \{\boldsymbol{A}\}$ space on which the initial state is uniformly distributed is restricted by the constraints in Section 1 and has the volume:

$$\mathcal{V}_{n\ell} = \iint \delta(|\boldsymbol{L}| - \ell\hbar)\delta(|\boldsymbol{A}| - \hbar\sqrt{n^2 - \ell^2}) \times \delta(\boldsymbol{L} \cdot \boldsymbol{A})\,\mathrm{d}\boldsymbol{L}\,\mathrm{d}\boldsymbol{A} \tag{24}$$

which integrates to

$$\mathcal{V}_{n\ell} = 8\pi^2\ell\sqrt{n^2 - \ell^2}\hbar^2$$

Each point within this manifold evolves during the collision according to the above solutions for $\boldsymbol{A}(t)$ and $\boldsymbol{L}(t)$, so that only a fraction of possible initial states can have the final angular momentum ℓ' after the collision. Following the definition (24), the overlap volume of accessible $(\boldsymbol{L}, \boldsymbol{A})$ space which contains both initial and final states is

$$\mathcal{V}_{n\ell\ell'} = \iint \delta(|\boldsymbol{L}| - \ell\hbar)\delta(|\boldsymbol{L}'| - \ell'\hbar) \times \delta(|\boldsymbol{A}| - \hbar\sqrt{n^2 - \ell^2})\delta(\boldsymbol{L} \cdot \boldsymbol{A})\,\mathrm{d}\boldsymbol{L}\,\mathrm{d}\boldsymbol{A} \tag{25}$$

The transition probability is defined as the ratio

$$P^{(n)}_{\ell'\ell} = \frac{\mathcal{V}_{n\ell\ell'}}{\mathcal{V}_{n\ell}} \tag{26}$$

of phase space volumes. The classical transition probability is therefore defined in this new $(\boldsymbol{A}, \boldsymbol{L})$ phase

space, designed to exploit the dynamical symmetry, as the normalized volume of phase space accessible to both initial and final states. This overlap volume is the volume occupied by those final states which originate from the initial states and is illustrated in Fig. 2.

Upon integrating (25), the classical transition probability obtained [16,17] from (26) is written as the following analytic expression

$$P^{(n)}_{\ell'\ell}(\chi) = \frac{2(\ell'/n)}{\pi\hbar|\sin\chi|} \begin{cases} 0, & \text{if } |\sin\chi| < |\sin(\eta_1-\eta_2)| \\ \dfrac{K\{[\sin^2(\eta_1+\eta_2)-\sin^2(\eta_1-\eta_2)]/\sin^2\chi-\sin^2(\eta_1-\eta_2)\}}{\sqrt{\sin^2\chi-\sin^2(\eta_1-\eta_2)}}, & \text{if } |\sin\chi| > |\sin(\eta_1+\eta_2)| \\ \dfrac{K\{[\sin^2\chi-\sin^2(\eta_1-\eta_2)]/\sin^2(\eta_1+\eta_2)-\sin^2(\eta_1-\eta_2)\}}{\sqrt{\sin^2(\eta_1+\eta_2)-\sin^2(\eta_1-\eta_2)}}, & \text{if } |\sin\chi| < |\sin(\eta_1+\eta_2)|. \end{cases} \tag{27}$$

The classical probability is a function of the same collisional parameter χ basic to the quantal result (17) and given by (18), and also of the angles η_1 and η_2 determined by

$$\cos\eta_1 \equiv \frac{\ell}{n} = \epsilon \quad \text{and} \quad \cos\eta_2 \equiv \frac{\ell'}{n} = \epsilon', \tag{28}$$

the initial and final state ratios $\epsilon = \ell/n$ and $\epsilon' = \ell'/n$. Note that the eccentricities $\epsilon_{i,f}$ of the initial and final classical Kepler orbits are $\sin\eta_{1,2}$. The collision parameter χ increases monotonically with the Stark parameter $\alpha = 3Z/2\tilde{b}\tilde{v}$ as

$$\chi \approx 2\alpha\sin\left(\frac{\Delta\Phi}{2}\right) + \mathcal{O}(\alpha^3)$$

The transition probability $P^{(n)}_{\ell'\ell}(\chi)$ can be also interpreted as the distribution of final states with angular momentum ℓ' which originate from one initial state of angular momentum ℓ and result from collision with a charged projectile. The probability (27) satisfies detailed balance $2\ell P_{\ell'\ell} = 2\ell' P_{\ell\ell'}$, where 2ℓ is the classical weight of the state $n\ell$. Moreover, the classical limit of the full quantal probability (17) can be directly and easily obtained to provide a result identical with (27).

6. Results

6.1. Quantal–classical convergence

The classical function $nP^{(n)}_{\epsilon'n,\epsilon n}(\chi)$ of (27) is independent of n. Such universal functions can be uncovered within classical treatments, in general, and this feature will be exploited, to explore the rapid convergence of the quantal results onto the classical frame as n is increased. Fig. 3 illustrates the rapid convergence with n for all transitions from a given initial ℓ at a given collision parameter $\chi \sim 1/bv$. Fig. 4 demonstrates the rapid convergence with n for a specific $\ell \to \ell'$ transition over all χ. The quantal results oscillate in general about the universal classical frame. The structure of the classical frames of Figs. 3 and 4 can be explained in terms of two distinct regions within the classical accessible region, and two classical inaccessible regions. This structure remains obscured within the quantal results.

6.2. Structure

Representative probabilities as a function of ℓ' are presented in Fig. 5 for the $n = 28, \ell = 18 \to 28, \ell'$ transitions in atomic hydrogen. The increasing values of $\chi \sim 1/bv \sim \tau_{\text{coll}}/b^2$ corresponds to a series of collisions either at fixed impact parameter b and decreasing v, or vice-versa. Increasing χ therefore corresponds to lengthening the duration of a collision at fixed b. Since the dipole interaction couples $\ell \to \ell \pm 1$ states, the sequence of transitions which occur during the time τ_c of collision is then $\ell \rightleftharpoons (\ell-1) \rightleftharpoons (\ell-2) \rightleftharpoons \cdots \rightleftharpoons \ell'_{\min}$ and $\ell \rightleftharpoons (\ell+1) \rightleftharpoons (\ell+2) \rightleftharpoons \cdots \rightleftharpoons \ell'_{\max}$. For the shorter collision times τ_c,

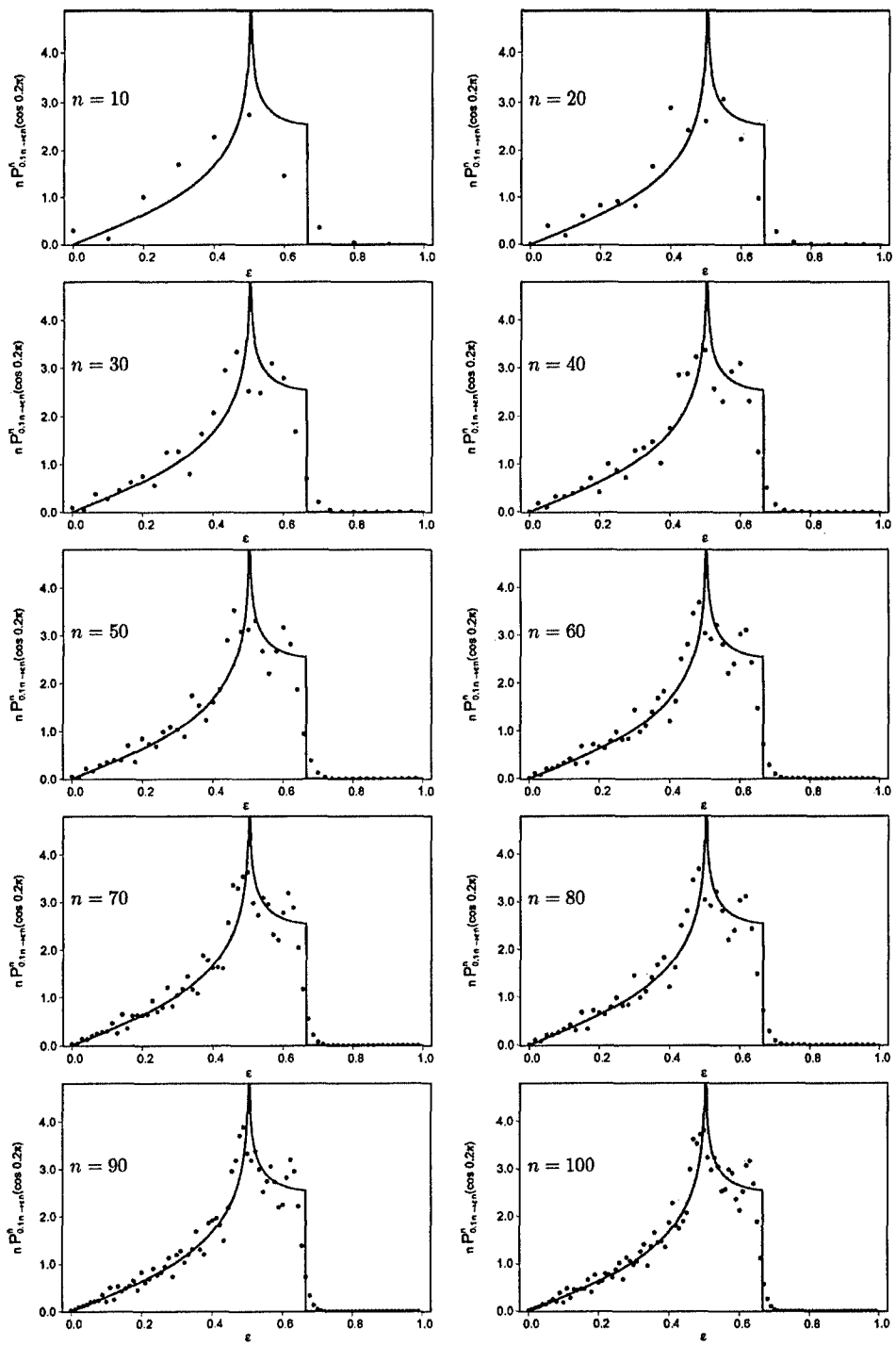

Fig. 3. Plots of the scaled transition probability $nP^{(n)}_{\ell\to\epsilon n}(\chi)$ as a function of the ratio $\epsilon = \ell'/n$ illustrating, as n increases, the convergence of the exact quantal results (blue dots) onto the fixed classical framework (red line), at constant values of the ratios $\ell/n = 0.1$ and collision parameter $\chi = 0.2\pi$.

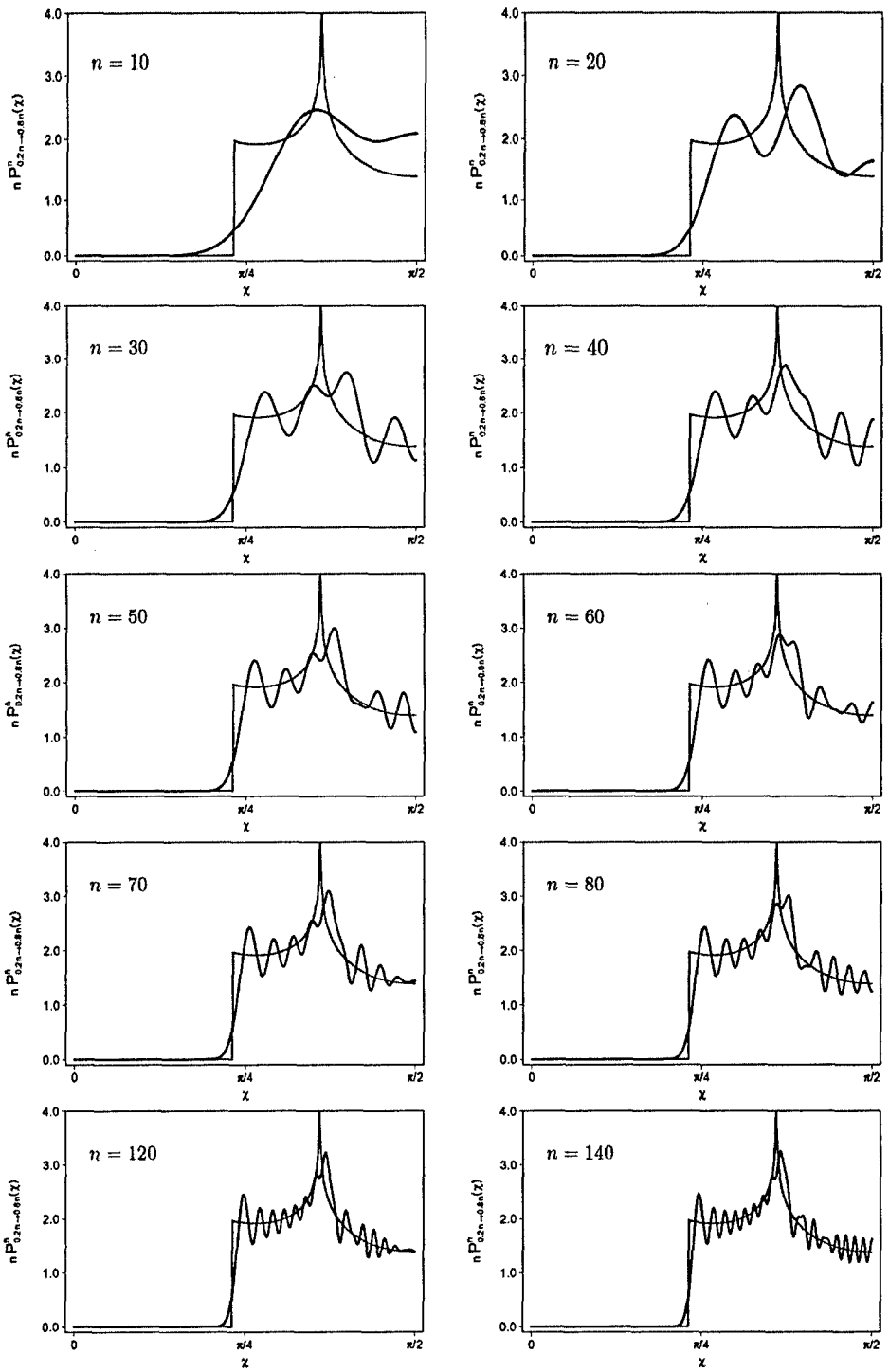

Fig. 4. Plots of the scaled transition probability $nP^{(n)}_{\epsilon n \to \epsilon' n}(\chi)$ as a function of collision parameter χ illustrating, as n increases, the convergence of the exact quantal result (blue line) onto the fixed classical framework (red line), for constant values of the ratios $\epsilon = \ell/n$ and $\epsilon' = \ell'/n$.

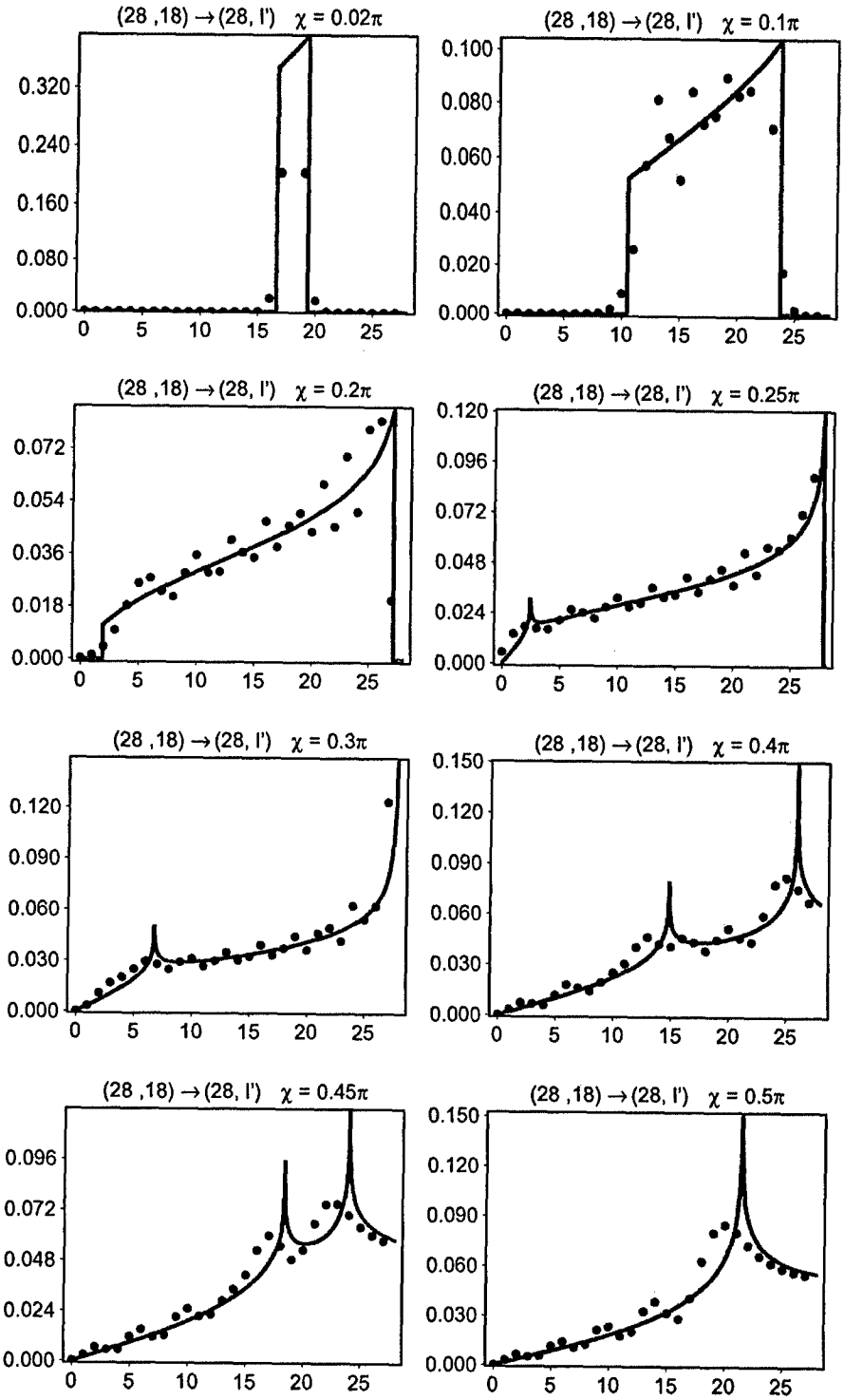

Fig. 5. Quantal and classical transition probabilities $P^{(n)}_{\ell'\ell}(\chi)$ for Stark mixing from initial $\ell = 11$ to final ℓ' states within the $n = 28$ energy shell at specific values of the collision parameter χ.

corresponding to small χ, $\ell'_{\min}$ and $\ell'_{\max}$ do remain well within the boundary values 0 and $n-1$ of the angular momentum. There is insufficient time to sequentially access the highest or lowest values of ℓ' during the collision. Steps then appear in the classical structure. Within the classical inaccessible regions, the quantal results exhibit the characteristic exponentially decreasing and increasing variation. When the extreme limits, $\ell' = 0$ and $\ell' = n-1$, of angular momentum can be accessed during the collision, then these limits act, in turn, as additional sources which then proceed to populate the $\ell' = 1, 2, \ldots$ and $\ell = n-2, n-3, \ldots$ states from below and above, throughout the duration of the collision. The classical probabilities then exhibit two distinct cusps arising from these secondary sources. These cusps merge into one as the collision duration time continues to increase with increasing values of the collision parameter χ. The ℓ'-locations of the classical steps and cusps in (27) are determined by the solutions of $|\sin(\eta_1 - \eta_2)| = |\sin\chi|$ and $|\sin(\eta_1 + \eta_2)| = |\sin\chi|$, respectively. The structure in Fig. 3 (which corresponds to one of the structures in Fig. 5) can therefore be physically explained.

A map of the various classical zones in the plane of reduced initial and final angular momenta $(\ell/n, \ell'/n)$ is displayed in Fig. 6 for the four values, $\alpha = 0.2, 0.4, 0.6$ and 0.8 of the Stark parameter and for $\Delta\Phi = -\pi$, appropriate to an undeflected classical path. Quantities

$$\mathcal{A} = |\sin\chi| - |\sin(\eta_1 + \eta_2)| \tag{29}$$

and

$$\mathcal{B} = |\sin\chi| - |\sin(\eta_1 - \eta_2)| \tag{30}$$

are useful to describe the various possibilities. In the central region $\mathcal{A}$ is negative and $\mathcal{B}$ is positive. Within the lower left and upper right corners both $\mathcal{B}$ and $\mathcal{A}$ are positive. The transition is classically forbidden where $\mathcal{B} < 0$ in the upper left and lower right corners (gray zones). Across the separatrix (dotted line) which separates the classical inacessible/accessible regions, the

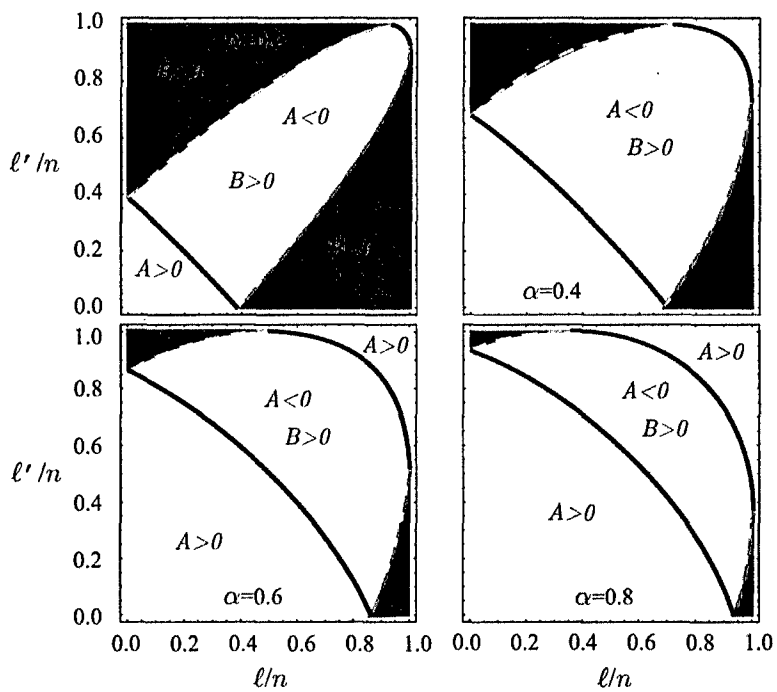

Fig. 6. Contour plots of the solutions of $\mathcal{A} = 0$ (solid line) and $\mathcal{B} = 0$ (dotted line) for various values of α. In gray zones $\mathcal{B} < 0$ and the transition is classically forbidden.

transition probability jumps from zero (in the gray zone) to some finite value (in the central zone). Along the solid line, for which $\mathcal{A} = 0$, the transition probability has a logarithmic (cusp) singularity. As $\alpha \to 0$, the two inaccessible regions (where $\mathcal{B} < 0$) broaden until the central region with $\mathcal{B} > 0$ and $\mathcal{A} < 0$ becomes an elongated line strip lying along the diagonal $\ell = \ell'$. Only elastic and dipole transitions are therefore permitted in the limit $\alpha \to 0$. As α increases to unity the classically forbidden zones diminish and the collision becomes more and more effective in its ability to induce larger angular momentum changes. By appeal to Fig. 6, the structures in Figs. 3 and 5 can be fully explained.

Fig. 7 presents maps corresponding to Fig. 6. The same characteristic regions are now displayed in the plane of final reduced angular momentum ℓ'/n and the Stark parameter α for four values of the initial reduced angular momentum $\ell/n = 0.071$, 0.36, 0.64, and 0.93. Again, the classically forbidden regions (gray zones), correspond to the condition $\mathcal{B} < 0$, in the left upper and lower corners. The elastic $\ell' = \ell$ transitions are always possible, even when $\alpha \to 0$. Again, along the solid ($\mathcal{A} = 0$) and dotted ($\mathcal{B} = 0$) lines, the transition probabilities have cusp and step singularities. When α (or χ) increases the span of possible final angular momentum, for given angular momentum, increases. Large (small) angular momentum transfer is only possible for collisions with large (small) Stark parameters. This behavior is exhibited in the quantal/classical probabilities of Fig. 8 as a function of collision parameter χ. The structure in Fig. 4 corresponds to one of the structures in Fig. 8. In summary, both Figs. 6 and 7 are key to interpretation of Figs. 5 and 8 for the variation of the probabilities $P_{\ell'\ell}(\alpha)$ with both ℓ' and χ, respectively.

6.3. Quantal–classical correspondence

This is illustrated by Fig. 9 where the quantal probabilities are greatest in the vicinity of the classical cusp solid lines and exponentially decay as they transverse

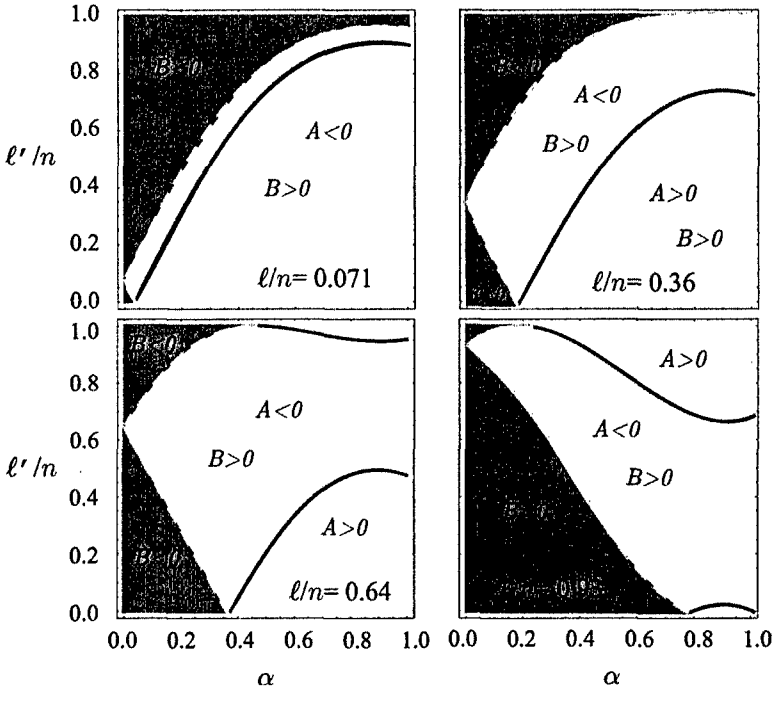

Fig. 7. Contour plots of the solutions of $\mathcal{A} = 0$ (solid line) and $\mathcal{B} = 0$ (dotted line) for various values of ℓ. In gray zones $\mathcal{B} < 0$ and the transition is classically forbidden.

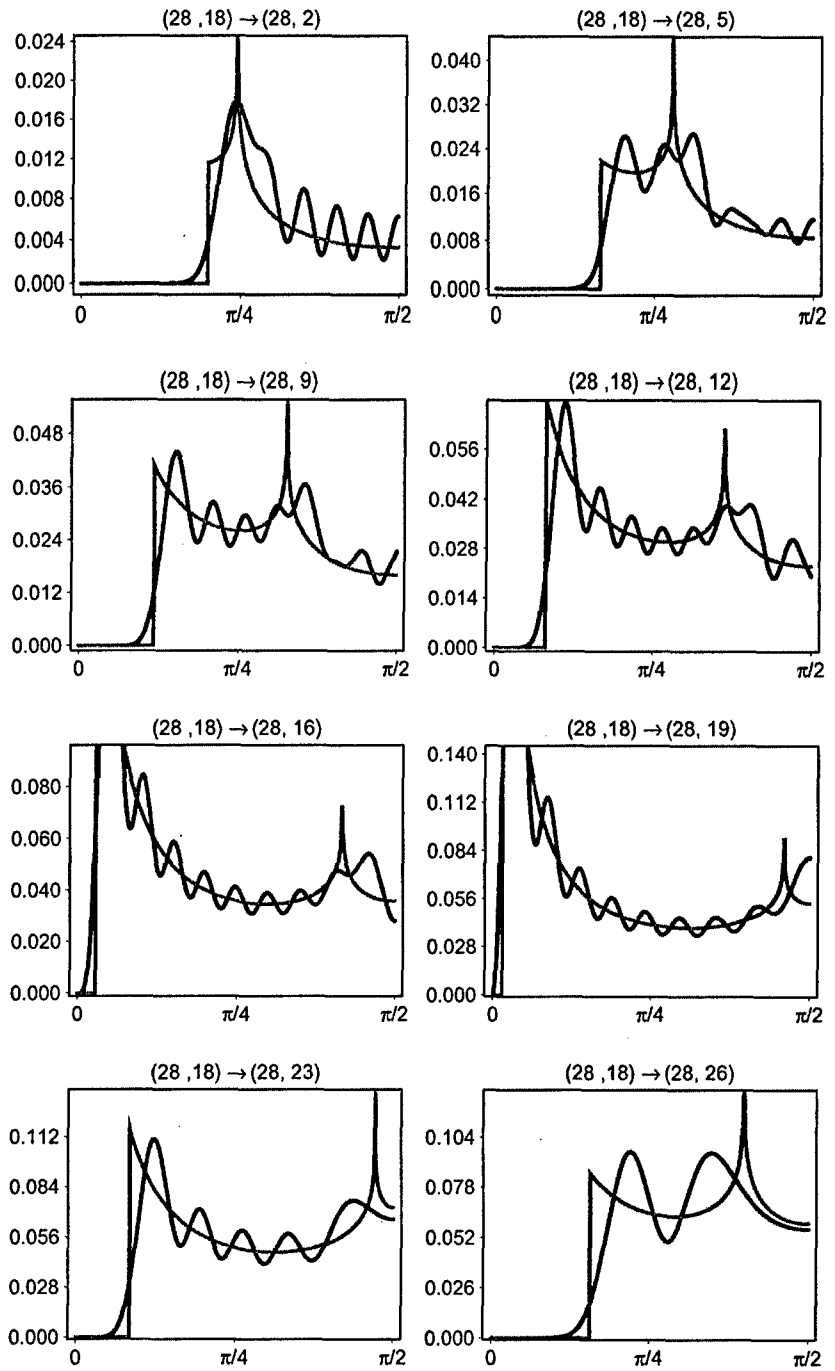

Fig. 8. Quantal and classical probabilities $P^{(n)}_{\ell'\ell}(\chi)$ for specific $\ell \rightarrow \ell'$ Stark mixing transitions within the $n = 28$ energy shell as a function of collision parameter χ.

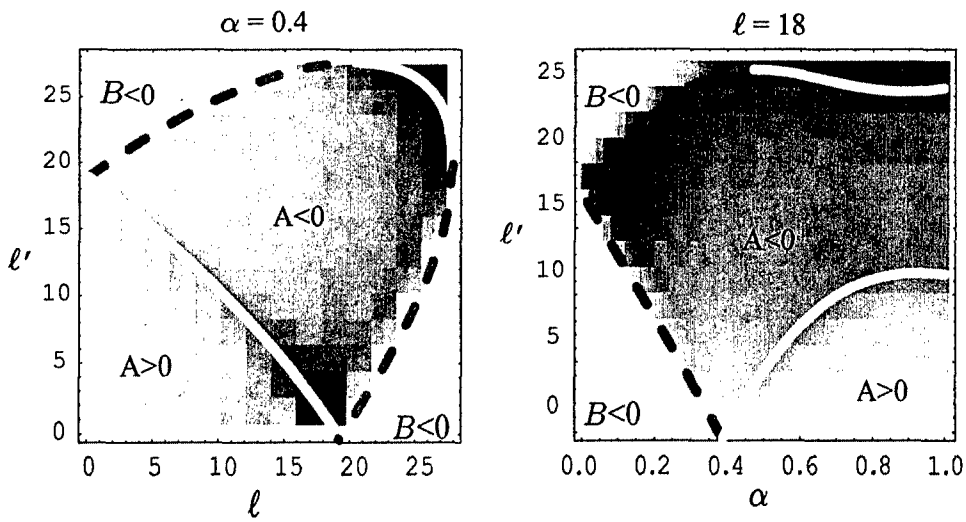

Fig. 9. Quantal–classical correspondence: variation with ℓ, ℓ' and Stark parameter α of quantal probabilities over the classical accessible and inaccessible regions. The higher probabilities (darker regions) are confined to the classical cusp (solid line) regions while the smaller exponentially decreasing probabilities are apparent in the classical inaccessible (dashed line) regions.

past the classical inaccessible (dashed line) regions. Figs. 5 and 8 are obtained from various cuts through Fig. 9.

7. Born limit

In the limit of weak coupling at all collision energies, the Born approximation

$$P^{\mathrm{B}}_{\ell\to\ell'} = \frac{1}{\hbar^2}\frac{1}{2\ell+1}\sum_{m,m'}\left|\int_{-\infty}^{\infty} V_i f[R(t)]\mathrm{e}^{i\omega_{ij}t}\,\mathrm{d}t\right|^2$$

for the probability of $\ell \to \ell' = \ell \pm 1$ transitions, which involve an energy defect $\epsilon_{fi} = \hbar\omega_{fi}$, yields

$$P^{\mathrm{B}}_{n\ell\to n'\ell'} = \left(\frac{2Ze^2\omega_{fi}}{\hbar v^2}\right)^2 \frac{1}{2\ell+1} \times \sum_{m,m'}\left[|y^{n'\ell'm'}_{n\ell m}|^2 K_0^2\left(\frac{\omega_{fi}b}{v}\right) + |z^{n'\ell'm'}_{n\ell m}|^2 K_1^2\left(\frac{\omega_{fi}b}{v}\right)\right] \quad (31)$$

in terms of the y and z components of the dipole matrix element, $\langle\phi_{n'\ell'm'}|\boldsymbol{r}|\phi_{n\ell m}\rangle$, and the modified Bessel functions $K_{0,1}$. The collision takes place in the YZ-plane of Fig. 1. For atomic hydrogen, $\phi_{n\ell m} = R_{n\ell}Y_{\ell m}(\hat{r})$ so that $\sum_{m,m'}|y^{n'\ell\pm1m'}_{n\ell m}|^2 = (\ell_>/3)R^2_{n\ell,n'\ell\pm1}$ with $m' = m \pm 1$ and $\sum_{m,m'}|z^{n'\ell'm'}_{n\ell m}|^2 = (\ell_>/3)R^2_{n\ell,n'\ell\pm1}$, with $m = m'$. The dipole radial matrix element $R_{n\ell,n'\ell'}$ involving the radial wavefunctions $R_{n\ell}$ is $\int_0^\infty R_{n\ell}R_{n'\ell'}r^3\,\mathrm{d}r$. Hence,

$$\begin{aligned} P^{\mathrm{B}}_{n\ell\to n'\ell\pm1} &= 4Z^2\left(\frac{v_0}{v}\right)^4\left(\frac{\epsilon_{fi}}{\epsilon_0}\right)^2\frac{\ell_>}{3(2\ell+1)} \times\left(\frac{R_{n\ell,n'\ell\pm1}}{a_0}\right)^2[K_0^2(\beta)+K_1^2(\beta)] \\ &= 4Z^2\left(\frac{a_0v_0}{bv}\right)^2\frac{\ell_>}{3(2\ell+1)}\left(\frac{R_{n\ell,n'\ell\pm1}}{a_0}\right)^2 \times\beta^2[K_0^2(\beta)+K_1^2(\beta)] \end{aligned} \quad (32)$$

where a_0, v_0 and ϵ_0 are atomic units and the parameter β is $\omega_{fi}b/v \sim \omega_{fi}/\omega_{\mathrm{coll}} \sim \tau_{\mathrm{coll}}/\tau_{\mathrm{tran}}$, the ratio of the collision time to the time τ_{tran} for the transition. When convenient, $P^{\mathrm{B}}_{n\ell\to n'\ell\pm1}$ may also be expressed in terms of the oscillator strength

$$f_{n\ell,n'\ell\pm1} = \frac{2\ell_>}{3(2\ell+1)}\left(\frac{\epsilon_{fi}}{\epsilon_0}\right)\left(\frac{R_{n\ell,n'\ell\pm1}}{a_0}\right)^2$$

For Stark mixing collisions, $n = n'$, $\beta^2[K_0^2(\beta) + K_1^2(\beta)] = 1$ and $R^2_{n\ell,n'\ell\pm1} = (9n^2/4)(n^2 - \ell_>^2)a_0^2$, so that (32) yields

$$P^{\mathrm{B}}_{n\ell\to n'\ell\pm1} = 3Z^2\frac{\ell_>}{2\ell+1}n^2(n^2-\ell_>^2)\left(\frac{a_0v_0}{bv}\right)^2 = \frac{4}{3}\frac{\ell_>}{2\ell+1}n^2(n^2-\ell_>^2)\alpha^2 \quad (33)$$

which is identical, as expected, with the weak-coupling dipole contribution (32), the first term ($L = 1$) of (19).

8. Rydberg states with quantum defects

Rydberg atoms and molecules have quantum defects only for states with core penetrating electron orbits i.e., those with $\ell = 0$–2. These low-ℓ Rydberg wavefunctions, which are assumed known, are expanded here in terms of a hydrogenic basis set $|n\ell m\rangle$ as,

$$|RyN\ell m\rangle = \sum\int_n w_n^{(N\ell)}|n\ell m\rangle$$

and the amplitudes $w_n^{(N\ell)}$ determined. There is a small energy defect $\epsilon_{fi} = \hbar\omega_{fi}$ involved in transitions from low ℓ.

In order to account approximately for the probability of small energy transfer and by analogy with Section 7, it can be shown that the Stark Mixing quantal transition probability (17) becomes modified to

$$P_{N\ell\to N'\ell'} = (2\ell'+1)\sum_L(2L+1)\times\left[\sum\int_n\frac{(-1)^n}{\sqrt{n}}w_n^{(N'\ell')}w_n^{(N\ell)}\times\begin{Bmatrix}\ell' & \ell & L\\ j & j & j\end{Bmatrix}H_{jL}(\chi)\right]^2\left(\frac{\omega_{fi}b}{v}\right)^2\times\left[K_0^2\left(\frac{\omega_{fi}b}{v}\right)+K_1^2(\omega_{fi}b/v)\right] \quad (34)$$

The weak coupling limit of (34) is (32). While the present theory has been developed for individual $n\ell \to n\ell'$ transitions in Rydberg atoms, the only available measurements of Stark Mixing are those of Sun and MacAdam [6] who provided normalized measured fractional populations for Na(28d) → Na(28f), Na(28g + 28h), Na(28f + 28g + 28h) transitions in Na^+–Na(28d) collisions. Fig. 10 illustrates the general agreement between the measurements and our corresponding calculations based on (34).

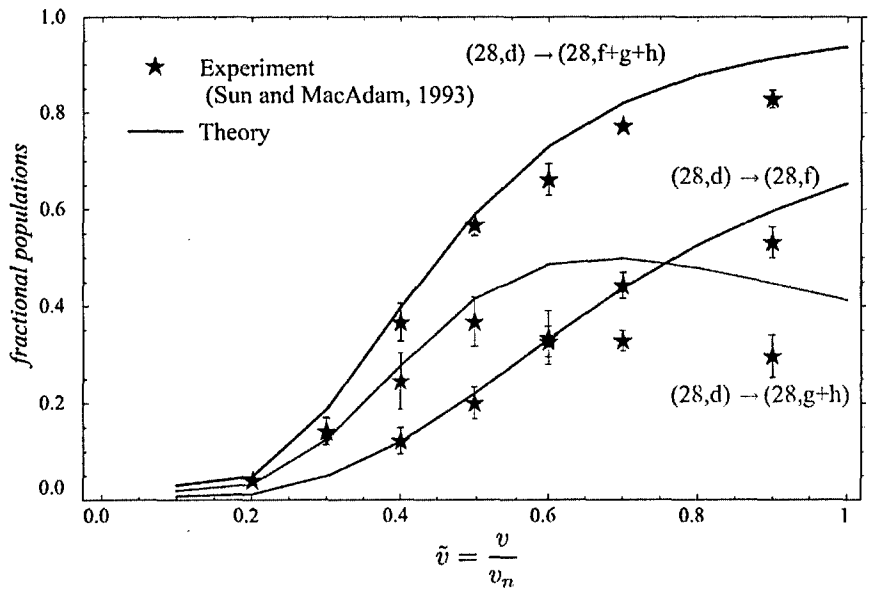

Fig. 10. Fractional populations for Na(28d) → Na(28f), Na(28g + 28h), Na(28f + 28g + 28h) transitions.

9. Summary and conclusions

We have presented here a case study of collisional Stark mixing within the full array of $n\ell \rightarrow n\ell'$ transitions induced by ion–Rydberg atom collisions at ultralow energies. The inherent group dynamic symmetry permits development of exact solution in both quantal and classical formulations. The solutions are presented in compact form reflecting the mathematical beauty of the problem as well as pragmatic value. The quantal (17) and classical (27) results complement each other. The leading (dipole) term (20) of the weak coupling limit (19) is identical, as expected, with the Born result (33) for $\ell \rightarrow \ell \pm 1$ dipole transitions alone. A universal classical probability $nP^{(n)}_{\epsilon' n,\epsilon n}(\chi)$ was deduced which allowed illustration of rapid convergence of the quantal to the classical results with increasing principal quantum number n. The structure exhibited in the variation of $P^{(n)}_{\ell'\ell}$ with ℓ' is explained and a quantal–classical correspondence is manifest. A modified theory (34) was then provided to acknowledge quantum defects (low ℓ) in non-hydrogenic systems. Essential agreement is obtained with measurements [6]. Collisional Stark mixing at ultralow energies is probably one of the last remaining problems in collision physics capable of exact theoretical solution.

Acknowledgements

This research has been supported by AFOSR Grant No. 49620-99-1-0277 and NSF Grant No. 01-00890.

References

[1] M.R. Flannery, D. Vrinceanu, in: E. Oks, M.S. Pindzola (Eds.) Atomic Processes in Plasmas, 11th APS Topical Conference, AIP Press, New York, 1998, p. 317.
[2] F. Merkt, R.N. Zare, J. Phys. Chem. 101 (1994) 3495.
[3] S.R. Lundeen, in: J.B.A. Michell, S.L. Guberman (Eds.), Dissociative Recombination: Theory, Experiment, and Applications, World Scientific, Singapore, 1989, p. 182.
[4] R.J.T. Gougousi, M.F. Golde, Int. J. Mass. Spectrom. Ion Process. 149/150 (1995) 131.
[5] M.R. Flannery, D. Vrinceanu, in: S.L. Guberman (Ed.), Dissociative Recombination: Theory, Experiment, and Applications, Kluwer Academic/Plenum Press, Singapore, 2002.
[6] X. Sun, K.B. MacAdam, Phys. Rev. A 47 (1993) 3913.
[7] R.M. Pengelly, M.J. Seaton, Monthly Notices Roy. Astronom. Soc. 127 (1964) 165.
[8] I.C. Percival, D. Richards, J. Phys. B 12 (1979) 2051.
[9] Y.N. Demkov, B.S. Monozon, V.N. Ostrovskii, Sov. Phys. JETP 30 (1970) 775.
[10] I.L. Beigman, V.S. Lebedev, Phys. Rep. 250 (1995) 95.
[11] P. Bellomo, D. Farrelly, T. Uzer, J. Chem. Phys 107 (1995) 2499.
[12] A.K. Kazansky, V.N. Ostrovsky, Phys. Rev. A 53 (1995) 1811.
[13] A.K. Kazansky, V.N. Ostrovsky, J. Phys. B 29 (1996) 3651.
[14] A.K. Kazansky, V.N. Ostrovsky, Phys. Rev. Lett. 77 (1996) 3094.
[15] A.K. Kazansky, V.N. Ostrovsky, Sov. Phys. JETP 83 (1996) 1095.
[16] D. Vrinceanu, M.R. Flannery, Phys. Rev. Lett. 85 (2000) 4880.
[17] D. Vrinceanu, M.R. Flannery, Phys. Rev. A 63 (2001) 32701.
[18] D. Vrinceanu, M.R. Flannery, J. Phys. B 33 (2000) 721.
[19] D. Vrinceanu, M.R. Flannery, J. Phys. B 34 (2001) 1.
[20] M. Born, The Mechanics of the Atom, Ungar, New York, 1960, p. 235.
[21] W. Pauli, Z. Phys. 36 (1926) 336.
[22] D.A. Varshalovich, A.N. Moskalev, V.K. Khersonskii, Quantum theory of angular momentum, World Scientific, Singapore, 1988, p. 260.

Classical and quantal atomic form factors for $nlm \rightarrow n'l'm$ transitions

M. R. Flannery and D. Vrinceanu
School of Physics, Georgia Institute of Technology, Atlanta, Georgia 30332-0430
(Received 17 July 2001; published 4 January 2002)

An analytical expression for the classical form factor or impulsive probability $P_{if}(\mathbf{q})$ for $nlm \rightarrow n'l'm$ transitions is derived directly from the "phase-space distribution" method [Phys. Rev. A **60**, 1053 (1999)] and is compared with quantal results. Exact universal scaling laws are derived for the classical probability for any $i \rightarrow f$ transition. As n is increased, convergence of the quantal to classical results is obtained and it becomes even more rapid upon averaging in succession over the m and then the l substates. The classical results reveal the basic reason for the underlying structure in the variation of P_{if} with momentum transfer $\mathbf{q}$. Classical form factors can operate as an effective averaged version of the exact quantal counterpart.

DOI: 10.1103/PhysRevA.65.022703 PACS number(s): 32.80.Cy, 34.50.−s, 31.15.Gy

I. INTRODUCTION

State-to-state collisional atomic form factors

$$P_{nlm \rightarrow n'l'm'}(\mathbf{q}) = |\langle \psi_{n'l'm'}(\mathbf{r}) | e^{i\mathbf{q}\cdot\mathbf{r}/\hbar} | \psi_{nlm}(\mathbf{r}) \rangle|^2 \quad (1)$$

are important in theoretical analysis of experiments involving initially oriented or aligned target atoms. Equation (1) is the probability [1,2] for transitions induced by an impulsive perturbation generated, for example, by a short unipolar electromagnetic pulse [3–5] or by sudden collisions with an aligned neutral atom [6–10]. The internal momentum $\mathbf{p}_i$ of the target system with wave function $\psi_i = \psi_{nlm}$ increases impulsively by $\mathbf{q}$ to the momentum $\mathbf{p}_f = \mathbf{p}_i + \mathbf{q}$, of the final state $\psi_f = \psi_{n'l'm'}$. The form factor (1) is also important to the analysis of high angular momentum l states in cold Rydberg gases [11] and in theories [12] of atomic collisions with Rydberg atoms.

There are several ways to create an unbalanced population of magnetic substates in target atoms, e.g., by application of a polarized laser, a weak external static field, or a unidirectional electromagnetic field pulse. The quantum numbers (nlm) appropriate to spherical coordinates can then be used to specify the initial and final states and Eq. (1) is used directly. This is in contrast to experiments [4] with very high n Rydberg atoms in strong external fields when parabolic quantum numbers must be used, since angular momentum is not a conserved quantity.

Highly oscillatory wave functions for the Rydberg electron render unfeasible the direct numerical calculation of the quantal form factor, particularly for $n \geq 40$. The classical limit is, however, well defined [1] and provides [13], in the limit of large quantum numbers, good agreement for $nl \rightarrow n'l'$, $nl \rightarrow n'$, and $n \rightarrow n'$ transitions. Classical [14] and quantal [15,16] form factors for transitions between parabolic quantum numbers are available. On writing the $\exp(i\mathbf{q}\mathbf{r}/\hbar)$ operator in terms of the generators for SO(4,2) noncompact symmetry group of the hydrogen atom [16], the quantal form factor has been derived in an elegant fashion for $nlm \rightarrow n'lm$ transitions, with $\Delta l = 0$ and $\Delta m = 0$.

When $\hat{\mathbf{q}}$ is taken as the quantization axis of the system, as in electromagnetic field pulse experiments, Eq. (1) is nonzero only for transitions with $\Delta m \equiv m' - m = 0$. This is also true classically since the projection

$$\mathbf{L}_f \cdot \hat{\mathbf{q}} = \mathbf{r} \cdot (\mathbf{p}_f \times \hat{\mathbf{q}}) = \mathbf{L}_i \cdot \hat{\mathbf{q}}$$

of the final $\mathbf{L}_f = \mathbf{r} \times \mathbf{p}_f$ angular momentum along the momentum-change direction $\hat{\mathbf{q}}$ equals the corresponding projection of the initial $\mathbf{L}_i = \mathbf{r} \times \mathbf{p}_i$ angular momentum.

In this paper, the phase-space distribution (PSD) method previously presented [13] for $nl \rightarrow n'l'$ transitions is extended to provide an analytic expression for the classical form factor for $nlm \rightarrow n'l'm$ transitions in a Rydberg atom for a general electron-core interaction $V(r)$. The derived expression agrees with that deduced by Bersons *et al.* [17] from a different approach based on the kinematics of an electron moving in an elliptical orbit under Coulomb attraction. An advantage of the present PSD method is that general classical scaling laws can immediately be derived in transparent form. These are then used to explore the convergence of the quantal form factors onto the classical background as the principal quantum number n is increased. This convergence is important for cases when n is very large ($n \simeq 400$ in half-cycle experiments of Bromage and Stroud [4]) where accurate quantal calculations are unfeasible, if not impossible. Reliance on the use of classical form factors must, therefore, be established and justified for state-to-state transitions, as here.

II. PHASE-SPACE DISTRIBUTION METHOD

The quantal probability (1) for transitions in which momentum $\mathbf{q}$ is impulsively transferred to the target particle can be rewritten [1] as

$$P_{if}(\mathbf{q}) = (2\pi\hbar)^3 \frac{\int \rho_i(\mathbf{r},\mathbf{p}) \rho_f(\mathbf{r},\mathbf{p}+\mathbf{q}) d\mathbf{r} d\mathbf{p}}{\int \rho_i(\mathbf{r},\mathbf{p}) d\mathbf{r} d\mathbf{p}}, \quad (2)$$

where quantal densities

$$\rho_j^q(\mathbf{r},\mathbf{p}) = (2\pi\hbar)^{-3/2} \phi_j^*(\mathbf{p}) \exp(-i\mathbf{p}\cdot\mathbf{r}/\hbar) \psi_j(\mathbf{r}) \quad (3)$$

are expressed in terms of the spatial and momentum wave functions $\psi_j(\mathbf{r})$ and $\phi_j(\mathbf{p})$, respectively for the initial i and final f states. This function (3), which is the standard ordered version of the Wigner PSD, is normalized to unity and may be interpreted as the quantal PSD. The probability

$$\mathcal{P}_{if}(\mathbf{q})=(2\pi\hbar)^3\int \rho_i(\mathbf{r},\mathbf{p})\rho_f(\mathbf{r},\mathbf{p}+\mathbf{q})d\mathbf{r}d\mathbf{p} \tag{4}$$

from all degenerate states i with statistical weights

$$g_i=\int \rho_i(\mathbf{r},\mathbf{p})d\mathbf{r}d\mathbf{p}$$

satisfies detailed balance $\mathcal{P}_{if}(\mathbf{q})=\mathcal{P}_{fi}(-\mathbf{q})$ and is symmetric in i and f.

A. Classical distributions

The volume of phase space occupied by particles moving under Hamiltonian $H=p^2/2m+V(r)$ in a symmetrical potential $V(r)$ with specified energy E, angular momentum $\mathbf{L}=\mathbf{r}\times\mathbf{p}$ and L_z, its component along a fixed direction $\hat{\mathbf{z}}$ of atomic quantization, in the range $dEdLdL_z$ centered about (E,L,L_z) is

$$\begin{aligned}\mathcal{V}_{ELL_z}&=dEdLdL_z\int \delta(H(r,p)-E)\delta(|\mathbf{r}\times\mathbf{p}|-L)\\&\quad\times\delta((\mathbf{r}\times\mathbf{p})\cdot\hat{\mathbf{z}}-L_z)d\mathbf{r}d\mathbf{p}\\&=\mathcal{V}_{nlm}dndldm.\end{aligned} \tag{5}$$

The number of bound nlm states within volume $\mathcal{V}_{nlm}$ is

$$g_{nlm}\equiv\frac{\mathcal{V}_{nlm}}{(2\pi\hbar)^3}=\int \rho^c_{nlm}(\mathbf{r},\mathbf{p})d\mathbf{r}d\mathbf{p}. \tag{6}$$

The classical PSD of nlm states is therefore

$$\begin{aligned}\rho^c_{nlm}(\mathbf{r},\mathbf{p})&=\frac{1}{(2\pi\hbar)^3}\left(\frac{dE}{dn}\right)\left(\frac{dL}{dl}\right)\left(\frac{dL_z}{dm}\right)\delta(H(r,p)-E)\\&\quad\times\delta(|\mathbf{r}\times\mathbf{p}|-L)\,\delta((\mathbf{r}\times\mathbf{p})\cdot\hat{\mathbf{z}}-L_z),\end{aligned} \tag{7}$$

which, upon integration, yields

$$g_{nlm}=\frac{1}{(2\pi\hbar)^3}\left(\frac{dE}{dn}\right)\left(\frac{dL}{dl}\right)\left(\frac{dL_z}{dm}\right)\left(\frac{8\pi^3}{\omega_{nl}}\right)$$

for the number (6) of bound nlm states. The angular frequency for bounded radial motion is given, in terms of the radial action, by $\omega_{nl}\equiv 2\pi\partial H/\partial J$. Under the substitutions, $dE/dn=\hbar\omega_{nl}$, $dL/dl=\hbar$ and $dL_z/dm=\hbar$, for the spacings between neighboring states, the phase volume is $\mathcal{V}_{nlm}=(2\pi\hbar)^3$ and the number of states $g_{nlm}=1$. The corresponding nlm one-particle PSD is then

$$\begin{aligned}\rho^c_{nlm}(\mathbf{r},\mathbf{p})&=\frac{\hbar\omega_{nl}}{(2\pi\hbar)^3}\delta(H(r,p)-E)\,\hbar\,\delta(|\mathbf{r}\times\mathbf{p}|-L)\\&\quad\times\hbar\,\delta((\mathbf{r}\times\mathbf{p})\cdot\hat{\mathbf{z}}-L_z),\end{aligned} \tag{8}$$

which is normalized to one particle. The volume of phase space occupied by particles in state nl is

$$\mathcal{V}_{nl}=\left(\frac{dE}{dn}\right)\left(\frac{dL}{dl}\right)\int \delta(H(r,p)-E)\delta(|\mathbf{r}\times\mathbf{p}|-L)d\mathbf{r}d\mathbf{p}. \tag{9}$$

The degeneracy g_{nl} is $(2\pi\hbar)^{-3}\mathcal{V}_{nl}=2l$. The classical PSD appropriate to these $2l$ bound nl states is then

$$\rho^c_{nl}(\mathbf{r},\mathbf{p})=\frac{\hbar\omega_{nl}}{(2\pi\hbar)^3}\delta(H(r,p)-E)\hbar\,\delta(|\mathbf{r}\times\mathbf{p}|-L). \tag{10}$$

The classical PSD appropriate to the degenerate $g_n=n^2$ bound hydrogenic states within level n is similarly

$$\rho^c_n(\mathbf{r},\mathbf{p})=\frac{\hbar\omega_n}{(2\pi\hbar)^3}\delta(H(r,p)-E). \tag{11}$$

The classical correspondence with Eq. (2) may now be established.

B. Classical-quantal probability correspondence

The phase-space volume occupied by those final $(n'l')$ states that can be accessed only from the initial distribution of (nl) states via an impulsive transfer of momentum $\mathbf{q}$ at electronic separation $\mathbf{r}$ is

$$\begin{aligned}\mathcal{V}_{nl,n'l'}(\mathbf{q})&=\left(\frac{dE_i}{dn}\frac{dL_i}{dl}\frac{dE_f}{dn'}\frac{dL_f}{dl'}\right)\int d\mathbf{r}d\mathbf{p}\{\delta(H(r,p)\\&\quad-E)\delta(|\mathbf{r}\times\mathbf{p}|-L)\}\{\delta(\mathbf{r}'-\mathbf{r})\,\delta(\mathbf{p}'-(\mathbf{p}+\mathbf{q}))\}\\&\quad\times\{\delta(H(r',p')-E')\\&\quad\times\delta(|\mathbf{r}'\times\mathbf{p}'|-L')\}d\mathbf{r}'d\mathbf{p}'.\end{aligned} \tag{12}$$

The number $g_{nl,n'l'}$ of final $(n'l')$ states originating from the (nl) states is $\mathcal{V}_{nl,n'l'}/(2\pi\hbar)^3$. The classical probability for transitions from one initial state to the band of final states is then the ratio

$$P_{nl,n'l'}=g_{nl,n'l'}/g_{nl}=\mathcal{V}_{nl,n'l'}/\mathcal{V}_{nl} \tag{13}$$

of final to initial populations or, alternatively, the ratio of the overlap phase volume (12) to the initial volume (9). The classical probability for $nl\rightarrow n'l'$ transitions can therefore be expressed in terms of the classical PSD (10) for bound states by

$$P^c_{nl,n'l'}(\mathbf{q}) = (2\pi\hbar)^3 \int \rho^c_{nl}(\mathbf{r},\mathbf{p})\rho^c_{n'l'}(\mathbf{r},\mathbf{p}+\mathbf{q})d\mathbf{r}d\mathbf{p} \Big/ \int \rho^c_{nl}(\mathbf{r},\mathbf{p})d\mathbf{r}d\mathbf{p}. \tag{14}$$

Comparison between Eqs. (14) and (2), therefore, establishes directly the classical-quantal correspondence between the impulsive probabilities given as the normalized overlap of the corresponding initial and final PSD's. The probability for transitions from the degenerate $g_{nl}=2l$ initial states i to the $2l'$ final states f is the overlap

$$\mathcal{P}^c_{nl,n'l'}(\mathbf{q}) \equiv g_{nl}P^c_{nl,n'l'}(\mathbf{q}) = (2\pi\hbar)^3 \int \rho^c_{nl}(\mathbf{r},\mathbf{p})\rho^c_{n'l'}(\mathbf{r},\mathbf{p}+\mathbf{q})d\mathbf{r}d\mathbf{p},$$

which also satisfies the relation $\mathcal{P}^c_{nl,n'l'}(+\mathbf{q}) = \mathcal{P}^c_{n'l',nl}(-\mathbf{q})$ for a detailed balance. The classical probability for transitions from the degenerate n^2 initial states in level n of hydrogenic atoms to the n'^2 final states in level n' is

$$\mathcal{P}^c_n(\mathbf{q}) = (2\pi\hbar)^3 \int \rho^c_n(\mathbf{r},\mathbf{p})\rho^c_{n'}(\mathbf{r},\mathbf{p}+\mathbf{q})d\mathbf{r}\,d\mathbf{p}.$$

C. State-to-state transition probabilities

The classical probability (form factor) for $i \equiv nlm \to f \equiv n'l'm'$ transitions is

$$P_{nlm,n'l'm'}(\mathbf{q}) = \frac{1}{(2\pi\hbar)^3}\left(\frac{dE_i}{dn}\frac{dL_i}{dl}\frac{dL_{iz}}{dm}\frac{dE_f}{dn'}\frac{dL_f}{dl'}\frac{dL_{fz}}{dm'}\right)V_{nlm,n'l'm'}(\mathbf{q}) \tag{15}$$

in terms of the overlapped volume density (of initial and final states),

$$V_{if}(\mathbf{q}) = \int \delta(H(r,p)-E_i)\delta(|\mathbf{r}\times\mathbf{p}|-L_i) \times \delta(H(r,|\mathbf{p}+\mathbf{q}|)-E_f)\delta(|\mathbf{r}\times(\mathbf{p}+\mathbf{q})|-L_f) \times \delta((\mathbf{r}\times\mathbf{p})\cdot\hat{\mathbf{z}}-L_{iz})\delta([\mathbf{r}\times(\mathbf{p}+\mathbf{q})]\cdot\hat{\mathbf{z}}-L_{fz})d\mathbf{r}d\mathbf{p}, \tag{16}$$

which is simply the phase-space overlap integral of δ functions involving states $i=(E_i,L_i,L_{iz})$ and $f=(E_f,L_f,L_{fz})$. This overlap is illustrated in Fig. 1. Evolution to the final-state manifold is achieved via the allowed phase-space trajectories indicated.

For hydrogenic states, $E=\epsilon_0/2n^2, L=l\hbar, L_z=m\hbar$ where ϵ_0 is the atomic unit of energy, and the transition probability is obtained upon setting $dE/dn=\hbar\omega_n=\epsilon_0/n^3$, $dL/dl=\hbar$, and $dL_z/dm=\hbar$ to give

$$P_{nlm,n'l'm'}(\mathbf{q}) = \frac{\epsilon_0^2\hbar}{8\pi^3 n^3 n'^3}V_{nlm,n'l'm'}(\mathbf{q}) \tag{17}$$

in terms of the volume density (16). The probabilities for $nl\to nl'$ and in $n\to n'$ transitions from all degenerate initial levels are

$$\mathcal{P}_{nl,n'l'}(\mathbf{q}) = \frac{(\epsilon_0^2/\hbar)}{8\pi^3 n^3 n'^3}V_{nl,n'l'}(\mathbf{q}) \tag{18}$$

and

$$\mathcal{P}_{n,n'}(\mathbf{q}) = \frac{(\epsilon_0^2/\hbar^3)}{8\pi^3 n^3 n'^3}V_{n,n'}(\mathbf{q}), \tag{19}$$

respectively, in terms of the corresponding volume densities

$$V_{nl,n'l'}(\mathbf{q}) = \int \delta(H(r,p)-E_i)\delta(|\mathbf{r}\times\mathbf{p}|-L_i) \times \delta(H(r,|\mathbf{p}+\mathbf{q}|)-E_f)\delta(|\mathbf{r}\times(\mathbf{p}+\mathbf{q})|-L_f)d\mathbf{r}d\mathbf{p} \tag{20}$$

and

$$V_{n,n'}(\mathbf{q}) = \int \delta(H(r,p)-E_i)\delta(H(r,|\mathbf{p}+\mathbf{q}|)-E_f)d\mathbf{r}d\mathbf{p}, \tag{21}$$

respectively.

D. Classical scaling rules

An advantage of the classical formulation above is that very useful universal scaling laws for the probabilities can be derived. On introducing a scaling factor α, such that $p'=\alpha p$ and $r'=r/\alpha^2$ for hydrogenic systems, then $H' \equiv H(p',r')=\alpha^2 H(p,r)$, $E'=\alpha^2 E$ and $\mathbf{L}'=\mathbf{r}'\times\mathbf{p}'=\mathbf{L}/\alpha$. It follows that the continuum PSD

$$\rho^c_{ELL_z}(\mathbf{r},\mathbf{p}) = (2\pi\hbar)^{-3}dE dL dL_Z \delta(H-E)\delta(|\mathbf{r}\times\mathbf{p}|-L) \times \delta(\mathbf{L}\cdot\hat{\mathbf{z}}-L_z) \tag{22}$$

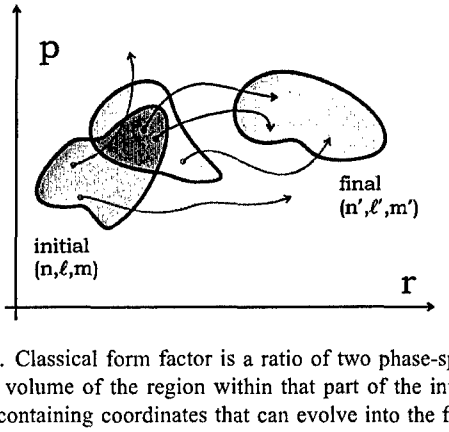

FIG. 1. Classical form factor is a ratio of two phase-space volumes: the volume of the region within that part of the initial-state manifold containing coordinates that can evolve into the final-state manifold, and the total volume of the initial-state manifold.

and the associated L_z and (L_z,L) integrated PSD's, ρ^c_{EL} and ρ^c_E, therefore scale as

$$\rho^c_\Gamma(\mathbf{r},\mathbf{p})=\rho^c_{\Gamma'}(\mathbf{r}',\mathbf{p}'),$$

an invariant for all sets $\Gamma\equiv(ELL_z),(EL),E$. For continuum-continuum transitions, the symmetric probabilities

$$\mathcal{P}_{\Gamma_i,\Gamma_f}(\mathbf{q})=(2\pi\hbar)^3\int\rho^c_{\Gamma_i}(\mathbf{r},\mathbf{p})\rho^c_{\Gamma_f}(\mathbf{r},\mathbf{p}+\mathbf{q})d\mathbf{r}\,d\mathbf{p}$$

therefore scale, independently of Γ, as

$$\mathcal{P}_{\Gamma_i,\Gamma_f}(\mathbf{q})=\alpha^3\mathcal{P}_{\Gamma_i,\Gamma_f}(\mathbf{q}'),$$

where $\mathbf{q}'=\alpha\mathbf{q}$. Since $n=\alpha n'$, $l=\alpha l'$ and $m=\alpha m'$, the bound state PSD's (8), (10) and (11) however scale according to

$$\rho^c_{nlm}(\mathbf{r},\mathbf{p})=\alpha^{-3}\rho^c_{n'l'm'}(\mathbf{r}',\mathbf{p}'),\tag{23}$$

$$\rho^c_{nl}(\mathbf{r},\mathbf{p})=\alpha^{-2}\rho^c_{n'l'}(\mathbf{r}',\mathbf{p}'),\tag{24}$$

$$\rho^c_{n}(\mathbf{r},\mathbf{p})=\alpha^{-1}\rho^c_{n'}(\mathbf{r}',\mathbf{p}').\tag{25}$$

The probabilities

$$\mathcal{P}_{\Gamma_i,nlm}(\mathbf{q})=(2\pi\hbar)^3\int\rho^c_{\Gamma_i}(\mathbf{r},\mathbf{p})\rho^c_{nlm}(\mathbf{r},\mathbf{p}+\mathbf{q})d\mathbf{r}\,d\mathbf{p}$$

for continuum-bound (recombination) transitions therefore scale as

$$\mathcal{P}_{ELL_z,nlm}(\mathbf{q})=\mathcal{P}_{E'L'L'_z,n'l'm'}(\mathbf{q}'),\tag{26}$$

$$\mathcal{P}_{EL,nl}(\mathbf{q})=\alpha\mathcal{P}_{E'L',n'l'}(\mathbf{q}'),\tag{27}$$

$$\mathcal{P}_{E,n}(\mathbf{q})=\alpha^2\mathcal{P}_{E',n'}(\mathbf{q}').\tag{28}$$

The probabilities for bound-bound transitions

$$\mathcal{P}_{if}(\mathbf{q})=g_iP_{if}=(2\pi\hbar)^3\int\rho_i(\mathbf{r},\mathbf{p})\rho_f(\mathbf{r},\mathbf{p}+\mathbf{q})d\mathbf{r}d\mathbf{p}\tag{29}$$

from the g_i initial states scale as

$$P_{n_il_im_i,n_fl_fm_f}(\mathbf{q})=\alpha^{-3}P_{n'_il'_im'_i,n'_fl'_fm'_f}(\mathbf{q}'),\tag{30}$$

$$P_{n_il_im_i,n_fl_f}(\mathbf{q})=\alpha^{-2}P_{n'_il'_im'_i,n'_fl'_f}(\mathbf{q}'),\tag{31}$$

$$\mathcal{P}_{n_il_i,n_fl_f}(\mathbf{q})=\alpha^{-1}\mathcal{P}_{n'_il'_i,n'_fl'_f}(\mathbf{q}'),\tag{32}$$

$$\mathcal{P}_{n_il_i,n_f}(\mathbf{q})=\alpha^{0}\mathcal{P}_{n'_il'_i,n'_f}(\mathbf{q}'),\tag{33}$$

$$\mathcal{P}_{n_i,n_f}(\mathbf{q})=\alpha\mathcal{P}_{n'_i,n'_f}(\mathbf{q}').\tag{34}$$

Summation over the initial/final substates is implied when the corresponding quantum numbers do not appear as subscripts.

Applications

(A) By choosing $\alpha=n_i$, for example, it can then be shown that the $i\to f$ symmetric probabilities (30)–(34) written as $\mathcal{P}(i;f;\mathbf{q})$ satisfy the rules

$$n_i^3P(n_il_im_i;n_fl_fm_f;\mathbf{q}/n_i)=P(1,\epsilon_i,\mu_i;\eta_f,\epsilon_f,\mu_f;\mathbf{q}),\tag{35}$$

$$n_i^2P(n_il_im_i;n_fl_f;\mathbf{q}/n_i)=P(1,\epsilon_i,\mu_i;\eta_f,\epsilon_f,\mu_i;\mathbf{q}),\tag{36}$$

$$n_i\mathcal{P}(n_il_i;n_fl_f;\mathbf{q}/n_i)=\mathcal{P}(1,\epsilon_i;\eta_f,\epsilon_f;\mathbf{q}),\tag{37}$$

$$n_i^{-1}\mathcal{P}(n_i;n_f;\mathbf{q}/n_i)=\mathcal{P}(1;\eta_f;\mathbf{q}),\tag{38}$$

where the parameters are $\epsilon_j=l_j/n_i$, $\mu_j=m_j/n_i$ and $\eta_f=n_f/n_i$. The transition arrays for *all* n_i can, therefore, be deduced from the array from a single value of n_i, e.g., $n_i=1$. The dimensionality of the transition arrays is then reduced by one.

(B) The quasielastic transition arrays $(n_il_im_i\to n_il_fm_f)$ and $(n_il_i\to n_il_f)$ can be scaled similarly by choosing $\alpha=l_i$ to provide the rules

$$l_i^3P(n_il_im_i;n_il_fm_f;\mathbf{q}/l_i)=P(\beta_i,1,\delta_i;\beta_i\gamma_f\delta_f;\mathbf{q}),\tag{39}$$

$$l_i\mathcal{P}(n_il_i;n_il_f;\mathbf{q}/l)=\mathcal{P}(\beta_i,1;\beta_i\gamma_f\delta_f;\mathbf{q}),\tag{40}$$

where $\beta_i=n_i/l_i$, $\gamma_f=l_f/l_i$, and $\delta_j=m_j/l_i$.

III. ANALYTICAL EXPRESSION FOR THE PROBABILITY

The volume density phase-space integration (16) for state-to-state transitions is accomplished by noting that the δ functions of the initial and final Hamiltonians, $H_i=p^2/2\mu+V(r)$ and $H_f=|\mathbf{p}+\mathbf{q}|^2/2\mu+V(r)$, are

$$\delta(H_i-E_i)=(\mu/p)\,\delta(p-[2\mu(E_i-V(r))]^{1/2}),\tag{41}$$

$$\delta(H_f-E_f)=(\mu/pq)\,\delta\left[\cos\chi-\frac{E_f-H_i-q^2/2\mu}{pq/\mu}\right],\tag{42}$$

where χ is the angle between $\mathbf{p}$ and $\mathbf{q}$ such that

$$H_f(\mathbf{p},\mathbf{r})=\frac{p^2+2\mathbf{p}\cdot\mathbf{q}+q^2}{2\mu}+V(r)=H_i+\frac{q^2}{2\mu}+\frac{pq}{\mu}\cos\chi.$$

It now proves extremely advantageous to adopt the spherical bifocal coordinates u_i and u_f introduced previously in Ref. [18] and represented in Fig. 2. The δ functions of the angular momentum are

$$\delta(|\mathbf{r}\times\mathbf{p}|-L_i)=\frac{\delta(u_i-U_i)+\delta(u_i-(\pi-U_i))}{rp|\cos U_i|},\tag{43}$$

$$\delta(|\mathbf{r}\times(\mathbf{p}+\mathbf{q})|-L_f)=\frac{\delta(u_f-U_f)+\delta(u_f-(\pi-U_f))}{r|\mathbf{p}+\mathbf{q}||\cos U_f|},\tag{44}$$

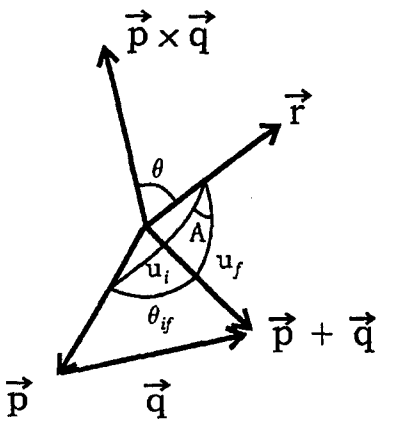

FIG. 2. Basic geometry involved in the calculation of the classical state-to-state form factor.

where the angles u_j are determined by $\cos u_i = \hat{\mathbf{r}}\cdot\hat{\mathbf{p}}$ and $\cos u_f = \hat{\mathbf{r}}\cdot(\widehat{\mathbf{p}+\mathbf{q}})$. Also

$$\sin U_i = \frac{L_i}{rp}; \quad \sin U_f = \frac{L_f}{r|\mathbf{p}+\mathbf{q}|}.$$

The phase-space volume element can then be expressed [18] in terms of the u_i and u_f in Fig. 2 as

$$d\mathbf{p}\,d\mathbf{r} = [p^2 dp\, d(\cos\theta_p) d\phi_p]\left\{\frac{2du_i du_f}{\sin A}\right\} r^2 dr,$$

where (θ_p, ϕ_p) are the polar and azimuthal angles of $\mathbf{p}$ relative to a fixed set of axis and where A is determined from

$$\cos A = \frac{p^2 + |\mathbf{p}+\mathbf{q}|^2 - q^2 - 2p|\mathbf{p}+\mathbf{q}|\cos u_i \cos u_f}{2p|\mathbf{p}+\mathbf{q}|\sin u_i \sin u_f}.$$

Subsequent calculation of Eq. (16) or Eq. (20) depends on whether or not there is a fixed direction of space as specified by an electric or magnetic field.

(a) When no fixed axis is specified, then θ_p can be identified with the angle χ between $\mathbf{p}$ and $\mathbf{q}$. Under the constraints (41)–(45), $p|\mathbf{p}+\mathbf{q}||\cos u_i||\cos u_f| = \mu^2 R_i R_f$, where the radial speeds $R_{i,f}(r) = \dot{r}_{i,f}$ are determined from energy conservation

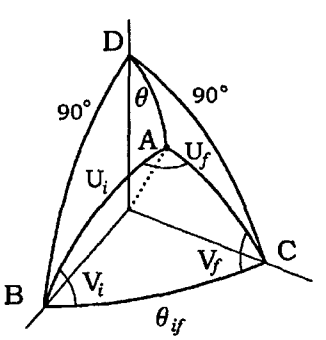

FIG. 3. In spherical bifocal coordinates, point A is identified by angles U_i and U_f of arcs BA and CA on the unit sphere. The area element is $dS = dU_i dU_f/\sin A$, where A is the angle between arcs BA and CA.

$$E_{i,f} = \frac{1}{2}\mu \dot{r}_{i,f}^2 + V(r) + \frac{L_{i,f}^2}{2\mu r^2} \tag{45}$$

as functions only of r for specified energy and angular momentum. The phase-space integrations in the volume density (20) for $nl \to n'l'$ transitions can then be performed directly to yield

$$\begin{aligned} V_{nl,n'l'}(\mathbf{q}) &= \frac{8\pi}{q}\int_{\mathcal{R}} \frac{dr}{R_i(r)R_f(r)}\left[\frac{1}{\sin A_+} + \frac{1}{\sin A_-}\right]\Theta(r,q) \\ &= \frac{16\pi L_i L_f}{q}\int_{\mathcal{R}} \frac{dr/r^2}{R_i(r)R_f(r)} \\ &\quad \times\left\{\left[\frac{4L_i^2L_f^2}{r^4} - C_+^2(r)\right]^{-1/2} \right. \\ &\quad \left. + \left[\frac{4L_i^2L_f^2}{r^4} - C_-^2(r)\right]^{-1/2}\right\}\Theta(r,q), \end{aligned} \tag{46}$$

where quantities $C_\pm$ are defined as

$$\begin{aligned} C_\pm(r) &= 2\mu[E_i + E_f - 2V(r)] \pm 4\mu\left[E_i - V(r) - \frac{L_i^2}{r^2}\right]^{1/2} \\ &\quad \times\left[E_f - V(r) - \frac{L_f^2}{r^2}\right]^{1/2} - q^2 \\ &= \mu^2[R_i(r) \pm R_f(r)]^2 + \frac{(L_i^2 + L_f^2)}{r^2} - q^2. \end{aligned}$$

The step function Θ is unity provided $V(r) \leqslant E_i - \mu(E_f - E_i - q^2/2\mu)^2/2q^2$ and zero otherwise. The region $\mathcal{R}$ of radial integration, within which $A_\pm$ are real, is determined by the condition $C_\pm^2(r) \leqslant 4L_i^2L_f^2/r^4$. The above result (46) is identical with that calculated previously [13] via a different integration method. The integrand of Eq. (46) is an ingredient [12] in classical impulsive theories of $A - B(nl)$ collisions when the cross section $\sigma(g,q)$ for scattering of the Rydberg electron by A at relative speed g is a function of both g and the momentum q transferred. When σ is a function only of q, the full integral (46) is then applicable [12].

(b) For transitions between m sublevels, there is a fixed direction of atomic quantization and the calculation is more difficult. The δ function involving L_{fz} is

$$\delta([\mathbf{r}\times(\mathbf{p}+\mathbf{q})]\cdot\hat{\mathbf{z}} - L_{fz}) = \delta(\mathbf{r}\cdot(\mathbf{q}\times\hat{\mathbf{z}}) - (L_{fz} - L_{iz})), \tag{47}$$

where $\mathbf{q}\times\hat{\mathbf{z}}$ is a fixed direction in space. For the impulse $\mathbf{q}$ directed along the quantization axis $\hat{\mathbf{z}}$, then (47) reduces to $\delta(L_{fz} - L_{iz})$ and only transitions with $L_{iz} = L_{fz} \equiv L_z$ occur. Moreover, the azimuthal angle ϕ_p of $\mathbf{p}$ may now rotate freely in the range $[0 - \pi]$ and $\mathbf{r}$, for fixed U_i and U_f, is attached to the rotated $\mathbf{p}$. With the aid of the spherical bifocal coordinates [18], it can be shown (see Fig. 3 as well as the Appendix) that the δ function of L_{iz} in Eq. (16) reduces to

$$\delta((\mathbf{r}\times\mathbf{p})\cdot\hat{\mathbf{z}}-L_{iz})=\delta\left(\frac{L_iL_f}{qr}\sin A-L_{iz}\right). \tag{48}$$

Under the conditions (41)–(43), it can be expressed as

$$\begin{aligned}&\delta((\mathbf{r}\times\mathbf{p})\cdot\hat{\mathbf{z}}-L_{iz})\\&=\frac{8q^2L_z}{r^2}\delta\left(C_{\pm}^2(r)+\left(\frac{2qL_z}{r}\right)^2-\left(\frac{2L_iL_f}{r^2}\right)^2\right)\\&=\frac{8q^2L_z}{r^2}\left\{\sum_k\frac{\delta(r-r_k)}{|\partial F_{\pm}(r_k)/\partial r|}\right\},\end{aligned} \tag{49}$$

where the summation includes all roots r_k of

$$F_{\pm}(r;q)=C_{\pm}^2(r)+\left(\frac{2qL_z}{r}\right)^2-\left(\frac{2L_iL_f}{r^2}\right)^2=0,$$

where the $nlm\rightarrow n'l'm$ transitions occur classically. The six-fold integration in the probability (17) for $nlm\rightarrow n'l'm$ transitions resulting from the impulse $\hbar\mathbf{q}$ directed along the z axis of atomic quantization then reduces to the following exact result:

$$P_{nlm\rightarrow n'l'm}(\mathbf{q})$$

$$=\frac{(2l)(2l')}{\pi^2n^3n'^3}(\hbar\epsilon_0^2)\sum_k\frac{1}{|r_k^3R_i(r_k)R_f(r_k)\partial F_{\pm}(r_k)/\partial r|}, \tag{50}$$

where ϵ_0 is the atomic unit of energy. This result reduces to that in Ref. [17] for Coulomb attraction and, when summed over m to the earlier result [13] for $nl\rightarrow n'l'$ transitions. There are always two or four roots r_k. When two roots accidentally coalesce, where $\partial F_{\pm}(r)/\partial r$ vanishes, the classical transition probability has a singularity. The basic variation of the classical form factor (50) with q for the $n=5,l=4,m=1\rightarrow 8,2,1$ transition in atomic hydrogen is displayed in Fig. 4, together with the q-variation of corresponding roots $r_k(q)$, given by the intersection of the surfaces $z=F_{\pm}(r;q)$ with the $z=0$ plane. It is seen that cusp singularities are exhibited in $P_{nlm\rightarrow n'l'm}(q)$ when the line $q=$ const is tangential to the $r_k(q)$ curves . This occurs at four places in Fig. 4. The magnitude of the probability between the singularities is proportional to the number k of contributing radial roots where the m transitions occur. The probabilities $P_{nlm\rightarrow n'l'm}(q)$ are, of course, zero in the classical inaccessible region shown.

The probability (50) obeys the following scaling law:

$$n^2P_{nlm\rightarrow n'l'm}(\mathbf{q}/n)=P_{1,l/n,m/n\rightarrow n'/n,l'/n,m/n}(q),$$

cf. Eq. (36), which will be used to explore the quantal-classical convergence as n is increased.

IV. QUANTAL FORM FACTOR

Here, a numerical technique is devised for accurate calculation of the quantal form factor, even for high $n\sim 100$. An analytic expression for the quantal form factor (1) can be

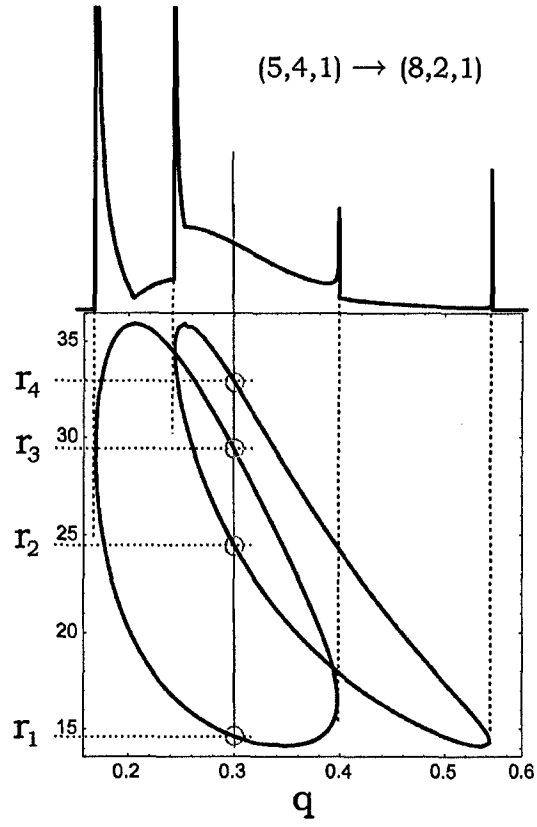

FIG. 4. Contour lines for equation $F_{\pm}(r;q)=0$ in the $q-r$ plane. In the upper part of the diagram, classical probability for transition $(n=5,l=4,m=1)\rightarrow(n'=8,l'=2,m'=1)$. Singularities arise when two roots r_k are equal.

obtained by using the expansion of the exponential function in terms of spherical Bessel functions and spherical harmonics. Upon integration,

$$P^{Q}_{nlm\rightarrow n'l'm}(q)=\left|\mathscr{I}\sum_{k=l+l'+2}^{n+n'}w_kd_k(-q^2/\alpha^2)\right|^2, \tag{51}$$

where the prefactor is

$$\begin{aligned}\mathscr{I}&=\frac{1}{4\alpha}\sqrt{\frac{2l'+1}{2l+1}}\sqrt{\frac{(n-l-1)!}{(n+l)!}}\\&\times\sqrt{\frac{(n'-l'-1)!}{(n'+l')!}}\left(\frac{2}{n}\right)^{l+2}\left(\frac{2}{n'}\right)^{l'+2}\left(\frac{q}{\alpha}\right)^{|l-l'|},\end{aligned}$$

in terms of $\alpha=1/n+1/n'$. The w_k term is the coefficient of the power r^k in the expansion of the product of radial polynomials

$$(r/\alpha)^2R_{nl}R_{n'l'}=\sum_{k=l+l'+2}^{n+n'}w_kr^k,$$

where

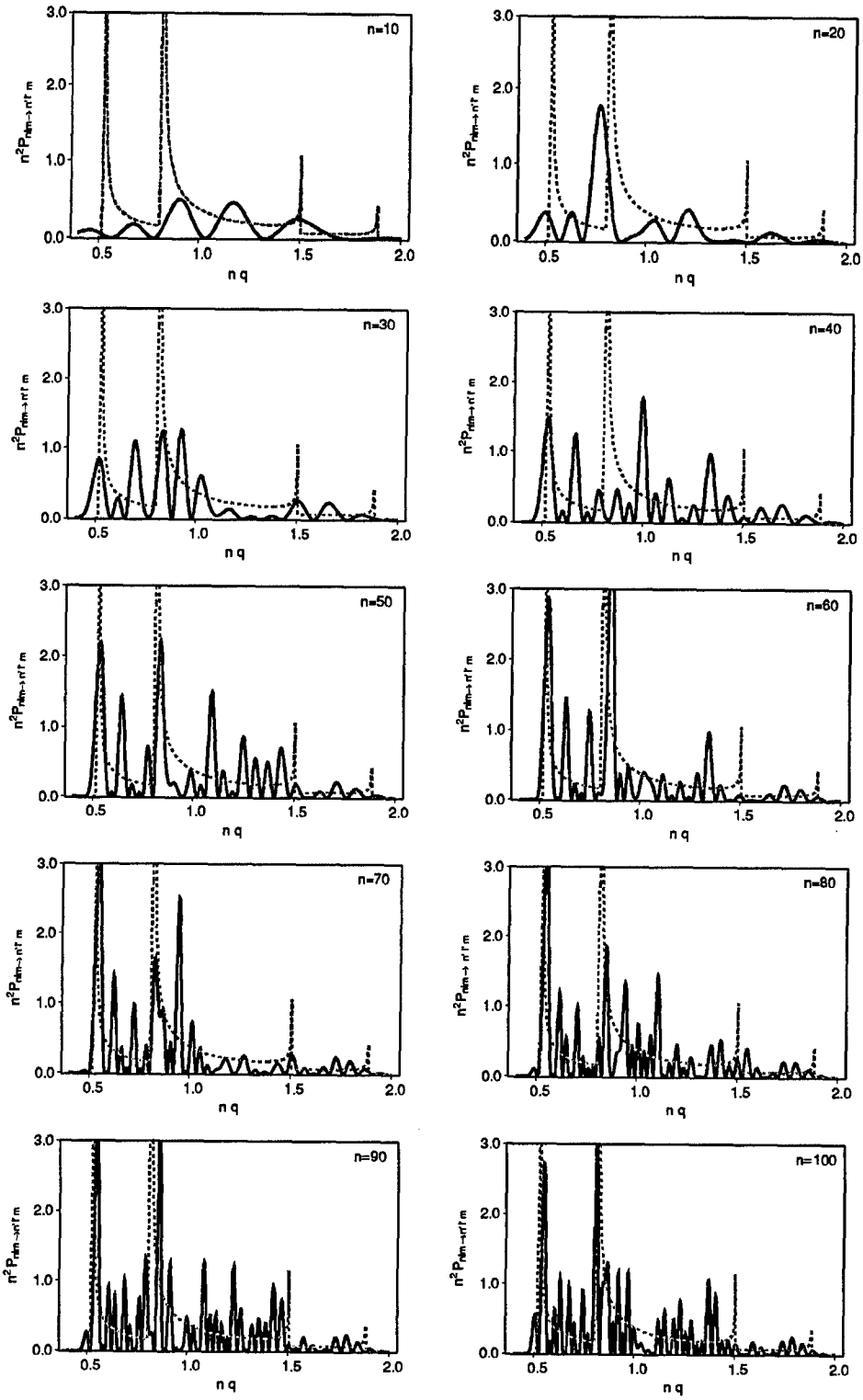

FIG. 5. Classical (dotted line) and quantal (solid line) scaled form factors as a function of scaled momentum transfer $\bar{q}=nq$ for $nlm\to n'l'm$ transitions. For transitions with fixed parameters $l/n=3/10$, $n'/n=14/10$, $l'/n=12/10$, and $m/n=1/10$ convergence is obtained as n is increased from $n=10$ to $n=100$.

$$R_{nl}=(r/\alpha)^l L_{n-l-1}^{(2l+1)}\left(\frac{2r}{n\alpha}\right)$$

is the polynomial part of the radial hydrogenic wave function defined in terms of Laguerre polynomials $L_n^{(a)}(x)$. Finally, the q dependence of the quantal form factor (51) is contained within the functions d_k defined by

$$d_k(x)=\frac{1}{(1-x)^k}\sum_{s=0}^{\min(l,l')} C_{l'0L0}^{l0}C_{l'mL0}^{lm}\frac{(k+L)!}{(2L-1)!!}$$
$$\times x^s\,{}_2F_1\left[\frac{L-k+1}{2},\frac{L-k}{2}+1,L+3/2;x\right],$$

where C are Clebsch-Gordan coefficients for the addition of

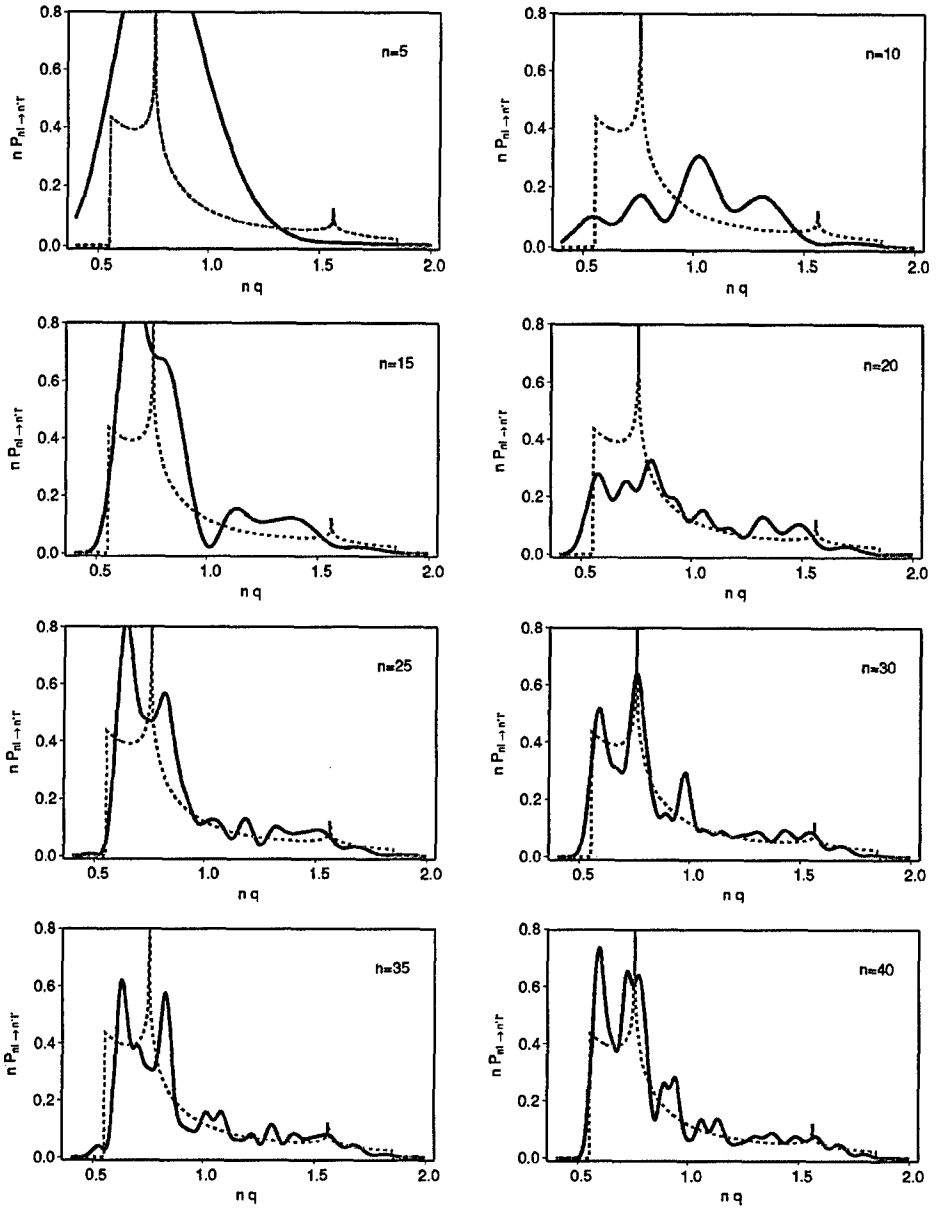

FIG. 6. Classical (dotted line) and quantal (solid line) symmetric scaled form factors as a function of scaled momentum transfer $\bar{q}=nq$ for $nl\rightarrow n'l'$ transitions. For fixed parameters $l/n=1/5$, $n'/n=7/5$, and $l'/n=6/5$, convergence is obtained as n is increased from $n=5$ to $n=40$.

angular momenta l and l'. The resulting angular momentum L is given by $L=|l-l'|+2s$, such that L takes values between $|l-l'|$ and $l+l'$ with the same parity as $l+l'$. The hypergeometric function ${}_2F_1$ reduces to a polynomial that obeys a simple recursion relation since either the first or the second argument of ${}_2F_1$ is a negative integer. The quantal form factor has, therefore, a very simple structure as a function of momentum transfer q, being a polynomial divided by $(1+q^2/\alpha^2)^{n+n'}$. Unfortunately, factorials of large arguments lead to very large but integer coefficients in the polynomial expression. Accurate results for $n>40$ cannot be obtained by using the usual floating-point machine accuracy. By using integer and rational number arithmetic, calculation can, however, be performed in infinite precision if the momentum transfer is approximated by a rational number. The result, in turn, is obtained as an exact rational number, with an extremely large numerator and denominator. Even though the form factor can be calculated in this way for arbitrary quantum numbers (computer time and memory being the only constraints), the results exhibit an increasing number of oscillations, as seen in $n>80$ subplots of Fig. 5. The usefulness of the exact, rigorous, quantal results, therefore, becomes questionable for such large quantum numbers and only an averaging procedure can provide practical quantitative results. The classical form factor has the ability to operate as an effective averaged version of the exact quantal counterpart, as illustrated in Fig. 5.

V. QUANTAL-CLASSICAL CONVERGENCE

Quantal-classical correspondence is evident when the classical curve provides the essential framework on which the quantal oscillatory structure is superimposed. In this sense, Fig. 5 illustrates the convergence of the scaled quantal

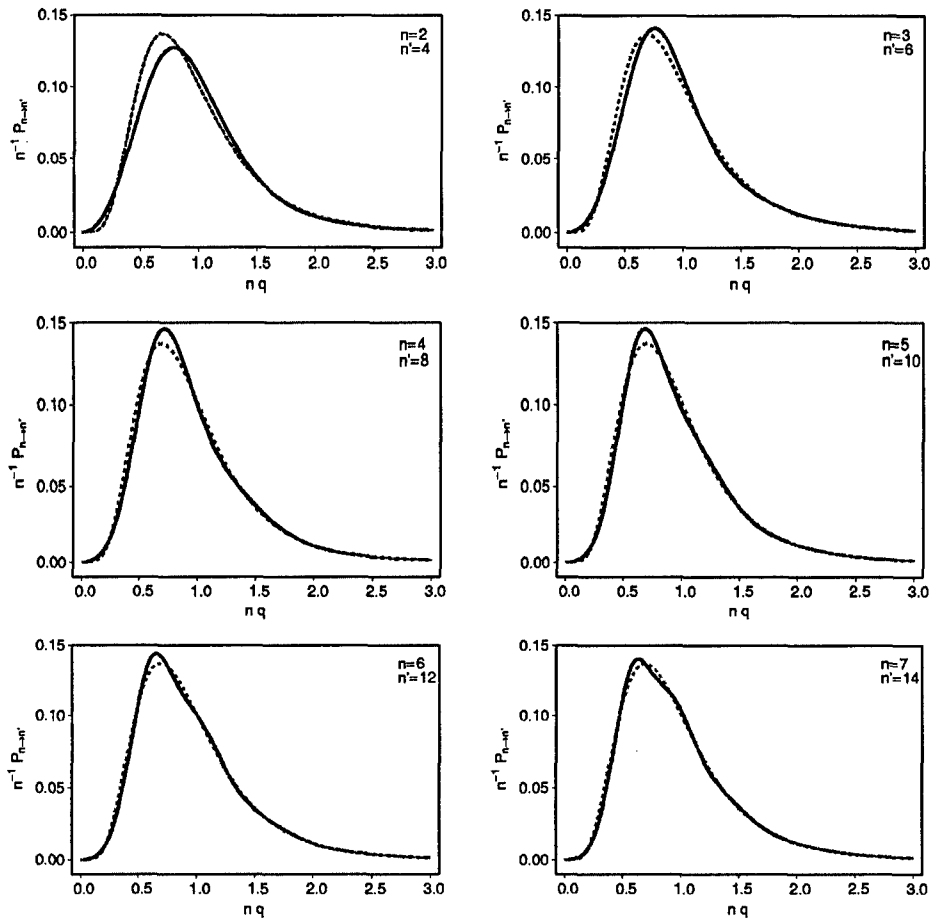

FIG. 7. Classical (dotted line) and quantal (solid line) scaled form factors as a function of scaled momentum transfer $\bar{q}=nq$ for $n\to n'$ transitions. For transitions with constant ratio $n'/n=2$, convergence is obtained as n increases from $n=2$ to $n=7$.

form factors $n^2P^{Q}_{nlm\to n'l'm}(\mathbf{q}/n)$ onto the universal classical curve $P^{C}_{1,l/n,m/n\to n'/n,l'/n,m/n}$ as a function of scaled q for $nlm\to n'l'm$ transitions. Convergence ranges from good for n as low as 30 to excellent for $n\geq 80$. The oscillations can be attributed to interference effects between phases (quantal or semiclassical) of the contributions to the amplitude that arises from each location r_k.

Convergence to the classical results is much faster when the results are averaged over all m values, as for the scaled probabilities $nP_{nl\to n'l'}$ for $nlm\to n'l'm$ transitions, displayed in Fig. 6. Finally, in Fig. 7, the classical and quantal probabilities $n^{-1}P_{n\to n'}$ for the l,m-averaged transitions contain no oscillatory structure and agree for n as low as 2. This result is well known and is the basis for classical descriptions of $n\to n'$ collisional transitions.

VI. CONCLUSION

Using the PSD formulation [13], the classical-quantal correspondence has been established by showing that the atomic form factor (1) for state-to-state transitions in a general one-electron atom can be written in the generic form (2) where the quantal and classical distributions are given by Eqs. (3) and (7), respectively. Exact calculations of the derived probability (50) for $nlm\to n'l'm$ transitions are presented. The classical state-to-state form factor (50) is expressed analytically in terms of the radial electronic locations r_k where the transitions occur. Agreement with previously published results [17] is obtained for the special case of atomic hydrogen (Coulombic potential).

The classical background contains two classical inaccessible regions (at small and large momentum transfers q) and four singularities attributed to four cases where two roots r_k converge for four values of q. The method also permits the construction of important classical scaling laws obeyed by the form factor for any $i\to f$ transition, involving bound or continuum states. Use of these scaling rules then facilitates a detailed investigation of the rate of convergence of the quantal results to the classical background, as n is increased. The quantal results at high n are shown to reduce to oscillatory structure superimposed on the classical background, as in Fig. 5. The rate of this convergence is accelerated upon averaging, in succession, over the m substates and then the l states, as for the $nl\to n'l'$ and $n\to n'$ transitions displayed in Figs. 6 and 7, respectively. Figures 5–7 also illustrate that classical form factors have the capability to operate as an effective and reliable averaged version of its quantal counterpart. This is of particular significance to experiments that involve very high values of $n\simeq 400$, as in the half-cycle experiments of Bromage and Stroud [4].

In summary, the phase-space distribution method [13] has permitted (a) universal scaling laws for the classical form factor to be immediately derived in transparent form, (b) the construction of an analytic expression (50) for the form factor for state-to-state transitions in a system with general interaction $V(r)$, and (c) the detailed numerical investigation

of the convergence of the quantal form factors onto the classical background.

ACKNOWLEDGMENTS

This work has been supported by AFOSR Grant No. 49620-99-1-0277 and NSF Grant No. 01-00890.

APPENDIX: COMPONENT OF ANGULAR MOMENTUM ALONG $\hat{\mathbf{q}}$

When the axis $\hat{\mathbf{z}}$ of atomic quantization is along the direction $\hat{\mathbf{q}}$ of the impulse, then

$$(\mathbf{r}\times\mathbf{p})\cdot\hat{\mathbf{z}}\equiv\frac{\mathbf{r}}{q}\cdot[\mathbf{p}\times(\mathbf{p}+\mathbf{q})]=\left[\frac{rp}{q}|\mathbf{p}+\mathbf{q}|\right]\sin\theta_{if}\cos\theta,$$

where the angles θ_{if} and θ are depicted in Fig. 3.

From the spherical triangles ABC and ABD, then

$$\frac{\sin V_i}{\sin U_f}=\frac{\sin V_f}{\sin U_i}=\frac{\sin A}{\sin\theta_{if}}$$

and

$$\cos\theta=\sin U_i\sin V_i,$$

respectively, so that

$$(\mathbf{r}\times\mathbf{p})\cdot\hat{\mathbf{z}}=\left[\frac{rp}{q}|\mathbf{p}+\mathbf{q}|\right]\sin U_i\sin U_f\sin A.$$

Since $\sin U_i=L_i/rp$ and $\sin U_f=L_f/r|\mathbf{p}+\mathbf{q}|$, then

$$(\mathbf{r}\times\mathbf{p})\cdot\hat{\mathbf{z}}=\left(\frac{L_iL_f}{qr}\right)\sin A,$$

as in Eq. (48) of the text. From spherical triangle ABC, the angle A is determined from

$$\cos A=\frac{\cos\theta_{if}-\cos U_i\cos U_f}{\sin U_i\sin U_f},$$

where

$$\cos\theta_{if}=\frac{p^2+|\mathbf{p}+\mathbf{q}|^2-q^2}{2p|\mathbf{p}+\mathbf{q}|}.$$

Since $p\cos u_i=\mu\dot{r}_i$ and $|\mathbf{p}+\mathbf{q}|\cos u_f=\mu\dot{r}_f$ in terms of the radial speeds, then A is determined from

$$\cos A_\pm=\left(\frac{r^2}{2L_iL_f}\right)[p^2+|\mathbf{p}+\mathbf{q}|^2\pm2\mu^2\dot{r}_i\dot{r}_f].$$

Under the constraints (41) and (42), then

$$\cos A_\pm=\frac{r^2}{2L_iL_f}C_\pm(r),$$

where

$$\begin{aligned}C_\pm(r)&=2\mu[E_i+E_f-2V(r)]\pm2\mu^2\dot{r}_i\dot{r}_f-q^2\\&=2\mu[E_i+E_f-2V(r)]\pm4\mu\left[E_i-V(r)-\frac{L_i^2}{r^2}\right]^{1/2}\\&\quad\times\left[E_f-V(r)-\frac{L_f^2}{r^2}\right]^{1/2}-q^2,\end{aligned}$$

as in Eq. (46) of the text.

[1] D. Vrinceanu and M. R. Flannery, Phys. Rev. Lett. **82**, 3412 (1999).
[2] M. R. Flannery, Phys. Rev. A **22**, 2408 (1980).
[3] C. O. Reinhold, J. Burgdörfer, M. T. Frey, and F. B. Dunning, Phys. Rev. Lett. **79**, 5226 (1997).
[4] J. Bromage and C. R. Stroud, Phys. Rev. Lett. **83**, 4963 (1999).
[5] B. E. Tannian *et al.*, J. Phys. B **32**, L517 (1999).
[6] E. M. Spain *et al.*, J. Chem. Phys. **102**, 9522 (1995).
[7] E. M. Spain *et al.*, J. Chem. Phys. **102**, 9532 (1995).
[8] W. A. Isaacs and M. A. Morrison, Phys. Rev. A **57**, R9 (1998).
[9] M. A. Morrison, E. G. Layton, and G. A. Parker, Phys. Rev. Lett. **84**, 1415 (2000).
[10] N. E. Shafer-Ray, M. A. Morrison, and G. A. Parker, J. Chem. Phys. **113**, 4274 (2000).
[11] S. K. Dutta *et al.*, Phys. Rev. Lett. **86**, 3993 (2001).
[12] M. R. Flannery and D. Vrinceanu, Phys. Rev. Lett. **85**, 1 (2000).
[13] D. Vrinceanu and M. R. Flannery, Phys. Rev. A **60**, 1053 (1999).
[14] I. Bersons and A. Kulsh, Phys. Rev. A **55**, 1674 (1997).
[15] K. Omidvar, Phys. Rev. **188**, 140 (1969).
[16] A. O. Barut and H. Kleinert, Phys. Rev. **160**, 1149 (1967).
[17] I. Bersons, A. Kulsh, and R. Veilande, Phys. Lett. A **277**, 223 (2000).
[18] D. Vrinceanu and M. R. Flannery, Phys. Rev. A **63**, 032701 (2001).

PHYSICAL REVIEW A **68**, 030502(R) (2003)

Quantal and classical radiative cascade in Rydberg plasmas

M. R. Flannery[1,2] and D. Vrinceanu[2]
[1]*School of Physics, Georgia Institute of Technology, Atlanta, Georgia 30332, USA*
[2]*ITAMP, Harvard-Smithsonian Center for Astrophysics, Harvard University, Cambridge, Massachusetts 02138, USA*
(Received 4 February 2003; published 11 September 2003)

Atoms in high-(n,ℓ) states formed in cold Rydberg plasmas decay to the ground state in a succession of radiative transitions populating intermediate excited states. A classical treatment presents radiative cascade in a physically transparent way and reveals the "trajectory" in $n\ell$ space obeyed by the cascade, scaling rules, and other aspects hidden within the quantal approach. Quantal-classical correspondence in radiative decay is directly demonstrated. Classical transition probabilities are also presented and are in excellent agreement with quantal transition probabilities, even for moderate quantum numbers.

DOI: 10.1103/PhysRevA.68.030502 PACS number(s): 32.70.Cs, 31.15.Gy, 32.30.Jc, 32.80.Rm

Cold Rydberg plasmas, wherein electrons and ions coexist with atoms $R(nl)$ in highly excited Rydberg states n,ℓ have recently been produced by direct laser excitation [1] or ionization [2] of atoms initially prepared at submillikelvin temperatures. In the ATRAP experiment at CERN, levels $n \geqslant 50$ of antihydrogen at 4 K are observed [3]. In these three experiments, the basic processes [4] include three-body recombination which mainly produces Rydberg or anti-Rydberg atoms in high-$\ell \sim n-1$ circular states, which have very long lifetimes $\tau_{n\ell} \sim n^3\ell^2$ towards spontaneous radiative decay. Stark mixing [5] by the electric microfields and collision with ultraslow ions then produce a redistribution of the angular momentum towards much lower ℓ, which, because of the increased electrodynamical $e^- - R^+$ interaction at the pericenter of the highly eccentric orbits, radiate $\sim n^2$ times faster than the high-ℓ states. Theoretical analysis of ultracold Rydberg plasmas involves the distribution of Rydberg atoms over *both* n and ℓ so that the standard collisional-radiative models [6] must be extended. Such an inclusion increases dramatically the computational and numerical difficulties, since the dimension of the required array increases from n^2 to n^4, enough to render direct calculation unfeasible and physical interpretation intractable. Moreover, the well-known Gordon formula [7] for the required radiative transition probabilities becomes numerically unstable for $n \geqslant 50$, even with special numerical algorithms and substantial numerical effort. Some physical transparency is therefore required.

In this paper, we investigate the energy route preferred in radiative cascade of an excited atom in an initially prepared Rydberg level $n\ell$. In so doing, we advance a remarkably accurate classical theory of the subsequent trajectory in $n\ell$ space produced by radiative cascade and illustrate a powerful classical-quantal correspondence at work. A classical treatment of the transition probability (Einstein A coefficient) is also provided. It is worth noting that classical theory of radiative decay was not vigorously pursued after 1930, presumably due to its prediction that the accelerating spiraling electron will ultimately pass through the Coulomb force center, an untenable feature evident for those lowest-n and -ℓ states, the only states then accessible to experimental observation. For high-n states, however, we shall show that the classical picture developed here works remarkably well, even for states with $\ell/n \geqslant 0.2$ which includes the majority of Rydberg states created in the ultracold Rydberg plasmas recently observed [1–3].

The instantaneous classical power of photon emission from an atom with energy E is given by the Larmor formula [8,9]

$$I = \frac{2}{3}\frac{e^2}{c^3}|\ddot{\mathbf{r}}|^2 = -\frac{dE}{dt} = -\mathbf{F}\cdot\dot{\mathbf{r}}, \tag{1}$$

where $\mathbf{F}$ is the (Abraham-Lorentz) force [8] exerted on the atom during photoemission. On assuming that $\mathbf{F}$ is small compared with the Coulomb attraction, then on averaging over the electronic period $T_n = 2\pi n^3 \tau_{au}$, where τ_{au} is the *au* of time, and following Refs. [8,9], the secular rate of change in quantum number n is given by

$$\frac{dn}{dt} = -\frac{A_0}{\ell^5}\left(1 - \frac{\ell^2}{3n^2}\right), \tag{2}$$

where $A_0 = \alpha_{FS}^3/\tau_{au} = 1.6065 \times 10^{10}\ \mathrm{s}^{-1}$ is the characteristic rate for radiative processes and α_{FS} is the fine-structure constant. The secular rate of change in angular momentum $L = l\hbar$ is obtained upon similar averaging [8,9] as

$$\frac{d\ell}{dt} = -\frac{2}{3}\frac{A_0}{n^3\ell^2}. \tag{3}$$

A classical estimate [10] of the characteristic time $\tau_{n\ell}$ of radiative decay to all lower $n,\ell-1$ states is obtained by equating (3) with $-1/\tau_{n\ell}$ to yield $\tau_{n\ell} = 93.37 n^3\ell^2$ ps. Many orbits occur during radiative decay, since this radiative decay time $\tau_{n\ell} \gg T_n$, the orbital period.

Combining Eqs. (2) and (3) yields

$$\frac{dn}{d\ell} = \frac{3}{2}\frac{n^3}{\ell^3}\left(1 - \frac{\ell^2}{3n^2}\right). \tag{4}$$

Since Eq. (4) is always positive, both n and ℓ change in the same direction, in accord with the quantal propensity rule [6]. The solution of Eq. (4) yields $n^2 = \ell^2/(1 - C\ell^3)$, where the quantity

$$C(n_0,\ell_0) = \frac{1 - \ell_0^2/n_0^2}{\ell_0^3} = \frac{1 - \ell^2/n^2}{\ell^3} \tag{5}$$

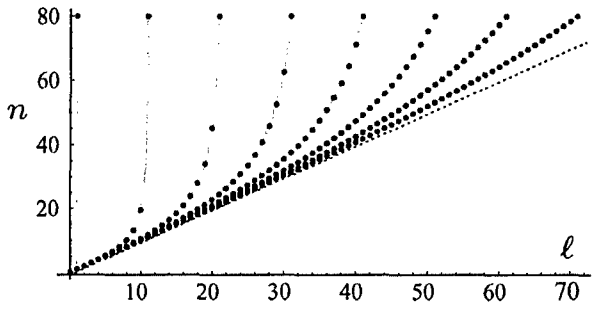

FIG. 1. (Color online) "Trajectories" in (n,ℓ) space for initial states $l_0=1,11,21,31,41,51,61,71$ within the $n_0=80$ shell. Dots correspond to a change of one unit of angular-momentum quantum number ($\Delta\ell=-1$). The dashed diagonal line $\ell=n$ represents transitions between circular states.

is determined by the initial state $n_0\ell_0$ and remains conserved throughout the radiative cascade process. The $n\ell$ states subsequently populated are illustrated in Fig. 1 where ℓ successively decreases by one unit. Each trajectory is characterized by different values of $C(n_0,\ell_0)$, which can vary between 0, for circular ($\ell_0=n_0$) states, and 1, for eccentric ($\ell_0=1$) high-n_0 states. Circular states decay along the diagonal line ($C=0$) of Fig. 1 as $(n,\ell=n)\rightarrow(n-1,\ell'=n-1)\rightarrow(n-2,\ell''=n-2),\ldots,$ while states with lower angular momentum (and $C>0$) will decay by making increasingly larger jumps

$$\Delta n_c=n-\frac{\ell-1}{\left[1-(1-\ell^2/n^2)\left(\frac{\ell-1}{\ell}\right)^3\right]^{1/2}}, \tag{6}$$

from level n in the $\ell\rightarrow\ell-1$ transition. Direct calculation of the corresponding quantal expression for the averaged change in the principle quantum number

$$\Delta n_q=\left(\sum_{n'=\ell}^{n-1}(n-n')A_{n\ell\rightarrow n'\ell-1}\right)\Big/\sum_{n'=\ell}^{n-1}A_{n\ell\rightarrow n'\ell-1}$$

in terms of probabilities $A_{i\rightarrow j}$ for $i\rightarrow j$ transitions show agreement with the classical prediction (6), even for moderate $n\sim20$, over an extensive range of ℓ.

Thus, the Bohr correspondence (which predicts $\Delta n=1$ transitions along the diagonal line of circular states) is generalized via Eq. (6) for decay of general noncircular states. Figure 1 also clearly illustrates that any initial orbit will eventually become increasingly circular during the cascade process. The coupled equations (2) and (3) can be solved in analytic form to provide the duration τ of $n_0\ell_0\rightarrow n,\ell$ transitions as

$$A_0\tau=\frac{n_0\ell_0^5}{\left(1+\frac{\ell_0}{n_0}\right)^2}-\frac{n\ell^5}{\left(1+\frac{\ell}{n}\right)^2}. \tag{7}$$

It is worth noting that Eq. (7) predicts $A_0\tau=3n^5/2$ for transitions between circular states, in agreement with the high n limit of the calculated quantal transition rate

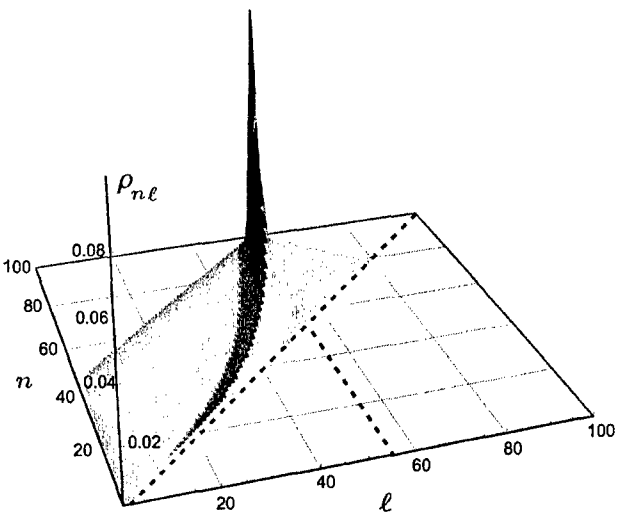

FIG. 2. (Color online) The steady-state quantal distribution $\rho_{n\ell}$ of $n\ell$ states populated by the radiative cascade originating from a source maintained at level $n_0=100$, $\ell_0=55$. The quantal ridge follows the prescribed classical trajectory (5).

$$A_{n,n-1\rightarrow n-1,n-2}=\frac{(2n-1)A_0}{3n^4(n-1)^2}\left[\frac{2^4n^2(n-1)^2}{(2n-1)^4}\right]^n. \tag{8}$$

The set of coupled rate equations for the time-dependent quantal evolution of population $\rho_{n\ell}(t)$ involved in the cascade from the initially populated level (n_0,ℓ_0) are

$$\frac{d\rho_{n\ell}}{dt}=\sum_{n'=n+1}^{n_0}\rho_{n'\ell+1}(t)A_{n'\ell+1\rightarrow n\ell}+\sum_{n'=n+1}^{n_0}\rho_{n'\ell-1}(t)A_{n'\ell-1\rightarrow n\ell}-\rho_{n\ell}(t)\left(\sum_{n'=\ell}^{n-1}A_{n\ell\rightarrow n'\ell-1}+\sum_{n'=\ell}^{n-1}A_{n\ell\rightarrow n'\ell+1}\right).$$

The steady-state solution, subject to the constant source represented as $\rho_{n_0\ell_0}(t)=1$ at all times, is shown in Figs. 2 and 3. It is seen that the quantal distribution over the $n\ell$ plane exhibits (a) a sharp ridge which follows the deduced classical trajectory (5) and is (b) skewed (Fig. 3) towards the left, indicating the predominance of $\ell\rightarrow\ell-1$ downward transitions, in accord with a propensity rule [7]. The quantal-classical correspondence illustrated by Figs. 2 and 3 may be explained as follows. The quantal rate that energy $E_{if}=\hbar\omega_{if}$ is radiated is the power [7]

$$I_{if}=\hbar\omega_{if}A_{if}=\frac{4}{3}\frac{e^2}{c^3}(E_{if}/\hbar)^4|\mathbf{r}_{if}|^2, \tag{9}$$

where $\mathbf{r}_{if}$ is the dipole electronic matrix element $\langle\phi_{n_f\ell_fm_f}|\mathbf{r}|\phi_{n_i\ell_im_i}\rangle$. Since $\ddot{\mathbf{r}}_{if}=-\omega_{if}^2\mathbf{r}_{if}$ exactly, when exact wave functions $\phi_{i,f}$ are used, the total power radiated into all lower states is

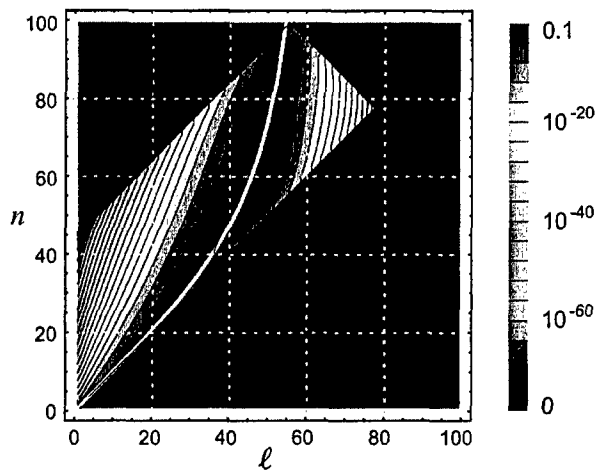

FIG. 3. (Color online) Two-dimensional representation of Fig. 2 but with quantal isodistributions represented by lines with magnitudes determined by each color code on the right hand side. The white line is the classical ridge (5).

$$I_i=\frac{4}{3}\frac{e^2}{c^3}\sum_{f<i}|\ddot{\mathbf{r}}_{if}|^2.$$

The sum $\Sigma_{allf}|\ddot{\mathbf{r}}_{if}|^2=\langle\ddot{\mathbf{r}}^2\rangle_i$ is dominated by a symmetric band of states centered about the highly excited level i. Then $\Sigma_{f<i}|\ddot{\mathbf{r}}_{if}|^2=\frac{1}{2}\langle\ddot{\mathbf{r}}^2\rangle_i$ and

$$I_i=\frac{2}{3}\frac{e^2}{c^3}\langle\ddot{\mathbf{r}}^2\rangle_i \tag{10}$$

in agreement with Larmor's theorem (1), from which Eqs. (5) and (6) followed upon a corresponding classical average. The present classical approach based on Eq. (1) is therefore expected to be valid for n and ℓ large enough that radiative decay is confined to within a band of neighboring levels. It is therefore expected to be inadequate for low-ℓ core penetrating electrons where the stronger interactions induce larger quantum jumps to levels outside the band. Based on the success that the quantal ridge in Figs. 2 and 3 follows the energy route classically prescribed by Fig. 1, it is now worthwhile exploring classical rates for $i\rightarrow f$ transitions between two discrete levels. The position $\mathbf{r}$ of the electron in initial state $i\equiv n_i\ell_i m_i$ and executing bounded periodic motion with constant angular frequency ω can be Fourier decomposed as

$$\mathbf{r}(i;\theta,\psi,\phi)=\sum_{\mathbf{s}}\mathbf{r}_{\mathbf{s}}(i)\exp i(s_1\theta+s_2\psi+s_3\phi), \tag{11}$$

where the sum is over all $\mathbf{s}\equiv\{s_1,s_2,s_3\}$, where $\theta=\omega t+\delta$ is the angular position of the particle in the orbital plane whose orientation is determined by the constant Euler angles ($\Theta=\cos^{-1}m/l,\phi,\psi$). This permits the time average $\langle I\rangle_{T_n}$ of the Larmor power (1) to be decomposed as $\Sigma_{\mathbf{s}\geq\mathbf{0}}I_{\mathbf{s}}$, where each component

$$I_{\mathbf{s}}=\frac{4}{3}\frac{e^2}{c^3}(s_1\hbar\omega/\hbar)^4|\mathbf{r}_{\mathbf{s}}(i)|^2. \tag{12}$$

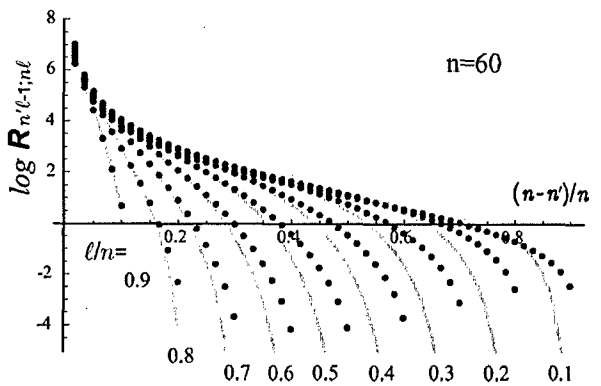

FIG. 4. (Color online) Quantal (blue dots) and classical [(13), red lines] radial matrix elements as a function of scaled change $s/n=(n-n')/n$ for various initial-state ratios ℓ/n from 0.9 to 0.1 in steps of 0.1. The ordinate axis uses a base-10 logarithm.

When compared with Eq. (9), Eq. (12) provides the Bohr [11]-Van Vleck [12] correspondence principle, which equates the power of line spectra between equally spaced levels $E_{if}=s_1\hbar\omega$ (the Bohr frequency theorem [11]) with the power associated with the sth harmonic of the classical motion of state i. The correspondence also holds provided $\mathbf{r}_{if}=\mathbf{r}_{\mathbf{s}}(i)$, where $s_1=n_f-n_i, s_2=\ell_f-\ell_i, s_3=m_f-m_i$, which is the Heisenberg form [13] of a correspondence principle for matrix elements. Since $\mathbf{r}$ is real, $\mathbf{r}_{\mathbf{s}}(i)=\mathbf{r}_{-\mathbf{s}}(i)$, as also assumed within the derivation of Eq. (10). Moreover, $\mathbf{r}_{if}\approx\mathbf{r}_{\mathbf{s}}(i)$ and $\mathbf{r}^*_{fi}\approx\mathbf{r}^*_{-\mathbf{s}}(f)$, where i or f denote taking the parameters for the initial or final orbits, respectively. For $i=n_i\ell\rightarrow f=n_f\ell\pm1$ transitions, calculation of the Fourier coefficients $\mathbf{r}_{\mathbf{s}}(j)$ in Eq. (11) for the initial and final classical orbits $j=i,f$ then provides the new correspondence

$$|\mathbf{r}_{if}|^2=\mathbf{r}_{if}\mathbf{r}^*_{fi}\approx\mathbf{r}_{\mathbf{s}}(i)\mathbf{r}^*_{-\mathbf{s}}(f)=\frac{\ell_>}{2\ell+1}R_i(s)R_f(s), \tag{13}$$

which is symmetrical with respect to the "classical" radial matrix elements

$$R_j(s)=\frac{a_j}{2s}\left[\left(1-\Delta\ell\frac{\ell_j}{n_j}\right)J_{s-1}(s\epsilon_j)-\left(1+\Delta\ell\frac{\ell_j}{n_j}\right)J_{s+1}(s\epsilon_j)\right].$$

Here $a_j=n_j^2a_0, \epsilon_j=(1-\ell_j^2/n_j^2)^{1/2}$, $s=(n_i-n_f)>0$, $\Delta\ell=\mp1$, and $J_{s\pm1}$ are Bessel functions of order $s\pm1$. Since $R_i(s)R_f(s)$ in Eq. (13) is our classical representation of the standard [7] quantal radial matrix element $R^2_{n_i\ell,n_f\ell\pm1}$, then under radial correspondence alone, our classical version of the A coefficient for $i\rightarrow f$ transitions in Eq. (9) is, therefore,

$$A_{n_i\ell_i\rightarrow n_f\ell_f}=\frac{4A_0}{3}\frac{\ell_>}{2\ell+1}\left(\frac{n_i^2-n_f^2}{2n_i^2n_f^2}\right)^3R_i(s)R_f(s), \tag{14}$$

where only the Heisenberg correspondence $\mathbf{r}_{if}\approx\mathbf{r}_{\mathbf{s}}(i)$ and $\mathbf{r}^*_{fi}\approx\mathbf{r}^*_{-\mathbf{s}}(f)$ is used. Expressions (13) and (14), symmetric in the initial and final states, are proved to be valid and much more accurate over a much more extensive range of $s=(n_i-n_f)$ than those obtained [14] from the assumption in Eq. (12) that $|\mathbf{r}_{if}|^2\approx R_i(s)^2/2$. This distinction, as derived in the

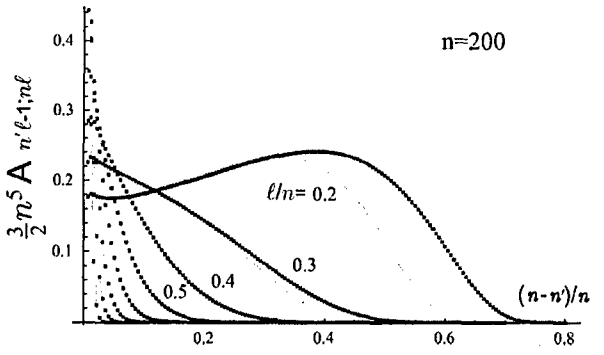

FIG. 5. (Color online) Quantal (blue dots) and classical [(13), red lines] transition rates $A_{200\ell\to n'\ell-1}$ times $\tau_{n,n\to n-1,n-1}=3n^5/2A_0$, as a function of $(n-n')/n$ for various initial scaled angular-momentum values ℓ/n from 0.9 to 0.2 in steps of 0.1.

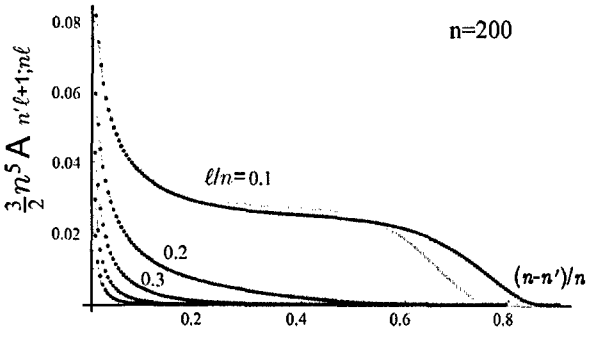

FIG. 6. (Color online) As in Fig. 5, but for $[200,\ell\to n',(\ell+1)]$ transitions for $\ell/n=0.1-0.5$.

new correspondence (14) is important, particularly for intermediate and large values of s when the approximation $R_i(s)\approx R_f(s)$ breaks down, being valid only for $s\sim 1,2,3$. Figure 4 for $n\ell\to n'(\ell-1)$ transitions shows that the quantal and classical radial matrix elements, $R^2_{n\ell,n'\ell\pm1}$ are in excellent agreement over an extensive range in $s=n-n'$ as ℓ is varied from $0.9n$ to $0.1n$. Figure 4 illustrates also that the stronger e-ion interaction at the pericenter for low ℓ orbits induces transitions over a broader range of s, in contrast to transitions with small s characteristic of near circular (higher ℓ) orbits.

The quantal and classical transition probabilities are compared in Figs. 5 and 6 for $\ell\to\ell\mp1$ downward transitions. The agreement is excellent, particularly for large angular momenta, circular states, in accord with Bohr's $\Delta n=1$ correspondence. It is less good for elongated states with low angular momenta (which favor larger n changes) because the equally spaced levels approximation within the Heisenberg correspondence becomes less accurate and because the E^3_{if} factor in Eq. (14) amplifies any error in $R_{i,f}(s)$. Note that the probabilities for $\ell\to\ell-1$ downward transitions are much higher by a factor of 10^2 than those for $\ell\to\ell+1$ transitions, as illustrated also in Figs. 2 and 3. The extent of quantal-classical agreement shown in Figs. 2–6 is representative for all $n\geq 10$. The present classical radiative rates are much easier to evaluate correctly than their quantal counterparts.

In summary, the classical treatment of radiative decay outlined here has proven to be accurate, particularly for Rydberg states with $\ell/n\geq 0.1$ (preponderant in recombination) and has provided an accurate yet physically transparent picture of radiative cascade of Rydberg states. The deduced trajectory in $n\ell$ space obeyed by radiative cascade origination from a constant source is confirmed by quantal calculation. The deduced classical invariant (5) has, as yet, no quantal analog, indicating a hidden symmetry. The theory is further developed, via Eq. (13) in Eq. (9), to provide here a symmetrized new version of the power correspondence (12) and a classical version (14) of Einstein transition rates, to a high degree of accuracy. It is particularly appropriate for the analysis of Rydberg plasmas over (n,ℓ) and for the proposed deactivation of the high $n\geq 50$ states in the ATRAP experiment by laser deexcitation methods, subjects of intense current theoretical and experimental interest.

This work was supported by AFOSR Grant No. 49620-02-1-0338 and NSF Grant No. 01-00890 and by a NSF Grant to ITAMP at the Harvard University-Smithsonian Astrophysical Observatory.

[1] M.P. Robinson *et al.*, Phys. Rev. Lett. **85**, 4466 (2000).
[2] T.C. Killian *et al.*, Phys. Rev. Lett. **86**, 3759 (2001).
[3] G. Gabrielse *et al.*, Phys. Rev. Lett. **89**, 213401 (2002).
[4] M.R. Flannery and D. Vrinceanu, in *Atomic Processes in Plasmas*, edited by E. Oks and M.S. Pindzola (AIP Press, New York, 1998), pp. 317–333.
[5] D. Vrinceanu and M.R. Flannery, Phys. Rev. **63**, 032701 (2001).
[6] B. Zygelman, J. Phys. B **36**, L31 (2003)
[7] H.A. Bethe and E.E. Salpeter, *Quantum Mechanics of One-and Two-Electron Atoms* (Plenum, New York, 1977), pp. 262, 259, and 250.
[8] J.D. Jackson, *Classical Electrodynamics* (Wiley, New York, 1998), p. 770.
[9] L.D. Landau and E.M. Lifshitz, *The Classical Theory of Fields* (Pergamon, Oxford, 1987), p. 187.
[10] K. Omidvar, Phys. Rev. **26**, 3053 (1982); E.S. Chang, *ibid.* **31**, 495 (1985); H. Marxer and L. Spruch, *ibid.* **43**, 1268 (1991).
[11] N. Bohr, in *Sources of Quantum Mechanics*, edited by B.L. Van der Waerden (Dover, New York, 1968), p. 95.
[12] J.H. Van Vleck, Phys. Rev. **24**, 330 (1924).
[13] W. Heisenberg, Z. Phys. **33**, 879 (1925); in *Sources of Quantum Mechanics* (Ref. [11]), p. 261.
[14] P.F. Naccache, J. Phys. B **5**, 1308 (1972); I.C. Percival and D. Richards, Adv. At., Mol., Opt. Phys. **11**, 1 (1975).

INSTITUTE OF PHYSICS PUBLISHING JOURNAL OF PHYSICS B: ATOMIC, MOLECULAR AND OPTICAL PHYSICS

J. Phys. B: At. Mol. Opt. Phys. **38** (2005) S279–S293 doi:10.1088/0953-4075/38/2/020

Long-range interaction between polar Rydberg atoms

M R Flannery[1,2], D Vrinceanu[2] and V N Ostrovsky[3]

[1] School of Physics, Georgia Institute of Technology, Atlanta, GA 30332, USA
[2] ITAMP, Center for Astrophysics, Harvard University, Cambridge, MA 02138, USA
[3] V Fock Institute of Physics, St Petersburg State University, 198904 St Petersburg, Russia

Received 16 August 2004
Published 5 January 2005
Online at stacks.iop.org/JPhysB/38/S279

Abstract

The most attractive and the most repulsive potential-energy curves for interaction between two Rydberg atoms in a broad superposition of internal angular momentum states are studied. The extreme Stark states have the largest dipole moments and provide the dominant contribution to the interaction which is then expressed as a long-range expansion involving the *permanent* multipole moments Q_j of each *polar* atom. Analytical expressions are obtained for all Q_j associated with principal quantum number n of H(n) and permit the long-range expansion for the H(n)–H(n') *first-order interaction* to be explicitly expressed analytically in terms of n, n' and internuclear distance R. Possible quasi-molecular formation is investigated. Direct calculations show that the H($n = 2$)–H($n' = 2$) interaction is capable of supporting 47 bound vibrational levels. As n increases, the long-range interaction becomes increasingly attractive so that molecular formation at large internuclear distances is expected to be scarcely possible for these extreme Stark levels.

(Some figures in this article are in colour only in the electronic version)

1. Introduction

A new branch of atomic physics—the interactions, dynamics and collisions in ultracold ($T \ll 1K$) systems—has naturally evolved from recent advances in the cooling and trapping of neutral gases. Giant helium dimer molecules have been recently produced [1] via photo-association of ultracold metastable atoms. Such long-range molecules attract considerable attention [1–4], with possible application to quantum computing [5] and dipole blockade [6]. The long-range molecules considered up to now are those formed from atoms [1–4] with low-ℓ electron-core penetrating states, as He(2^3S_1) and He(2^3P_0), appropriate to photo-association experiments.

We now consider the interaction between two Rydberg atoms with internal electronic angular momentum spread over a broad distribution of ℓ values, characteristic of Rydberg atoms placed in a weak electric field. Three-body electron–ion recombination produces

Rydberg atoms mainly in high ℓ-states. Subsequent Stark mixing [7, 8] within the Rydberg manifold by collision with ions provides Rydberg atoms with a broad superposition of ℓ states. The relative number of states which do not penetrate the non-Coulomb core with consequent vanishingly small quantum defects increases with n. They remain degenerate, just as for atomic hydrogen, being easily intermixed [7, 8] within the n-manifold even by the slightest perturbations by microfields or ion impact. These states are sufficiently flexible that a *permanent dipole* and higher *permanent multipoles* Q_j are created quite easily out of the large number $\sim n^2$ of degenerate angular momentum states ℓ within the energy shell. These Rydberg atoms can be called 'polar' because they possess permanent multipole moments.

In this paper, we present the physics of the long-range interaction between these polar Rydberg atoms and investigate the possible formation of long-range molecules from two Rydberg atoms with the same (or different) principal quantum numbers n, but with a broad superposition of many degenerate (non-core-penetrating) angular momentum states ℓ. In the long-range interaction between two Rydberg atoms, the degeneracy of the energy shells has profound and decisive consequences. Its account represents a challenging quantum mechanical problem which has not received any previous theoretical attention. Our aim here is to first identify the physics and mechanism of the interaction between two degenerate Rydberg atoms. We then obtain analytical expressions for the various multipoles Q_j as a function of n which allows the coefficients of the long-range expansion to be calculated purely in algebraic terms. The long-range interactions so determined are of basic interest in this rapidly evolving field and will also be useful for various processes involving ultracold Rydberg atoms e.g., for Penning ionization, an important process required to sustain ultracold Rydberg plasmas.

2. Theory

Interaction between atoms in low $n \approx 2, 3$ levels can be calculated [4] by conventional *ab initio* numerical techniques, but for highly excited atoms $n \gg 1$, the treatment becomes prohibitively difficult and impractical. Binding of the purely long-range molecule $He(2^3S_1)$–$He(2^3P_0)$ depends only on the long-range part of the atom–atom interaction, and the internuclear distance is always large compared with ordinary bond lengths [1]. The physically important region for the present Rydberg–Rydberg interaction is also over large nuclear separations R, dominated by long-range interactions which permit the use of a two-centre multipole expansion. The leading term is the dipole–dipole interaction $V_{dd} \sim R^{-3}$ and is given by *first-order degenerate* perturbation theory [9, 10]. The origin of this interaction is quite different from the weaker resonant excitation-transfer interaction [11] between an excited and unexcited atom of the same species, say in the s and p states, which also has the $\sim R^{-3}$ dependence. The next non-vanishing multipole contribution to the interaction also appears in *first-order degenerate* perturbation theory and is the electrostatic quadrupole–quadrupole interaction V_{qq} and the dipole–octupole interaction V_{do}, both of which $\sim R^{-5}$. In the absence of degeneracy, the interaction between two atoms in the same isolated state is the much weaker and shorter range induced dipole-induced dipole (van der Waals) potential $\sim R^{-6}$ which appears only in *second-order* perturbation theory. The aim here is now to calculate analytically the first-order interaction in terms of all the permanent multipoles associated with level n.

2.1. Multipole expansion

The interaction operator

$$\hat{V} = \frac{1}{R} - \frac{1}{r_{1B}} + \frac{1}{r_{12}} - \frac{1}{r_{2A}}$$

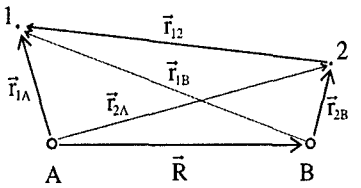

Figure 1. Two-centre coordinate system: two nuclei (A, B) and two electrons (1, 2).

between two atoms (figure 1) is given, at large separation R between the nuclei A and B located along the z-axis, by the multipole expansion [12]

$$\hat{V}(R\hat{\mathbf{z}}, \mathbf{r}_{1A}, \mathbf{r}_{2B}) = \sum_{L_1,L_2=1}^{\infty} \sum_{M=-L_<}^{L_<} \frac{(-1)^{L_2} f_{L_1L_2M}}{R^{L_1+L_2+1}} \hat{Q}_{L_1M}(\mathbf{r}_{1A}) \hat{Q}_{L_2-M}(\mathbf{r}_{2B}), \tag{1}$$

where the multipole operator for each atom with composite electronic coordinates $\mathbf{r}$ relative to each nucleus is

$$\hat{Q}_{LM}(\mathbf{r}) = \left\{ \frac{4\pi}{2L+1} \right\}^{1/2} r^L Y_{LM}(\hat{r}), \tag{2}$$

and where

$$f_{L_1L_2M} = \frac{(L_1+L_2)!}{[(L_1+M)!(L_1-M)!(L_2+M)!(L_2-M)!]^{1/2}}. \tag{3}$$

The phase factor $(-1)^{L_2}$ included here arises [12] from the A $\rightarrow$ B direction of $\mathbf{R}$ joining the nuclei, as in figure 1. Even with neglect of electron spin for the generic case of two interacting hydrogen atoms, H(n)–H(n), with equal principal quantum numbers n, there are as many as n^4 degenerate states within this $\{n, n\}$ manifold to be perturbed by the atom–atom interaction. As the internuclear distance R decreases from infinity, the degeneracy is first lifted by the dipole–dipole interaction operator and the dense bundle of initially degenerate electronic states broadens. These quasi-continuous energy bands, similar to the bands formed in periodic systems, originate from the large number of angular momentum states available in each atom. In general, highly correlated quasi-molecular states $\Psi(\mathbf{r}_{1A}, \mathbf{r}_{2B})$ emerge with the electron coordinates $\mathbf{r}_{1A}$ and $\mathbf{r}_{2B}$ quite intricately entangled [10]. The situation, however, becomes drastically simplified in the $n \gg 1$ case, for those states in the manifold which provide the strongest attraction or repulsion. These are given by a simple product of two one-electron orbitals, each of which is just the most elongated Stark (parabolic) state $\psi_{(n-1)00}(\mathbf{r})$ with the greatest dipole moment $d = 3n(n-1)/2$. Maximum interaction is ensured when both atomic dipoles are aligned along the molecular axis $\mathbf{R}$, so that

$$\Psi_{\mathrm{dd}}(\mathbf{r}_{1A}, \mathbf{r}_{2B}) = \psi_{(n-1)00}(\mathbf{r}_{1A})\, \psi_{(n-1)00}(\mathbf{r}_{2B}), \tag{4}$$

where $\psi_{n_1n_2m}(\mathbf{r})$ is the wavefunction (table 1) for the set of parabolic quantum numbers $\{n_1, n_2, m\}$, with $n = n_1 + n_2 + |m| + 1$ and with dipole moment $d = 3n(n_1 - n_2)/2$. The atomic wavefunctions in (4) are eigenstates of the dipole moments $\mathbf{r}_{1A}$ and $\mathbf{r}_{2B}$. The deviation of (4) from being an eigenfunction of the dipole–dipole operator,

$$\hat{V}_{\mathrm{dd}} = [\mathbf{r}_{1A} \cdot \mathbf{r}_{2B} - 3(\mathbf{r}_{1A} \cdot \hat{\mathbf{R}})(\mathbf{r}_{2B} \cdot \hat{\mathbf{R}})]R^3 \tag{5}$$

is measured by the mean square deviation

$$\langle (\Delta V)^2 \rangle = \langle \Psi_{\mathrm{dd}} | \hat{V}_{\mathrm{dd}}^2 | \Psi_{\mathrm{dd}} \rangle - \langle \Psi_{\mathrm{dd}} | \hat{V}_{\mathrm{dd}} | \Psi_{\mathrm{dd}} \rangle^2. \tag{6}$$

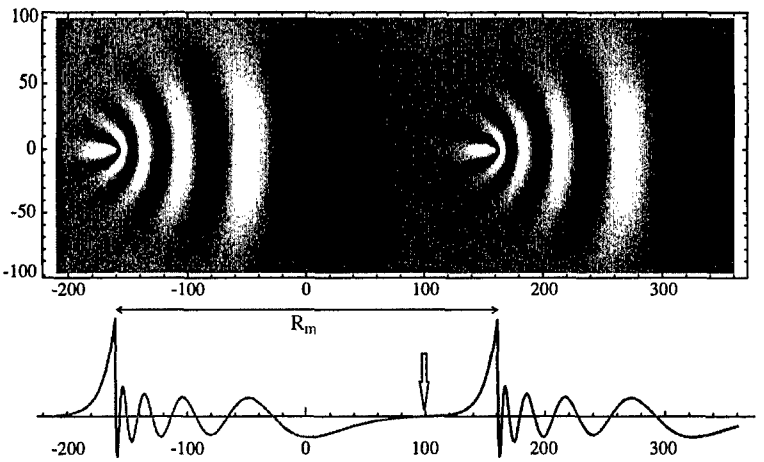

Figure 2. Wavefunctions for the two most elongated Stark orbitals, $\psi_{(n-1)00}(\mathbf{r} \pm \mathbf{R}_m/2)$ with $n = 10$, aligned along internuclear axis **R**. Each orbital is centred at its own nucleus with typical separation R_m (cf section 6). The orbital overlap is strongly suppressed and is maximum at the arrow.

Table 1. Four bases [8] useful for describing the quantal states of the hydrogen atom.

Basis	Quantum numbers	Complete set of commuting observable	Origin
Spherical	$\|n\ell m\rangle_O$	H_0, L^2, L_3	Standard for spherical coordinates; describes correctly the states of the field-free atom.
Parabolic	$\|n_1 n_2 m\rangle_P$	H_1, H_2, L_3	Separation of Hamiltonian $H = H_1 + H_2$ in parabolic coordinates, $\xi = r + z$, $\eta = r - z$, $\tan\varphi = y/x$; $= n_1 + n_2 + \|m\| + 1$.
Stark	$\|nkm\rangle_S$	H_0, A_3, L_3	Parabolic basis; describes the Stark states for small electric fields $\vec{\mathcal{E}} = \mathcal{E}\hat{k}$, diagonalizes the interaction $e\mathcal{E}z$ and gives energy shifts $\Delta E = \frac{3}{2}nke\mathcal{E} = -\vec{d}\cdot\vec{\mathcal{E}}$ where $k = n_1 - n_2$ is the electric quantum number and $\vec{d}$ is the vector dipole.
Algebraic	$\|nm_1m_2\rangle_A$	H_0, J_{13}, J_{23}	The two rotation groups in which the dynamic symmetry group $SO(4) \equiv SO(3) \oplus SO(3)$ is decomposed; the equivalent angular momentum for both $SO(3)$ representation is $j = (n-1)/2$; $m_1 = (m+k)/2$ and $m_2 = (m-k)/2$.

Direct numerical integration yields the dispersion in V_{dd} to be $\langle(\Delta V)^2\rangle^{1/2} = A(n)/R^3$ where $A = 6, 30, 152$ and 485 for $n = 1, 2, 3$ and 4, respectively. At $R = 4n^2$, the corresponding variances are then $(38.2, 7.32, 3.26, 1.85) \times 10^{-3}$, respectively. Therefore (4) becomes a better eigenfunction of the dipole–dipole operator (5) with increasing n provided R also increases as n^2 with the result that the variance tends to zero as n^{-2}. See also [10] for a similar conclusion. The wavefunction (4) is shown in figure 2.

From the four interesting basis sets in table 1 appropriate for the one electron hydrogen-like atom, it is sometimes convenient to adopt the equivalent $SO(3) \otimes SO(3)$ algebraic basis $|nm_1m_2\rangle$ where m_1 and m_2 are projections on the Z-axis of the two angular momentum

operators $\mathbf{J}_1$ and $\mathbf{J}_2$, given by

$$\mathbf{J}_1 = \tfrac{1}{2}(\mathbf{L}+\mathbf{A}), \qquad \mathbf{J}_2 = \tfrac{1}{2}(\mathbf{L}-\mathbf{A}), \tag{7}$$

where $\mathbf{A}$ is the electronic Runge–Lenz vector. Then $\mathbf{J}_1^2 = \mathbf{J}_2^2 = j(j+1) = \frac{1}{4}(n^2-1)$ with $j = \frac{1}{2}(n-1)$. This basis set permits exact quantal and classical solutions to be obtained [8] for collisional ℓ-mixing by the ion–dipole interaction in ion–Rydberg atom collisions. It is also valuable for expressing operators such as the dipole, quadrupole and octupole by equivalent operators [14] involving $\mathbf{J}_{1,2}$ so that all matrix elements can be evaluated algebraically.

The Stark (parallel and anti-parallel) states most stretched along the positive and negative directions of the Z-axis are respectively,

$$\psi_{(n-1)00}(\mathbf{r}_{1A}) \equiv |+\rangle = |n, j, -j\rangle, \tag{8}$$

$$\psi_{0(n-1)0}(\mathbf{r}_{2B}) \equiv |-\rangle = |n, -j, j\rangle, \tag{9}$$

in the parabolic and algebraic basis (table 1), respectively. Atom A in any of the states $|\alpha\rangle = |\pm\rangle$ has expectation value,

$$Q_L^A \equiv \langle\alpha|\hat{Q}_{LM}|\alpha\rangle = \langle\alpha|\hat{Q}_{L0}|\alpha\rangle\delta_{M0}, \tag{10}$$

where the multipole operator (2) is now

$$\hat{Q}_{L0} = r^L P_L(\hat{r}\cdot\hat{z}). \tag{11}$$

The expectation values Q_1, Q_2, Q_3 and Q_4 are the strengths of the dipole, quadrupole, octupole and hexadecapole, respectively. The average of interaction (1) over states $|\alpha\rangle_A$ of atom $A(n)$ and $|\beta\rangle_B$ of atom $B(n')$,

$$V(R) =_B \langle\beta|_A\langle\alpha|V(R\hat{\mathbf{z}}, \mathbf{r}_{1A}, \mathbf{r}_{2B})|\alpha\rangle_A|\beta\rangle_B, \tag{12}$$

is first order and can now be expanded in terms of the averaged multipoles Q_i for each atom in the form

$$V(R) \equiv \sum_{i=1}^{N}\sum_{j=1}^{N'} V_{ij} = \sum_{i=1}^{N}\sum_{j=1}^{N'}(-1)^j \frac{(i+j)!}{i!\,j!}\frac{Q_i^A Q_j^B}{R^{i+j+1}}, \tag{13}$$

where $N = 2(n-1)$ and $N' = 2(n'-1)$. Multipoles higher than Q_N^A and $Q_{N'}^B$ all vanish, due to angular momenta considerations. The interaction of the dipole Q_1^A of A with the various $(j = 1, 2, \ldots, 5)$ multipoles Q_j^B of B is

$$V_1 = \sum_{j=1}^{5} V_{1j} = -\frac{2}{R^3}Q_1^A Q_1^B + \frac{3}{R^4}Q_1^A Q_2^B - \frac{4}{R^5}Q_1^A Q_3^B + \frac{5}{R^6}Q_1^A Q_4^B - \frac{6}{R^7}Q_1^A Q_5^B.$$

The interaction of the quadrupole $\left(Q_2^A\right)$ of A with the $(j = 1, 2, 3, 4)$-multipoles of B is

$$V_2 = \sum_{j=1}^{4} V_{2j} = -\frac{3}{R^4}Q_2^A Q_1^B + \frac{6}{R^5}Q_2^A Q_2^B - \frac{10}{R^6}Q_2^A Q_3^B + \frac{15}{R^7}Q_2^A Q_4^B.$$

The interaction between the octupole $(i = 3)$ of A and the $(j = 1, 2, 3)$-multipoles of B is

$$V_3 = \sum_{j=1}^{3} V_{3j} = -\frac{4}{R^5}Q_3^A Q_1^B + \frac{10}{R^6}Q_3^A Q_2^B - \frac{20}{R^7}Q_3^A Q_3^B.$$

The interaction between the $i = 4$ multipole of A and the dipole and quadrupole of B is

$$V_4 = \sum_{j=1}^{2} V_{4j} = -\frac{5}{R^6}Q_4^A Q_1^B + \frac{15}{R^7}Q_4^A Q_2^B.$$

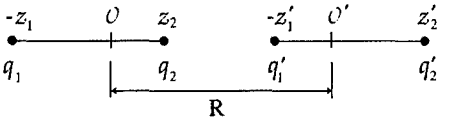

Figure 3. Two aligned linear charge distributions (q_1, q_2) and (q_1', q_2') with arbitrary origins O and O′ separated by distance R.

The interaction between the $i = 5$ multipole of A and the dipole of B is

$$V_5 = V_{51} = -\frac{6}{R^7} Q_5^A Q_1^B.$$

The full long-range multipole–multipole expansion (13) of the first-order interaction (12) to $O(R^{-8})$ is therefore

$$\begin{aligned} V(R) = &-\frac{2}{R^3} Q_1^A Q_1^B - \frac{3}{R^4}\left(Q_1^A Q_2^B - Q_2^A Q_1^B\right) - \frac{2}{R^5}\left[2\left(Q_1^A Q_3^B + Q_3^A Q_1^B\right) - 3Q_2^A Q_2^B\right] \\ &- \frac{5}{R^6}\left[\left(Q_1^A Q_4^B - Q_4^A Q_1^B\right) - 2\left(Q_2^A Q_3^B - Q_3^A Q_2^B\right)\right] - \frac{1}{R^7}\left[6\left(Q_1^A Q_5^B + Q_5^A Q_1^B\right)\right. \\ &\left. - 15\left(Q_2^A Q_4^B + Q_4^A Q_2^B\right) + 20 Q_3^A Q_3^B\right] + O(R^{-8}). \end{aligned} \tag{14}$$

Higher-order terms involve inclusion of multipoles higher than Q_5. It is apparent from the structure of (14) that symmetry considerations may reduce the overall number of terms in the expansion. For parallel aligned identical ($A = B$) linear systems, $Q_j^A = Q_j^B$ and the series (14) does not contain even powers of $1/R$. For anti-parallel aligned identical linear systems, $Q_j^A = (-1)^j Q_j^B$ and the series (14) contains all powers of $1/R$.

2.2. *Classical analogy*

Consider the two linear charge distributions displayed in figure 3. From electrostatics, the classical long-range interaction between them can be written as,

$$\begin{aligned} V(R) = &\frac{Q_0 Q_0'}{R} + \frac{Q_0 Q_1' - Q_1 Q_0'}{R^2} + \frac{Q_0 Q_2' - 2Q_1 Q_1' + Q_2 Q_0'}{R^3} \\ &+ \frac{Q_0 Q_3' - 3Q_1 Q_2' + 3Q_2 Q_1' - Q_3 Q_0'}{R^4} \\ &+ \frac{Q_0 Q_4' - 4Q_1 Q_3' + 6Q_2 Q_2' - 4Q_3 Q_1' + Q_4 Q_0'}{R^5} + \cdots, \end{aligned} \tag{15}$$

where $Q_n = q_1 z_1^n + (-1)^n q_2 z_2^n$ are the various classical multipoles for each distribution. For equal and opposite charges, $q_1 = -q_2 = q$, the monopole Q_0 is zero and (14) and (15) are formally identical. This is because the quantal interaction is electrostatic in origin and includes no second-order induced effects between the distributions. For parallel aligned identical systems, symmetry considerations eliminate terms in even powers of $1/R$, as with the quantal case (14). For zero monopole, only the dipole Q_1 is independent of the origin O. In general, the first non-zero multipole is origin independent. When O is taken at the centre of the charge distribution, then all even multipoles Q_{2n} vanish. When O is located at the nuclear charge q, as in figure 1, all the multipoles are non-zero. Also note that the quadrupole–quadrupole R^{-5}-term is always repulsive, classically and quantally.

3. Calculation of multipole matrix elements

The multipoles of interest are [13],

$$\hat{Q}_{L0} = \sqrt{\frac{4\pi}{2L+1}} r^L Y_{L0}(\hat{r}) = L! \sum_{\substack{q,r=0 \\ 2q+r=L}} \frac{1}{q!q!r!} \left(-\frac{x^2+y^2}{4}\right)^q z^r.$$

Calculation of the associated matrix elements for the atomic multipoles is best performed with parabolic coordinates ($\zeta = r+z, \eta = r-z, \varphi = \arctan y/x$) of table 1. The multipole operator then simplifies to

$$\hat{Q}_{L0} = \frac{1}{2^L} \sum_{s=0}^{L} \frac{(-1)^{L-s} L!^2}{(L-s)!^2 s!^2} \zeta^s \eta^{L-s}.$$

The most stretched Stark states are now,

$$|+\rangle = u_{n-100}(\zeta, \eta) = u_{n-1}(\zeta) u_0(\eta) = \frac{\mathrm{e}^{-(\zeta+\eta)/2n}}{(n-1)! n^2 \sqrt{\pi}} L_{n-1}(\zeta/n),$$

where $L_a(x)$ are Laguerre polynomials. The matrix elements of $\zeta^\alpha \eta^\beta$ are

$$\langle +|\zeta^\alpha \eta^\beta|+\rangle = \int u_{n-1}(\zeta)^2 \zeta^\alpha \eta^\beta \frac{\zeta+\eta}{4} \,\mathrm{d}\zeta \,\mathrm{d}\eta \,\mathrm{d}\varphi = \frac{n^{\alpha+\beta-1}}{2} \left[\beta! J_{n-10}^{(\alpha+1)} + (\beta+1)! J_{n-10}^{(\alpha)}\right],$$

where the elementary integrals J, as defined by Bethe and Salpeter [15], are

$$J_{\lambda\mu}^{(\sigma)} = \frac{1}{\lambda!^2} \int_0^\infty \mathrm{e}^{-\rho} \rho^{\mu+\sigma} \left[L_\lambda^\mu(\rho)\right]^2 \,\mathrm{d}\rho.$$

For the case of interest here, the matrix elements of the multipole operators of any order for the $|+\rangle$ states are therefore,

$$Q_L(+) \equiv \langle +|\hat{Q}_{L0}|+\rangle = \frac{n^{L-1}}{2^{L+1}} \sum_{s=0}^{L} \frac{(-1)^{L-s} L!^2}{s!^2 (L-s)!} \left[J_{n-1,0}^{(s+1)} + (L-s+1) J_{n-1,0}^{(s)}\right], \tag{16}$$

where $J_{\lambda\mu=0}^{(\sigma)}$ reduces to the analytical expression

$$J_{\lambda 0}^{(\sigma)} = (-1)^\sigma \sum_{r=\min(0,\sigma-\lambda)}^{\sigma} \frac{(-1)^r (\lambda+r)!^2}{r!(\sigma-r)!(\lambda+r-\sigma)!}. \tag{17}$$

A similar calculation provides the matrix elements over $|-\rangle$ states as

$$Q_L(-) \equiv \langle -|Q_{L0}|-\rangle = (-1)^L Q_L(+). \tag{18}$$

The matrix elements between all the Stark states of the algebraic basis (table 1) can also be calculated by equivalent operator techniques [14].

4. Analytical expressions for the permanent multipoles Q_L

Specific calculations are now required to investigate the attractive/repulsive nature of potential $V(R)$ when atomic electrons are in particular quantum states. We are interested in the case where both electrons are in the most stretched Stark states $|\pm\rangle$ aligned along the internuclear z-axis, both in the same direction [$V(R) \equiv V_{\rightarrow,\rightarrow}(R)$] or in opposite directions [$V(R) \equiv V_{\rightarrow,\leftarrow}(R)$]. These one-electron states are building blocks of the quasi-molecular state (4). We will then trace how the interaction responds to the successive introduction of the

quadrupole, octupole and higher multipoles into the long-range expansion (14). The input for this study are the permanent multipoles Q_L of individual atoms in the extreme Stark stretched states $|\pm\rangle$ of H(n). These are explicitly calculated as,

$$Q_0(+) = +Q_0(-) = 1,$$

$$Q_1(+) = -Q_1(-) = \frac{3}{2^1}n^1(n-1) \sim \frac{3}{2}n^2,$$

$$Q_2(+) = +Q_2(-) = \frac{2}{2^2}n^2(n-1)(5n-7) \sim \frac{5}{2}n^4,$$

$$Q_3(+) = -Q_3(-) = \frac{5}{2^3}n^3(n-1)(n-2)(7n-9) \sim \frac{35}{8}n^6,$$

$$Q_4(+) = +Q_4(-) = \frac{6}{2^4}n^4(n-1)(n-2)(21n^2-77n+62) \sim \frac{63}{8}n^8,$$

$$Q_5(+) = -Q_5(-) = \frac{42}{2^5}n^5(n-1)(n-2)(n-3)(11n^2-39n+30) \sim \frac{231}{16}n^{10},$$

$$Q_6(+) = +Q_6(-) = \frac{12}{2^6}n^6(n-1)(n-2)(n-3)$$
$$\times (143n^3-990n^2+2077n-1270) \sim \frac{429}{16}n^{12},$$

$$Q_7(+) = -Q_7(-) = \frac{9}{2^7}n^7(n-1)(n-2)(n-3)(n-4)$$
$$\times (715n^3-4862n^2+9977n-5950) \sim \frac{6435}{128}n^{14},$$

$$Q_8(+) = +Q_8(-) = \frac{10}{2^8}n^8(n-1)(n-2)(n-3)(n-4)$$
$$\times (2431n^4-27\,170n^3+105\,677n^2-165\,946n+85\,848) \sim \frac{12\,155}{128}n^{16},$$

$$Q_9(+) = -Q_9(-) = \frac{22}{2^9}n^9(n-1)(n-2)(n-3)(n-4)(n-5)$$
$$\times (4199n^4-46\,410n^3+178\,165n^2-275\,730n+140\,616) \sim \frac{46\,189}{256}n^{18},$$

$$Q_{10}(+) = +Q_{10}(-) = \frac{12}{2^{10}}n^{10}(n-1)(n-2)(n-3)(n-4)(n-5)$$
$$\times (29\,393n^5-482\,885n^4+298\,4605n^3-855\,8875n^2+111\,710\,82n$$
$$-515\,8440) \sim \frac{88\,179}{256}n^{20}.$$

The multipoles $Q_i(+)$ for parallel states $|+\rangle$ are all positive, while only the odd multipoles $Q_i(-)$ for anti-parallel states $|-\rangle$ are negative. Higher permanent multipoles are introduced as n increases. The $n = 2$ state possesses only a dipole and quadrupole while $n = 3$ has a dipole Q_1, quadrupole Q_2, octupole Q_3 and hexadecapole Q_4. Each multipole Q_i varies as n^{2i}. From the angular momenta addition scheme, it follows straightforwardly that the highest non-zero multipole associated with level n is Q_N where $N = 4j = 2(n-1)$. It turns out, even for low n, that a large number of multipoles with large magnitudes must be included in the long-range expansion. Expressions, similar to those above, have been obtained for the higher-order multipoles, Q_N, $N > 10$ as a function of n.

5. H(n)–H(n) long-range interactions

We can now consider the generic case of two interacting hydrogen atoms, H(n)–H(n), with the same principal quantum numbers n. For parallel-aligned dipoles $Q_i^A = Q_i^B = Q_i$, the multipole interaction is then

$$V_{\rightarrow,\rightarrow}(R) = -\frac{2}{R^3}Q_1^2 - \frac{2}{R^5}\left[4Q_1Q_3 - 3Q_2^2\right] - \frac{2}{R^7}\left[6Q_1Q_5 - 15Q_2Q_4 + 10Q_3^2\right] - O(R^{-9}), \tag{19}$$

a series consisting only of odd powers of $1/R$. The fact that the R^{-4} term is absent was already deduced from symmetry considerations (see also [10]). We have shown here that symmetry precludes, in general, any even power of $1/R$, e.g., the coefficient of the R^{-6}-term in section 2.1 is $-5\left[\left(Q_1^AQ_4^B - Q_4^AQ_1^B\right) - 2\left(Q_2^AQ_3^B - Q_3^AQ_2^B\right)\right]$ which vanishes when $Q_i^A = Q_i^B$. The coefficients of even powers of $1/R$ are all anti-symmetric in $Q_i^AQ_j^B = Q_iQ_j$ with respect to i, j interchange. For anti-parallel-aligned dipoles $Q_i^A = (-1)^iQ_i^B = Q_i$, the multipole interaction,

$$V_{\leftarrow,\rightarrow}(R) = +\frac{2}{R^3}Q_1^2 + \frac{6}{R^4}Q_1Q_2 + \frac{2}{R^5}\left[4Q_1Q_3 + 3Q_2^2\right]\left[Q_1Q_4 + 2Q_2Q_3\right] + \frac{2}{R^7}\left[6Q_1Q_5 + 15Q_2Q_4 + 10Q_3^2\right] + O(R^{-8}), \tag{20}$$

consists of all integral powers $j = 3, 4, 5, \ldots$ of $1/R$ and is always repulsive because $Q_i > 0$. The first terms of (19) and (20) have the following significance. For general orientation of the dipoles, the averaged-dipole–averaged-dipole interaction is

$$V_{\rm dd}(\mathbf{R}) = [\mathbf{d}_1 \cdot \mathbf{d}_2 - 3(\mathbf{d}_1 \cdot \hat{\mathbf{R}})(\mathbf{d}_2 \cdot \hat{\mathbf{R}})]R^3, \tag{21}$$

where $\mathbf{d} = -\langle\mathbf{r}\rangle = (3n/2)\mathbf{A}$ is the dipole vector. With the Z-axis along $\hat{\mathbf{R}}$, then

$$V_{\rm dd}(R) = -[2d_{1z}d_{2z} - (d_{1x}d_{2x} + d_{1y}d_{2y})]R^3 \tag{22}$$

$$= -d_1d_2[2\cos\theta_1\cos\theta_2 - \sin\theta_1\cos\theta_2\cos(\phi_1 - \phi_2)]R^3, \tag{23}$$

where (d_x, d_y, d_z) and (d, θ, ϕ) are the Cartesian and spherical components of $\mathbf{d}$. For parallel and anti-parallel dipole-aligned atoms, $\hat{\mathbf{d}}_1 = \hat{\mathbf{d}}_2$ and $\hat{\mathbf{d}}_1 = -\hat{\mathbf{d}}_2$, and $V_{\rm dd}(R) = \mp 2d_1d_2/R^3$ is attractive or repulsive, in agreement with the first terms of (19) and (20), respectively. When the dipole is aligned along the z-axis, then $d_z = (3n/2)A_3 = (3n/2)[J_{13} - J_{23}]$ operates on its eigenstate (8) to give eigenvalue $(3n/2)k = 3nj = (3n/2)(n-1)$, cf, table 1, in agreement with the multipole $Q_1(+)$ of section 4. Such algebraic techniques can also be utilized [14] with advantage for higher multipoles.

6. Investigation of possible long-range Rydberg–Rydberg molecules

By ignoring the octupole and higher moments, (19) reduces to,

$$V_{\rm dq}^{(+)}(R) = -\frac{2}{R^3}Q_1^2 + \frac{6}{R^5}Q_2^2, \tag{24}$$

where only the terms with dipoles and quadrupoles are retained. Since the quadrupole–quadrupole interaction is always repulsive (classically and quantally) and grows rapidly as R decreases, it will eventually serve to stabilize the dipole–dipole *attraction* for parallel-aligned dipoles. For each $\{n, n\}$ manifold, the potential $V_{\rightarrow,\rightarrow}(R)$ exhibits a well, of depth

$$V_{\rm min} = -\frac{4}{5}\frac{Q_1^2}{R_e^3} = -\frac{4}{25\sqrt{5}}\frac{Q_1^5}{Q_2^3} \sim -3.5 \times 10^{-2}/n^2; \qquad R_e = \sqrt{5}\,\frac{Q_2}{Q_1} \sim 3.7n^2, \tag{25}$$

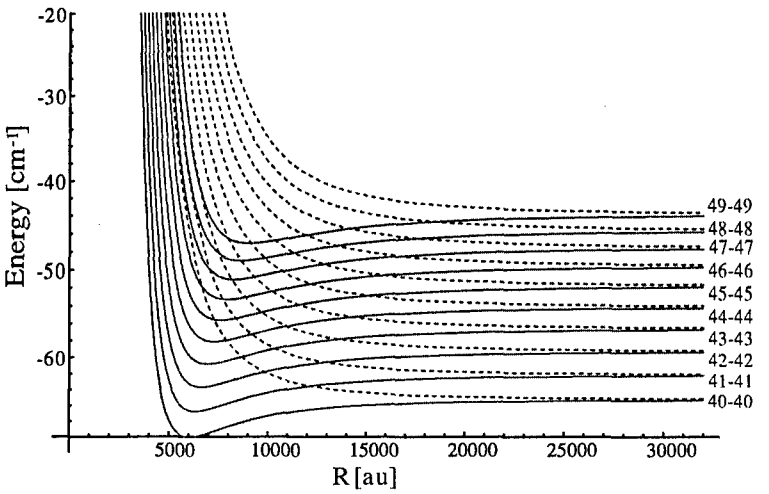

Figure 4. Potential curves for the H(n)–H(n) Rydberg–Rydberg system for several adjacent $n-n$ manifolds. Solid and dotted lines refer to the parallel and anti-parallel dipole–dipole configurations of equations (24) and (26). (1 cm^{-1} ≡ 1.5 K.)

at the equilibrium nuclear separation R_e. The corresponding interaction potential for anti-parallel alignment is

$$V_{\mathrm{dq}}^{(-)}(R) = \frac{2}{R^3}Q_1^2 + \frac{6}{R^4}Q_1Q_2 + \frac{6}{R^5}Q_2^2, \tag{26}$$

which is fully repulsive. Both sets of curves, with the asymptotic electronic energy $-n^{-2}$ au added, are displayed in figure 4 for n in the range, $40 \leqslant n \leqslant 49$. The attractive R^{-3} dipole–dipole and the repulsive R^{-5} quadrupole–quadrupole interactions therefore suggest the possible formation of long-range (i.e., $R_e \geqslant 4n^2$) Rydberg–Rydberg molecules. However, it is only for the $n = 2$ system, H($n = 2$)–H($n = 2$), that the octupole and higher multipoles are absent. As n increases, an increasing number of permanent multipoles up to order $N = 2(n-1)$ interact. In addition to the quadrupole–quadrupole repulsion, the attractive dipole–octupole interaction is the only other contribution to the R^{-5}-term which now has coefficient

$$2\left(3Q_2^2 - 4Q_1Q_3\right) = -\tfrac{3}{2}n^4(n-1)^2[5n(2n-9)+41], \tag{27}$$

which is always negative for $n \geqslant 4$, so that pure attraction dominates! The dipole–octupole attraction has therefore offset the quadrupole–quadrupole repulsion. Inclusion of the dipole–octupole R^{-5}-interaction has changed the physical nature of the interaction from one with a potential well (figure 4), capable of supporting many vibrational levels, to a potential which is now purely attractive for those R for which there is no electron overlap. Although the dipole–quadrupole attractive interaction is only 7/5 times the repulsive quadrupole–quadrupole interaction i.e., is 20% larger, it is sufficient to offset the repulsion. We have found, in general, that all permanent multipoles must be included in order to determine the correct coefficients of the first-order long-range expansion. Explicit calculations, including all multipoles Q_j; $j = 1, 2, 3, \ldots, N = 2(n-1)$ appropriate for a given $n = 2, 3, \ldots, 50$, show that the net contributions arising from all the multipoles except that due to the last multipole, Q_{2n-2}, are all attractive. Net repulsion arises only from the final multipole which introduces terms $\sim R^{2N-1} = R^{4n-3}$ into the expansion. Potential wells are indeed exhibited

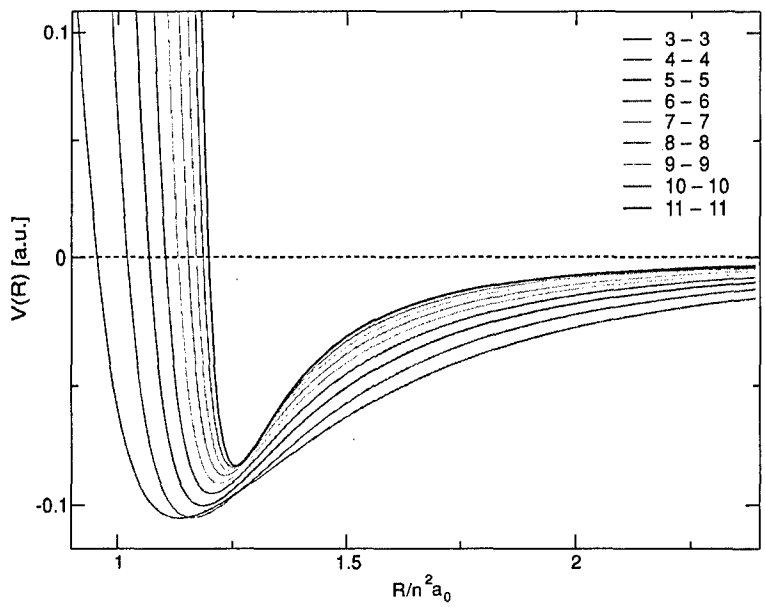

Figure 5. H(n)–H(n) Rydberg–Rydberg molecular potentials (19) for several adjacent $n - n$ manifolds with $n = 3, 4, 5, 6, 7, 8, 9, 10, 11$.

for all H(n)–H(n) and the steepness of the repulsive wall increases with n. Representative results are shown in figure 5. We note that these potential curves are much deeper than those in figure 4 and that the minima are located at shorter equilibrium separations $R_m \sim 1.2n^2$ au, where the multipole expansion may no longer be accurate. At small internuclear separations R, the adoption of electronic functions with the form (4), which are only diagonal with respect to each dipole operator, is also subject to question, and a larger basis set (diagonal in the full long-range interaction) may be required. Moreover, second-order effects (as the van der Waals attraction) and electronic overlap may no longer be ignored at these smaller R_m.

In the limit of high $n \gg 1$, the attractive portions of the parallel-aligned dipole potentials of figure 5 take the asymptotic form,

$$V_{\rightarrow,\rightarrow}(R) \approx -\frac{1}{n^2}\left[\frac{9}{2}\left(\frac{n^2}{R}\right)^3 + 15\left(\frac{n^2}{R}\right)^5 + \frac{833}{16}\left(\frac{n^2}{R}\right)^7\right] + O(R^{-9}). \qquad (28)$$

The second-order van der Waals ($\sim R^{-6}$) term is not included within this expression but is the subject of separate study.

7. H(n)–H(n') long-range interactions

Figure 6 illustrates several potential curves for interaction between two 'polar' Rydberg atoms in different levels n and n' but having their dipoles oriented in the same direction. The principal quantum number of one of the atoms is $n = 10$, while the other Rydberg atom has n' ranging from 3 to 11. It is seen that the well becomes much deeper and steeper as n' increases, as expected from the increasingly attractive contributions from the additional multipoles. The minima, however, are still located at about 1.2 min (n^2, n'^2), where distortions, mentioned previously for the $n = n'$ case may also be in evidence. It therefore seems highly unlikely that long-range Rydberg–Rydberg molecules can be formed from the extreme Stark states with the

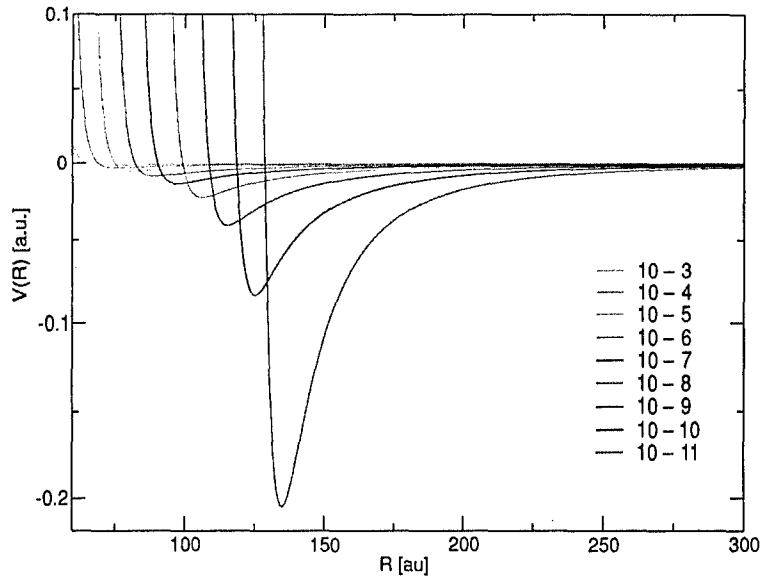

Figure 6. H(10)–H(n') Rydberg–Rydberg molecular potentials (19) for parallel dipole–dipole configuration with $n' = 3, 4, 5, 6, 7, 8, 9, 10, 11$.

greatest dipole moment. The attraction proves just too overwhelming so that repulsion finally sets in at separations R too small for validity of the long-range expansion.

8. The H($n = 2$)–H($n = 2$) long-range interaction

Because H($n = 2$) contains no octupole and higher moments, it is worth exploring the $n = 2$ case. For small n, the approximation (4) for the eigenfunction of dipole–dipole interaction operator (5) breaks down, because the wavefunction (4) using the extreme Stark orbital $\psi_{(n-1)00}(\mathbf{r})$ becomes an eigenstate of the dipole–dipole operator (5) to high accuracy only for large $n \gg 1$. It is, nevertheless, possible to exactly determine the interaction [9, 4] and associated vibrational levels for the $n = 2$ case. The exact $n = 2$ eigenfunction which diagonalizes the dipole–dipole interaction (5) is [9]

$$\tfrac{1}{\sqrt{2}}|2s2s\rangle + \tfrac{1}{\sqrt{3}}|2p_0 2p_0\rangle + \tfrac{1}{\sqrt{12}}[|2p_1 2p_{-1}\rangle + |2p_{-1}2p_1\rangle] \tag{29}$$

within the $\{n = 2, n = 2\}$ sub-manifold of Hilbert space. The associated long-range interaction (12) is then

$$V(R) = -\frac{\alpha}{R^3} + \frac{\beta}{R^5} + O(R^{-6}) \tag{30}$$

with $\alpha = 9\sqrt{6} \approx 22$ and $\beta = 648$. Polar H($n = 2$) possesses only permanent dipole and quadrupole moments, so that the long-range interaction (30) is exact up to $O(R^{-6})$.

The H($n = 2$)–H($n = 2$) potential (30) displays a minimum $V(R_m) = -2\alpha/5\,(3\alpha/5\beta)^{3/2}$ at equilibrium separation $R_m = \sqrt{5\beta/3\alpha} \approx 7a_0$. Direct numerical solution of the Schrödinger equation for vibrational motion of the atomic nuclei shows that the interaction (30) accommodates 47 vibrational levels. Although the potential (30) will be distorted by the second-order van der Waals correction and overlap of atomic orbitals, it is nevertheless clear that such a long-range molecular state has a rich ro-vibrational spectrum.

A new type of doubly-excited states for a long-range quasi-molecule is therefore predicted for the $n = 2$ case. It is very difficult to populate the states under consideration by conventional means such as photon or electron-impact excitation from the ground state of H_2, because of vanishing Frank–Condon factors. However, modern schemes such as photoassociation could allow the hydrogen molecule to be formed in such exotic states.

It is worth noting that the extreme Stark $n = 2$ orbital is $\psi_{(n-1)00} = (|2s\rangle - |2p_0\rangle)/\sqrt{2}$. The present high-$n$ analysis, when applied to this low n case, of course yields the correct form (30) for the interaction, but with coefficients, $\alpha = 2d_1d_2 = 18$ and $\beta = 6Q_2^2 = 216$, appropriate to the extreme Stark states with dipoles aligned parallel along the internuclear axis $\hat{R}$. The $n = 2$ level is obviously too low for (4) to be considered as an accurate eigenstate of the dipole–dipole operator (5), as expected (cf section 2.1).

9. A comment on destruction processes

Any long-range Rydberg–Rydberg quasi-molecule is subject to various destruction processes as radiation decay, autoionization and predissociation. The detailed account of stability issues is beyond the scope of this paper. We can show [14] however that the radiation lifetime for the states under consideration scales as $\tau_S \sim n^{13/3}$, which is much longer than $\tau \sim n^3$ for core penetrating states, but shorter than the maximum possible lifetime $\tau_c \sim n^5$ for circular states. The autoionization width Γ_{au} is evaluated within the dipole–dipole approximation for the $n = 2$ case [9]. It decreases rather rapidly with internuclear distance as $\sim R^{-6}$ and is quite small at equilibrium separation R_m. Significantly, the autoionization rate is three orders of magnitude smaller than the vibrational frequency so that autoionization occurs only after many molecular vibrations. In fact, Léonard *et al* [1] have recently noted that 'the autoionization process is blocked by the extremely large size of the $He(2^3S_1)$–$He(2^3P_0)$ dimers'. This blockage will be even more evident in any true long-range Rydberg–Rydberg molecule. Predissociation arises from the crossing of the lowermost attractive curves (figure 4) in one $\{n, n\}$ manifold with the uppermost repulsive curves in the lower-lying $\{n - \Delta, n - \Delta\}$ manifold. Interaction between such curves corresponds to the flip of one of the atomic dipoles which is strongly suppressed.

10. Summary

The flexibility of the energy shell of a Rydberg atom in a broad superposition of angular momentum states changes dramatically the nature of the interaction between such atoms. These Rydberg atoms are termed 'polar' because they have permanent multipoles Q_j. Higher-order permanent multipoles are introduced as n increases. The highest non-zero multipole associated with level n is Q_N where $N = 4j = 2(n - 1)$. Analytical expressions for the electrostatic long-range first-order interaction between polar Rydbergs in extreme (the most stretched) Stark states have been obtained in terms of Q_i, expressed analytically as functions of principal quantum number n. Each multipole Q_i varies as n^{2i}.

By including only the attractive dipole–dipole $\sim R^{-3}$ and the repulsive quadrupole–quadrupole $\sim R^{-5}$ interactions, we have shown (figure 4) that molecules could possibly be formed with relatively large equilibrium separations $R_m \approx 3.7n^2$. Addition of the dipole–octupole attraction, which also $\sim R^{-5}$, however offsets the quadrupole–quadrupole repulsion and destroys this possibility; except for the $n = 2$ case, which has no octupole and higher moments.

We have also shown that all the multipoles associated with a given n must be included within the long-range expansion in order to determine the correct nature of the first-order

interaction. The net contribution from all the multipoles is purely attractive, except for the last multipole $Q_{2(n-1)}$ which provides repulsion, which becomes increasingly steeper with n. Potential minima however occur at relatively modest internuclear distances $R \approx 1.2n^2$, where other effects such as second-order van der Waal's attraction and electron overlap become effective, thereby compromising the validity of the long-range expansion at such low R. As n increases, the interaction becomes increasingly attractive so that long-range molecular formation is expected to be scarcely possible for these extreme Stark levels.

The long-range interactions provided here for these polar Rydberg atoms could be probed by an optical lattice, a regular 3D arrangement of cold trapped atoms. Atoms can be excited to Rydberg states. It is then possible to selectively populate specific Stark levels with a given m by applying a moderate electric field aligned with one of the principal axes of the lattice. The electric field would also protect these Stark states by lifting their degeneracy within the hydrogenic manifold. For all atoms in the lattice, the electron clouds will be stretched in the same direction and the strong dipole–dipole interaction will be operative and can be probed by laser spectroscopy. Isolated atoms in the lattice will be resonant on the unperturbed Stark line. For a pair of neighbouring atoms, sidebands could therefore be observed on the red side of the 'naked' Stark transition. The parameters of the optical lattice can be so chosen as to maintain the atoms at a distance of several times n^2, where the dipole–dipole interaction prevails. As the laser field creating the optical lattice is switched off, the atoms accelerated by attraction fall towards each other and the 'polar Rydberg arrangement' in the optical lattice collapses in a time long enough for laser probing to be completed.

We have concentrated here on Rydberg–Rydberg states with zero projection $\Lambda = 0$ of total orbital electron momentum along the internuclear axis. States with non-zero Λ have a weaker dipole–dipole interaction.

In summary, we have therefore provided the first detailed investigation of the full first-order long-range interactions between 'polar' Rydberg atoms. This work has opened up a very promising and interesting new field with many theoretical and experimental possibilities and challenges ahead.

Acknowledgments

This work is supported by AFOSR grant no 49620-02-1-0338 and NSF grant no 01-00890 to Georgia Institute of Technology and by NSF grant to ITAMP at Harvard University, where MRF and VNO were long-term visitors.

References

[1] Léonard J, Walhout M, Mosk A P, Müller T, Leduc M and Cohen-Tannoudji C 2003 *Phys. Rev. Lett.* **91** 073203
[2] Stwalley W C, Uang Y-H and Pichler G 1978 *Phys. Rev. Lett.* **41** 1164
Stwalley W C and Wang H 1999 *J. Mol. Spectrosc.* **195** 194
[3] de Oliveira A L, Mancini M W, Bagnato V S and Marcassa L G 2003 *Phys. Rev. Lett.* **90** 143002
Avdeenkov A V and Bohn J L 2003 *Phys. Rev. Lett.* **90** 043006
Venturi V, Leo P J, Tiesinga E, Williams C J and Whittingham I B 2003 *Phys. Rev.* A **68** 022706
Boisseau C, Simbotin L and Côté R 2002 *Phys. Rev. Lett.* **88** 133004
Greene C H, Dickinson A S and Sadeghpour H R 2000 *Phys. Rev. Lett.* **85** 2458
[4] Jonsell S, Saenz A, Froelich P, Forrey R C, Côté R and Dalgarno A 2002 *Phys. Rev.* A **65** 42501
[5] Jaksch D, Cirac J I, Zoller P, Rolston S I, Côté R and Lukin M D 2001 *Phys. Rev. Lett.* **87** 037901
[6] Lukin M D, Fleischhauer M, Côté R, Duan L M, Jaksch D, Cirac J I and Zoller P 2000 *Phys. Rev. Lett.* **85** 2208
[7] Kazansky A K and Ostrovsky V N 1996 *Phys. Rev. Lett.* **77** 3094
[8] Vrinceanu D and Flannery M R 2000 *Phys. Rev. Lett.* **85** 4880
Vrinceanu D and Flannery M R 2001 *Phys. Rev.* A **63** 032701
Flannery M R and Vrinceanu D 2003 *Int. J. Mass Spectrom.* **223–224** 473

[9] Nikitin S I, Ostrovsky V N and Prudov N V 1986 *Zh. Eksp. Teor. Fiz.* **91** 1262
Nikitin S I, Ostrovsky V N and Prudov N V 1986 *Sov. Phys.–JETP* **64** 745
[10] Braun P A, Ostrovsky V N and Prudov N V 1993 *Phys. Rev.* A **48** 941
[11] Margenau H and Kestner N R 1969 *Theory of Intermolecular Forces* (Oxford: Pergamon) p 265
[12] Fontana P R 1961 *Phys. Rev.* **123** 1865
[13] Varshalovich D A, Moskalev A N and Khersonski V K 1988 *Quantum Theory of Angular Momentum* (Singapore: World Scientific)
[14] Ostrovsky V N, Flannery M R and Vrinceanu D in preparation
[15] Bethe H A and Salpeter E E 1997 *Quantum Mechanics of One- and Two-Electron Atoms* (New York: Plenum) p 14

The enigma of nonholonomic constraints

M. R. Flannery[a)]
School of Physics, Georgia Institute of Technology, Atlanta, Georgia 30332

(Received 16 February 2004; accepted 8 October 2004)

The problems associated with the modification of Hamilton's principle to cover nonholonomic constraints by the application of the multiplier theorem of variational calculus are discussed. The reason for the problems is subtle and is discussed, together with the reason why the proper account of nonholonomic constraints is outside the scope of Hamilton's variational principle. However, linear velocity constraints remain within the scope of D'Alembert's principle. A careful and comprehensive analysis facilitates the resolution of the puzzling features of nonholonomic constraints. © *2005 American Association of Physics Teachers.*
[DOI: 10.1119/1.1830501]

I. INTRODUCTION

The action integral,

$$S=\int_{t_1}^{t_2} L(\mathbf{q},\dot{\mathbf{q}},t)dt, \tag{1}$$

plays a central role in the dynamics of physical systems described by a Lagrangian L. Hamilton's principle states that the actual path $\mathbf{q}(t)$ of a particle is the path that makes the action S a minimum. It is well known that Hamilton's principle,

$$\delta S=\delta\int_{t_1}^{t_2} L(\mathbf{q},\dot{\mathbf{q}},t)dt=0, \quad \text{(Hamilton's principle)}, \tag{2}$$

when applied to problems involving c-holonomic constraints with the geometric form,

$$f_k(q_1,q_2,\ldots,q_n,t)=0, \quad (k=1,2,\ldots,c), \tag{3}$$

leads to Lagrange's equations of motion whose solution provides the time dependence of the $(n-c)$ independent generalized coordinates q_j for the unconstrained degrees of freedom.

For problems that require additional calculation of the forces Q_j^c of holonomic constraint, Hamilton's principle may be generalized to yield correct results simply by replacing L in Eq. (2) by

$$L^{\dagger}=L(\mathbf{q},\dot{\mathbf{q}},t)+\sum_{k=1}^{c}\lambda_k(t)f_k(\mathbf{q},t), \tag{4}$$

where the λ_k are Lagrange multipliers. Equation (2) is therefore replaced by Hamilton's generalized principle,

$$\delta S^{\dagger}=\delta\int_{t_1}^{t_2} L^{\dagger}(\boldsymbol{\eta},\dot{\boldsymbol{\eta}},t)dt=0, \quad \text{(Hamilton's generalized principle)}, \tag{5}$$

from which the Euler–Lagrange equations

$$\frac{d}{dt}\left(\frac{\partial L^{\dagger}}{\partial\dot{\eta}_j}\right)-\frac{\partial L^{\dagger}}{\partial\eta_j}=0, \quad (j=1,2,\ldots,n+c) \tag{6}$$

can be derived via *free* variations of the extended set $\boldsymbol{\eta}\equiv\{\mathbf{q}(q_1,q_2,\ldots,q_n),\boldsymbol{\lambda}(\lambda_1,\lambda_2,\ldots\lambda_c)\}$ of the $(n+c)$ variables involved in Eq. (5). Because $f_k(\mathbf{q},t)$ are independent of the generalized velocity $\dot{\mathbf{q}}$, the first n-equations of the Euler–Lagrange set (6) provide the correct equations of state. Because Eq. (4) is independent of $\dot{\lambda}_k$, the last c equations of the Euler–Lagrange set (6) for the λ_k $(k=1,2\ldots,c)$ simply reproduce the equations (3) of holonomic constraint.

A recurring theme[1–4] is whether Hamilton's principle (2) may be similarly generalized so as to treat nonholonomic (dynamic) constraints,

$$g_k(\mathbf{q},\dot{\mathbf{q}},t)=0, \tag{7}$$

which depend on generalized velocities $\dot{\mathbf{q}}$, simply by substituting

$$L^{*}=L+\sum_{k=1}^{c}\lambda_k(t)g_k(\mathbf{q},\dot{\mathbf{q}},t) \tag{8}$$

for L in Eq. (2). A theorem in the calculus of variations appears, at first sight, tailor-made for such a conjecture. The theorem[5–7] states that the path $\mathbf{q}(t)$ that makes the action Eq. (1) have an extremum under the side conditions (7) is the same as the path that makes the modified functional, $S^{*}=\int_{t_1}^{t_2}L^{*}(\boldsymbol{\eta},\dot{\boldsymbol{\eta}},t)dt$, an extremum, without any side conditions imposed. On the basis of this multiplier rule, the conjecture, the substitution of Eq. (8) in Eq. (2), was simply adopted without reservation for the general case (7) and equations of state were published.[1–3]

This conjecture becomes problematic, particularly because the multiplier rule does not yield the standard equations of state as obtained from D'Alembert's more basic principle for systems with less general nonholonomic constraints,

$$g_k^{(L)}(\mathbf{q},\dot{\mathbf{q}},t)=\sum_{j=1}^{n}A_{kj}(\mathbf{q},t)\dot{q}_j+B_k(\mathbf{q},t)=0, \tag{9}$$

which are now only linear in the velocities $\dot{q}_j$. Yet, the same multiplier rule[5–7] works for the holonomic constraints in Eq. (3).

The question of whether the use of Eq. (8) in Eq. (2) is a viable generalization of Hamilton's principle is of interest here, because Ref. 1 advocates its use and cites the equations of state derived from it.[3] However, this generalization had previously been acknowledged[4] as being incorrect because it did not reproduce the correct equations of state for systems under linear constraints in Eq. (9). Some textbooks[8–11] also have indicated the fallacy of using Eq. (8) in Eq. (2). However, the basic reason for its failure has remained obscure.

The multiplier rule[5–7] is indeed correct, as stated, so the fact that it works for holonomic constraints (3), but not for nonholonomic constraints (7) poses a dilemma.

Many examples can be given that explicitly illustrate that Eq. (8) does not provide the correct results as obtained from Newtonian mechanics.[12] In this paper, we search for the reason why the procedure fails and, in so doing, we also explain why the proper account of nonholonomic constraints given by Eqs. (7) and (9) is outside the scope of Hamilton's principle, even though the linear constraints in Eq. (9) remain within the scope of D'Alembert's principle. We will find the conditions that Eq. (8) must satisfy for valid substitution into Eq. (2). We also will indicate why the general nonholonomic constraints in Eq. (7) are outside the scope of a principle based on virtual displacements. Rather than beginning from Eq. (2) and showing, as has been done, that an application involving Eq. (7) or (9) leads to erroneous results,[4,8–12] more insight can be gained by tracing the various stages of development of the variational principle, Eq. (2), from the more fundamental principle of D'Alembert. The essential reason will then become apparent.

Because variational theorems and methods are essential tools of modern analytical dynamics and because various fallacies underlying their use are subtle and are not generally well appreciated, it is hoped that the following account will help illuminate their scope of application.

II. THEORY

We first outline some standard deductions of D'Alembert's principle, which is then expressed in a useful variational form that will provide a "royal road" from which Hamilton's principle can be easily extracted. The resolution of why the extended Lagrangian Eq. (4) works, while Eq. (8) does not, in Hamilton's principle, Eq. (2), will then become apparent via this approach.

A. Differential form of D'Alembert's principle

The motion of a system of particles, $i=1,2,\ldots,N$ of mass m_i located at $\mathbf{r}_i(t)$ in an inertial frame of reference is governed by Newton's equations,

$$\mathbf{F}_i+\mathbf{F}_i^c=m_i\ddot{\mathbf{r}}_i, \tag{10}$$

where the net force acting on each particle is decomposed into an active force $\mathbf{F}_i$ and a force $\mathbf{F}_i^c$ of constraint. A virtual displacement $\delta\mathbf{r}_i$ is an instantaneous variation from a given configuration $\mathbf{r}_i$ performed at a fixed time t and taken consistent with the constraints at that time. The summation convention, $a_{ij}q_j\equiv\Sigma_{j=1}^{n}a_{ij}q_j$ for repeated indices j will be adopted.

Assume that the total virtual work $\mathbf{F}_i^c\cdot\delta\mathbf{r}_i$ performed by all the constraining forces is zero. D'Alembert's principle, in both Newtonian $\mathbf{r}_i$ $(i=1,2,\ldots,N)$ and generalized q_j $(j=1,2,\ldots,3N)$ coordinate versions, states that[1,8–10,13]

$$(m_i\ddot{\mathbf{r}}_i-\mathbf{F}_i)\cdot\delta\mathbf{r}_i=\left[\frac{d}{dt}\left(\frac{\partial T}{\partial\dot{q}_j}\right)-\frac{\partial T}{\partial q_j}-Q_j\right]\delta q_j=0, \tag{11}$$

where the total kinetic energy $T=\frac{1}{2}m_i\dot{\mathbf{r}}_i^2(\mathbf{q},\dot{\mathbf{q}},t)$ is expressed in terms of the $n=3N$ generalized coordinates of all the particles. The generalized force,

$$Q_j\equiv\mathbf{F}_i\cdot\frac{\partial\mathbf{r}_i}{\partial q_j}, \tag{12}$$

is such that the virtual work $Q_j\delta q_j=\mathbf{F}_i\cdot\delta\mathbf{r}_i$ is equivalent in both representations and may be decomposed into a potential part,

$$Q_j^{(P)}(\mathbf{q},\dot{\mathbf{q}},t)\equiv\frac{d}{dt}\left(\frac{\partial U}{\partial\dot{q}_j}\right)-\frac{\partial U}{\partial q_j}, \tag{13}$$

derived from a generalized monogenic (the same for all particles) potential $U(\mathbf{q},\dot{\mathbf{q}},t)$ and a nonpotential part $Q_j^{\mathrm{NP}}=\mathbf{F}_i^{\mathrm{NP}}\cdot\partial\mathbf{r}_i/\partial q_j$. D'Alembert's principle is then

$$\left[\frac{d}{dt}\left(\frac{\partial L}{\partial\dot{q}_j}\right)-\frac{\partial L}{\partial q_j}-Q_j^{\mathrm{NP}}\right]\delta q_j=0, \quad \text{(D'Alembert's principle)}, \tag{14}$$

where the Lagrangian is

$$L(\mathbf{q},\dot{\mathbf{q}},t)=T(\mathbf{q},\dot{\mathbf{q}},t)-U(\mathbf{q},\dot{\mathbf{q}},t). \tag{15}$$

B. Holonomic constraints

When the c-constraint conditions in Eq. (3) are utilized to reduce the number of generalized coordinates from n to the minimum number $(n-c)$ of actual independent degrees of freedom, that is, when the constraints are embedded within the problem at the outset, then all the $(n-c)$ δq_j's in Eq. (14) are independent of each other. Because each displacement can take on any value at each t, the satisfaction of D'Alembert's principle, Eq. (14), demands that each coefficient of δq_j in Eq. (14) separately vanishes to yield Lagrange's equations,[1,8–10,13]

$$\frac{d}{dt}\left(\frac{\partial L}{\partial\dot{q}_j}\right)-\frac{\partial L}{\partial q_j}=Q_j^{\mathrm{NP}}, \tag{16}$$

for the $(n-c)$ independent degrees of freedom.

When the holonomic constraints Eq. (3) are not used to reduce the set of generalized coordinates to this minimum number, that is, when they are instead "adjoined," then c of the δq_j's in Eq. (14) depend on the independent $(n-c)$ coordinates and are constrained by the c conditions,

$$\frac{\partial f_k}{\partial q_j}\delta q_j=0, \quad (k=1,2,\ldots,c) \tag{17}$$

which is obtained by differentiating Eq. (3) and keeping t fixed. The Lagrange multipliers $\lambda_k(t)$ can then be introduced by subtracting the quantity $\lambda_k(\partial f_k/\partial q_j)\delta q_j=0$ from the left-hand side of Eq. (14) to give

$$\left[\frac{d}{dt}\left(\frac{\partial L}{\partial\dot{q}_j}\right)-\frac{\partial L}{\partial q_j}-\lambda_k(t)\frac{\partial f_k(\mathbf{q},t)}{\partial q_j}-Q_j^{\mathrm{NP}}\right]\times\delta q_j(t)=0. \quad (j=1,2,\ldots,n). \tag{18}$$

Nonpotential forces Q_j^{NP} are included in Eq. (18). If we denote the $m=n-c$ independent (free) coordinates by $q_1,q_2,\ldots,q_m$ and the c-dependent ones by $q_{m+1},q_{m+2},\ldots,q_n$, then the previously unassigned c multipliers, λ_k, are now chosen to satisfy the c equations,

$$\frac{d}{dt}\left(\frac{\partial L}{\partial\dot{q}_j}\right)-\frac{\partial L}{\partial q_j}=\lambda_k(t)\frac{\partial f_k(\mathbf{q},t)}{\partial q_j}+Q_j^{\mathrm{NP}} \quad (j=m+1,m+2,\ldots,n). \tag{19}$$

Equation (18) then reduces to

$$\left[\frac{d}{dt}\left(\frac{\partial L}{\partial \dot{q}_j}\right)-\frac{\partial L}{\partial q_j}-\lambda_k(t)\frac{\partial f_k(\mathbf{q},t)}{\partial q_j}-Q_j^{\mathrm{NP}}\right]\times\delta q_j(t)=0,\quad (j=1,2,\ldots,m) \tag{20}$$

for the free $m=n-c$ coordinates. Because the m δq_j's in Eq. (20) are all independent and arbitrary, each of the δq_j coefficients in Eq. (20) must separately vanish. The set,

$$\frac{d}{dt}\left(\frac{\partial L}{\partial \dot{q}_j}\right)-\frac{\partial L}{\partial q_j}=\lambda_k(t)\frac{\partial f_k(\mathbf{q},t)}{\partial q_j}+Q_j^{\mathrm{NP}},\quad (j=1,2,\ldots,n), \tag{21}$$

therefore represents the equations of state for the full array of dependent and independent variables $q_1,q_2,\ldots,q_n$.

Now adjoin the constraint equations (3) to the Lagrangian set in Eq. (21) of n-equations to provide $n+c$ equations for the $n+c$ unknowns, the n q_j's and the c λ_k's, so that the sets $\mathbf{q}\equiv\{q_j\}$ and $\boldsymbol{\lambda}\equiv\{\lambda_k\}$ may in principle be determined. By comparing Eq. (21) with Eq. (16), it is seen that $Q_j^c=\lambda_k(\partial f_k/\partial q_j)$ are additional forces acting on the system. These Q_j^c must therefore be the forces of constraint which, because of Eq. (17), do no virtual work, as required for the validity of D'Alembert's principle. Although standard,[1,8–13] the above review will help provide the context to what now follows.

Because f_k is independent of the velocities $\dot{\mathbf{q}}$, a generalized D'Alembert principle,

$$\left[\frac{d}{dt}\left(\frac{\partial L^\dagger}{\partial \dot{\eta}_j}\right)-\frac{\partial L^\dagger}{\partial \eta_j}-Q_j^{\mathrm{NP}}\right]\delta\eta_j=0,\quad (j=1,2,\ldots,n+c)$$

(D'Alembert generalized principle), (22)

can therefore be introduced where $L^\dagger(\dot{\boldsymbol{\eta}},\boldsymbol{\eta},t)=L+\lambda_k(t)f_k(\mathbf{q},t)$ is an augmented Lagrangian over an extended set of coordinates $\boldsymbol{\eta}\equiv(\mathbf{q},\boldsymbol{\lambda})$. On regarding all η_j as free, then

$$\frac{d}{dt}\left[\frac{\partial(L+\lambda_k f_k)}{\partial \dot{\eta}_j}\right]-\frac{\partial(L+\lambda_k f_k)}{\partial \eta_j}=Q_j^{\mathrm{NP}},\quad (j=1,2,\ldots,n+c) \tag{23}$$

are the generalized Lagrange equations for the extended set η_j. The first n equations of Eq. (23) reproduce the correct equations of state, (21), and the last c equations reproduce the constraint equations, $f_k=0$. Hence, D'Alembert's principle in Eq. (14), with the displacements δq_j subject to the c conditions in Eq. (17), is equivalent to the generalized principle, Eq. (22), with all coordinates η_j free. The replacement of the basic principle Eq. (14) with the subsidiary conditions Eq. (17) by the generalized principle Eq. (22) without subsidiary conditions is the Lagrange multiplier rule. Both principles provide identical equations of state, Eq. (21), and the multiplier rule in Eq. (22) provides the shortcut.

It is important to note that the displaced paths $q_j+\delta q_j$, not only comply with the essential conditions in Eq. (17) for the displacements, but also satisfy the equations of constraint,

$$f_k(\mathbf{q}+\delta\mathbf{q},t)=f_k(\mathbf{q},t)+\delta f_k(\mathbf{q},t)=0, \tag{24}$$

because there is no change $\delta f_k=(\partial f_k/\partial q_j)\delta q_j=0$ to the constraint Eq. (3). The displaced paths are therefore all geometrically possible because they all conform to Eq. (24). The key requirement for application of the multiplier rule is that the displaced paths must be geometrically possible by satisfying the equations (24) of constraint. As will be shown next, this condition is violated, in general, by nonholonomic constraints.

C. Nonholonomic constraints

The virtual displacements δq_j for nonholonomic systems with c linear constraints,

$$g_k^{(L)}(\mathbf{q},\dot{\mathbf{q}},t)=A_{kj}(\mathbf{q},t)\dot{q}_j+B_k(\mathbf{q},t)=0, \tag{25}$$

obeyed by the actual path, are themselves constrained to obey c instantaneous conditions

$$A_{kj}(\mathbf{q},t)\,\delta q_j=0,\quad (k=1,2,\ldots,c) \tag{26}$$

obtained by first writing Eq. (25) in differential form as

$$g_k^{(L)}dt=A_{kj}(\mathbf{q},t)dq_j+B_k(\mathbf{q},t)dt, \tag{27}$$

and then by setting $dt=0$ and $dq_j=\delta q_j$ as prescribed. As with Eq. (17), the linear conditions (26) also may be absorbed in D'Alembert's principle because Eq. (14) is linear in δq_j. By adding $\lambda_k A_{kj}\delta q_j=0$ to the right-hand side of Eq. (14), and by proceeding as before in Sec. II B, the equations of state under the linear constraints in Eq. (25) are obtained in the form

$$\frac{d}{dt}\left(\frac{\partial L}{\partial \dot{q}_j}\right)-\frac{\partial L}{\partial q_j}=\lambda_k(\mathbf{q},t)A_{kj}(\mathbf{q},t)+Q_j^{\mathrm{NP}},\quad (j=1,2,\ldots,n) \tag{28}$$

for all the coordinates. We now examine the validity of D'Alembert's generalized principle

$$\left\{\frac{d}{dt}\left[\frac{\partial(L+\mu_k g_k)}{\partial \dot{\eta}_j}\right]-\frac{\partial(L+\mu_k g_k)}{\partial \eta_j}-Q_j^{\mathrm{NP}}\right\}\delta\eta_j=0,\quad (j=1,2,\ldots,n+c), \tag{29}$$

applied to nonholonomic constraints Eq. (7), where $\mu_k(t)$ are a different set of multipliers and where all $\delta\eta_j$ are regarded as free. On introducing G_{kj}, where

$$G_{kj}=\left[\frac{d}{dt}\left(\frac{\partial g_k}{\partial \dot{q}_j}\right)-\frac{\partial g_k}{\partial q_j}\right]\quad (j=1,2,\ldots,n), \tag{30}$$

and is zero for $j>n$, Eq. (29) can be rewritten as

$$\left[\frac{d}{dt}\left(\frac{\partial L}{\partial \dot{\eta}_j}\right)-\frac{\partial L}{\partial \eta_j}+\dot{\mu}_k\frac{\partial g_k}{\partial \dot{\eta}_j}+\mu_k G_{kj}-g_k\frac{\partial \mu_k}{\partial \eta_j}-Q_j^{NP}\right]\delta\eta_j=0,\quad (j=1,2,\ldots,n+c). \tag{31}$$

The first n equations of Eq. (31) provides the equation of state,

$$\frac{d}{dt}\left(\frac{\partial L}{\partial \dot{q}_j}\right)-\frac{\partial L}{\partial q_j}=-\dot{\mu}_k\frac{\partial g_k}{\partial \dot{\eta}_j}-\mu_k G_{kj}+Q_j^{NP}\quad (j=1,2,\ldots,n), \tag{32}$$

as derived from D'Alembert's generalized principle, Eq. (29). The last c equations of Eq. (31) yield the constraint equations (7), as expected. But Eq. (32) reproduces the correct equation (28) of state for the linear constraints in Eq. (25), only when Eq. (30) for linear constraints vanishes, that is, provided

$$G_{kj}^{(L)}=\left[\left(\frac{\partial A_{kj}}{\partial q_i}-\frac{\partial A_{ki}}{\partial q_j}\right)\dot{q}_i+\left(\frac{\partial A_{kj}}{\partial t}-\frac{\partial B_k}{\partial q_j}\right)\right]=0. \tag{33}$$

Because condition Eq. (30) is basic to validity of Eq. (29), the significance of this auxiliary restriction on the linear constraints (25) will now be explored.

In order for Eq. (25) to be a perfect (exact) differential of a function $f_k(\mathbf{q},t)$, we must have

$$A_{ki}(\mathbf{q},t)\dot{q}_i+B_k(\mathbf{q},t)=\frac{d}{dt}f_k=\frac{\partial f_k}{\partial q_i}\dot{q}_i+\frac{\partial f_k}{\partial t}. \tag{34}$$

The correspondence $A_{ki}=\partial f_k/\partial q_i$ and $B_k=\partial f_k/\partial t$ provides the (necessary and sufficient) conditions

$$\frac{\partial A_{ki}}{\partial q_j}=\frac{\partial^2 f_k}{\partial q_j\partial q_i}=\frac{\partial^2 f_k}{\partial q_i\partial q_j}=\frac{\partial A_{kj}}{\partial q_i}, \tag{35}$$

$$\frac{\partial B_k}{\partial q_i}=\frac{\partial^2 f_k}{\partial q_i\partial t}=\frac{\partial^2 f_k}{\partial t\partial q_i}=\frac{\partial A_{ki}}{\partial t}, \tag{36}$$

for the "exactness" of Eq. (25). Provided the linear constraints (25) satisfy conditions (35) and (36), an integrated form f_k therefore exists but may be unknown. Such constraints are termed *semiholonomic* and are denoted by $g_k^{(\mathrm{sh})}(\mathbf{q},\dot{\mathbf{q}},t)=0$. But the conditions (35) and (36) for exactness yield condition Eq. (33), for all $\dot{q}_i$ which satisfy the constraints. Semiholonomic constraints can therefore be correctly treated by D'Alembert's generalized principle, Eq. (29). In addition to exactness, semiholonomic constraints ($G_{kj}^{(L)}=0$) possess a further important property. The equations of constraint appropriate to the displaced paths $\mathbf{q}+\delta\mathbf{q}$ are

$$g_k(\mathbf{q}+\delta\mathbf{q},\dot{\mathbf{q}}+\delta\dot{\mathbf{q}},t)=g_k(\mathbf{q},\dot{\mathbf{q}},t)+\delta g_k(\mathbf{q},\dot{\mathbf{q}},t). \tag{37}$$

Because $g_k(\mathbf{q},\dot{\mathbf{q}},t)=0$ for the true dynamical path $\mathbf{q}(t)$, the constraint equations for the displaced paths change by

$$\delta g_k=\frac{\partial g_k}{\partial q_j}\delta q_j(t)+\frac{\partial g_k}{\partial \dot{q}_j}\delta\dot{q}_j(t). \tag{38}$$

With the aid of $\delta\dot{q}_j(t)=d[\delta q_j(t)]/dt$, this difference is

$$\delta g_k=\frac{d}{dt}\left[\frac{\partial g_k}{\partial \dot{q}_j}\delta q_j(t)\right]-G_{kj}\delta q_j(t). \tag{39}$$

The condition for the displaced paths to be all geometrically possible is that $g_k(\mathbf{q}+\delta\mathbf{q},\dot{\mathbf{q}}+\delta\dot{\mathbf{q}},t)=0$, that is $\delta g_k=0$ and the constraints are invariant to displacements. For the linear constraints (25), Eq. (39) reduces to

$$\delta g_k^{(L)}=\frac{d}{dt}(A_{kj}\delta q_j)-G_{kj}^{(L)}\delta q_j. \tag{40}$$

On invoking the basic restriction (26) on the displacements and the exactness condition $G_{kj}^{(L)}=0$, Eq. (40) reduces to $\delta g_k^{(\mathrm{sh})}=0$, which implies geometrically possible paths. D'Alembert's generalized principle (29) with Eq. (25) therefore holds for semiholonomic systems where the displaced paths are all geometrically possible. Semiholonomic systems are, in essence, holonomic, although the integrated holonomic form $f_k=0$ may not be known.

Linear constraints (25) can be integrable and yet violate the exactness condition (33). For example, the constraint,

$$g_1^{(\mathrm{sh})}(\mathbf{q},\dot{\mathbf{q}})=(3q_1^2+2q_2^2)\dot{q}_1+4q_1q_2\dot{q}_2=0, \tag{41}$$

is exact because (33) is satisfied and it integrates directly to give $f_1=q_1^3+2q_2^2q_1=\text{constant}$. The constraint,

$$g_2^{(I)}(\mathbf{q},\dot{\mathbf{q}})=(4q_1+3q_2^2)\dot{q}_1+2q_1q_2\dot{q}_2=0, \tag{42}$$

is not exact but can be integrated via the integrating factor $\Phi_2\ (=q_1^2)$ to give $f_2=q_1^4+q_1^3q_2^2=\text{constant}$. All exact constraints are therefore integrable, but all integrable constraints are not necessarily exact. The conditions (35) and (36) are too restrictive for integrable constraints $g_k^{(I)}$, which can however be rendered in exact form by multiplying by the integrating factor $\Phi_k(\mathbf{q},t)$. Then $g_k^{(\mathrm{sh})}=\Phi_k g_k^{(I)}$ now satisfies the condition (33) for both exactness and geometrically possible displaced paths. For example, the constraint,

$$g_2^{(\mathrm{sh})}(\mathbf{q},\dot{\mathbf{q}})=\Phi_2 g_2^{(I)}=(4q_1^3+3q_1^2q_2^2)\dot{q}_1+2q_1^3q_2\dot{q}_2=0, \tag{43}$$

now satisfies condition (33) and is therefore in exact (semiholonomic) form. A known integrating factor Φ_k implies a known integrated holonomic form $f_k=0$, so that the simpler holonomic result Eq. (23) can be used rather than D'Alembert's generalized principle (29).

The linear constraints (25) which do not satisfy the exactness condition (33) are classified as nonholonomic. D'Alembert's generalized principle (29) is therefore not appropriate for nonholonomic constraints (25), as is also confirmed by the fact that Eq. (32) is not the correct equation (28) of state, because $G_{kj}^{(L)}\neq 0$, in general.

D'Alembert's basic principle, Eq. (14), is not amenable to general nonholonomic constraints (7), because there is now no relation such as Eq. (26) which connects the displacements δq_j in a linear form. The fact that Eq. (7) is, in general, not a linear function of $\dot{q}_j$ prohibits writing a linear interrelation between the δq_j's essential for the application of D'Alembert's principle. General nonholonomic constraints (7) are therefore outside the scope of all principles based on virtual displacements.

The key conclusions of Secs. II B and II C are the following:

(1) D'Alembert's basic principle, Eq. (14), is applicable to holonomic and linear nonholonomic constraints, as is already known.
(2) D'Alembert's generalized principle, Eq. (22), applies to holonomic constraints and Eq. (29) applies to semiholonomic systems, because the displaced paths are also geometrically possible paths, an essential criterion for the validity of the underlying multiplier rule. The solution of both sets provides the actual path $\{q_j(t)\}$ and the constraint forces $\{Q_j^c\}$.
(3) The displaced paths $q_j+\delta q_j$ for linear nonholonomic systems are not geometrically possible and therefore do not satisfy the multiplier-rule condition.
(4) It is important to distinguish restrictions imposed on virtual displacements, such as Eq. (26), from the actual equations of constraint, such as Eq. (9), which must only be satisfied within the equations of state that are eventually determined by some variational procedure. The constraint equations $g_k(\mathbf{q},\dot{\mathbf{q}},t)=0$ satisfied by the true dynamical path $\mathbf{q}(t)$ do not necessarily imply that the corresponding equations $g_k(\mathbf{q}+\delta\mathbf{q},\dot{\mathbf{q}}+\delta\dot{\mathbf{q}},t)=0$ are satisfied by the displaced paths.
(5) General nonholonomic constraints (7) are completely outside the scope of even the most fundamental principle

of D'Alembert. The generalization[1-3] of any principle based on Eq. (14) to general nonholonomic constraints is without foundation.

D. The δL version of D'Alembert's principle

The Lagrangian for the varied paths is

$$L(\mathbf{q}+\delta\mathbf{q},\dot{\mathbf{q}}+\delta\dot{\mathbf{q}},t)=L(\mathbf{q},\dot{\mathbf{q}},t)+\delta L(\mathbf{q},\dot{\mathbf{q}},t), \tag{44}$$

where the change in L due to the virtual displacement δq_j from the actual path $\mathbf{q}$ is

$$\delta L=\frac{\partial L}{\partial q_j}\delta q_j(t)+\frac{\partial L}{\partial \dot{q}_j}\delta\dot{q}_j(t). \tag{45}$$

With the aid of $\delta\dot{q}_j(t)=d[\delta q_j(t)]/dt$, the change is

$$\delta L=\frac{d}{dt}[p_j\delta q_j(t)]-\left[\frac{d}{dt}\left(\frac{\partial L}{\partial \dot{q}_j}\right)-\frac{\partial L}{\partial q_j}\right]\delta q_j(t), \tag{46}$$

where the generalized momentum is defined as $p_j=\partial L/\partial\dot{q}_j$. D'Alembert's basic principle (14) can then be recast in δL form as

$$\delta L=\frac{d}{dt}(p_j\delta q_j)-Q_j^{\mathrm{NP}}\delta q_j. \tag{47}$$

The differential version, Eq. (14), and the δL version, Eq. (44), of D'Alembert's principle are equivalent and are fundamental equations of dynamics. When the holonomic constraints (3) are adjoined, rather than embedded, there are c δq_j's in Eq. (46) that are dependent on the remaining $(n-c)$ displacements. Because there is no change, $\delta f_k=0$, to the holonomic equations (3) among the varied paths, we may add $\delta[\lambda_k(t)f_k]=0$ to the left-hand side of Eq. (47). By utilizing the augmented Lagrangian $L^\dagger$ over the extended set of free generalized coordinates $\boldsymbol{\eta}\equiv(\mathbf{q},\boldsymbol{\lambda})$, the generalized version of D'Alembert's principle, Eq. (47), is

$$\delta L^\dagger(\dot{\boldsymbol{\eta}},\boldsymbol{\eta},t)=\delta[L+\lambda_k(t)f_k(\mathbf{q},t)]=\frac{d}{dt}(p_j\delta\eta_j)-Q_j^{\mathrm{NP}}\delta\eta_j. \tag{48}$$

If we use the definition (46) for δL, the generalized version (48) reproduces the correct equations of state, Eq. (21), and provides another example of the multiplier rule.

For semiholonomic systems, the Lagrangian L can also be replaced by $L^{(\mathrm{sh})}=L+\mu_k g_k^{(\mathrm{sh})}$ because the constraints $g_k^{(\mathrm{sh})}(\mathbf{q},\dot{\mathbf{q}},t)=0$ are exact, thereby satisfying the condition $\delta g_k^{(\mathrm{sh})}=0$ for geometrically possible paths. D'Alembert's generalized principle (47) therefore yields the equations of state

$$\frac{d}{dt}\left[\frac{\partial(L+\mu_k g_k^{(\mathrm{sh})})}{\partial\dot{\eta}_j}\right]-\frac{\partial(L+\mu_k g_k^{(\mathrm{sh})})}{\partial\eta_j}=Q_j^{\mathrm{NP}},\quad (j=1,2,\ldots,n+c) \tag{49}$$

for the extended coordinates $(\boldsymbol{\eta}\equiv\mathbf{q},\boldsymbol{\mu})$ for a semiholonomic system. The multiplier rule of replacing L in Eq. (47) by $L^*=L+\mu_k g_k$ is, however, not valid for inexact linear or general nonholonomic constraints, because the displaced paths are not geometrically possible paths, as explained in Sec. II C.

E. Generalization of Hamilton's variational principle

Hamilton's integral principle,

$$\int_{t_1}^{t_2}\delta L\,dt=\delta\int_{t_1}^{t_2}L\,dt=[p_j\delta q_j]_{t_1}^{t_2}-\int_{t_1}^{t_2}[Q_j^{\mathrm{NP}}\delta q_j]dt, \tag{50}$$

is D'Alembert's principle, Eq. (47), integrated between the times t_1 and t_2. The δ operator does not affect the time and was therefore taken outside the integral. The appropriate Eq. (28) for linear nonholonomic constraints is recovered by making the time integration in Eq. (50) redundant. The application of Eq. (50) then reduces simply to an application of D'Alembert's basic principle (14), as in Sec. II C. The main advantage, however, of the integral principle Eq. (50) is that it becomes a variational principle,

$$\delta S=\delta\int_{t_1}^{t_2}L\,dt=0, \tag{51}$$

by admitting only those paths $q_j(t)$ that pass through the fixed end points, $\delta q_j(t_{1,2})=0$, and by considering only potential systems, that is, $Q_j^{\mathrm{NP}}=0$. The virtual variation δ ensures that the transit time $\tau=t_2-t_1$ remains the same for all the varied paths. Equation (51) is Hamilton's principle for the least action $S=\int_{t_1}^{t_2}L\,dt$.

When attempting to generalize Hamilton's variational principle, Eq. (51), the conditions for generalization of the more fundamental differential and δL versions, Eqs. (14) and (47) of D'Alembert's principle by the multiplier rule, are still in effect. Equation (51) can be directly applied to holonomic systems with the embedded constraints in Eq. (3) to recover the correct equations of state (16) with $Q_j^{\mathrm{NP}}=0$. When holonomic constraints are adjoined in order to determine the constraint forces, then L in Eq. (51) can be replaced by $L^\dagger=L+\lambda_k(t)f_k(\mathbf{q},t)$, because $\delta f_k=0$, to give Hamilton's generalized principle

$$\delta S^\dagger=\delta\int_{t_1}^{t_2}L^\dagger(\dot{\boldsymbol{\eta}},\boldsymbol{\eta},t)dt=\delta\int_{t_1}^{t_2}[L+\lambda_k(t)f_k(\mathbf{q},t)]dt=0, \tag{52}$$

where the $\delta\eta_j$'s involved are free and independent. For semiholonomic constraints, Hamilton's principle is generalized to

$$\delta S^{(\mathrm{sh})}=\delta\int_{t_1}^{t_2}L^{(\mathrm{sh})}(\dot{\boldsymbol{\eta}},\boldsymbol{\eta},t)dt=\delta\int_{t_1}^{t_2}[L+\mu_k(t)g_k^{(\mathrm{sh})}(\mathbf{q},\dot{\mathbf{q}},t)]dt=0. \tag{53}$$

The essential reason for the validity of (52) and (53) is that the paths $\mathbf{q}+\delta\mathbf{q}$ admitted into the variational procedures are all geometrically possible, that is $\delta f_k=0$ and $\delta g_k^{(\mathrm{sh})}=0$ and that the δ and $\int$ operations commute. The correct equations of state (19) and (49) with $Q_j^{\mathrm{NP}}=0$ are recovered from (52) and (53), respectively. Because $g_k^{(\mathrm{sh})}$ is, by definition, the perfect differential df_k/dt, then provided that f_k is known, Eq. (53) reduces to

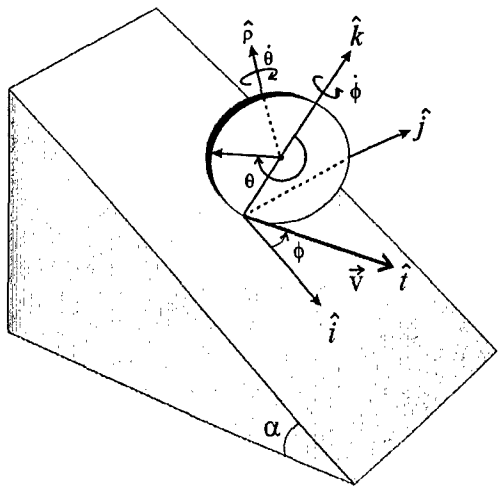

Fig. 1. An upright coin rolls and spins down an inclined plane of angle α. Directions of space-fixed axes are $\hat{i}$, $\hat{j}$, and $\hat{k}$, as indicated. Coin rolls with angular velocity $\vec{\omega}_{\text{Rol}}=\dot{\theta}\hat{\rho}$ about axis $\hat{\rho}$ which in turn spins with angular velocity $\vec{\omega}_S=\dot{\phi}\hat{k}$ about fixed axis $\hat{k}$. The center of mass has velocity $\vec{v}=R\dot{\theta}\hat{t}$.

$$\delta S^{(\text{sh})}=\delta\int_{t_1}^{t_2}\left[L+\frac{d}{dt}(\mu_k f_k)-\dot{\mu}_k f_k\right]dt$$

$$=\delta\int_{t_1}^{t_2}[L-\dot{\mu}_k(t)f_k(\mathbf{q},t)]dt=0, \tag{54}$$

the holonomic form (52), as expected. The relationship between the multipliers is $\lambda_k=-\dot{\mu}_k$, as also shown in Sec. II C.

Hamilton's variational principle (51) cannot be generalized to inexact linear or more general nonholonomic constraints, Eq. (9) or (7), by replacing L by $L+\mu_k g_k$ in Eq. (51), as has been suggested.[1-3] The fact that $\delta g_k\neq 0$ for these cases implies that the varied paths are not geometrically possible. We have shown that generalization of Hamilton's and D'Alembert's principles rests on the multiplier rule which demands that the varied paths be geometrically possible, a property reserved only for holonomic and semiholonomic systems.

F. Validity of generalized principles and multiplier rule

The generalized principles of D'Alembert and Hamilton are effected by the multiplier rule (see the Appendix). The theorem (rule) applies only when all varied paths $(\mathbf{q}+\delta\mathbf{q})$ preserve the side conditions $g_k(\mathbf{q}+\delta\mathbf{q},\dot{\mathbf{q}}+\delta\dot{\mathbf{q}},t)=0$, that is the $\delta\mathbf{q}$ variation causes no change $\delta g_k=0$ to g_k. The displaced paths are then geometrically possible in that they satisfy the same equations of constraint. It is only for holonomic and semiholonomic constraints that the appropriate criteria, $\delta f_k=0$ and $\delta g_k^{(\text{sh})}=0$, are satisfied. For all nonholonomic constraints, the conditions $g_k=0$ cannot be satisfied by the displaced paths and are therefore not good constant side conditions, as the multiplier rule demands. The invariance of the constraint equations to displacements is the key condition for application of the multiplier rule. The application of Eq. (6) to nonholonomic constraints is therefore without justification.

III. A TEST CASE

Some of these key points may be tested by the physical system depicted in Fig. 1. The solution of this spinning–rolling problem does not appear to have been provided in any standard textbook, although the limiting cases of rolling without spinning down a plane[1] and rolling–spinning on a horizontal plane[8,10] have been analyzed. Let $\mathbf{r}_{\text{c.m.}}=x\hat{i}+y\hat{j}+z\hat{k}$ be the Cartesian coordinate of the center of mass (c.m.) of the coin of mass M and radius R, where the origin O is at the top of plane and where the directions $\hat{i}$, $\hat{j}$, and $\hat{k}$ form a Cartesian (X,Y,Z) fixed set of axes, with $\hat{i}$ pointing directly downward along the plane. Let θ and ϕ be the angles associated with the rolling and spinning motions about the symmetry axis (which is perpendicular to the coin) and the axis pointing along $\hat{k}$, the fixed outward normal to the plane. The Lagrangian is

$$L=\tfrac{1}{2}M(\dot{x}^2+\dot{y}^2)+\tfrac{1}{2}I_S\dot{\theta}^2+\tfrac{1}{2}I_D\dot{\phi}^2+Mgx\sin\alpha, \tag{55}$$

where $I_S=\beta MR^2$ and I_D are the moments of inertia of the body about the symmetry axis and the fixed Z-figure axis, respectively. Cases involving a solid sphere, coin, solid cylinder, spherical shell, hoop, or cylindrical shell, can be treated by taking $\beta=2/5$, 1/2, 1/2, 2/3, 1, and 1, respectively.

Rolling without spinning: $\dot{y}=0$, $\dot{\phi}=0$. This example is a simple test of our proof that semiholonomic (exact linear) constraints $g_k^{(\text{sh})}(\mathbf{q},\dot{\mathbf{q}},t)=0$ are covered by D'Alembert's and Hamilton's generalized principles, Eq. (49) or Eq. (53), respectively. The rolling constraint $g=\dot{x}-R\dot{\theta}=0$ is exact so that the generalized principles should work. If we apply either Eq. (49) or (53) to the augmented Lagrangian,

$$L^{(\text{sh})}(\boldsymbol{\eta},\dot{\boldsymbol{\eta}})=\tfrac{1}{2}M\dot{x}^2+\tfrac{1}{2}I_S\dot{\theta}^2+Mgx\sin\alpha+\mu(\dot{x}-R\dot{\theta}), \tag{56}$$

for the extended set $\boldsymbol{\eta}=(x,\theta,\mu)$ of free coordinates, we obtain the equations of state, $M\ddot{x}=Mg\sin\alpha-\dot{\mu}$, $I_S\ddot{\theta}=\dot{\mu}R$, and $\dot{x}=R\dot{\theta}$. When decoupled, these equations yield the acceleration $\ddot{x}=g\sin\alpha/(1+\beta)$ and the frictional constraint force $\dot{\mu}$ which produces the torque needed for rolling motion, $[(\beta/(1+\beta)]Mg\sin\alpha$, in agreement with standard results[1,8-10,13] obtained from holonomic theory, Eq. (22).

Rolling and spinning in two dimensions. We now test to see if linear conditions exist between the displacements δq_j needed for D'Alembert's basic principle (14) and then see if the constraints imply geometrically possible displaced paths, as needed for the generalized principles. The constraint for rolling is now

$$g_1'(\dot{x},\dot{y},\dot{\theta})=[\dot{x}^2+\dot{y}^2]^{1/2}-(R\dot{\theta})^2=0, \tag{57}$$

which is nonintegrable and quadratic in the generalized velocities. There is no velocity component perpendicular to $\hat{\mathbf{v}}$ so that a second constraint is

$$g_2(\dot{x},\dot{y})=\dot{x}\sin\phi-\dot{y}\cos\phi=0, \tag{58}$$

which is also nonintegrable, but linear in the generalized velocities. That the coin remains upright implies that the center of mass coordinates (x,y) are also those for the point of contact of the coin with the plane and that $z=R$, a holonomic constraint which can be embedded from the outset unless the normal reaction (constraint) of the plane on the

coin is sought. From Eqs. (57) and (58), the virtual displacements satisfy

$$(\delta x)^2+(\delta y)^2-R^2(\delta\theta)^2=0, \tag{59}$$

$$\delta x \sin\phi-\delta y\cos\phi=0. \tag{60}$$

The relation (60) is linear in δq_j and therefore amenable to being absorbed into D'Alembert's principle, Eq. (14). The quadratic relation (59) cannot be directly absorbed. Fortunately, for this case, the offending quadratic constraint (57) can be replaced by the combination $g_1^2=g_1'^2-g_2^2$ of g_1' and g_2 to give

$$g_1(\dot{x},\dot{y},\dot{\theta})=\dot{x}\cos\phi+\dot{y}\sin\phi-R\dot{\theta}=0, \tag{61}$$

which leads to the linear form,

$$\delta x\cos\phi+\delta y\sin\phi-R\delta\theta=0, \tag{62}$$

which is now suitable for application of D'Alembert's principle. The displaced paths $q_j+\delta q_j$ cause the changes,

$$\delta g_1=\delta\dot{x}\cos\phi+\delta\dot{y}\sin\phi-R\delta\dot{\theta} -(\dot{x}\sin\phi-\dot{y}\cos\phi)\delta\phi, \tag{63a}$$

$$\delta g_2=\delta\dot{x}\sin\phi-\delta\dot{y}\cos\phi+(\dot{x}\cos\phi+\dot{y}\sin\phi)\delta\phi, \tag{63b}$$

in the constraint conditions (58) and (61). Because $\delta\dot{q}_j=d(\delta q_j)/dt$, then, on using the time derivatives of Eqs. (60) and (62) together with the relations (58)–(62), δg_1 and δg_2 reduce to 0 and $R(\dot{\theta}\delta\phi-\dot{\phi}\delta\theta)$, respectively. Therefore, the constraint (61) is semiholonomic. Integration yields the holonomic form $x^2+y^2-R^2\theta^2=0$. Because the sum $\delta(\lambda_k g_k)=\delta(\lambda_2 g_2)\neq 0$, we cannot use D'Alembert's or Hamilton's generalized principles, Eqs. (29) and (53), respectively, as predicted.

Because the conditions (60) and (62) on the displacements are now all linear, the problem can be solved by D'Alembert's basic principle (14), or by its time-integrated version, Hamilton's integral principle (50). The solution is straightforward and reduces to the standard results[8,10] for horizontal motion ($\alpha=0$).

IV. SUMMARY AND CONCLUSIONS

This paper has presented the basic reason why Hamilton's variational principle and the more basic principle of D'Alembert cannot be generalized by substituting the augmented Lagrangian Eq. (8) in either Eq. (2) or Eq. (14) to cover general nonholonomic constraints, as the multiplier rule[5–7] in the calculus of variations might suggest.[1–3] The multiplier rule requires that the side conditions $g_k=0$ be satisfied by all varied paths, which must therefore be geometrically possible. The displacements δq_j in nonholonomic systems violate this rule because they cause nonzero changes $\delta g_k\neq 0$ in the constraint conditions and the displaced paths are not geometrically possible. The constraint $g_k=0$ is satisfied only by the actual physical path $\mathbf{q}(t)$ in configuration space and not by the individual members of the family of varied paths for nonholonomic systems. The multiplier rule cannot therefore be used to generalize Hamilton's or D'Alembert's principles to cover nonholonomic constraints. It can however be applied to all holonomic and semiholonomic (exact linear) constraints which have the property that all displaced paths are geometrically possible in accord with the multiplier rule.

We have traced the development of various generalized principles from D'Alembert's basic principle in such a way as to render transparent their scope of application. It is useful to keep the following conclusions in mind.

(1) D'Alembert's basic principle, Eq. (14), is the most fundamental of all the principles considered here.
(2) D'Alembert's basic principle, Eq. (14), and Hamilton's variational principle, Eq. (2), are well designed for holonomic systems. Equation (16) is the equation of state.
(3) When constraint forces in holonomic systems are sought, D'Alembert's generalized principle, Eq. (22), and Hamilton's generalized principle, Eq. (5), are appropriate, because the varied paths under holonomic constraints are all geometrically possible and the underlying multiplier rule is then valid. Equation (6) is the equation of state.
(4) The correct equations of state (28) for general linear nonholonomic constraints are furnished only by D'Alembert's basic principle, Eq. (14), or its time-integrated version, Hamilton's integral principle, Eq. (50).
(5) As shown here, the generalized principles, Eqs. (29) and (53), are valid for semiholonomic systems. In these generalized principles, the constraints are automatically included and the displacements $\delta\eta_j$ are all free. Equation (49) is the equation of state for semiholomic systems, that is, those which satisfy conditions for exactness and therefore geometrically possible displaced paths.
(6) Generalized principles are inappropriate for linear nonholonomic constraints, because the constraint equations $g_k=0$ are not exact and change from varied path to varied path. The underlying multiplier rule then loses validity.
(7) The theory for nonholonomic constraints with a general velocity dependence remains outside the scope of the most fundamental principle, Eq. (14) of D'Alembert. It is impossible to extract from the equations $g_k=0$ of general nonholonomic constraints the linear relation between the δq_j's required for the application of D'Alembert's principle unless the constraints are either linear in velocity or holonomic. Nonholonomic constraints are therefore outside the scope of any of the principles based on D'Alembert's principle.

The above conclusions reflect the intrinsic merit of reconstructing the variational principle, Eq. (2), from the more fundamental D'Alembert principle, Eq. (14) via Eq. (47), so that the validity of the various stages involved becomes directly exposed. Pitfalls[1–3] can easily occur by arbitrarily invoking the multiplier rule to assert generalized principles such as Eqs. (29) and (53), without first ascertaining the critical but hidden condition that the varied paths must be geometrically possible. We have shown here that the condition is satisfied only for holonomic and semiholonomic systems.

General nonholonomic constraints (7) can be analyzed by other principles[13] that involve, for example, the virtual velocity (Jourdain) displacements, constructed by maintaining both the configuration $\mathbf{q}$ and time t fixed, in contrast to virtual displacements δq_j which keep only t fixed. The Jourdain variational principle is the subject of a separate paper.[14]

APPENDIX: THE MULTIPLIER THEOREM

We will determine the paths $q_i(t)$; $i=1,2,\ldots,n$ that provide an extremum to the functional

$$J=\int_{t_1}^{t_2}F(\mathbf{q},\dot{\mathbf{q}},t)dt, \tag{A1}$$

subject to the $c<n$-finite auxiliary (side) conditions

$$g_k(\mathbf{q},\dot{\mathbf{q}},t)=0. \quad (k=1,2,\ldots,c). \tag{A2}$$

A basic theorem[5–7] in the calculus of variations can be invoked, provided we admit to the variational competition only those curves $\mathbf{q}(t)$ that satisfy fixed end-point conditions $\delta\mathbf{q}(t_{1,2})=0$ and c-finite fixed side conditions as in Eq. (A2). The varied curves must all be geometrically possible by satisfying $g_k(\mathbf{q}+\delta\mathbf{q},\dot{\mathbf{q}}+\delta\dot{\mathbf{q}},t)=g_k(\mathbf{q},\dot{\mathbf{q}},t)+\delta g_k(\mathbf{q},\dot{\mathbf{q}},t)=0$, so that $\delta g_k=0$. The physical path $\mathbf{q}(t)$ is then determined by the extremum determined by the free variation of the modified functional,

$$J^\dagger=\int_{t_1}^{t_2}F^\dagger(\mathbf{q},\dot{\mathbf{q}},t)dt\equiv\int_{t_1}^{t_2}[F(\mathbf{q},\dot{\mathbf{q}},t)+\lambda_k(t)g_k(\mathbf{q},\dot{\mathbf{q}},t)]dt, \tag{A3}$$

without any side conditions imposed. The physical path $\mathbf{q}(t)$ then satisfies the Euler–Lagrange system of equations,

$$\frac{d}{dt}\left(\frac{\partial F^\dagger}{\partial\dot{\eta}_j}\right)-\frac{\partial F^\dagger}{\partial\eta_j}=0, \quad (j=1,2,\ldots,n+c) \tag{A4}$$

for the extended set $\boldsymbol{\eta}\equiv\{q_1,q_2,\ldots,q_n,\lambda_1,\lambda_2,\ldots,\lambda_c\}$ of $(n+c)$ variables. Because $F^\dagger$ does not depend on $\dot{\lambda}_k(t)$, the last c members of the set of equations (A4) reproduce the side conditions (A2). The validity of the multiplier theorem, Eqs. (A3) and (A4), rests on the fact that conditions (A2) must be satisfied by *all* the varied paths therein, that is, $\delta g_k=0$. This condition is satisfied for holonomic and semiholonomic constraints. It is not satisfied for nonholonomic constraints because $\delta g_k\neq 0$ for this case; the condition $g_k=0$ is satisfied only by the physical path to be eventually determined. The theorem is therefore irrelevant to nonholonomic systems.

However, the multiplier theorem is directly relevant to the related principle[1,8,11,13]

$$\Delta S_A=\Delta\int_{t_1}^{t_2}p_i\dot{q}_i dt=[p_i\Delta q_i]_{t_1}^{t_2}=0 \tag{A5}$$

of least abbreviated action S_A, valid for varied curves, all chosen to obey the same constant Hamiltonian H and to pass through the end points, that is, $\Delta q_i(t_{1,2})=0$. It is similar in form to Eqs. (50) and (51). The Δ operator causes nonsimultaneous variations $\Delta q_i=\delta q_i+\dot{q}_i\Delta t$, which also involve displacements Δt in time, in addition to the usual virtual displacements δq_i. When the kinetic energy T reduces to a homogeneous quadratic function $T_2=\frac{1}{2}M_{ij}(\mathbf{q})\dot{q}_i\dot{q}_j$ of the generalized velocities $\dot{q}_i$, then $p_i\dot{q}_i=2T$ and the least action principle, Eq. (A5), reduces to the Euler–Lagrange–Maupertuis principle,[1,8,11,13]

$$\Delta\int_{t_1}^{t_2}2T\,dt=0, \tag{A6}$$

of least action. The multiplier theorem, Eqs. (A3) and (A4), can now be applied to extract Lagrange's equations from Eq. (A6). The condition for the variation (A6) is that the Hamiltonian H does not depend on time and remains fixed at the same value for all the paths considered. In the sense that $(t,-H)$ are conjugate variables, the principle (A6), which admits paths with the same constant H, is complementary to Hamilton's variational principle, Eq. (2), which admits only those paths with the same transit times $\tau=t_1-t_2$ into the variation. For $T=T_2$, H equals the total energy $E=T+V$, so that Eq. (A6) becomes modified, under the fixed constraint $g=(T+V)-E=0$ for all varied paths, to finding a stationary value of

$$\Delta\int_{t_1}^{t_2}[2T(\mathbf{q},\dot{\mathbf{q}})+\lambda(t)\{T(\mathbf{q},\dot{\mathbf{q}})+V(\mathbf{q})-E\}]dt=0. \tag{A7}$$

The application[8,11,13] of this modified version (A7) of the Euler–Lagrange–Maupertuis principle leads directly to the standard Lagrange's equations (16), with $Q_j^{\mathrm{NP}}=0$ for potential systems.

[a]Electronic mail: ray.flannery@physics.gatech.edu

[1]H. Goldstein, C. Poole, and J. Safko, *Classical Dynamics* (Addison–Wesley, New York, 2002), 3rd ed., pp. 46–48. This generalized action principle is retracted without explanation at ⟨http://astro.physics.sc.edu/Goldstein/⟩, pp. 356–360.
[2]G. H. Goedecke, "Undetermined multiplier treatments of the Lagrange problem," Am. J. Phys. **34**, 571–574 (1966).
[3]J. R. Ray, "Nonholonomic constraints," Am. J. Phys. **34**, 406–408 (1966).
[4]J. R. Ray, "Erratum: Nonholonomic constraints," Am. J. Phys. **34**, 1202–1203 (1966).
[5]D. A. Pierre, *Optimization Theory with Applications* (Dover, New York, 1986), p. 92.
[6]I. M. Gelfand and S. Fomin, *Calculus of Variations* (Dover, New York, 2000), p. 48.
[7]L. Elsgolc, *Calculus of Variations* (Addison–Wesley, Reading, MA, 1962), p. 136.
[8]R. M. Rosenberg, *Analytical Dynamics of Discrete Systems* (Plenum, New York, 1977), pp. 176–178, 220, 232–235, 265–268.
[9]D. T. Greenwood, *Classical Dynamics* (Dover, New York, 1997), pp. 159–162.
[10]J. V. José and E. J. Saletan, *Classical Dynamics* (Cambridge UP, Cambridge, 1998), pp. 114–116.
[11]L. A. Pars, *An Introduction to the Calculus of Variations* (Wiley, New York, 1962), pp. 253, 249.
[12]I. Gatland, "Nonholonomic constraints: A test case," Am. J. Phys. **72**, 941–942 (2004).
[13]L. A. Pars, *A Treatise on Analytical Dynamics* (Ox Bow, Woodbridge, CT, 1979), pp. 543–545.
[14]M. R. Flannery, "Theory for general nonholonomic constraints," (unpublished).

Magnetic stabilization of a Rydberg quasimolecule in circular states

M. R. Flannery[1] and E. Oks[2]
[1]*School of Physics, Georgia Institute of Technology, Atlanta, Georgia 30332, USA*
[2]*Physics Department, 206 Allison Lab., Auburn University, Auburn, Alabama 36849-5311, USA*
(Received 24 June 2005; published 13 January 2006)

An exact analytical classical solution for the electronic terms of circular Rydberg states (CRS) in the presence of a magnetic field B is obtained for two-Coulomb-center systems. The classical electronic terms are shown to be significantly affected by the magnetic field. In particular, a sufficiently strong magnetic field is shown to cause the appearance of CRS above the ionization threshold. These CRS are the classical molecular counterparts of the quantal atomic quasi-Landau levels (resonances). Study of the stability of the nuclear motion in this system reveals that the system in CRS is, in the absence of the magnetic field, not really a molecule, but only a quasimolecule with antibonding molecular orbitals. We also find that the magnetic field creates a deep minimum in one of the branches of the effective potential of the relative motion of the nuclei, and thereby stabilizes the nuclear motion. We have therefore shown that a magnetic field can transform the quasimolecule into a real, classically described molecule where one of the molecular orbitals becomes bonding. This result reveals a phenomenon—the magnetically controlled stabilization of the quasimolecules in CRS—which is appropriate for future experimental studies.

DOI: 10.1103/PhysRevA.73.013405 PACS number(s): 32.60.+i, 33.15.−e, 31.15.−p, 52.25.−b

I. INTRODUCTION

Circular Rydberg states (CRS) of atomic and molecular systems, with only one electron, correspond to $|m|=n-1 \gg 1$, where n and m are the principal and magnetic electronic quantum numbers, respectively. They have been extensively studied [1–4] both theoretically and experimentally for several reasons: (a) CRS have long radiative lifetimes and highly anisotropic collision cross sections, thereby enabling experiments on inhibited spontaneous emission and cold Rydberg gases [5,6], (b) classical CRS correspond to quantal coherent states, objects of fundamental importance, and (c) a classical description of CRS is the primary term in the quantal method based on the $1/n$ expansion (see, e.g. Ref. [7] and references therein). In the present paper we focus on the analytical classical description of CRS of two-Coulomb-center systems in a magnetic field B parallel to the internuclear axis. The system consists of two nuclei of charges Ze and $Z'e$, separated by a distance R, and one electron and is denoted as ZeZ'. Analytical results for the electronic terms $E(R)$ of the ZeZ' system for the field-free case were obtained [8,9] from first principles within a purely classical approach. The classical approach reproduces [8,9] several electronic terms and two of these terms undergo a V-shape crossing at separation R^*, so that CRS cannot exist for $R<R^*$.

In the present paper, an exact analytical classical solution is obtained for the electronic terms $E(R,B)$ for CRS of the ZeZ' system in the presence of a magnetic field B. The solution is exact and is valid for any strength of the magnetic field. We also study how the classical electronic terms are influenced by the magnetic field, including the case of a strong field. This is a fundamental problem in its own right.

The theory is then used to explore the stability of the nuclear motion in the ZeZ' system. It is found that the term $E(R,B)$ in the effective potential $V(R,B)=ZZ'/R+E(R,B)$ for the relative motion of the nuclei plays a crucial role. We find that the CRS system, in the absence of the magnetic field, is not a stable molecule, but is only a quasimolecule with antibonding molecular orbitals. A similar classical result was obtained by Pauli [10] for the hydrogen molecular-ion H_2^+. We find that a magnetic field creates a deep minimum in one of the branches of the effective potential $V(R,B)$ for relative motion of the nuclei, so as to render stable nuclear motion. The magnetic field can therefore be used to transform a quasimolecule into a real CRS molecule with a bonding molecular orbital. This finding initiates a phenomenon—*the magnetically-controlled stabilization of the CRS quasimolecules*—suitable for future experimental studies.

II. ELECTRONIC TERMS IN A MAGNETIC FIELD

Let the charge Z of the two-Coulomb-center system be fixed at the origin and the charge Z' be located along the OZ axis at nuclear separation R. For simplicity, let the plane of the electron's circular orbit of radius ρ centered at z be perpendicular to the internuclear axis OZ. For $z \ll R$ or for $(R-z) \ll R$ when the electron is mainly bound to the Z or the Z' ion and is perturbed by the other fully stripped ion, these circular orbits depict Stark states which correspond classically to zero projection of the Runge-Lenz vector [11] on the axis OZ and quantally to zero electric quantum number $k=n_1-n_2$, where n_1 and n_2 are the parabolic quantum numbers [12]. The classical Hamiltonian for fixed R of the ZeZ' system in the presence of a uniform magnetic field B parallel to the internuclear axis is given in *au* by

$$H(\rho,z) = M^2/(2\rho^2) - Z/(\rho^2+z^2)^{1/2} - Z'/[\rho^2+(z-R)^2]^{1/2} + \Omega M + \Omega^2\rho^2/2, \quad \Omega \equiv B/(2c). \tag{1}$$

Here M is the constant z component of the angular momentum and Ω is the Larmor frequency expressed in practical units as $\Omega(\mathrm{s}^{-1}) \approx 8.794 \times 10^6\, B(\mathrm{G})$.

Introduce the following scaled quantities:

$$b \equiv Z'/Z, \quad u \equiv \rho/R, \quad w \equiv z/R, \quad m \equiv M/(ZR)^{1/2},$$
$$\omega \equiv \Omega M^3/Z^2, \quad h \equiv HM^2/Z^2, \tag{2}$$

so that the scaled Hamiltonian is

$$h = (u,w,\omega) = m^2\epsilon(u,w,\omega),$$

$$\epsilon(u,w,\omega) \equiv m^2/(2u^2) - 1/(u^2+w^2)^{1/2} - b/[u^2+(1-w)^2]^{1/2} + \omega/m^2 + \omega^2u^2/(2m^6). \tag{3}$$

The conditions for dynamic equilibrium are

$$\partial h/\partial w = m^2\{w/(u^2+w^2)^{3/2} - b(1-w)/[u^2+(1-w)^2]^{3/2}\} = 0 \tag{4}$$

and

$$\partial h/\partial u = m^2\{-m^2/u^3 + u/(u^2+w^2)^{3/2} + bu/[u^2+(1-w)^2]^{1/2} + \omega^2u/m^6\} = 0. \tag{5}$$

Equation (4) shows that equilibrium along the internuclear axis does not depend on the scaled magnetic field ω. In terms of the equilibrium value w_0 of w, the equilibrium value of u can therefore be expressed as

$$u(w_0,b) = \{[w_0(1-w_0)^2]^{2/3} - b^{2/3}w_0^2\}^{1/2}/\{b^{2/3} - [w_0/(1-w_0)]^{2/3}\}^{1/2}. \tag{6}$$

which only exists within the following "allowed ranges"

$$0 \leq w_0 < b/(1+b) \text{ and } 1/(1+b^{1/2}) \leq w_0 \leq 1, \quad b < 1,$$

$$0 \leq w_0 \leq 1/(1+b^{1/2}) \text{ and } b/(1+b) < w_0 \leq 1, \quad b > 1,$$

$$0 \leq w_0 \leq 1, \quad b = 1 \tag{7}$$

of w_0. Equation (5), represents the condition for equilibrium in the orbital plane and can be rewritten in the form

$$m(w_0,b,\omega) = \pm\{f/4 + (f^2/4+j)^{1/2}/2 + [f^2/2 - j + (f^3/4)/(f^2/4+j)^{1/2}]^{1/2}/2\}^{1/2}, \tag{8}$$

where, in terms of $u(w_0,b)$, given by Eq. (6),

$$f(w_0,b,\omega) \equiv u^4(w_0,b)/[u^2(w_0,b)+w_0^2]^{3/2} + bu^4(w_0,b)/[u^2(w_0,b)+(1-w_0^2)]^{3/2} \tag{9}$$

and

$$j(w_0,b,\omega) \equiv [u^4(w_0,b)\omega^2/18]^{1/3}g - (4/g)[u^8(w_0,b)\omega^4/3]^{1/3}, \tag{10}$$

with

$$g(w_0,b,\omega) \equiv |-9f^2 + [81f^4 + 768u^4(w_0,b)\omega^2]^{1/2}|^{1/3}. \tag{11}$$

The plus and minus signs in Eq. (8) correspond, respectively, to the positive and negative projections of the angular momentum along the magnetic field. For each set $\{b,m,\omega\}$ of parameters, Eq. (8) determines the equilibrium value w_0 of the scaled z coordinate of the orbital plane.

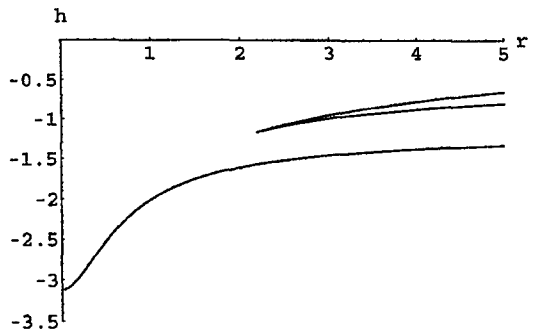

FIG. 1. The scaled electronic energy h versus the scaled internuclear distance r for the ratio of the nuclear charges $b=3/2$ at the absence of the magnetic field [h and r are defined by Eqs. (2) and (12), respectively].

The internuclear distance R as noted above was considered to be "frozen." In order to reproduce the electronic terms, i.e., the dependence of the electronic energy on the internuclear distance, one should now allow R to be a slowly varying adiabatic quantity (slowly varying with respect to the electronic motion, as in the Born-Oppenheimer approach [13]).

We consider energy terms of the *same symmetry* which, for the quantal ZeZ' problem, means terms with the same magnetic quantum number M [14–18]. Therefore, in our classical ZeZ' problem, from now on we consider fixed projection of the angular momentum M and study the behavior of the classical energy keeping M constant.

Introduce the scaled internuclear distance

$$r \equiv RZ/M^2 \tag{12}$$

which, under the fourth relation in Eq. (2), reduces to

$$r(w_0,b,\omega) = 1/m^2(w_0,b,\omega). \tag{13}$$

On substituting $w=w_0$ into Eq. (3), then

$$h(w_0,b,\omega) = m^2(w_0,b,\omega)\epsilon[u(w_0,b),w_0,\omega]. \tag{14}$$

Thus, for any positive ratio of the nuclear charges $b>0$ and for any value of the scaled magnetic field ω, the dependence of the scaled energy h on the scaled internuclear distance r is determined by Eqs. (13) and (14) in terms of the parameter w_0, which takes all values from the allowed ranges specified by Eq. (7), i.e., Eqs. (13) and (14) determine the *classical electronic energy terms* for any strength of the magnetic field, including the strong field case.

Figure 1 shows the scaled electronic energy h versus the scaled internuclear distance r for $b=3/2$ in the absence of magnetic field. There are three terms of the same symmetry, a totally counterintuitive result because there is more than one classical energy term. Moreover, two of these classical energy terms undergo a V-shape crossing.

We note that the upper and middle energy terms terminate at some $r=r_{\min}$, so that there are no CRS at $r<r_{\min}$ for these two energy terms. The classical energy of the CRS acquires an imaginary part at $r<r_{\min}$, corresponding quantally to vir-

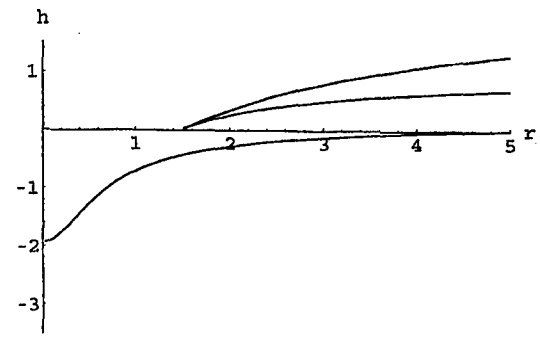

FIG. 2. Same as in Fig. 1, but at the scaled magnetic field $\omega=+1.1$. We note that $\omega>0$ corresponds to $BM>0$, while $\omega<0$ corresponds to $BM<0$; here B and M are z projections of the magnetic field and of the angular momentum, respectively; the Oz axis is directed from the charge Z toward the charge Z'.

tual states or resonances. There may well be noncircular Rydberg states at $r<r_{\min}$ in the same energy range, but this would be beyond the scope of the present paper.

We emphasize that the above example of $Z'/Z=3/2$ is fully representative. In fact, for any pair of Z and $Z'\neq Z$, there are three classical energy terms of the same symmetry and the upper term always crosses the middle term. (For $Z'=Z$ there is only one term in the corresponding plot and no crossing, as expected.)

Analysis, previously published [8,9], provided the following reason for these three energy terms. The lower term, as $R\to\infty$ corresponds to the energy $E\to-(Z_{\max}/M)^2/2$ of the hydrogen-like ion with nuclear charge $Z_{\max}\equiv\max(Z',Z)$ perturbed slightly by the other charge $Z_{\min}\equiv\min(Z',Z)$. As $R\to 0$, the lower term translates into the energy $E\to-(Z+Z')^2/(2M^2)$ of the hydrogenlike ion of the nuclear charge $Z+Z'$, i.e., to the united-atom limit [14–18].

The middle term as $R\to\infty$ corresponds to the energy $E\to-(Z_{\min}/M)^2/2$ of the hydrogenlike ion of nuclear charge $Z_{\min}$ slightly perturbed by the charge $Z_{\max}$. The upper term, as $R\to\infty$, evolves into a near-zero-energy state.

The analysis presented in Ref. [9] was not confined to circular orbits of the electron. In order to make the present work more transparent, we briefly outline here the scheme of that analysis. In cylindrical coordinates (z,ρ,ϕ), using the axial symmetry of the problem, the z and ρ motions, due to axial symmetry, can be separated from the ϕ motion. The ϕ motion can be determined from the calculated ρ motion. Equilibrium points of the two-dimensional motion in the $z\rho$ space were studied and a condition distinguishing between two physically different cases where the effective potential energy (1) has a two-dimensional minimum in the $z\rho$ space and (2) has a saddle point in the $z\rho$ space was explicitly derived. In particular, it turned out that the boundary between these two cases corresponds to the point of crossing of the upper and middle energy terms. For stable motion, the trajectory was found [9] to be a helix on the surface of a cone, with axis coinciding with the internuclear axis. In this *helical* state, the electron, while spiraling on the surface of the cone, oscillates between two end circles which result from cutting the cone by two parallel planes perpendicular to its axis.

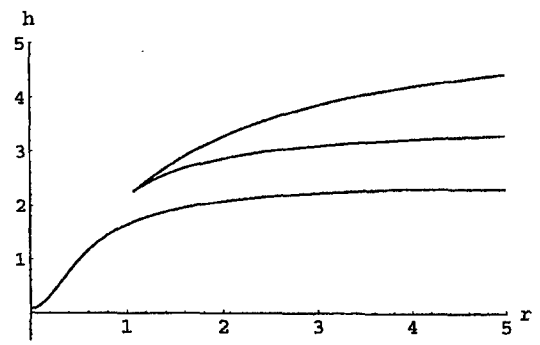

FIG. 3. Same as in Fig. 2, but at $\omega=+2.7$.

We now "turn on" the magnetic field—in contrast to the scope of papers [8,9]. Figure 2 shows the scaled electronic energy h versus the scaled internuclear distance r for $b=3/2$ at $\omega=+1.1$, i.e., at a moderate value of the magnetic field. We note that $\omega>0$ corresponds to $BM>0$, while $\omega<0$ corresponds to $BM<0$; remember B and M are the z projections of the magnetic field and of the angular momentum, respectively, and that the Oz axis is directed from the charge Z toward the charge Z'.

Figure 2 shows that the magnetic field corresponding to $\omega=+1.1$ and higher values, under the condition $BM>0$, lifts the entire upper and middle energy terms into the continuum. Figure 3 shows the scaled electronic energy h versus the scaled internuclear distance r for $b=3/2$ at $\omega=+2.7$, i.e., at a larger value of the magnetic field. It is seen that the magnetic field of this value (and of higher values), under the condition $BM>0$, lifts all three energy terms into the continuum.

These CRS above the ionization threshold, shown in Figs. 2 and 3, are *classical molecular counterparts of the quantal atomic quasi-Landau levels* or resonances. The latter were discovered experimentally by Garton and Tomkins [19] (for theoretical references on atomic quasi-Landau resonances, see, e.g., the book [20]).

III. MAGNETICALLY CONTROLLED STABILIZATION OF QUASIMOLECULES

The stability of the nuclear motion in the ZeZ' system is now explored. The electronic energy $E(R,B)$ becomes a crucial part of the effective internuclear potential

$$V(R,B)=ZZ'/R+E(R,B) \tag{15}$$

for the relative motion of the nuclei. The scaled internuclear potential

$$v\equiv VM^2/Z^2, \tag{16}$$

then reduces [cf. Eq. (14)] to

$$v(w_0,b,Z',\omega)=m^2(w_0,b,\omega)\{\epsilon[u(w_0,b),w_0,\omega]+Z'\}. \tag{17}$$

For any set $\{b,Z',\omega\}$, Eqs. (13) and (17) therefore determines the dependence of the scaled internuclear potential v on the scaled internuclear distance r in terms of the parameter w_0 which takes all values within the allowed ranges

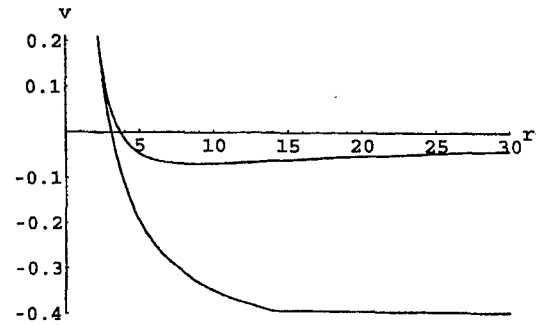

FIG. 4. The upper and middle branches of the scaled effective internuclear potential v [defined by Eqs. (15) and (16)] versus the scaled internuclear distance r for $Z=2$ and $Z'=3$ at the absence of the magnetic field.

specified by Eq. (7), i.e., Eqs. (13) and (17) determine the *classical effective internuclear potential* for any strength of the magnetic field, including the strong field case.

Figure 4 shows the upper and middle branches of the scaled effective internuclear potential v versus the scaled internuclear distance r for $Z=2$ and $Z'=3$ in the absence of the magnetic field. It is seen for any starting point at the middle branch that the system would "find" the way to lowering its potential energy without any obstacle and would end up at an infinitely large internuclear distance, thereby resulting in dissociation. The same is true for the lower branch (not shown in Fig. 4). In other words, in the absence of the magnetic field, the CRS system, associated with the middle or lower branches of the effective potential energy, is not really a molecule, but only a quasimolecule because the molecular orbital is *antibonding*. As we noted, the corresponding classical result was obtained previously by Pauli [10] for the molecular hydrogen ion H_2^+. The upper branch in Fig. 4 displays a very shallow minimum of $v=-0.0688$ located at $r=8.7$.

We now "turn on" the magnetic field. Figure 5 shows the upper and middle branches of the scaled effective internuclear potential v versus the scaled internuclear distance r for $Z=2$ and $Z'=3$ at a relatively small scaled magnetic field

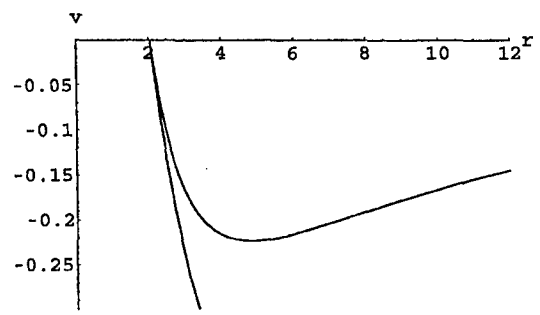

FIG. 5. The same as in Fig. 4, but at the scaled magnetic field $\omega=-0.3$ (note that $BM<0$).

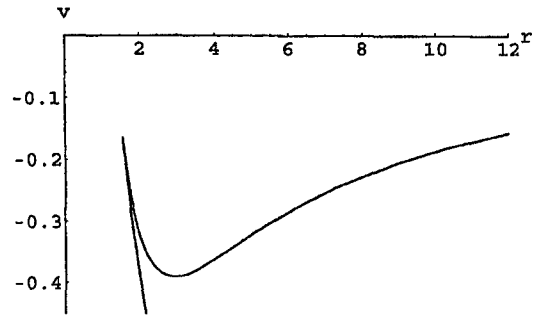

FIG. 6. The same as in Fig. 4, but at the scaled magnetic field $\omega=-1$.

$\omega=-0.3$ (with $BM<0$).[1] It is seen that the minimum in the upper branch became significantly deeper and moved towards lower r.

Figure 6 shows the same as Fig. 5, but for $\omega=-1$. As the magnetic field increased, it is seen that the minimum in the upper branch becomes further deepened and moves even closer to the origin.

The "cusp" formed by the upper and middle branches in Figs. 4–6 reflects the fact that the upper and middle energy terms for the corresponding electronic terms terminate at some $r=r_{\min}$—as already noted in Sec. II. Although present in CRS, this cusp may not appear in noncircular Rydberg states, a topic beyond the scope of the present CRS study.

Figures 4–6 reveal *magnetic stabilization of the nuclear motion* for the case of $BM<0$. Indeed, in the absence of the magnetic field, the potential well is very shallow. It is known that too shallow potential wells do not have any quantal discrete energy levels (see, e.g., Ref. [12]). Moreover, if this system is embedded in a plasma, then due to the known phenomenon of the "continuum lowering" by the plasma environment (see, e.g., books or reviews [21–23] and references therein), the minimum of this very shallow potential well in Fig. 4 could be "absorbed" by the lowered continuum. The magnetic field dramatically deepens the potential well and therefore stabilizes the system for the case of $BM<0$. The magnetic field can therefore transform the quasimolecule into a real, classically described molecule so that the molecular orbital becomes *bonding*.

The particular example of the system chosen for Figs. 4–6 corresponds to the CRS of an electron in the vicinity of the nuclei of He and Li. Both nuclei are usually present in magnetic fusion plasmas. Moreover, in such plasmas, Rydberg states of either of these nuclei result from charge exchange with ions of higher nuclear charge that are always present in magnetic fusion plasmas. Relatively large magnetic-field strengths are also present. It should be therefore possible to observe magnetic stabilization of the quasimolecule $HeLi^{4+}$ present in these practically important experimental devices.

The present analysis has also shown that a similar magnetic stabilization of Rydberg quasimolecules in CRS is displayed by other (though not all) ZeZ' systems characterized

[1]The scaled magnetic field $|\omega|=0.3$ would correspond to the magnetic field $B\sim 10^5$ G for $|M|\sim 30$. The magnetic field $B\sim 10^5$ G would be typical for magnetic fusion devices under construction.

by the ratio of the nuclear charges in the range: $1<Z'/Z<3$. Our results open up this phenomenon for *possible further theoretical and experimental investigation.*

IV. CONCLUSIONS

For two-Coulomb-center systems (ZeZ' systems), an *exact analytical classical solution for the electronic terms* $E(R,B)$ of CRS at the presence of the magnetic field **B** has been obtained. The solution, being exact, is valid for any strength of the magnetic field. We have shown that the classical electronic terms are significantly affected by the magnetic field. In particular, we have demonstrated that a sufficiently strong magnetic field causes the appearance of CRS above the ionization threshold—for the case of $BM>0$. These CRS are *classical molecular counterparts of the quantal atomic quasi-Landau levels* (or resonances) discovered experimentally by Garton and Tomkins [19].

As an application of the above results, we studied the stability of the nuclear motion in the ZeZ' system. We found that the nuclear motion for $B=0$ is unstable: two out of three branches of the effective potential energy do not have any minimum, while the third branch has only a very shallow minimum. In the absence of the magnetic field, the system in CRS is therefore not really a molecule, but only a quasimolecule and the molecular orbitals are *antibonding*. The magnetic field is shown to dramatically deepen the potential well, corresponding to the third branch, so that the nuclear motion of the system is therefore stabilized for the case of $BM<0$. We have demonstrated that the magnetic field can transform the quasimolecule into a real, classically described molecule where one of the molecular orbitals becomes *bonding*.

For example, it should be possible to observe the magnetic stabilization of the quasimolecule $HeLi^{4+}$ present in magnetic fusion devices. Some other highly excited ZeZ' systems, characterized by the ratio of the nuclear charges in the range $1<Z'/Z<3$, can also exhibit magnetic stabilization. Our present findings have introduced a phenomenon—*magnetically controlled stabilization of the quasimolecules in CRS*—for future theoretical and experimental studies.

ACKNOWLEDGMENTS

This work is supported by AFOSR Grant No. 49620-02-1-0338 and NSF Grant No. 04-00438 to Georgia Institute of Technology.

[1] E. Lee, D. Farrelly, and T. Uzer, Opt. Express **1**, 221 (1997).
[2] T. C. Germann, D. R. Herschbach, M. Dunn, and D. K. Watson, Phys. Rev. Lett. **74**, 658 (1995).
[3] C. H. Cheng, C. Y. Lee, and T. F. Gallagher, Phys. Rev. Lett. **73**, 3078 (1994).
[4] L. Chen, M. Cheret, F. Roussel, and G. Spiess, J. Phys. B **26**, L437 (1993).
[5] S. K. Dutta, D. Feldbaum, A. Walz-Flannigan, J. R. Guest, and G. Raithel, Phys. Rev. Lett. **86**, 3993 (2001).
[6] R. G. Hulet, E. S. Hilfer, and D. Kleppner, Phys. Rev. Lett. **55**, 2137 (1985).
[7] V. M. Vainberg, V. S. Popov, and A. V. Sergeev, Sov. Phys. JETP **71**, 470 (1990).
[8] E. Oks, Phys. Rev. Lett. **85**, 2084 (2000).
[9] E. Oks, J. Phys. B **33**, 3319 (2000).
[10] W. Pauli, Ann. Phys. **68**, 177 (1922).
[11] L. D. Landau and E. M. Lifshitz, *Mechanics* (Pergamon, Oxford, 1960).
[12] L. D. Landau and E. M. Lifshitz, *Quantum Mechanics* (Pergamon, Oxford, 1965).
[13] M. Born and R. Oppenheimer, Ann. Phys. **84**, 457 (1927).
[14] S. S. Gershtein and V. D. Krivchenkov, Sov. Phys. JETP **13**, 1044 (1961).
[15] J. Von Neumann and E. Wigner, Phys. Z. **30**, 467 (1929).
[16] L. I. Ponomarev and T. P. Puzynina, Sov. Phys. JETP **25**, 846 (1967).
[17] J. D. Power, Philos. Trans. R. Soc. London, Ser. A **A274**, 663 (1973).
[18] I. V. Komarov, L. I. Ponomarev, and S. Yu. Slavyanov, *Spheroidal and Coulomb Spheroidal Functions* (Nauka, Moscow, 1976) (in Russian).
[19] W. R. S. Garton and F. S. Tomkins, Astrophys. J. **158**, 839 (1969).
[20] M. Brack and R. K. Bhaduri, *Semiclassical Physics* (Addison-Wesley, Reading, MA, 1997), Sec. 1.4.2.
[21] D. Salzmann, *Atomic Physics in Hot Plasmas* (Oxford University Press, Oxford, 1998), Chaps. 2 and 3.
[22] M. S. Murillo and J. C. Weisheit, Phys. Rep. **302**, 1 (1998).
[23] H. R. Griem, *Principles of Plasma Spectroscopy* (Cambridge University Press, Cambridge, UK, 1997), Secs. 5.5 and 7.3.

Equivalent multipole operators for degenerate Rydberg states

V. N. Ostrovsky

V. Fock Institute of Physics, St. Petersburg State University, 198904 St. Petersburg, Russia

D. Vrinceanu

Theoretical Division, Los Alamos National Laboratory, Los Alamos, NM 87545, USA

M. R. Flannery

School of Physics, Georgia Institute of Technology, Atlanta, GA 30332, USA

(Dated: March 16, 2006)

Abstract

As shown by Pauli [Z. Phys. **36**, 336 (1926)], the electric dipole operator $\mathbf{r}$ can be replaced by the Runge-Lenz vector $\mathbf{A}$ when operating within the degenerate n-manifold of hydrogenic states of principal quantum number n. We seek to develop similar rules for higher multipole operators by expressing equivalent operators in terms only of the two vector constants of motion – the orbital angular momentum $\mathbf{L}$ and the Runge-Lenz vector $\mathbf{A}$ – appropriate to the degenerate hydrogenic shell. Equivalence of two operators means here that they yield identical matrix elements within a subspace of Hilbert space that corresponds to fixed n. Such equivalent operator techniques permit direct algebraic calculation of perturbations of Rydberg atoms by external fields and often exact analytical results for transition probabilities. Explicit expressions for equivalent quadrupole and octupole operators are derived, examples are provided and general aspects of the problem are discussed.

PACS numbers: 34.60.+z,34.10.+x,31.15.Hz,32.60.+i

I. INTRODUCTION

Highly excited Rydberg states with the same principal quantum number n have small deviations from pure hydrogenic behavior. The degenerate shell of these states forms the basis of a representation of the $O(4)$ symmetry group [1] associated with the $1/r$ Coulomb potential governing the dynamics of the Rydberg electron. Many structural properties of the Rydberg atom can then be calculated by using algebraic rules and group representation techniques. These features combine mathematical beauty with pragmatic usefulness. Moreover, such algebraic techniques facilitate direct quantal and classical solution of Rydberg atoms in static external electric and magnetic fields [2], slow collisions with Rydberg atoms [3–5], and intrashell dynamics of a Rydberg atom in time-dependent electric and magnetic field [6]. For example, analytical probabilities have been derived [3–5], without the need for any perturbative and numerical analysis, for the full array of $\ell \to \ell'$ transitions in atomic hydrogen $H(n\ell)$ induced by a time-varying weak electric field generated by adiabatic collision with slow ions.

The dimension of the degenerate subspace grows as n^2 (without electron spin) and traditional close-coupling (R-matrix) calculations using spatial wave functions become prohibitively difficult and ultimately impractical, either because of the sheer dimension of the space or because of the large number of oscillations. Rydberg states with n as large as several hundred are now accessible to observations and experiments. The group representation technique may therefore offer the only practical and effective way of solving problems involving such Rydberg states. In so doing, some essential underlying physics can be exposed, as an additional asset.

In particular, the theory of a Rydberg atom in weak external electric and magnetic fields is reduced to an algebraic problem that is extremely well poised towards extracting both quantitative analytical results and qualitative insight. This is possible provided the necessary operators of interaction with the fields can be represented in terms of integrals of motion– the angular momentum operator $\mathbf{L}$ (common to all central field problems) and the Runge-Lenz vector $\mathbf{A}$ (specific to the Coulomb potential alone). This key step, basic to the subsequent algebraic construction, can be only taken when the dynamics becomes restricted to the subspace of energy degenerate states i.e., when the external perturbation is so weak that it does not induce $n - n'$ coupling among shells of different energy.

All of the above work [2–6] was based on a paper [7], as old as quantum mechanics. There, Pauli [7] has shown that the electric dipole operator $\mathbf{r}$ becomes identical with the Runge-Lenz vector when the two operators are restricted to an energy shell with fixed principal quantum number n. This can most easily be seen by comparing all the matrix elements of these operators between states within the same energy shell. The power of this result comes from its general validity and utility for any shell with quantum number n.

The advantage of expressing the intrashell dynamics of Rydberg atoms in terms of the $\mathbf{A}, \mathbf{L}$ set of constants for electronic coulombic motion has already been demonstrated [3–5] for collisional ℓ mixing transitions induced by a projectile charge-Rydberg dipole interaction. Also the interaction between two Stark-stretched (polar) Rydberg atoms has recently been expressed [8] in terms of interactions between the permanent multipoles of each atom. A basic question now arises quite naturally from these studies [3–5, 8]. It is one which does not appear to have been previously posed or addressed. *Can all higher multipole interactions be equivalently expressed solely in terms of the* $\mathbf{A}, \mathbf{L}$ *integrals of motion on the energy shell?*

In an effort to answer this, the present paper considers general equivalent multipole operators in Sections II and III. A procedure is then presented and applied, with examples, to the explicit determination in Sections IV, V and VI of the equivalent operators for the dipole, quadrupole and octupole moments, respectively. The algebraic evaluation of the operators in terms of $(\mathbf{A}, \mathbf{L})$ is conducted in the Appendices. Our eventual aim is to provide, if possible, the full solution for general multipoles. Atomic units are used throughout the paper, unless otherwise noted.

II. INTRASHELL EQUIVALENT OPERATORS

The angular momentum $\mathbf{L}$ and the unrestricted Runge-Lenz vector

$$\mathbf{U} = \frac{1}{2}\left(\mathbf{p} \times \mathbf{L} - \mathbf{L} \times \mathbf{p}\right) - \frac{\mathbf{r}}{r}$$

are constants of motion for the internal Hamiltonian $H = p^2/2 - 1/r$ of the Rydberg atom. A more convenient form for the unrestricted Runge-Lenz vector is

$$\mathbf{U} = \frac{1}{2}\mathbf{r}p^2 - \mathbf{p}(\mathbf{r} \cdot \mathbf{p}) + \mathbf{r}H.$$

The vector operators $\mathbf{L}$ and $\mathbf{U}$ do not close under commutation to form a Lie algebra because

$$[U_i, U_j] = (-2H)\mathrm{i}\epsilon_{ijk}L_k,$$

where ϵ_{ijk} is the Levi-Civita antisymmetric symbol for indices $i, j, k = 1, 2, 3$. If, however, the action of operators $\mathbf{U}$ is restricted to the Hilbert subspace of states with principle quantum number n, then the Runge-Lenz vector for *bound* states of energy E_n can be defined as

$$\mathbf{A} = \frac{1}{\sqrt{-2E_n}} \left[\frac{1}{2} \mathbf{r} p^2 - \mathbf{p}(\mathbf{r} \cdot \mathbf{p}) + \mathbf{r} E_n \right] . \tag{1}$$

The six components of the vector operators $\mathbf{A}$ and $\mathbf{L}$ are generators of the symmetry group SO(4) of proper rotation in four dimensions. They satisfy the commutation relations — $[A_i, A_j] = \mathrm{i}\epsilon_{ijk} L_k$, $[L_i, L_j] = \mathrm{i}\epsilon_{ijk} L_k$ and $[L_i, A_j] = \mathrm{i}\epsilon_{ijk} A_k$. The discrete part of the hydrogenic spectrum is then exhibited [7] by the theory of irreducible representations of SO(4).

When redefined by Eq. (1), the Runge-Lenz vector $\mathbf{A}$ acts only on states within the n-shell and has non-zero matrix elements only between states within the n-shell. If P_n is the projector onto the n-shell subspace then one can write

$$\mathbf{A} = P_n \frac{\mathbf{U}}{\sqrt{-2H}} P_n$$

The operators $\mathbf{A}$ and $\mathbf{U}/\sqrt{-2H}$ are *equivalent* because all their matrix elements are equal when evaluated between all states within the same n-shell. In general, the operators $\mathcal{A}$ and $\mathcal{B}$ are *equivalent* within the n-shell if all their intrashell matrix elements are equal

$$\langle n\gamma | \mathcal{A} | n\gamma' \rangle = \langle n\gamma | \mathcal{B} | n\gamma' \rangle \ . \tag{2}$$

The quantum numbers γ label the basis set which spans the n^2 degenerate subspace. Spherical (n, ℓ, m), parabolic (n_1, n_2, m), Stark (n, k, m) or algebraic (n, m_1, m_2) quantum numbers are all useful hydrogenic sets (see, e.g., Ref [8], Table 1). When an operator has an n-shell equivalent which can be expressed in terms of the constants of motion $\mathbf{L}$ and $\mathbf{A}$, then its intrashell matrix elements are easily calculated in any basis of states, using the SO(4) irreducible matrix representations. For example, Pauli [7] has proven that

$$P_n \mathbf{r} P_n = -\frac{3n}{2} \mathbf{A} \ ,$$

so that the dipole operator $\mathbf{r}$ within the n-shell is *equivalent* to $-3n/2\mathbf{A}$. The dipole matrix elements between all (ℓ, m) states of the same n are therefore simply related to the matrix elements of $\mathbf{A}$, which are then algebraically determined most effectively in the algebraic or Stark bases.

III. MULTIPOLE AND MULTIPOLE-TYPE OPERATORS

Many applications require calculation of matrix elements of higher multipole operators and therefore it is useful to find their n-shell equivalents. The spherical-coordinate representation of the multipole operator of order λ is

$$\mathrm{Q}_\mu^{(\lambda)} = \sqrt{\frac{4\pi}{2\lambda+1}}\, r^\lambda Y_{\lambda\mu}(\hat{\mathbf{r}})\,, \tag{3}$$

where $\mathbf{r}$ is the electron position vector, with magnitude r and direction $\hat{\mathbf{r}}$, and where μ are the $2\lambda+1$ components with $-\lambda \le \mu \le \lambda$. Eq. (3) for $\lambda = 1, 2, 3$ provides the dipole, quadrupole and octupole operators, respectively. In general, as a function of coordinates, the multipole $\mathrm{Q}_\mu^{(\lambda)}$ is a solution of the Laplace equation in the entire free space (excluding the singular $\mathbf{r} = \mathbf{0}$ point).

Another definition [9], which directly reveals the irreducible tensor properties of the multipole operators, is

$$\mathrm{Q}_\mu^{(\lambda)} = \sqrt{\frac{(2\lambda-1)!!}{\lambda!}} \Big\{ \ldots \big\{ \{\mathbf{r}\otimes\mathbf{r}\}^{(2)} \otimes \mathbf{r} \big\}^{(3)} \ldots \otimes \mathbf{r} \Big\}_\mu^{(\lambda)}\,, \tag{4}$$

which represents Q as a multiple irreducible tensor product of vector $\mathbf{r}$ over itself λ times. A *multipole-type* operator is obtained if the identical factors $\mathbf{r}$ are replaced by different vectors $\mathbf{a}$, $\mathbf{b}$, $\mathbf{c}$, ... Theory based on this definition will not be developed here but will be the subject of future investigation.

Representation of the multipole operator by its cartesian components provide several advantages for the approach taken in the present paper. The tensor $q^{(\lambda)}$ of rank λ with cartesian components

$$q_{i_1 i_2 \ldots i_\lambda} = \frac{(-1)^\lambda r^{2\lambda+1}}{(2\lambda-1)!!}\, \partial_{i_1}\partial_{i_2}\ldots\partial_{i_\lambda}\frac{1}{r} \tag{5}$$

is a harmonic polynomial of power λ in the cartesian components x_j $(j = 1, 2, 3)$ of the electronic position vector $\mathbf{r}$. Harmonic polynomials, by definition, satisfy Laplace equation. For $\lambda > 1$, the tensor (5) can be expanded as a sum of terms, as a result of taking successive derivatives. One of the terms is $x_{i_1} x_{i_2} \cdots x_{i_\lambda}$, while the remaining terms contain at least one Kronecker delta symbol for a pair of indices. However, not all 3^λ components of the tensor $q^{(\lambda)}$ are independent because the tensor is fully symmetrical with regard to index permutation and has zero trace when any pair of indices is contracted. The fully symmetric tensor has $\binom{\lambda+2}{\lambda}$ independent components and there are $\binom{\lambda}{2}$ pairs of indices for which

the trace is zero. The tensor $q^{(\lambda)}$ has therefore only $\binom{\lambda+2}{\lambda} - \binom{\lambda}{2} = 2\lambda + 1$ independent components. The first three multipole operators have the following cartesian components

$$q_i^{(1)} = x_i \ , \tag{6}$$

$$q_{ij}^{(2)} = x_i x_j - \frac{1}{3} r^2 \delta_{ij} \ , \tag{7}$$

$$q_{ijk}^{(3)} = x_i x_j x_k - \frac{1}{5} r^2 (x_i \delta_{jk} + x_j \delta_{ik} + r_k \delta_{ij}) \ , \tag{8}$$

for the dipole, quadrupole and octupole moments, respectively. An alternative definition for the cartesian components (5) is obtained by starting from the monomial $x_{i_1} x_{i_1} \cdots x_{i_\lambda}$ and constructing from it the tensor components $q_{i_1 i_2 \ldots i_\lambda}$ by adding terms such that the result has both the required symmetry and the zero trace condition for all pairs of indices. As an example, the octupole operator is explicitly derived via this procedure in section VI. This is also the way one can construct *multipole-type* operators starting from a set of vectors (**L** and **A** in our present case) which replace the position vector. For example, if one begins with vectors **a**, **b**, **c**, ..., the multipole-type operator contains the cartesian components $a_{i_1} b_{i_2} c_{i_3} \cdots$ and the remaining terms are obtained by permutations and contractions. Care must however be exercised when the operators do not commute.

A relation between the spherical (3) and cartesian (5) components of the multipole operator is facilitated by using the following definition for the spherical harmonics

$$Y_{LM}(\hat{r}) = (-1)^{L-M} \, r^\ell \left(\frac{2L+1}{4\pi (L+M)!(L-m)!} \right)^{1/2} (\partial_1 + i\partial_2)^M \partial_3^{L-M} \, \frac{1}{r} \ ,$$

so that

$$\mathrm{Q}_M^{(L)} = \frac{(-1)^M (2L-1)!!}{[(L+M)!(L-M)!]^{1/2}} \sum_{k=0}^{M} i^k \binom{M}{k} q_{\underbrace{1\ldots1}_{M-k}\underbrace{2\ldots2}_{k}\underbrace{3\ldots3}_{L-M}}$$

provides the required result. Explicit relations are

$$\begin{aligned} Q_0^{(1)} &= q_3^{(1)} \, , \\ Q_1^{(1)} &= -(q_1^{(1)} + i q_2^{(1)})/\sqrt{2} \, , \end{aligned} \tag{9}$$

for the dipole operator,

$$\begin{aligned} Q_0^{(2)} &= \frac{3}{2} \, q_{33}^{(2)} \, , \\ Q_1^{(2)} &= -\sqrt{\frac{3}{2}} \, (q_{13}^{(2)} + i q_{23}^{(2)}) \, , \\ Q_2^{(2)} &= \frac{1}{2}\sqrt{\frac{3}{2}} \, (q_{11}^{(2)} + 2i q_{12}^{(2)} - q_{22}^{(2)}) \, , \end{aligned} \tag{10}$$

for the quadrupole operator and

$$\begin{aligned} Q_0^{(3)} &= \frac{5}{2}\, q_{333}^{(3)}\,, \\ Q_1^{(3)} &= -\frac{5}{4}\sqrt{3}\,(q_{133}^{(3)} + iq_{233}^{(3)})\,, \\ Q_2^{(3)} &= \frac{1}{2}\sqrt{\frac{15}{2}}\,(q_{113}^{(3)} + 2q_{123}^{(3)} - q_{223}^{(3)})\,, \\ Q_3^{(3)} &= -\frac{1}{4}\sqrt{5}\,(q_{111}^{(3)} + 3iq_{112}^{(3)} - 3q_{122}^{(3)} - iq_{222}^{(3)}) \end{aligned} \tag{11}$$

for the octupole operator. We now seek to obtain equivalent multipole operators within the n-shell by constructing general multipole-type operators

$$P_n \mathrm{Q}^{(\lambda)} P_n = \mathcal{F}^{(\lambda)}(\mathbf{L}, \mathbf{A})$$

from the two vector constants of motion $\mathbf{L}$ and $\mathbf{A}$. Because the multipole operator $\mathrm{Q}^{(\lambda)}$ of order λ is a uniform function of coordinates of order λ, coordinate scaling $\mathbf{r} \to \gamma\mathbf{r}$ implies that the operator scales as $\mathrm{Q}^{(\lambda)} \to \gamma^\lambda \mathrm{Q}^{(\lambda)}$. We therefore require a similar property for the equivalent operator, such that $\mathcal{F}$ contains products of λ terms, where each of them can be either $\mathbf{L}$ or $\mathbf{A}$. Further restrictions follow from parity (coordinate-inversion) considerations—the parity of $\mathrm{Q}^{(\lambda)}$ is $(-1)^\lambda$, the parity of $\mathbf{A}$ is -1 and the parity of $\mathbf{L}$ is $+1$. Multipoles of even order may therefore contain only products of even number of $\mathbf{L}$ operators. The equivalent dipole operator (with odd parity) is expressed only in terms of $\mathbf{A}$. The equivalent quadrupole operator (even-parity) has terms $\mathbf{AA}$ and $\mathbf{LL}$, but not the odd-parity terms with $\mathbf{AL}$. Because of parity considerations, the equivalent octupole operator can only contain the two odd-parity terms, $\mathbf{AAA}$ and $\mathbf{ALL}$, while the even parity term $\mathbf{AAL}$ is forbidden.

IV. EQUIVALENT DIPOLE OPERATOR

Using the general procedure outlined in the previous section, we seek the operator equivalent to the dipole operator (6) in the form

$$P_n q^{(1)} P_n = P_n \mathbf{r} P_n = a\mathbf{A} + b\mathbf{L}\,.$$

The operator $\mathbf{L}$ has the opposite parity of $q^{(1)}$ and is therefore precluded by setting $b = 0$. The coefficient a is calculated by comparing the matrix elements of $\mathbf{A}$ and $\mathbf{r}$. Because of identical rotation properties of the two vectors, it is sufficient to calculate the matrix elements

only along one direction. It is convenient to choose this direction as the z-direction. Because of the selection rules, the dipole operator $\mathbf{r}$ and the Runge-Lenz vector $\mathbf{A}$ have non-zero matrix elements only between states with angular momentum quantum numbers differing by one unit ($\ell' = \ell \pm 1$).

Using Eq. (9), the intrashell matrix elements of the z-component of the dipole are

$$\langle n\ell - 1m|z|n\ell m\rangle = (R_{n\ell-1}|r|R_{n\ell})(Y_{\ell-1m}|Y_{10}|Y_{\ell m}) = -\frac{3}{2}n\sqrt{\frac{(n^2-\ell^2)(\ell^2-m^2)}{(2\ell-1)(2\ell+1)}}, \qquad (12)$$

where the results (A3) and (A11) of Appendix A have been used.

On the other hand, the Runge-Lenz component A_z has the matrix elements

$$\langle n\ell - 1m|A_z|n\ell m\rangle = \sqrt{\frac{(n^2-\ell^2)(\ell^2-m^2)}{(2\ell-1)(2\ell+1)}}, \qquad (13)$$

easily deduced from Eq. (A17).

By comparing Eqs.(12) and (13), the coefficient is $a = -3n/2$. This reproduces, as expected, the result $\mathbf{r} \rightarrow -3n/2\mathbf{A}$ originally obtained by Pauli [7]. The position operator $\mathbf{r}$ can be therefore replaced by the Runge-Lenz vector, when restricted to states within the n-shell. This result is sometimes referred to as *Pauli's replacement rule*, which, in addition to Pauli's original proof [7] can also be derived from other approaches, as in Refs. [2, 3]. It is useful to note that the cartesian components commute when unrestricted ($[x, y] = 0$, for example), but behave as angular momentum vectors when restricted to the n-shell, because $[A_x, A_y] = iL_z$.

V. EQUIVALENT QUADRUPOLE OPERATOR

The quadrupole operator is a rank 2 tensor with cartesian components q_{ik} defined by Eq. (7). It is symmetrical ($q_{ik} = q_{ki}$) and has zero trace ($\sum_i q_{ii} = 0$). Two quadrupole-like operators, symmetrical, with zero trace and even parity, can be constructed from $\mathbf{A}$ and $\mathbf{L}$ and can contribute to the equivalent quadrupole operator. They are

$$O^{(1)}_{ij} = \frac{1}{2}(A_iA_j + A_jA_i) - \frac{1}{3}A^2\,\delta_{ij}\,, \qquad (14)$$

and

$$O^{(2)}_{ij} = \frac{1}{2}(L_iL_j + L_jL_i) - \frac{1}{3}L^2\,\delta_{ij}\,. \qquad (15)$$

where the end δ_{ij}-term insures zero trace. Mixed terms of the form $A_i L_j$ have odd parity (sign changes under coordinate inversion) and are therefore precluded. The equivalent quadrupole operator has therefore the general form

$$P_n q^{(2)} P_n = a\, O^{(1)} + b\, O^{(2)} ,$$

where the coefficients a and b are determined by comparing the matrix elements of specific tensor components, between states with angular momentum quantum number differing by 0 or 2 units, i.e. $(\ell' = \ell, \ell \pm 2)$.

It is convenient to calculate the matrix elements of the $_{zz}$, or $_{33}$, components of the quadrupole and quadrupole-like operators and then to solve the set of equations

$$\begin{aligned} \langle n\ell m|q^{(2)}_{33}|n\ell m\rangle &= a\langle n\ell m|O^{(1)}_{33}|n\ell m\rangle + b\langle n\ell m|O^{(2)}_{33}|n\ell m\rangle , \\ \langle n\ell' m|q^{(2)}_{33}|n\ell m\rangle &= a\langle n\ell' m|O^{(1)}_{33}|n\ell m\rangle + b\langle n\ell' m|O^{(2)}_{33}|n\ell m\rangle \end{aligned}$$

for the coefficients a and b, where $\ell' = \ell - 2$.

A. Implementation

Explicit calculations of the above matrix elements of $q^{(2)}_{33}$, $O^{(1)}_{33}$ and $O^{(2)}_{33}$ yield the results (A20), (A21) and (A24)-(A23), derived in Appendix A. The coefficients are thus calculated as $a = 5n^2/2$ and $b = -n^2/2$. The quadrupole equivalent-operator can therefore be expressed exclusively in terms of the **L** and **A** operators as,

$$\begin{aligned} P_n q^{(2)}_{ij} P_n &\equiv P_n \left(x_i x_j - \frac{1}{3} r^2 \delta_{ij} \right) P_n \\ &= \frac{5n^2}{4} \left(A_i A_i + A_j A_i - \frac{2}{3} A^2\, \delta_{ij} \right) - \frac{n^2}{4} \left(L_i L_j + L_j L_i - \frac{2}{3} L^2\, \delta_{ij} \right) . \end{aligned} \tag{16}$$

This is our desired rule which replaces the cartesian quadrupole components (7) by Eq. (16). From this general rule, the equivalent-operator relation

$$\rho^2 \equiv x^2 + y^2 = r^2 - z^2 = \frac{n^2}{2} \left(n^2 + 3 + L_z^2 + 4A^2 - 5A_z^2 \right) , \tag{17}$$

for the cylindrical diagonal element squared is readily deduced. Expression (17), originally proven by Solov'ev [10], was key to theoretical development for the hydrogen atom in weak magnetic fields and in crossed electric and magnetic fields (see [11], for example). The explicit rule (16) provides, of course, all five independent quadrupole tensor elements.

B. Equivalent operator for $n\ell m \to n\ell m'$ transitions

It is worth noting that a construction was developed earlier for the 3D rotational SO(3) group with generator $\mathbf{L}$ and the *unit* vector $\mathbf{n} = \mathbf{r}/r$, instead of the SO(4) group vector $\mathbf{r}$. In one of their problems [13], Landau and Lifshitz derive the equivalent operator relation

$$n_i n_k - \frac{1}{3}\delta_{ik} = -\frac{1}{(2\ell-1)(2\ell+3)}\left[L_i L_k + L_k L_i - \frac{2}{3}L^2\delta_{ik}\right] \tag{18}$$

to be compared with our equivalent operator (16). This relation (18) is valid for the Hilbert space of states on a unit sphere, within the subspace of states with definite total angular momentum ℓ (but with different m) i. e., for $n\ell m \to n\ell m'$ transitions. The definition of equivalent operators for this SO(3) group is

$$\langle n\ell\gamma|\mathcal{A}|n\ell\gamma'\rangle = \langle n\ell\gamma|\mathcal{B}|n\ell\gamma'\rangle \tag{19}$$

in contrast to the definition (2) of hydrogenic SO(4) equivalent operators. The present study provides the multipole operators, i.e. irreducible tensors built from electron coordinate $\mathbf{r}$, in terms of the hydrogenic SO(4) symmetry group generators $\mathbf{L}$ and $\mathbf{A}$ which permit all intrashell $n\ell m \to n\ell' m'$ transitions.

C. Quadrupole operator in the SO(3) ⊗ SO(3) representation

In the Coulomb problem, it is conventional to replace $\mathbf{L}$ and $\mathbf{A}$ by a pair of integrals of motion, $\mathbf{I}^{(1)}$ and $\mathbf{I}^{(2)}$ related by

$$\begin{aligned} \mathbf{I}^{(1)} &= \frac{1}{2}(\mathbf{L}+\mathbf{A}), \qquad \mathbf{I}^{(2)} = \frac{1}{2}(\mathbf{L}-\mathbf{A}); \\ \mathbf{L} &= \mathbf{I}^{(1)} + \mathbf{I}^{(2)}, \qquad \mathbf{A} = \mathbf{I}^{(1)} - \mathbf{I}^{(2)}. \end{aligned}$$

The operators $\mathbf{I}^{(1)}$ and $\mathbf{I}^{(2)}$ possess all the properties enjoyed by *independent* angular momentum quantum-mechanical operators

$$\begin{aligned} &\left(\mathbf{I}^{(1)}\right)^2 = \left(\mathbf{I}^{(2)}\right)^2 = j(j+1), \qquad j = \frac{1}{2}(n-1); \\ &\left[\mathbf{I}^{(1)}, \mathbf{I}^{(2)}\right] = 0. \end{aligned}$$

These *pseudospin* operators are generators of SO(3) ⊗ SO(3) representation of algebra of SO(4) symmetry group in quantum mechanics and provide the algebraic basis set [8] of wavefunctions with quantum numbers (n, m_1, m_2).

The equivalent quadrupole operator rule (16) can now be recast in terms of *pseudospin* vectors $\mathbf{I}^{(1)}$ and $\mathbf{I}^{(2)}$ as,

$$q_{ik}^{(2)} = n^2 \left[I_i^{(1)} I_k^{(1)} + I_k^{(1)} I_i^{(1)} + I_i^{(2)} I_k^{(2)} + I_k^{(2)} I_i^{(2)} \right] - 3n^2 \left[I_i^{(1)} I_k^{(2)} + I_i^{(2)} I_k^{(1)} \right] - \frac{1}{3} n^2 (n^2 - 1) + 2n^2 \left[\mathbf{I}^{(1)} \cdot \mathbf{I}^{(2)} \right] .$$

D. Application: Averaged ion-quadrupole interaction

In a number of physical problems, the angular momenta operators $\mathbf{I}^{(1)}$ and $\mathbf{I}^{(2)}$ are quantized with respect to independent axes $\boldsymbol{\omega}_1$ and $\boldsymbol{\omega}_2$ in space. One example is the hydrogen atom in crossed electric and magnetic fields, where the vectors $\boldsymbol{\omega}_1$ and $\boldsymbol{\omega}_2$ are expressed [2] in terms of the electric field strength and the magnetic field induction. This approach is extended also to time-dependent fields [6]. Another example appears in the theory [3, 5] of intrashell mixing in excited hydrogen atom by collision with a particle with charge Z_B. Here, in the co-rotating frame, the electric field is space-fixed and directed along the z axis towards charge Z_B, while the effective magnetic field is perpendicular to it and normal to the collision plane. The theory [3, 5] of intrashell mixing usually accounts only for the leading and dominant charge-dipole term in the expansion for the full charge (Z_B)-Rydberg atom interaction. The next term is the charge-quadrupole interaction which, in the co-rotating frame, is

$$3 Z_B \frac{q_{33}^{(2)}}{R^3} , \tag{20}$$

where $\mathbf{R}$ is a vector directed from the atomic nucleus of the target atom towards the projectile of charge Z_B and the component along $\mathbf{R}$ is denoted by subscript 3.

As a useful application of the present equivalent-operator method, we evaluate the average of interaction (20) appropriate to perturbation theory. Namely, we perform in the SO(3) $\otimes$ SO(3) representation of Section V C, the average of the quadrupole operator $q_{33}^{(2)}$ over the atomic state defined by two quantum numbers m_1 and m_2, where m_i, $i = 1, 2$ are the respective eigenvalues for projection of the vector operators $\mathbf{I}^{(i)}$ onto the respective axes $\boldsymbol{\omega}_i$. Let α_i, $i = 1, 2$ be the angle between vectors $\boldsymbol{\omega}_i$ and $\mathbf{R}$, and let β be the angle between vectors $\boldsymbol{\omega}_1$ and $\boldsymbol{\omega}_2$. Algebraic manipulation readily yields the important result

$$\langle m_1 m_2 | \, q_{33}^{(2)} | m_1 m_2 \rangle = n^2 \left[2m_1^2 \cos^2 \alpha_1 - 12 m_1 m_2 \cos \alpha_1 \cos \alpha_2 + 2m_2^2 \cos^2 \alpha_2 \right.$$

$$+\sqrt{(n^2-1)-4m_1^2}\sin^2\alpha_1+\sqrt{(n^2-1)-4m_2^2}\sin^2\alpha_2$$
$$-\frac{1}{3}(n^2-1)+2m_1m_2\cos\beta\Big]$$

for the quadrupole moment averaged over an algebraic basis set of wavefunctions with quantum numbers (n, m_1, m_2).

VI. EQUIVALENT OCTUPOLE OPERATOR

The cartesian components of the octupole moment as a tensor of rank 3 are defined by Eq. (8). The octupole-like combinations of **L** and **A** which have contributions to the equivalent octupole operator within the n-shell are based on **AAA** and **LLA**. Other combinations have even parity and are forbidden by the parity rule, as previously explained in Section III.

Following our general procedure, we seek the equivalent octupole operators in the form

$$P_n q^{(3)} P_n = a\,O^{(1)} + b\,O^{(2)},$$

where the tensor operator $O^{(1)}$ is derived from the set **AAA** and $O^{(2)}$ from the set **LLA**, respectively. The precise method for constructing these operators is now explained.

The matrix elements of the $_{333}$ tensor components between states with one and three units difference in angular momentum number are compared. The unknown coefficients a and b are then solutions of the set of equations,

$$\langle n\ell-1m|q^{(3)}_{333}|n\ell m\rangle = a\langle n\ell-1m|O^{(1)}_{333}|n\ell m\rangle + b\langle n\ell-1m|O^{(2)}_{333}|n\ell m\rangle\ ,$$
$$\langle n\ell-3m|q^{(3)}_{333}|n\ell m\rangle = a\langle n\ell-3m|O^{(1)}_{333}|n\ell m\rangle + b\langle n\ell-3m|O^{(2)}_{333}|n\ell m\rangle\ .$$

The cartesian components $O^{(1)}_{ijk}$ and $O^{(2)}_{ijk}$ of the octupole-like operators are now constructed from $A_iA_jA_k$ and $L_iL_jA_k$, respectively. Three operations are then applied to these elementary combinations to insure that the resulting operators possess the following properties: (1) they have zero trace when any pair of indices are contracted, (2) they are fully symmetric with respect to index permutations and (3) they are symmetric over the order of noncommuting factors.

Given three vector operators **a**, **b** and **c**, the ijk component of the most general octupole-type operator is given by

$$o_{ijk}(\mathbf{a},\mathbf{b},\mathbf{c}) = \mathcal{Z}\left[a_ib_jc_k - \frac{1}{5}\delta_{jk}\sum_{s=1}^{3}a_ib_sc_s - \frac{1}{5}\delta_{ij}\sum_{s=1}^{3}a_sb_sc_k - \frac{1}{5}\delta_{ik}\sum_{s=1}^{3}a_sb_jc_s\right], \qquad (21)$$

where $\mathcal{Z}$ represents the operation of symmetrization with respect to *both* index and vector permutations. For example,

$$\mathcal{Z}[a_i b_j c_k] = \frac{1}{36} \sum_{\rho} \sum_{\pi} \rho(a)_{\pi(i)}\, \rho(b)_{\pi(j)}\, \rho(c)_{\pi(k)} \ , \tag{22}$$

where ρ represents a permutation of the vector set $\{a, b, c\}$ and where π is a permutation of the index set $\{i, j, k\}$. It is easy to check that the combination (21) obtained in this way possess all of the above (1)-(3) required properties.

A. Implementation

According to the general prescription (21) above, the operator (8) takes the form $o_{ijk} = o_{ijk}(\mathbf{r}, \mathbf{r}, \mathbf{r})$ so that its $_{zzz}$ (or $_{333}$) component in cartesian representation is

$$q^{(3)}_{333} = o_{333}(\mathbf{r}, \mathbf{r}, \mathbf{r}) = x_3^3 - \frac{3}{5} r^2 x_3 \ ,$$

as expected. From vectors $\mathbf{L}$ and $\mathbf{A}$, two octupole operators with the same parity as for o_{ijk} can be constructed. One is $O^{(1)}_{ijk} = o_{ijk}(\mathbf{A}, \mathbf{A}, \mathbf{A})$ and the other is $O^{(2)}_{ijk} = o_{ijk}(\mathbf{A}, \mathbf{L}, \mathbf{L})$.

The $_{zzz}$ (or $_{333}$) component of the octupole-type operator $O^{(1)}$ is

$$O^{(1)}_{333} = o_{333}(\mathbf{A}, \mathbf{A}, \mathbf{A}) = \mathcal{Z}\left[A_3^3 - \frac{3}{5} \sum_s (A_s A_s) A_3 \right] . \tag{23}$$

With the aid of Eq. (22) and the commutation relations $[A_i, A_j] = \mathrm{i}\epsilon_{ijk} L_k$ and $[L_i, A_j] = \mathrm{i}\epsilon_{ijk} A_k$, expression (23) reduces eventually (see Appendix B 1) to simply

$$O^{(1)}_{333} = A_3^3 - \frac{3}{10}(A^2 A_3 + A_3 A^2) + \frac{1}{5} A_3 \ . \tag{24}$$

The second operator

$$O^{(2)}_{333} = o_{333}(\mathbf{L}, \mathbf{L}, \mathbf{A}) = \mathcal{Z}\left\{ L_3^2 A_3 - \frac{1}{5} \sum_s \left[(A_s L_s) L_3 + (L_s A_s) L_3 + (L_s L_s) A_3 \right] \right\} , \tag{25}$$

with the aid of similar algebraic reduction and the additional identity $\mathbf{A} \cdot \mathbf{L} = \mathbf{L} \cdot \mathbf{A} = 0$, eventually reduces (see Appendix B 2) to

$$O^{(2)}_{333} = L_3^2 A_3 - \frac{1}{10}(L^2 A_3 + A_3 L^2) + \frac{1}{5} A_3 \ . \tag{26}$$

Using Eqs. (A26), (A27), (A28) - (A31) of Appendix A, the solution of the set of equations of matrix elements yields the required coefficients to be $a = -\frac{35}{8} n^3$ and $b = \frac{15}{8} n^3$. The equivalent octupole operator within the n-shell is therefore

$$P_n q^{(3)}_{ijk} P_n = -\frac{35 n^3}{8}\, o_{ijk}\,(\mathbf{A}, \mathbf{A}, \mathbf{A}) + \frac{15 n^3}{8}\, o_{ijk}(\mathbf{L}, \mathbf{L}, \mathbf{A}) \ . \tag{27}$$

This is our desired rule which replaces the cartesian octupole (8) by Eq. (27), where the general components o_{ijk} are determined in the prescribed manner.

In particular, the sequences involved are provided in Appendix B for the o_{333} case, as an example characteristic of the overall calculational procedure. Specifically, Eq. (27), with the aid of $A^2 + L^2 + 1 = n^2$, yields the expression

$$P_n q^{(3)}_{333} P_n = \frac{5n^3}{8}\left[3L_3^2 A_3 + \frac{12}{5}(A^2 A_3 + A_3 A^2) - 7A_3^2\right] - \frac{n^3}{8}(3n^2 + 5) \tag{28}$$

for the equivalent octupole $_{333}$-component operator in the $(\mathbf{L}, \mathbf{A})$-representation.

VII. LIST OF EQUIVALENT MULTIPOLE OPERATORS AND A TEST EXAMPLE

We have shown that the cartesian dipole, quadrupole and octupole operators,

$$q_i^{(1)} = x_i\,, \tag{29}$$

$$q_{ij}^{(2)} = x_i x_j - \frac{1}{3} r^2 \delta_{ij}\,, \tag{30}$$

$$q_{ijk}^{(3)} = x_i x_j x_k - \frac{1}{5} r^2 (x_i \delta_{jk} + x_j \delta_{ik} + r_k \delta_{ij})\,. \tag{31}$$

have the equivalent intrashell dipole, quadrupole and octupole operators,

$$q_i^{(1)} = -\frac{3}{2} n A_i\,, \tag{32}$$

$$q_{ij}^{(2)} = -\frac{n^2}{4}\left(L_i L_j + L_j L_i - \frac{2}{3} L^2\,\delta_{ij}\right) + \frac{5n^2}{4}\left(A_i A_j + A_j A_i - \frac{2}{3} A^2\,\delta_{ij}\right), \tag{33}$$

$$q_{ijk}^{(3)} = -\frac{35}{8} n^3 O_{ijk}^{(1)} + \frac{15}{8} n^3 O_{ijk}^{(2)} \tag{34}$$

expressed explicitly in terms of the $\mathbf{L}$ and $\mathbf{A}$ integrals of the motion on the energy shell. Eq. (32) reproduces the Pauli [7] operator replacement rule, $\mathbf{r} \equiv -3n/2\mathbf{A}$, for the dipole cartesian component (29). Eqs. (33) and (34) summarize our replacement rules for both the quadrupole and octupole cartesian elements (30) and (31). The operators $O_{ijk}^{(1)} = o_{ijk}(\mathbf{A}, \mathbf{A}, \mathbf{A})$ and $O_{ijk}^{(2)} = o_{ijk}(\mathbf{L}, \mathbf{L}, \mathbf{A})$ are defined in Section VI and are calculated in Appendix B. The n^λ scaling law is apparent in Eqs. (32) - (34). Note that equivalent operators generally contain several terms with simple coefficients.

A. Application: Multipoles of extreme Stark states

As a test example, consider the permanent multipole moments associated with the extreme Stark hydrogenic states, i.e., for those Stark (parallel and antiparallel) states most stretched along the positive and negative direction of the Z-axis. With the aid of the replacement rules (32)-(34), the appropriate spherical multipole operators $Q_0^{(\lambda)}$ are

$$Q_0^{(1)} = q_3^{(1)} = -\frac{3n}{2} A_3 \ , \tag{35}$$

$$Q_0^{(2)} = \frac{3}{2}\, q_{33}^{(2)} = -\frac{3n^2}{4}\left(L_3^2 - \frac{1}{3}L^2\right) + \frac{15n^2}{4}\left(A_3^2 - \frac{1}{3}A^2\right), \tag{36}$$

$$\begin{aligned} Q_0^{(3)} = \frac{5}{2}\, q_{333}^{(3)} = &-\frac{175n^3}{16}\left(A_3^3 + \frac{1}{5}A_3 - \frac{3}{10}A^2A_3 - \frac{3}{10}A_3A^2\right) \\ &+ \frac{75n^3}{16}\left(L_3^2A_3 + \frac{1}{5}A_3 - \frac{1}{10}L^2A_3 - \frac{1}{10}A_3L^2\right). \end{aligned} \tag{37}$$

The parabolic and algebraic representation of these states are respectively,

$$\psi_{(n-1)\,0\,0}(\mathbf{r}) \equiv |+\rangle = |n,\ j,\ -j\rangle \ ,$$

$$\psi_{0\,(n-1)\,0}(\mathbf{r}) \equiv |-\rangle = |n,\ -j,\ j\rangle \ .$$

Any of these hydrogenic stretched states $|\alpha\rangle = |\pm\rangle$ has expectation value,

$$Q_0^{(\lambda)} \equiv \langle\alpha|Q_\mu^{(\lambda)}|\alpha\rangle = \langle\alpha|Q_0^{(\lambda)}|\alpha\rangle\delta_{\mu 0} \ . \tag{38}$$

For the "plus" states $|+\rangle = |n,\ j,\ -j\rangle$ of the algebraic basis, we have

$$Q_0^{(1)}(+) = \langle +|Q_0^{(1)}|+\rangle = -\frac{3n}{2}A_3(+) \ ,$$

where $A_3(+) = -2j = -(n-1)$, so that

$$Q_0^{(1)}(+) = \frac{3n(n-1)}{2}$$

is the permanent dipole moment for the extreme stretched Stark state. On using $L_3(+) = 0$, $L^2(+) = n-1$ and $A^2(+) = n(n-1)$, the quadrupole and octupole moments are

$$Q_0^{(2)}(+) = \frac{1}{2}\, n^2(n-1)(5n-7)$$

and

$$Q_0^{(3)}(+) = \frac{5}{8}\, n^3(n-1)(n-2)(7n-9) \ ,$$

respectively. All these moments are in exact agreement with the analytical results [8] of theory recently developed solely for the case of these extreme Stark states. Matrix elements of operators (35)-(37) over the $(n,\ \ell,\ m)$ basis have also been checked for $n = 1-6$.

VIII. CONCLUSIONS

We have shown that it is possible to construct both the quadrupole and octopole operators solely in terms of the $\mathbf{A}, \mathbf{L}$ operators which are integrals of motion on the energy shell with quantum number n. We have provided and illustrated the various steps involved with their construction and have derived explicit expressions for these operators. The basic importance of these expressions is that they furnish the ability to solve various structure and collision problems solely by algebraic group theoretical techniques and commutation relations based on the SO(4) symmetry of the hydrogen atom, when the dynamics is confined to the energy shell. We gave various useful averages of these operators. Our general theory readily provides the permanent dipole, quadrupole and octupole of polar Rydberg atoms in their extreme Stark states, a case which can be also solved by less-sophisticated standard techniques. The present treatment will be key to further developments in the theory of Stark ℓ- mixing via the combined charge-dipole, charge-quadrupole and charge-octupole interactions evident in ion-Rydberg atom collisions. The present study would also be important to investigation [14, 15] of Rydberg atoms in the field of electric multipoles.

Although the dipole, quadrupole and octupole are the most significant in many practical applications, the full general solution for any multipole remains, at present, elusive. Although plausible, the very existence of equivalent operators for a general multipole is not completely certain. Consider, for instance, the hexadecapole operator (i.e., Eq. 5 with $\lambda = 4$). Here three tensor operators are appropriate: $O^{(1)}$ derived from the set **AAAA**, $O^{(2)}$ derived from the set **AALL** and $O^{(3)}$ derived from the set **LLLL**, while the sets **AAAL** and **ALLL** with odd-parity are all forbidden. The equivalent operator can then be taken as the linear combination $aO^{(1)} + bO^{(2)} + cO^{(3)}$. Three non-zero non-diagonal intrashell matrix elements ($\ell' = \ell$, $\ell' = \ell - 2$ and $\ell' = \ell - 4$) are then used to fit the coefficients a, b, c, in the manner prescribed in Section VI.

Although this reasoning could, in principle, be extended to higher multipoles, the overall procedure ultimately becomes quite cumbersome for actual calculations for larger λ. The simplicity of the coefficients in formulae (32), (33) and (34) possibly indicates that there may well be simpler methods of derivation. Although fruitful, the present theoretical systematic pole-by-pole approach may not be sufficiently powerful for the general multipole case. Instead, some other more encompassing approach, probably based on study of commutation

relations (similar, in spirit to the derivation of Pauli replacement rule in the Appendix of Ref. [3]) could be developed.

Finally, we indicate that there is another context where equivalent operators are of key importance. Namely, higher order contributions from external fields might be expressed in terms of equivalent operators. These effects imply virtual intershell (n-changing) transitions conveniently expressed via Green functions. Although equivalent operators were constructed quite long ago by Solov'ev [12] for the second-order contributions from electric fields, higher orders have, as yet, not been considered. Equivalent operators of this type are beyond the scope of the present study.

Acknowledgments

Research is supported by AFOSR Grant No. 49620-02-1-0338 and NSF Grant No. 04-00438, and research of DV is performed under the auspices of the US Department of Energy through the Los Alamos National Laboratory under the LDRD-PRD program.

APPENDIX A: INTRASHELL MATRIX ELEMENTS

1. Radial and Angular Elements

A general expression for intrashell radial matrix elements of integer power of r is (see [16], for example)

$$(n\ell'|r^\beta|n\ell) = \int_0^\infty R_{n\ell'}(r)R_{n\ell}(r)r^{\beta+2}\,dr =$$
$$\frac{1}{4}\left(\frac{n}{2}\right)^{\beta-1}\left[\frac{(n+\ell_>)!(n-\ell_>-1)!}{(n+\ell_<)!(n-\ell_<-1)!}\right]^{1/2}(-1)^{\ell_>+\ell_<+\beta+1}\times$$
$$\sum_{i=i_0}^{\beta+1}\frac{(-1)^i}{i!(\beta+1-i)!}\frac{(n+\ell_<+i)!(n-\ell_<-1+i)!}{(n+\ell_>+i-(\beta+1))!(n-\ell_>-1+i-(\beta+1))!}\,,$$

where the lower limit in summation is $i_0 = \max[0, \beta+1-(n-\ell_>-1)]$, $\ell_> = \max(\ell,\ell')$ and $\ell_< = \min(\ell,\ell')$. This general equation yields the following useful matrix elements for low powers of r,

$$(n\ell|r^0|n\ell) = 1\,, \tag{A1}$$
$$(n\ell|r^1|n\ell) = \frac{1}{2}\left[3n^2-\ell(\ell+1)\right]\,, \tag{A2}$$

$$(n\ell-1|r^1|n\ell) = -\frac{3}{2}n\sqrt{n^2-\ell^2}\,, \tag{A3}$$

$$(n\ell|r^2|n\ell) = \frac{1}{2}n^2\left[5n^2-3\ell(\ell+1)+1\right], \tag{A4}$$

$$(n\ell-1|r^2|n\ell) = -\frac{1}{2}n(5n^2-\ell^2+1)\sqrt{n^2-\ell^2}\,, \tag{A5}$$

$$(n\ell-2|r^2|n\ell) = \frac{5}{2}n^2\sqrt{[n^2-\ell^2][n^2-(\ell-1)^2]}\,, \tag{A6}$$

$$(n\ell|r^3|n\ell) = \frac{1}{8}n^2\left[35n^4-5n^2(6\ell(\ell+1)-5)+3\ell(\ell-1)(\ell+1)(\ell+2)\right], \tag{A7}$$

$$(n\ell-1|r^3|n\ell) = -\frac{5}{8}n^3(7n^2-3\ell^2+5)\sqrt{n^2-\ell^2}\,, \tag{A8}$$

$$(n\ell-2|r^3|n\ell) = \frac{5}{8}n^2\left[7n^2-\ell(\ell-1)+2\right]\sqrt{[n^2-\ell^2][n^2-(\ell-1)^2]}\,, \tag{A9}$$

$$(n\ell-3|r^3|n\ell) = -\frac{35}{8}n^3\sqrt{[n^2-\ell^2][n^2-(\ell-1)^2][n^2-(\ell-2)^2]}\,. \tag{A10}$$

The standard angular integral is

$$\begin{aligned}(\ell_3 m_3|Y_{\ell_2 m_2}|\ell_1 m_1) = & \int d\Omega\, Y_{\ell_1 m_1}(\Omega)\, Y_{\ell_2 m_2}(\Omega)\, Y_{\ell_3 m_3}(\Omega)^* \\ = & \sqrt{\frac{(2\ell_1+1)(2\ell_2+1)}{4\pi(2\ell_3+1)}}\, C^{\ell_3 0}_{\ell_1 0\,\ell_2 0}\, C^{\ell_3 m_3}_{\ell_1 m_1\,\ell_2 m_2}\,.\end{aligned}$$

From standard tables (see [9], for example) of the Clebsch-Gordan coefficients $C^{\ell_3 m_3}_{\ell_1 m_1\,\ell_2 m_2}$, we obtain the following angular integrals for the quantum numbers of interest

$$(\ell-1m|Y_{10}|\ell m) = \sqrt{\frac{3}{4\pi}}\sqrt{\frac{\ell^2-m^2}{(2\ell-1)(2\ell+1)}}\,, \tag{A11}$$

$$(\ell m|Y_{20}|\ell m) = \sqrt{\frac{5}{4\pi}}\,\frac{\ell(\ell+1)-3m^2}{(2\ell-1)(2\ell+3)}\,, \tag{A12}$$

$$(\ell-2m|Y_{20}|\ell m) = \sqrt{\frac{5}{4\pi}}\,\frac{3}{4(2\ell-1)}\sqrt{\frac{(\ell^2-m^2)[(\ell-1)^2-m^2]}{(2\ell-3)(2\ell+1)}}\,, \tag{A13}$$

$$(\ell-1m|Y_{30}|\ell m) = \sqrt{\frac{7}{4\pi}}\,\frac{3}{2}\,\frac{\ell^2-5m^2-1}{(2\ell-3)(2\ell+3)}\sqrt{\frac{\ell^2-m^2}{(2\ell-1)(2\ell+1)}}\,, \tag{A14}$$

$$(\ell-3m|Y_{30}|\ell m) = \sqrt{\frac{7}{4\pi}}\,\frac{5}{2(2\ell-3)(2\ell-1)}\sqrt{\frac{(\ell^2-m^2)[(\ell-1)^2-m^2][(\ell-2)^2-m^2]}{(2\ell-5)(2\ell+1)}} \tag{A15}$$

2. Dipole Matrix Elements for Section IV

On using the relation (9), radial (A3) and angular (A11) integrals, the dipole matrix elements are

$$\langle n\ell-1m|q_3^{(1)}|n\ell m\rangle = \langle n\ell-1m|Q_0^{(1)}|n\ell m\rangle =$$

$$\sqrt{\frac{4\pi}{3}}(n\ell-1|r|n\ell)(\ell-1m|Y_{10}|\ell m)=-\frac{3n}{2}\sqrt{\frac{(n^2-\ell^2)(\ell^2-m^2)}{(2\ell-1)(2\ell+1)}}\,. \tag{A16}$$

3. A and L operators

The action of Runge-Lenz vector on n-shell states is (see Adams [1], p. 112, O. L. DeLange and R. E. Raab [1], p. 264 or Ref. [17], for example),

$$\begin{aligned} A_3|n\ell m\rangle \;=\; & \sqrt{\frac{(n^2-\ell^2)(\ell^2-m^2)}{(2\ell-1)(2\ell+1)}}\;|n\ell-1m\rangle \\ & +\sqrt{\frac{(n^2-(\ell+1)^2)((\ell+1)^2-m^2)}{(2\ell+1)(2\ell+3)}}\;|n\ell+1m\rangle\,. \end{aligned} \tag{A17}$$

The Pauli replacement rule $\mathbf{r}\;\rightarrow\;-3n/2\mathbf{A}$ immediately follows on comparing (A16) and (A17).

In terms of the coefficient

$$g_{n\ell}=\sqrt{\frac{(n^2-\ell^2)(\ell^2-m^2)}{(2\ell-1)(2\ell+1)}}, \tag{A18}$$

(A17) can be rewritten as the linear combination

$$A_3|n\;\ell\;m\rangle=g_{n\ell}\;|n\;\ell-1\;m\rangle+g_{n\ell+1}\;|n\;\ell+1\;m\rangle \tag{A19}$$

of $(n,\ell\pm1,m)$ states. The operators $A_\pm=A_1\pm\mathrm{i}A_2$ which change m by ±1, respectively, can also be written as the similar combinations

$$\begin{aligned} A_+|n\;\ell\;m\rangle \;&=\; +\beta_{\,m,\ell-1}\;c_{n\ell}\;|n\;\ell-1\;m+1\rangle-\gamma_{\,m,\ell+1}\;c_{n\ell+1}\;|n\;\ell+1\;m+1\rangle\,, \\ A_-|n\;\ell\;m\rangle \;&=\; -\beta_{-m,\ell-1}\;c_{n\ell}\;|n\;\ell-1\;m-1\rangle+\gamma_{-m,\ell+1}\;c_{n\ell+1}\;|n\;\ell+1\;m-1\rangle \end{aligned}$$

of $(n,\ell\pm1,m\pm1)$ states. The coefficients are

$$\begin{aligned} \beta_{m,\ell} \;&=\; \sqrt{(\ell-m+1)(\ell-m)}\,, \\ \gamma_{m,\ell} \;&=\; \sqrt{(\ell+m+1)(\ell+m)}\,, \\ c_{n\ell} \;&=\; \sqrt{(n^2-\ell^2)/(2\ell-1)(2\ell+1)}\,. \end{aligned}$$

For completeness with above, the components L_3 and $L_\pm=L_1\pm\mathrm{i}L_2$ of the $\mathbf{L}$ operator obey the standard relations,

$$L_3|n\;\ell\;m\rangle\;=\;m\;|n\;\ell\;m\rangle\,,$$

$$L_+|n\ \ell\ m\rangle\ =\ \omega_{\,m,\ell}\,|n\ \ell\ m+1\,\rangle\ ,$$
$$L_-|n\ \ell\ m\rangle\ =\ \omega_{-m,\ell}\,|n\ \ell\ m-1\,\rangle\ ,$$

where $\omega_{m,\ell}=\sqrt{(\ell-m)(\ell+m+1)}$.

In the subsequent reduction of the basic A_iA_j and L_iL_j operations within the quadrupole operators $O^{(1)}_{ij}$ and $O^{(2)}_{ij}$ and the $A_iA_jA_k$, $A_iL_jL_k$ and $L_iL_jA_k$ operations within the octupole operators $O^{(1)}_{ijk}$ and $O^{(2)}_{ijk}$, frequent use is made of the standard commutation relations $[A_i,A_j]=\mathrm{i}\epsilon_{ijk}L_k$, and $[L_i,L_j]=\mathrm{i}\epsilon_{ijk}L_k$ together with $[L_i,A_j]=\mathrm{i}\epsilon_{ijk}A_k$ (which relation rotates A_j about axis i to give A_k, thereby confirming the vector character of $\mathbf{A}$). We also employ the additional relations $\sum_s A_sL_s\equiv(\mathbf{A}\cdot\mathbf{L})=0$ and $\sum_s L_sA_s\equiv(\mathbf{L}\cdot\mathbf{A})=0$ for $O^{(2)}_{333}$ reduction.

4. Quadrupole Matrix Elements for Section V

On using the relation (10), radial (A4) and angular (A12) integrals, the quadrupole matrix elements are

$$\langle n\ell m|q^{(2)}_{33}|n\ell m\rangle=\frac{2}{3}\langle n\ell m|Q^{(2)}_0|n\ell m\rangle$$
$$=\ \frac{2}{3}\sqrt{\frac{4\pi}{5}}(n\ell|r^2|n\ell)(\ell m|Y_{20}|\ell m)=\frac{n^2}{3}\frac{\ell(\ell+1)-3m^2}{(2\ell-1)(2\ell+3)}\,(5n^2-3\ell^2-3\ell+1)\quad\text{(A20)}$$

and similarly, using eqs. (A6) and (A13),

$$\langle n\ell-2m|q^{(2)}_{33}|n\ell m\rangle=\frac{2}{3}\langle n\ \ell-2\ m|Q^{(2)}_0|n\ \ell\ m\rangle=\frac{2}{3}\sqrt{\frac{4\pi}{5}}(n\ell-2|r^2|n\ell)(\ell-2m|Y_{20}|\ell m)=$$
$$\frac{5n^2}{2(2\ell-1)}\sqrt{\frac{(n^2-\ell^2)[n^2-(\ell-1)^2](\ell^2-m^2)[(\ell-1)^2-m^2]}{(2\ell-3)(2\ell+1)}}\ .\qquad\text{(A21)}$$

On using Eq. (A19), direct algebraic calculation of the matrix elements of the quadrupole operators (14) and (15) yields

$$\langle n\ell m|O^{(1)}_{33}|n\ell m\rangle\ =\ g^2_{n\ell}+g^2_{n\ell+1}-\frac{1}{3}\left[n^2-\ell(\ell+1)-1\right]\,,\qquad\text{(A22)}$$
$$\langle n\ell-2m|O^{(1)}_{33}|n\ell m\rangle\ =\ g_{n\ell}g_{n\ell-1}\,,\qquad\text{(A23)}$$
$$\langle n\ell m|O^{(2)}_{33}|n\ell m\rangle\ =\ -\frac{1}{3}\left[\ell(\ell+1)-3m^2\right]\,,\qquad\text{(A24)}$$
$$\langle n\ell-2m|O^{(2)}_{33}|n\ell m\rangle\ =\ 0\,,\qquad\text{(A25)}$$

in terms of the $g_{n\ell}$ coefficient (A18). The relation $A^2+L^2=n^2-1$ has been used for Eq. (A22).

5. Octupole Matrix Elements for Section VI

The octupole matrix elements calculated using Eqs. (11), (A8), (A10), (A14) and (A15) are

$$\langle n\ell - 1m|q^{(3)}_{333}|n\ell m\rangle = \frac{2}{5}\sqrt{\frac{4\pi}{7}}(n\ell - 1|r^3|n\ell)(\ell - 1m|Y_{30}|\ell m) =$$
$$-\frac{3n^3}{8}\frac{(7n^2 - 3\ell^2 + 5)(\ell^2 - 5m^2 - 1)}{(2\ell - 3)(2\ell + 3)}\sqrt{\frac{(n^2 - \ell^2)(\ell^2 - m^2)}{(2\ell - 1)(2\ell + 1)}} \tag{A26}$$

and

$$\langle n\ell - 3m|q^{(3)}_{333}|n\ell m\rangle = \frac{2}{5}\sqrt{\frac{4\pi}{7}}(n\ell - 3|r^3|n\ell)(\ell - 3m|Y_{30}|\ell m) = -\frac{35n^3}{8(2\ell - 3)(2\ell - 1)}$$
$$\sqrt{\frac{(n^2 - \ell^2)[n^2 - (\ell - 1)^2][n^2 - (\ell - 2)^2](\ell^2 - m^2)[(\ell - 1)^2 - m^2][(\ell - 2)^2 - m^2]}{(2\ell - 5)(2\ell + 1)}} \tag{A27}$$

Direct calculation based on Eq. (A19) then provides the following octupole matrix elements

$$\langle n\ell - 1m|O^{(1)}_{333}|n\ell m\rangle = g_{n\ell}\left[g^2_{n\ell-1} + g^2_{n\ell} + g^2_{n\ell+1} + \frac{1}{5} - \frac{3}{5}(n^2 - \ell^2 - 1)\right], \tag{A28}$$
$$\langle n\ell - 3m|O^{(1)}_{333}|n\ell m\rangle = g_{n\ell}g_{n\ell-1}g_{n\ell-2}, \tag{A29}$$
$$\langle n\ell - 1m|O^{(2)}_{333}|n\ell m\rangle = -\frac{1}{5}g_{n\ell}(\ell^2 - 5m^2 - 1), \tag{A30}$$
$$\langle n\ell - 3m|O^{(2)}_{333}|n\ell m\rangle = 0, \tag{A31}$$

in terms of the coefficient (A18). The relation $A^2 + L^2 = n^2 - 1$ has been used in Eq. (A28).

APPENDIX B: (A, L)-REPRESENTATION FOR OPERATORS $O^{(1)}_{333}$ AND $O^{(2)}_{333}$

We illustrate here the procedure for evaluating, in terms of $(\mathbf{A}, \mathbf{L})$, the $O^{(1)}_{333}$ and $O^{(2)}_{333}$ operators from their basic definitions (23) and (25). At the outset, proper account must be taken of the inherent $\mathcal{Z}$-operation prescribed by formula (22) for symmetrization with respect to *both* index and vector permutations.

1. The $O^{(1)}_{333}$ component

The definition of $O^{(1)}_{333}$ is

$$O^{(1)}_{333} = o_{333}(\mathbf{A}, \mathbf{A}, \mathbf{A}) = \mathcal{Z}\left[A^3_3 - \frac{3}{5}\sum_s (A_s A_s)A_3\right]. \tag{B1}$$

The first term $\mathcal{Z}A_3^3 = A_3^3$ is left unaffected. The symmetrized sum can be evaluated via the following progression of steps:

$$
\begin{aligned}
& \mathcal{Z}\sum_s (A_s A_s) A_3 \\
&= \frac{1}{6}\sum_s (A_s A_s A_3 + A_s A_3 A_s + A_s A_s A_3 + A_s A_3 A_s + A_3 A_s A_s + A_3 A_s A_s) \\
&= \frac{1}{3}(A^2 A_3 + A_3 A^2) + \frac{1}{3}\sum_s A_s A_3 A_s \\
&= \frac{1}{3}(A^2 A_3 + A_3 A^2) + \frac{1}{6}\sum_s (A_s A_s A_3 - A_s A_s A_3 + 2A_s A_3 A_s - A_3 A_s A_s + A_3 A_s A_s) \\
&= \frac{1}{2}(A^2 A_3 + A_3 A^2) + \frac{1}{6}\sum_s (A_s\,[A_3,\, A_s] - [A_3,\, A_s]\,A_s) \\
&= \frac{1}{2}(A^2 A_3 + A_3 A^2) + \frac{1}{6}\,[A_1 i L_2 - i L_2 A_1 + A_2(-iL_1) - (-iL_1)A_2] \\
&= \frac{1}{2}(A^2 A_3 + A_3 A^2) + \frac{1}{6} i\Big([A_1,\, L_2] - [A_2,\, L_1]\Big) \\
&= \frac{1}{2}(A^2 A_3 + A_3 A^2) + \frac{1}{6} i(iA_3 + iA_3) \\
&= \frac{1}{2}(A^2 A_3 + A_3 A^2) - \frac{1}{3}A_3\ .
\end{aligned}
$$

The $O_{333}^{(1)}$ operator, Eq. (B1), therefore reduces to

$$O_{333}^{(1)} = A_3^3 - \frac{3}{10}(A^2 A_3 + A_3 A^2) + \frac{1}{5}A_3 \tag{B2}$$

as stated by Eq. (24) of the text.

2. The $O_{333}^{(2)}$ component

$O_{333}^{(2)}$ is defined by

$$O_{333}^{(2)} = o_{333}(\mathbf{L},\mathbf{L},\mathbf{A}) = \mathcal{Z}\left\{L_3^2 A_3 - \frac{1}{5}\sum_s [(A_s L_s)L_3 + (L_s A_s)L_3 + (L_s L_s)A_3]\right\}. \tag{B3}$$

Because the operators L_3 and A_3 commute, the first term $\mathcal{Z}\,L_3^2 A_3 = L_3^2 A_3$ is left unaffected. Symmetrization of the remaining terms proceeds via the following steps:

$$
\begin{aligned}
& \mathcal{Z}\sum_s [(A_s L_s)L_3 + (L_s A_s)L_3 + (L_s L_s)A_3] \\
&= \frac{1}{6}\sum_s (A_s L_s L_3 + A_s L_3 L_s + L_s A_s L_3 + L_s L_3 A_s + L_3 A_s L_s + L_3 L_s A_s \\
&\quad + L_s A_s L_3 + L_s L_3 A_s + A_s L_s L_3 + A_s L_3 L_s + L_3 L_s A_s + L_3 A_s L_s
\end{aligned}
$$

$$
\begin{aligned}
&+L_sL_sA_3 + L_sA_3L_s + L_sL_sA_3 + L_sA_3L_s + A_3L_sL_s + A_3L_sL_s) \\
&= \frac{1}{3}\sum_s (A_sL_sL_3 + A_sL_3L_s + L_sA_sL_3 + L_sL_3A_s + L_3A_sL_s + L_3L_sA_s) \\
&+\frac{1}{3}\left(L^2A_3 + A_3L^2\right) + \frac{1}{3}\sum_s L_sA_3L_s \\
&= \frac{1}{3}\sum_s (A_sL_3L_s + L_sL_3A_s) + \frac{1}{3}\left(L^2A_3 + A_3L^2\right) + \frac{1}{3}\sum_s L_sA_3L_s \ . \qquad \text{(B4)}
\end{aligned}
$$

The first sum in the RHS of (B4) transforms from

$$
\begin{aligned}
S_1 \equiv \sum_s (A_sL_3L_s + L_sL_3A_s) &= \sum_s (A_sL_3L_s - A_sL_sL_3 + L_sL_3A_s - L_3L_sA_s) \\
&= \sum_s (A_s\,[L_3,\,L_s] - [L_3,\,L_s]\,A_s)\,.
\end{aligned}
$$

to

$$
S_1 = A_1iL_2 - iL_2A_1 + A_2(-i)L_1 - (-i)L_1A_2 = i\,[A_1,\,L_2] - i\,[A_2,\,L_1] = -2A_3.
$$

The second sum in the RHS of (B4) becomes reduced by the following steps from

$$
\begin{aligned}
S_2 \equiv \sum_s L_sA_3L_s &= \frac{1}{2}\sum_s (L_sL_sA_3 - L_sL_sA_3 + 2L_sA_3L_s + A_3L_sL_s - A_3L_sL_s) \\
&= \frac{1}{2}\left(L^2A_3 + A_3L^2\right) + \frac{1}{2}\sum_s (L_s\,[A_3,\,L_s] - [A_3,\,L_s]\,L_s) \\
&= \frac{1}{2}\left(L^2A_3 + A_3L^2\right) + \frac{1}{2}\,(L_1iA_2 - iA_2L_1 - L_2iA_1 + iA_1L_2) \\
&= \frac{1}{2}\left(L^2A_3 + A_3L^2\right) + \frac{1}{2}\,(i\,[L_1,\,A_2] - i\,[L_2,\,A_1]) \\
&= \frac{1}{2}\left(L^2A_3 + A_3L^2\right) + \frac{1}{2}\,(iiA_3 + (-i)(-i)iA_3) \qquad \text{(B5)}
\end{aligned}
$$

to

$$
S_2 = \frac{1}{2}\left(L^2A_3 + A_3L^2\right) - A_3\ .
$$

The full $O^{(2)}_{333}$ operator, Eq. (B3), is therefore,

$$
O^{(2)}_{333} = L_3^2A_3 - \frac{1}{10}\left(L^2A_3 + A_3L^2\right) + \frac{1}{5}A_3\ , \qquad \text{(B6)}
$$

as stated by Eq. (26) of the text. The end term of Eq. (B6), being extracted from the detailed algebraic calculation above is the least obvious.

---

[1] B. G. Adams, *Algebraic Approach to Simple Quantum Systems*, (Springer-Verlag, Berlin, 1994). O. L. DeLange and R. E. Raab, *Operator Methods in Quantum Mechanics*, (Clarendon

Press, Oxford, 1991). C. E. Wulfman, in *Group Theory and its Applications*, edited by E. M. Loebl, (Academic Press, New York, 1977). B. G. Wybourne, *Classical Groups for Physicists* (Wiley, New York, 1974). M. J. Englefield, *Group Theory and the Coulomb Problem* (Wiley, New York, 1972).

[2] Yu. N. Demkov, B. S. Monozon, and V. N. Ostrovsky, Zh. Eksp. Teor. Fiz. **57**, 1431 (1969) [Sov. Phys.-JETP **30**, 775 (1970)].

[3] D. Vrinceanu and M. R. Flannery, Phys. Rev. A **63**, 032701 (2001); J. Phys. B: At. Mol. Opt. Phys. **34**, L1 (2001); Phys. Rev. Lett. **85**, 4880 (2000).

[4] M. R. Flannery and D. Vrinceanu, Int. Journ. Mass Spectrom. **223-224**, 473 (2003).

[5] A. K. Kazansky and V. N. Ostrovsky, Phys. Rev. A **52**, R1811 (1995); J. Phys. B **29**, 3651 (1996); Phys. Rev. Lett. **77**, 3094 (1996); Zh. Eksp. Teor. Fiz. **110**, 1988 (1996) [JETP **83**, 1095 (1996)].

[6] A. K. Kazansky and V. N. Ostrovsky, J. Phys. B **29**, L855 (1996); D. Fregenal, T. Ehrenreich, B. Henningsen, E. Horsdal-Pedersen, L. Nyvang, and V. N. Ostrovsky, Phys. Rev. Lett. **87**, 223001 (2001); E. Horsdal-Pedersen and V. N. Ostrovsky, Phys. Rev. A **67**, 033408 (2003); D. Fregenal, E. Horsdal-Pedersen, L. B. Madsen, M. Førre, J. P. Hansen, and V. N. Ostrovsky, Phys. Rev. A **69**, 031401(R) (2004); V. N. Ostrovsky and E. Horsdal-Pedersen, Phys. Rev. A **70**, 033413 (2004).

[7] W. Pauli, Z. Phys. **36**, 336 (1926).

[8] M. R. Flannery, D. Vrinceanu and V. N. Ostrovsky, J. Phys. B: Atom. Molec. and Opt.Phys. **38**, S279 (2005).

[9] D. A. Varshalovich, A. N. Moskalev, and V. K. Khersonsky, *Kvantovaya Tera Uglovogo Momenta* (Nauka: Leningrad, 1975) [English Translation: *Quantum Theory of Angular Momentum* (World Scientific: Singapore, 1988)].

[10] E. A. Solov'ev, Zh. Eksp. Teor. Fiz. **82**, 1762 (1982) [Sov. Phys. - JETP **55**, 1017 (1982)].

[11] P. A. Braun and E. A. Solov'ev, Zh. Eksp. Teor. Phys. **86**, 68 (1984) [Sov. Phys. - JETP **59**, 38 (1984)].

[12] E. A. Solov'ev, Zh. Eksp. Teor. Fiz. **85**, 109 (1983) [Sov. Phys. - JETP **58**, 63 (1983)].

[13] L. D. Landau and E. M. Lifshitz, *Quantum Mechanics*, (Butterworth-Heinemann: Oxford, 1997), Sect. 29, p. 96.

[14] A. K. Kazansky and V. N. Ostrovsky, Zh. Eksp. Teor. Fiz. **97**, 78 (1990) [Sov. Phys. - JETP

70, 43 (1990)].

[15] W. Clark and C. H. Greene, Rev. Mod. Phys. **71**, 821 (1999).

[16] J. Morales and J. J. Pena, Phys. Rev. A **45**, 4259 (1992).

[17] O. L. deLange and R. E. Raab, Phys. Rev. A **34**, 1650 (1986); A. C. Kalloniatis, J. Phys. A **21**, L573 (1988).

Plasma Screening within Rydberg Atoms in Circular States

M. R. Flannery* and E. Oks**

* School of Physics, Georgia Institute of Technology, Atlanta, GA 30332, USA
** Physics Department, 206 Allison Lab., Auburn University, Auburn, AL 36849, USA

Abstract

A Rydberg atom embedded in a plasma can experience penetration by slowly moving electrons within its volume. The original pure Coulomb potential must now be replaced by a screened Coulomb potential which contains either a screening length R_s or a screening factor $A = R_s^{-1}$. For any given discrete energy level, there is a Critical Screening Factor (CSF) A_c beyond which the energy level disappears (by merging into the continuum). Analytical results are obtained for the classical dependence of the energy on the screening factor, for the CSF, and for the critical radius of the electron orbit for Circular Rydberg States (CRS) in this screened Rydberg atom. The results are derived for *any general form of the screened Coulomb potential* and are applied to the particular case of the Debye potential. We also show that CRS can temporarily exist above the ionization threshold and are therefore the *classical counterparts of quantal discrete states embedded into continuum*. The results are significant not only to Rydberg plasmas, but also to fusion plasmas, where Rydberg states of multi-charged hydrogen-like ions result from charge exchange with hydrogen or deuterium atoms.

PACS numbers: 34.60.+z, 31.70.-f, 31.50.Df

1. Introduction

A new branch of atomic physics – the interactions, dynamics, and collisions in ultra-cold ($T << 1K$) systems – has naturally evolved from recent advances in the cooling and trapping of neutral gases. In ultra-cold Rydberg plasmas [1 - 3], three-body recombination [4] mainly populates Rydberg states *Ry(n, l)* with high principal and azimuthal quantum numbers *n, l*. Quantal and classical theories have already been presented [5 - 10] of relevant processes: (a) Stark mixing [5 - 8] by collision of *Ry(n, l)* with ultra-cold ions redistributes the internal angular momentum among all states l', (b) radiative cascade [6] from *Ry(n, l)* into all lower n'-states, and (c) the first order interactions between the *permanent* multi-poles of two Rydberg atoms [10] generated by the resulting broad distribution of l-states. The physics of ultra-cold Rydberg gases [11 – 13] also requires the same kind of physical transparency.

In this regard, we are concerned here with the possibility that the large volume of the Rydberg atom can be exposed to penetration by a swarm of slowly moving electrons, thereby introducing plasma screening between the Rydberg electron and its parent ionic core. Plasma screening of a test charge is a well-known phenomenon. For a hydrogen atom or a hydrogen-like ion (an H-atom, for short), it is effected by replacing the pure Coulomb potential by a screened Coulomb potential which contains a physical parameter – the screening length R_s or its inverse $R_s^{-1} = A$ known as the screening factor. For example, the Debye-Hückel (or Debye) interaction of an electron with the electronic shielded field of an ion of charge Z is

$$V(R) = -(Ze^2/R)\exp(-R/R_s), \quad (1)$$

where $R_s = [kT/(4\pi e^2 N_e)]^{1/2} \approx 1.304 \times 10^4 (10^{10}/N_e)^{1/2} T^{1/2} a_0$ for plasmas of the electron density N_e (cm^{-3}) and of the temperature T(K). For ultra-cold plasmas, N_e can be as large as $\sim 10^{10}$ cm^{-3} and the temperature as low as 1K to give $R_s = 1.3 \times 10^4$ a_0. Therefore $R_s < n^2 a_0$ for levels $n > 114$. Thus, the effects of screening may be important for low temperature Rydberg plasmas.

Outside R_s collective effects weaken the interaction of the Rydberg electron with the nucleus. Bound states are mostly eliminated outside R_s, while within R_s bound states are possible. As the screening becomes stronger, R_s decreases and the screening factor A increases, so that the number of Discrete Energy Levels (DELs) of a screened H-atom becomes reduced and the degree of degeneracy of the DELs also reduces from n^2 to $2l+1$ (because the degeneracy of l-states is lifted). For any specific DEL, there is some Critical Screening Factor (CSF) A_c , such that for $A > A_c$ this DEL disappears by merging into the continuum.

The DELs and A_c's were calculated for a (Debye) screened H-atom by various authors (e.g., see a recent Ref. [14] and references therein). However, most of this work was concerned only with numerical results for relatively low lying *n, l* states. Because Rydberg plasmas involve high $n > 20$ and high *l*, it is important to have A_c and the corresponding DELs for screened Rydberg atoms where quantal numerical calculations become prohibitively difficult and ultimately impractical.

Some analytical results have already been published [15 – 17]. Smith [15] presented DELs for arbitrary states of a screened H-atom, calculated by the perturbation theory using the basis of the wave functions of the unscreened Coulomb potential. These results [15] are therefore only valid when the difference between the screened and unscreened Coulomb potentials is relatively small. The CSFs for high n-levels correspond, however, to the opposite case and thus cannot be obtained from the results of Ref. [15]. Bessis et al [16] presented DELs for a screened H-atom, calculated by the perturbation theory using the basis of the wave functions of the Hulthen potential (see also references therein to previous results of this kind). However, the method provides rigorous results only for the states of zero angular momentum ($l = 0$). As for the $l > 0$-states most relevant to Rydberg atoms, only some model results were obtained by adding an approximate rotational term. Rogers et al [17] presented classical results for the energy of circular Rydberg states in a screened H-atom. However, it was only some basic starting formula for the energy – the dependence of the energy on the screening factor was not derived in any usable form. It should be also pointed out that Ref. [17] contained no calculations of the CSF and/or the critical radius of the electron orbit where DELs disappear.

All the above referenced results were obtained for the Debye potential – the most commonly used form of the screened Coulomb potential. However, the actual screened Coulomb potential in plasmas may be more complicated than the Debye potential (see, e.g., Ref. [18]).

In the present paper, we provide classical analytical results for the dependence of the energy on the screening factor, for the CSF, and for the critical radius of the electron orbit for Circular Rydberg States (CRS) in a screened H-atom. We obtained the results for a *general form of the screened Coulomb potential*. As far as we know, there are, as yet, no published results of any kind on the CSF and the critical radius of the electron orbit for the general form of the screened Coulomb potential.

After deriving the results for general screened interactions, we consider a particular case of the Debye potential. Here, we obtain even more explicit analytical results for the dependence of the

energy on the screening factor, for the CSF, and for the critical radius of the electron orbit. We also obtain the analytical dependence of the energy on the screening parameter.

Finally, we demonstrate the existence of the CRS above the ionization threshold. They are *classical counterparts of quantal discrete states embedded into continuum* [19]. We show that some of these states correspond to unstable motion, while the remainder of the CRS above the ionization threshold corresponds to stable motion.

Before proceeding with our theory, we note that CRS have been extensively studied both theoretically and experimentally for several reasons (see, e.g., [20 - 23] and references therein). Firstly, CRS have long radiative lifetimes and highly anisotropic collision cross sections, thereby enabling experimental observation of inhibited spontaneous emission and other cold Rydberg gases phenomena [11 -13]. Secondly, classical CRS correspond to quantal coherent states that are objects of fundamental importance. Thirdly, the classical description of CRS provided here serves as the leading and primary term in the quantal theory based on the 1/n-expansion (see, e.g. [24] and references therein).

2. Classical analytical results for the general form of the screened Coulomb potential

Consider the H-atom, with nucleus of charge Z is stationary at the origin, embedded in a plasma. Rydberg plasmas correspond to the case with Z=1. We confine ourselves to circular electronic orbits of constant radius R. The classical Hamilton function in atomic units $e = m_e = 1$ is

$$H(R, A) = M^2/(2R^2) - f(AR)Z/R = E, \qquad (2)$$

where E and M are the energy and the absolute value of the angular momentum which are constant. The screened Coulomb potential in its general form (i.e., not necessarily the Debye potential) is $V(R) = -f(AR)/R$ where $A = 1/R_s$ is the screening factor, the inverse value of the screening radius R_s. The function f(x) which represents the departure from the pure Coulomb attraction has the following properties

$$f(x) > 0 \text{ at } 0 < x < \infty; \qquad f(0) = 1, \qquad f(\infty) = 0, \qquad (3)$$

so that the pure Coulomb potential is recovered for A = 0, while the potential vanishes as $A \to \infty$.

On introducing the following scaled quantities,

$$r = RZ/M^2, \quad a = AM^2/Z, \quad v = VM^2/Z^2, \quad \varepsilon = EM^2/Z^2, \qquad (4)$$

the scaled Hamilton function is

$$h(r, a) = HM^2/Z^2 = 1/(2r^2) - f(ar)/r. \qquad (5)$$

Dynamic equilibrium occurs when

$$dh/dr = -1/r^3 + f/r^2 - af'/r = 0, \qquad f' = df/dx, \qquad (6)$$

one of the conditions required to determine the equilibrium value $r_0(a)$ of the scaled radius of the orbit for a given scaled screening factor a. It can be re-written in the form:

$$a = [f(s) - s\,f'(s)]s, \qquad (7)$$

where $s \bullet \bullet a r_0$. The scaled energy $\bullet\theta$ at $r = r_0$ is

$$\bullet\theta = 1/2r_0^2 - f(s)/r_0. \qquad (8)$$

As the scaled screening factor a increases and exceeds some critical value a_c, the scaled energy becomes positive, which corresponds to the disappearance of the bound state of the Rydberg atom (i.e., to the merging of the bound state into the continuum). This critical value a_c is determined by substituting $a = a_c$ into the right side of Eq. (8) with $\bullet\theta = 0$ to give

$$2r_0 f(s_c) = 1, \qquad (9)$$

where $s_c \bullet \bullet a_c r_0$. Equation (9) can be rewritten in the form:

$$a_c = 2s_c\,f(s_c), \qquad (10)$$

which, with Eq. (7) for $a = a_c$, yields

$$2s_c\,f(s_c) = [f(s_c) - s_c\,f'(s_c)]s_c, \qquad (11)$$

or the equivalent equation

$$f(s_c) = -s_c\,f'(s_c) \qquad (12)$$

with respect to only one unknown quantity s_c. The solution s_{c0} of Eq. (12) is then substituted into the right side of the Eq. (10) to finally give the critical value of the scaled screening factor as

$$a_c = 2s_{c0}\,f(s_{c0}). \qquad (13)$$

Because the corresponding critical value of the scaled radius of the orbit is $r_{0c} = s_{c0}/a_c$, from Eq. (9), we also obtain

$$r_{0c} = 1/[2f(s_{c0})]. \qquad (14)$$

By substituting $r_0 = s/a$ in Eq. (8) and then using the expression for a(s) from Eq. (7), we obtain the analytical dependence of the energy $\bullet\epsilon(s)$,

$$\bullet\epsilon(s) = \{[s\,f'(s)]^2 - [f(s)]^2\}/2, \qquad (15)$$

on the screening factor a(s), from Eq. (7), via one parameter s.

3. Classical analytical results for the Debye potential

Application of the preceding general theory is now made to the important particular case of the Debye potential

$$v(r, a) = - [\exp(-ar)]/r. \tag{16}$$

The scaled energy at the equilibrium radius $r = r_0$ is

$$\bullet_{\theta}(s, r_0) = 1/2r_0^2 - \exp(-s)/r_0. \tag{17}$$

Eq. (7) for the screening parameter yields

$$a(s) = s(1 + s) \exp(-s). \tag{18}$$

On expressing exp(-s) from Eq. (18) and substituting the result in Eq. (17), we obtain

$$\bullet_{\theta}(s, r_0) = (s - 1)/[2r_0^2 (s + 1)] \tag{19}$$

in agreement with an equivalent expression previously presented by Rogers et al [17]. Because the equilibrium scaled radius is

$$r_0 = s/a(s) = \exp(s)/(1+s), \tag{20}$$

Eq. (17) can be expressed as the pure function

$$\bullet_{\theta}(s, r_0) = -[(1-s^2)/2]\exp(-2s) \tag{21}$$

of s alone.

Eq. (21) predicts that the critical value s_c at which $\bullet_{\theta} = 0$ is $s_{c0} = 1$. Then Eq. (18) predicts that the critical screening factor $a_c = a(s_{c0})$ at which the corresponding DEL is just about to merge into the continuum is

$$a_c = 2/e \bullet \bullet 0.735759. \tag{22}$$

The classical scaled radius of this CRS orbit is

$$r_{0c} = s_{c0}/a_c = e/2 \bullet \bullet 1.359141. \tag{23}$$

Eqns. (18) and (21) provide the analytical dependence of the energy $\bullet_{\theta}$ on the screening factor a via one parameter s. The variation of a(s) and $\bullet_{\theta}(s)$ with s is illustrated in Figs. 1 and 2, respectively. Both functions display their maximal values

$$a_m \bullet \bullet 0.839962, \qquad \bullet_m \bullet \bullet 0.0318091 \tag{24}$$

at $s = s_m = (1 + 5^{1/2})/2$ • •1.61803. Figure 3 exhibits directly the dependence of the energy •ß on the screening parameter a. The maxima of the functions a(s) and •ß(s) in Figs. 1 and 2 correspond to the ">"-shape crossing of the two energy branches in Fig. 3. A simple analysis shows that the lower energy branch in Fig. 3 corresponds to *stable* equilibrium, while the upper energy branch in Fig. 3 corresponds to *unstable* equilibrium. For the case of two crossing classical energy branches, identification of the lower branch with stable equilibrium and the upper branch with unstable equilibrium was also previously shown in several different classical problems [25 – 27].

From Fig. 1, it is seen that there are two equilibrium values of r: r_1 and $r_2 > r_1$ for any $a < a_m$ • • 0.839962.The radius r_1 corresponds to stable equilibrium and thus to a bound (or quasi-bound) state. The value r_2 associated with unstable equilibrium corresponds to the electron escaping to become free.

From Fig. 2, it is seen that there are only quasi-bound states for $a_c < a < a_m$ (i.e., for $0.735759 < a < 0.839962$). These are *classical counterparts of quantal discrete states embedded into continuum* [19].

Our classical analytical results for the critical screening factor (CSF) for Rydberg atoms can now be compared with the quantal numerical calculations for relatively low lying states available in the literature. Harris [28] and Rogers et al [17] have both presented quantal numerical results up to the level with $n = 9$ and $l = 8$, i.e., up to the quasi-circular state 9k. For this state, Harris obtained a_c^{Har} • •0.77 (Table VI of Ref. [28]) – to be compared with our present asymptotic analytical result $a_c = 2/e$ • •0.735759. For the same 9k-state, Rogers et al [17] obtained the scaled critical screening length $1/a_c^{Rog}$ • •1.31 (Table III of Ref. [17]) – to be compared with our asymptotic analytical result $1/a_c = e/2$ • •1.359141. For the rest of our results (i.e., for the overwhelming majority of them), there is, to the best of our knowledge, nothing in the literature available for comparison.

4. Conclusion

For a *general form of the screened Coulomb potential* in a plasma, we have obtained classical analytical results for the dependence of the energy on the screening factor, for the critical screening factor, and for the critical radius of the electron orbit for circular Rydberg states (CRS). We have applied the general theory to a particular example of the Debye potential and derived even more explicit classical analytical results for the above three physical quantities.

We have also demonstrated the existence of the CRS above the ionization threshold. They are the *classical counterparts of quantal discrete states embedded into continuum*. Some of these states correspond to unstable motion, but the remaining CRS above the ionization threshold correspond to stable motion.

Although this entire study is motivated by the new research area of the physics of cold Rydberg plasmas, the results are also relevant to other types of plasmas. Examples are *fusion plasmas*, where Rydberg states of multicharged hydrogenlike ions result from charge exchange with hydrogen or deuterium atoms.

Acknowledgement

This work is supported by AFOSR Grant No. 49620-02-1-0338 and NSF Grant No. 01-00890.

References

1. M.P. Robinson, B.L. Tolra, M.W. Noel, T.F. Galagher, and P. Pillet 2000 *Phys. Rev. Lett.* **85** 4466
2. T.C. Killian, M.J. Lim, S. Kulin, R. Dumke, S.D. Bergeson, and S.L. Rolston 2001 *Phys. Rev. Lett.* **86** 3759
3. T.C. Killian, S. Kulin, S.D. Bergeson, L.A. Orozco, C. Orzel, and S.L. Rolston 1999 *Phys. Rev. Lett.* **83** 4776
4. M.R. Flannery and D. Vrinceanu 1998 in *Atomic Processes in Plasmas: 11th APS Topical Conf.*, edit. E. Oks and M. Pindzola (New York: AIP Press) p. 317
5. D. Vrinceanu and M.R. Flannery 2000 *Phys. Rev. Lett.* **85** 4880
6. D. Vrinceanu and M.R. Flannery 2001 *Phys. Rev.* **63** 032701
7. D. Vrinceanu and M.R. Flannery 2001 *J. Phys. B: At. Mol. Opt. Phys.* **34** L1
8. M.R. Flannery and D. Vrinceanu 2003 *Int. J. Mass Spectrom.* **223-224** 473
9. M.R. Flannery and D. Vrinceanu 2003 *Phys. Rav. A* **68** 030502(R)
10. M.R. Flannery, D. Vrinceanu, and V.N. Ostrovsky 2005 *J. Phys. B: At. Mol. Opt. Phys.* **38** S279
11. S.K. Dutta, D. Feldbaum, A. Walz-Flannigan, J.R. Guest, and G. Raithel 2001 *Phys. Rev. Lett.* **86** 3993
12. R.G. Hulet, E.S. Hilfer, and D. Kleppner 1985 *Phys. Rev. Lett.* **55** 2137
13. K.B. MacAdam and E. Horsdal-Petersen 2003 *J. Phys. B: At. Mol. Opt. Phys.* **36** R167
14. D. Ray and T.K. Roy 2000 *Eur. Phys. J. D* **10** 189
15. C.R. Smith 1964 *Phys. Rev.* **134** A1235
16. N. Bessis, G. Bessis, G. Gorbel, and B. Dakhel 1975 *J. Chem. Phys.* **63** 3744
17. F.J. Rogers, H.C. Graboske, and D.J. Harwood 1970 *Phys. Rev. A* **1** 1577
18. D. Salzmann 1998 *Atomic Physics in Hot Plasmas* (New York: Oxford Univ. Press)
19. L.D. Landau and E.M. Lifshitz 1965 *Quantum Mechanics* (Oxford: Pergamon)
20. E. Lee, D. Farrelly, and T. Uzer 1997 *Optics Express* **1** 221
21. T.C. Germann, D.R. Herschbach, M. Dunn, and D.K. Watson 1995 *Phys. Rev. Lett.* **74** 658
22. C.H. Cheng, C.Y. Lee, and T.F. Gallagher 1994 *Phys. Rev. Lett.* **73** 3078
23. L. Chen, M. Cheret, F. Roussel, and G. Spiess 1993 *J. Phys. B: At. Mol. Opt. Phys.* **26** L437
24. V.M. Vainberg, V.S. Popov, and A.V. Sergeev 1990 *Sov. Phys. JETP* **71** 470
25. E. Oks 2000 *Phys. Rev. Lett.* **85** 2084
26. E. Oks 2000 *J. Phys. B: Atom. Mol. Opt. Phys.* **33** 3319
27. E. Oks 2004 *Eur. Phys. J. D* **28** 171
28. G.M. Harris 1962 *Phys. Rev.* **125** 1131

Figures with captions

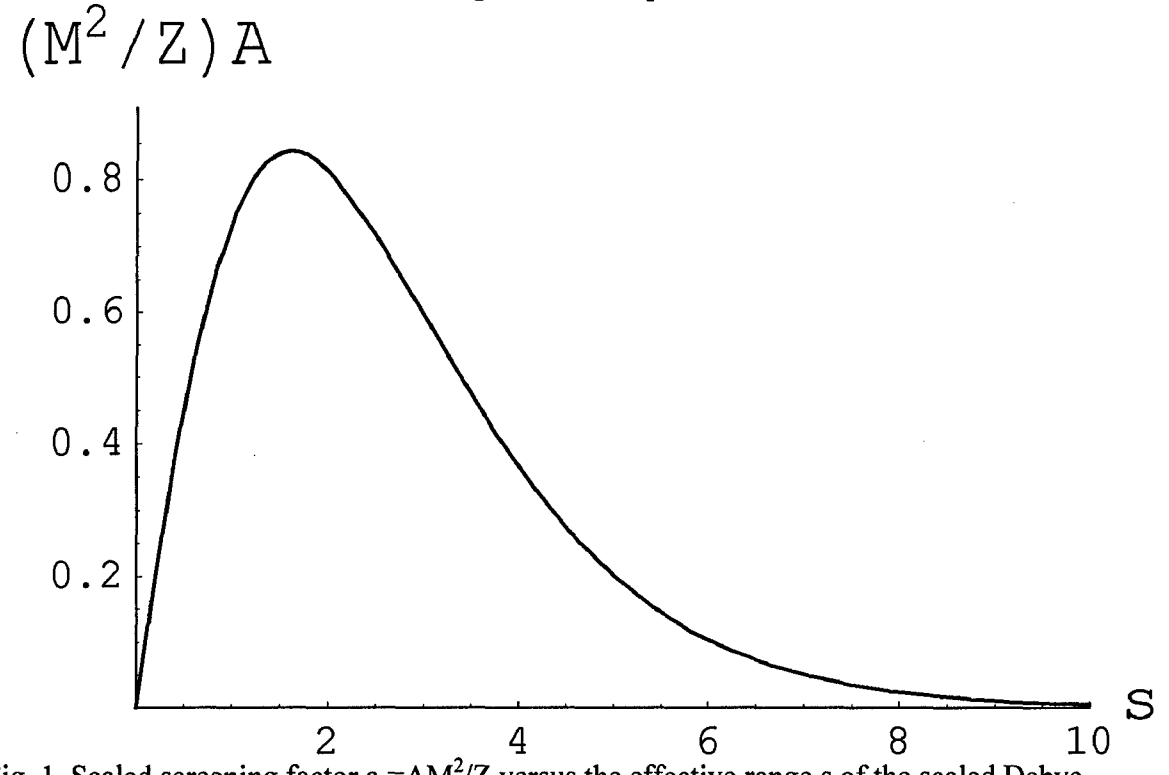

Fig. 1. Scaled screening factor a =AM^2/Z versus the effective range s of the scaled Debye potential v = – [exp(-s)]/r.

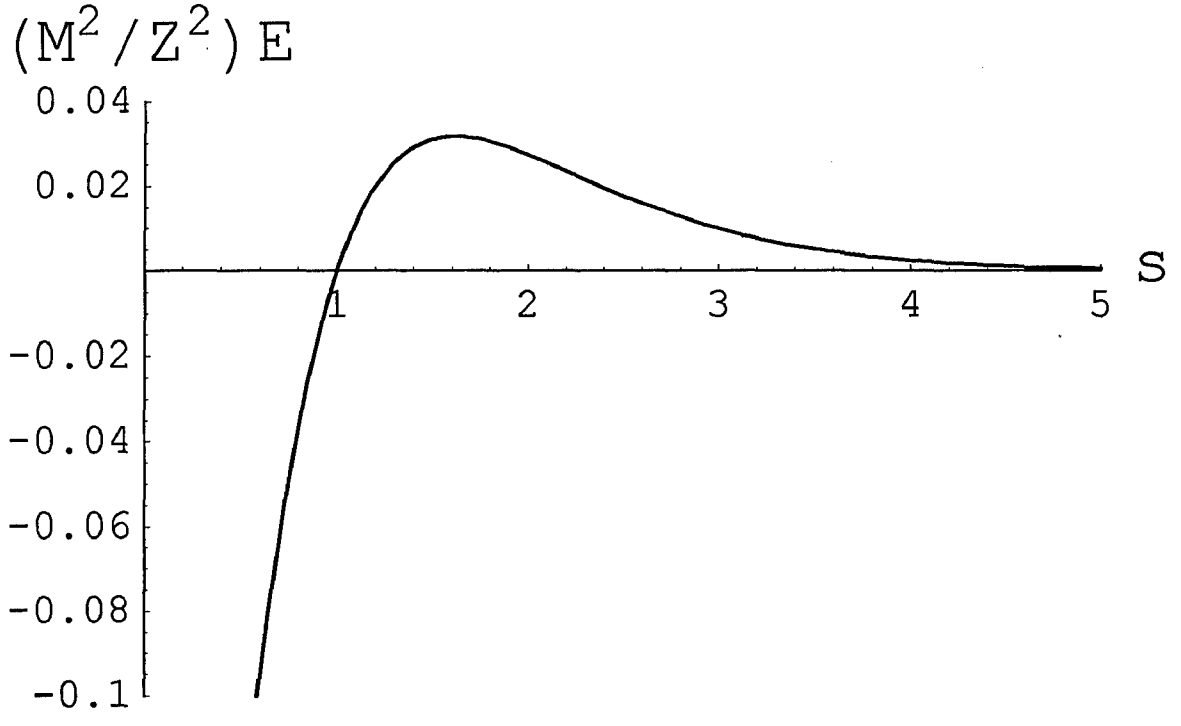

Fig. 2. Scaled energy $\bullet_0 = EM^2/Z^2$ versus the effective range s of the scaled Debye potential v = – [exp(-s)]/r.

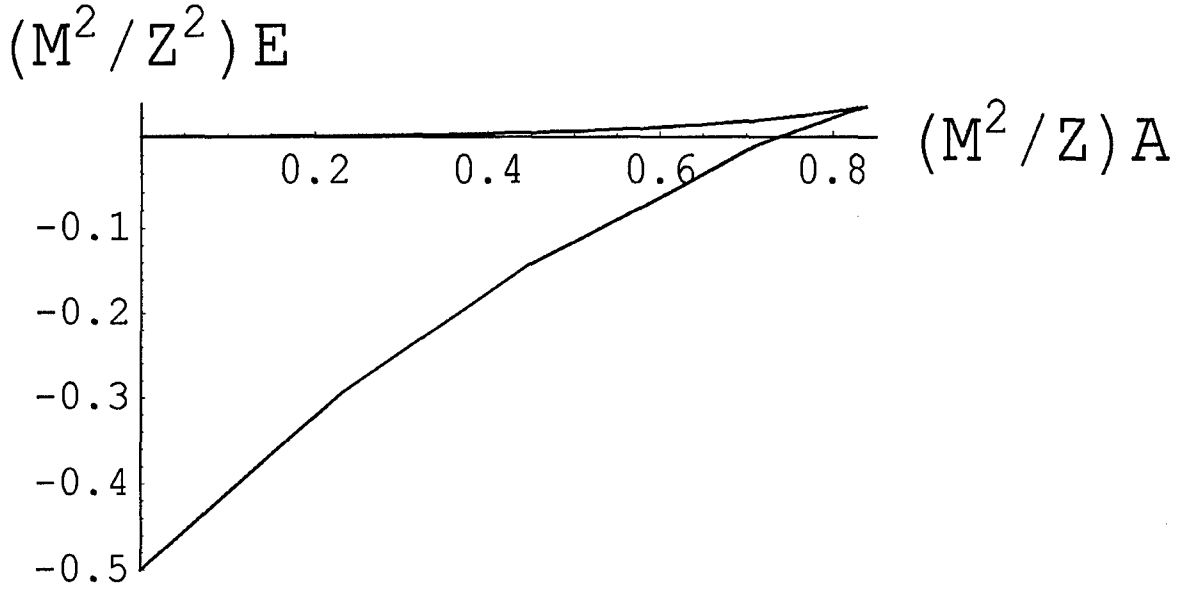

Fig. 3. Scaled energy $\bullet_0 = EM^2/Z^2$ of the circular state versus the scaled screening factor $a = AM^2/Z$ for the scaled Debye potential $v = -[\exp(-ar)]/r$.